Experimental Study and Numerical Simulation of Hydration and Microstructure Development of Ternary Cement-Based Materials

Zhijun Tan

Promotoren: prof. dr. G. Ye, prof. dr. ir. G. De Schutter
Proefschrift ingediend tot het behalen van de graad van
Doctor in de Ingenieurswetenschappen: Bouwkunde

Vakgroep Bouwkundige Constructies
Voorzitter: prof. dr. ir. L. Taerwe
Faculteit Ingenieurswetenschappen en Architectuur
Academiejaar 2015 - 2016

UNIVERSITEIT GENT

ISBN 978-90-8578-856-0
NUR 955
Wettelijk depot: D/2015/10.500/100

Supervisors:
Prof. dr. ir. Guang Ye
Prof. dr. ir. Geert De Schutter
Examination committee:
Prof. Luc Taerwe, chair (UGent)
Prof. Guang Ye and Prof. Geert De Schutter, promoters (UGent)
Prof. Klaas van Breugel (TUDelft)
Prof. Özlem Cizer (KULeuven)
Prof. Veerle Boel (UGent)
Dr. Elke Gruyaert (UGent)

Research institute
Magnel Laboratory for Concrete Research, Department of Structural Engineering, Faculty of Engineering and Architecture, Ghent University
This research was financially supported by the Special Research Fund (BOF) of Ghent University.

Acknowledgments

This thesis would not have been possible without the support from many people.

I would like to express my gratitude to my two supervisors, Prof. Guang Ye and Prof. Geert De Schutter, for their guidance and support over the years. They spent a great amount of time and effort to help me finishing the project, meetings, discussions, paper revising, conferences, etc.

These two gentlemen have been giving me free space to explore the world of cement. Prof. Ye is always ready to offer me his serious and critical thinking on every possible academic questions, which is definitely crucial to the development of a doctoral student like me. Prof. De Schutter is a very excellent scholar. He is always happily to help me to arrange experimental plan that is beyond my resources. In addition to the core academic research, he has always been supporting me when I am facing challenges or frustrating times.

Besides the research at work, my two supervisors are nice husbands, fathers of their families, which are also my examples when I am pursing happy life.

Great gratitude is also to the dedicated technician team of Magnel Laboratory for Concrete Research. Without their help, in particular Mr. Nicolas Coppieters, Mr. Dieter Hillewaere and Ms. Sandra De Buck, those experimental work would not be so easy.

I would like to show my great appreciation to the secretary team of Magnel Laboratory for Concrete Research, i.e. Ms. Marijke Reunes, Ms. Christel Malfait and Ms. Viviane Van Gaver, for their hard work in terms of meeting, travelling, financial management and other related office work.

Special thanks are given to colleagues Prof. Luc Taerwe, Prof. Nele De Belie for their occasional support, and also colleagues Mr. Vansweevelt Philip, Dr. Els Bruneel, Prof. Isabel Van Driessche (from the Department of Inorganic and Physical Chemistry of Ghent University), Dr. Lieven Machiels (Katholieke Universiteit Leuven) and Mr Yong Zhang (Delft University of Technology) for their support and cooperation on experimental work.

I appreciate the careful review and reading from the examination committee of this thesis. The comments and suggestions from Prof. Klaas van Breugel (TUDelft), Prof. Özlem Cizer (KULeuven), Prof. Veerle Boel (UGent) and Dr. Elke Gruyaert (UGent) are significant important for improving the quality of the thesis.

Among these years staying in Magnel laboratory, I thank the help and happy time from all colleagues in this lovely laboratory, i.e. all Chinese colleagues and non-Chinese colleagues, who made my research life in Belgium so enjoyable.

This project is financially supported by the Special Research Fund (BOF) of Ghent University, thus I show my deep appreciation to the tax-payers of Belgium as Ghent University is a public state university.

Last but not least, I express my love and gratitude to my beloved parents, elder brother and sister. It is their endless support and understanding that makes me have finished the whole duration of my studies from childhood to adulthood. In particular, the support from my wife Mrs Hongli Fu is also greatly appreciated. She has been looking after my own small family when I was working on this project.

This thesis is a gift for my son, Fuyouyang Tan, who was born in the first year (2010) of my doctoral study. Meanwhile, the thesis is dedicated to my two grandmothers, who passed away in the third year (2012) of my doctoral study.

Cement Chemical Nomenclature and other Abbreviations

Cement Chemistry

AFt = Al_2O_3-Fe_2O_3-tri
AFm = Al_2O_3-Fe_2O_3-mono
A = $A_{12}O_3$
C = CaO
$\overline{C}$ = CO_2
F = Fe_2O_3
H = H_2O
K = K_2O
M = MgO
N = Na_2O
P = P_2O_5
S = SiO_2
$\overline{S}$ = SO_3
T = TiO_2

Abbreviations

BFS = Blast-furnace slag
BSE = Backscattered electron
DTA = Differential thermal analysis
EDTA = Ethylenediaminetetraacetic acid
ESEM = Environmental scanning electron microscope
GGBFS = Ground granulated blast-furnace slag
MIP = Mercury intrusion porosimetry
OPC = Ordinary Portland cement
PB = Portland cement + Blast-furnace slag
PBL = Portland cement + Blast-furnace slag + Limestone powder
PC = Portland cement
PL = Portland cement + Limestone powder
QXRD = Quantitative X-ray diffraction
RH = Relative humidity

SCMs = Supplementary cementing materials

SEM = Scanning electron microscopy

TG = Thermogravimetry

TGA = Thermogravimetric analysis

w/c = Water-to-cement ratio

w/p = Water-to-powder ratio

XRD = X-ray diffraction

XRF = X-ray fluorescence

Summary

The work presented in this thesis systematically studied the hydration of blended cement by means of experimental and modeling methods. The work firstly intended to experimentally investigate the hydration mechanism, microstructure development of ternary blended cement paste consisting of Portland cement, slag and limestone powder (30% cement + 60% slag +10% limestone powder, by mass) as well as the relevant references. Based on the experimental results, a numerical model was developed to simulate the hydration process of ternary blended cement paste. Inspired by the existing HYMOSTRUC model for Porland cement, the numerical modeling work in this study includes the development, calibration and validation for binary and ternary blended cement systems.

Reaction Kinetics of Slag Activated by $Ca(OH)_2$ Solution

The first experimental work is investigating the reaction kinetics of slag particles activated by $Ca(OH)_2$ solution. Slags from two sources were sieved into groups of different sizes. The reaction heat evolution of slag was monitored by isothermal calorimetry method (TAM Air). The cumulative heat evolution was converted to degree of reaction. The penetration speed of the reacting front surface of each individual slag particle was calculated based on the measured degree of reaction. According to the calculated results, factors governing the reaction kinetics of slag were analyzed.

It is found that specific surface area of slag plays an important role in the overall reaction. The overall reaction degree of slag consisting of fine particles develops faster than that of coarse slag. However, coarse slag particles in this study have higher content of CaO but relatively lower content of MgO, Al_2O_3 and SiO_2, resulting in higher reactivity index of $(CaO + Al_2O_3 + MgO)/SiO_2$, implying higher reactivity at particle level. Calculated results show that the rate of increase of the reacting layer thickness (k value) of a coarse slag particle is higher than that of fine particles. The calculated k values were used for modeling of slag reaction in Chapter 7 and 8.

Experimental Research on Blended Cement Pastes

The second experimental work focused on the hydration kinetics, hydration products and microstructure of blended cement paste. Four groups of pastes were prepared by different combinations of Portland cement, slag and limestone powder.

The hydration of pastes at early age was monitored by isothermal calorimetry method to investigate the interaction among Portland cement, slag and limestone powder. The quantities of bound water, unreacted limestone powder and calcium hydroxide were measured by thermogravimetric analysis (TGA) at curing ages from 1 day up to 91 days. The amount of unreacted slag in the hydrating paste was determined by Ethylenediaminetetraacetic acid (EDTA) selective dissolution method. Meanwhile, Quantitative X-ray Diffraction(XRD/Rietveld) technique was applied to quantify the amounts of unhydrated cement clinker and hydration products of each sample at different curing ages. In order to understand the hydration behavior, pore solution of each paste at different ages was extracted and analyzed by Ion Chromatography.

The pore size distribution and porosity of the hydrating pastes were investigated by mercury intrusion porosimetry (MIP) method. Different types of density of hydrating pastes were also measured by MIP. Based on the MIP results, volumetric expansion ratios of hydration products were calculated, which were later applied as input for the simulation of proposed model. Besides MIP test, Backscattered electron (BSE) images were acquired to observe the microstructure of hydrating pastes. Mechanical strength of pastes and mortars were measured, aiming to observing the performance of the materials at macro level.

According to the experimental results, the hydration of calcium silicate phases of cement in ternary blended pastes was enhanced by the presence of limestone powder, but hampered by the addition of slag. The hydration of calcium alumina phases of cement was greatly accelerated by the addition of slag. It was also enhanced by the presence of limestone powder in binary blended limestone cement paste at early age. However, the coexistence of limestone powder with slag in ternary blended cement paste shows that limestone powder restrained the hydration of calcium alumina phases of cement. The hydration of cement clinker was distinctly accelerated by the single addition of slag or limestone powder within 91 days of hydration. The coexistence of slag and limestone powder in ternary blended cement accelerated the hydration of cement clinker at early age but shows negative influence at later age (after 14 days).

Isothermal calorimetry tests indicate that the addition of limestone power in blended pastes brought positive effect on the rate of heat evolution of hydration, which is in line with the increased production of $Ca(OH)_2$ in limestone blended cement paste. Slag reduced the cumulative heat evolution of slag blended cement pastes at early age due to its relative low reactivity.

The reaction of slag was activated at least after about 100 hours of hydration in this study. The pH of pore solution from all pastes is higher than 13 during the whole curing age, which is sufficiently high for the activation of slag even at the very early age of hydration. The hydration of slag consumed $Ca(OH)_2$, and the amount of $Ca(OH)_2$ was sufficient for slag in the ternary blended paste of this research even after 91 days of hydration. The degree of reaction of slag in blended cement pastes is about 8% (by weight) and 35% at 1 and 91 days of curing, respectively, which is almost not influenced by the addition of limestone powder. TGA tests show that a small amount of limestone powder, i.e. around 2% (by weight) of the total solid raw materials, has reacted in pastes, mainly at early age.

The hydration products of all pastes are mainly C-S-H gel, $Ca(OH)_2$, and alumina related assemblages such as ettringite, monosulphate, monocarboaluminate, hydrogarnet and hydrotalcite phases. The presence of limestone powder increased the amount of monocarboaluminate, but decreased the content of ettringite and monosulphate, showing distinct reaction with alumina phases from slag and cement. The formation of C-S-H gel in slag blended cements was largely reduced due to the relatively slow hydration of slag, which is more evident in the case of ternary blended cement paste. Calculation based on experimental results shows that the total amount of bound water for complete hydration of cement and slag in this research is 40% and 46.8%, respectively.

BSE images reveal that the slag particle still maintains its original shape, showing low degree of hydration even after 91 days of hydration. The addition of slag greatly improved the pore system of blended cement paste, reducing both the total porosity and critical pore size after 91 days of hydration. However, the presence of limestone powder showed negative influence on the pore system. Calculation based on MIP results indicates that the volumetric expansion ratio of hydration products of cement and slag is 2.3 and 3.1, respectively, which are two important values for developing hydration and microstructure model of ternary blended system (cement + slag + limestone powder). Compressive strength of slag blended cement paste and mortar is very low at early age but superior to counterparts containing no slag at later age. The single addition of limestone powder in cement reduced the compressive strength during the whole curing age, but improved the compressive strength at least at early age when coexisted with slag, showing synergistic effect in ternary blended cement, which is even more distinct in the case of flexural strength of mortars.

Modeling the Hydration of Ternary Blended Cement Paste

Based on the experimental results, a theoretical hydration model for (binary and ternary) blended cement paste was proposed, which was inspired by the existing HYMOSTRUC model for Portland cement paste. The model aims to simulate the hydration kinetics of each component in the blended cement system. The integrated kinetics algorithm implemented in the model bears several features. It is explicitly based on particle size distribution of each material. Each chemical reaction is considered as affected by physical contact among hydrating cement particles, i.e. interaction between hydration kinetics and microstructural development. The core of the algorithm is calculating the volume of the particles embedded in the outer product layer of each particle. The embedded particles induce further expansion of the outer product layer and thus influence the water available for the hydration. Water shortage in the capillary pore system is taken into account. Besides, influence of limestone powder on cement, and replacement level of cement by slag are also included in the model.

The proposed theoretical model was calibrated by part of the experimental results of this research and then validated by the other part of experimental results. The calculation of the model is implemented by computer programming using MATLAB language, achieving good calculation efficiency allowing practical simulation. Besides the predicted hydration degree of each component in the blended system, which is the main output of the model, other properties such as total porosity of paste at different curing ages can also be predicted.

Simulation indicates that the hydration of slag at late age (later than 91 days) is still remarkable, and finally reaches about 58% after two years of hydration in this study. The simulation of hydration of the ternary blended paste (Portland cement + slag + limestone powder) also reveals that the availability of water and space in the paste limits the potential maximum degree of hydration, which is essentially related to the water to powder ratio.

Samenvatting

Het werk voorgesteld in deze thesis bestudeert op systematische wijze de hydratatie van samengestelde cementen door middel van experimenten en numerieke modellering. In eerste instantie beoogt het werk de experimentele studie van de hydratatiemechanismen en microstructuurontwikkeling van ternair samengestelde cementpasta bestaande uit Portland cement, hoogovenslak en kalksteenmeel, samen met een studie van de relevante literatuur. Op basis van de experimentele resultaten wordt een model ontwikkeld voor de simulatie van het hydratatieproces van ternair samengestelde cementpasta. Geïnspireerd op het bestaande HYMOSTRUC model voor Portland cement omvat deze studie de ontwikkeling, kalibratie en validatie van een numeriek model voor binaire en ternaire cementmengsels.

Reactiekinetiek van hoogovenslak geactiveerd door een $Ca(OH)_2$-oplossing

Het eerste deel van het experimenteel programma betreft de studie van de reactiekinetiek van slakdeeltjes geactiveerd door een $Ca(OH)_2$-oplossing. Twee types hoogovenslak van verschillende oorsprong werden door zeving opgedeeld in groepen met verschillende korrelafmetingen. De evolutie van de hydratatiewarmte werd uitgezet in functie van de reactiegraad. De penetratiesnelheid van het reactiefront in de individuele slakkorreltjes werd berekend op basis van de experimenteel bepaalde reactiegraad. Gebaseerd op de resultaten van deze berekening worden de verschillende invloedsfactoren op de reactiekinetiek geanalyseerd.

Er wordt vastgesteld dat de specifieke oppervlakte van de hoogovenslak een belangrijke rol speelt in de globale reactie. De globale reactiegraad van fijnere hoogovenslak evolueert sneller dan deze van grovere hoogovenslak. Echter, grove slakdeeltjes zoals onderzocht in deze studie hebben een hoger gehalte aan CaO en een relatief lager gehalte aan MgO, Al_2O_3 en SiO_2, resulterend in een hogere reactiviteitsindex $(CaO + Al_2O_3 + MgO)/SiO_2$, wat een hogere reactiviteit impliceert op deeltjesniveau. Berekeningen tonen aan dat de snelheid waarmee de reactielaag in dikte toeneemt (k-waarde) voor een grove slakkorrel groter is dan deze voor een fijne slakkorrel. De berekende k-waarden worden verder aangewend in de numerieke modellering van de slakreactie in hoofdstuk 7 en 8.

Experimenteel onderzoek op samengestelde cementpasta's

Het tweede deel van het experimenteel onderzoek betreft de studie van de reactiekinetiek, de hydratatieproducten en de microstructuur van samengestelde cementpasta's. Vier groepen pasta's werden vervaardigd met verschillende combinaties van Portland cement, hoogovenslak en kalksteenmeel.

De hydratatie van cementpasta op jonge ouderdom werd opgevolgd door middel van isotherme hydratatieproeven teneinde de interactie te bestuderen tussen Portlandcement, hoogovenslak en kalksteenmeel. De hoeveelheden gebonden water, niet-gereageerd kalksteenmeel en calciumhydroxide werden experimenteel bepaald door middel van thermogravimetrie (TGA) op een ouderdom van 1 tot 91 dagen. De hoeveelheid niet-geregeerd hoogovenslak in de hydraterende cementpasta werd bepaald door een selectieve oplossingsmethode met behulp van EDTA. Kwantitatieve X-stralendiffractie (XRD/Rietveld) werd toegepast voor de kwantificering van de hoeveelheden niet-gehydrateerd Portland cement en de hydratatieproducten in elke pasta op verschillende ouderdom. Voor een beter begrip van het hydratatiegedrag werd poriënoplossing geëxtraheerd op verschillende ouderdom, en geanalyseerd door middel van ionenchromatografie.

De poriëndistributie en de porositeit van de hydraterende pasta's werd bestudeerd door middel van kwikporosimetrie (MIP). Op basis van de bekomen resultaten werden de volumetrische expansieratio's van de verschillende hydratatieproducten berekend. Deze ratio's werden later ingevoerd in het ontwikkelde simulatiemodel. Naast kwikporosimetrie werd ook elektronenmicroscopie toegepast voor de observatie van de microstructuur van de hydraterende pasta's. De mechanische sterkte van pasta's en mortel werd eveneens experimenteel bepaald, met het oog op de studie van de performantie van de materialen op macro-niveau.

Volgens de bekomen experimentele resultaten wordt de vorming van calciumsilicaathydraatfasen in ternaire samengestelde pasta's bevorderd door de aanwezigheid van kalksteenmeel, doch belemmerd door de toevoeging van hoogovenslak. De hydratatie van de calciumaluminaatfasen werd sterk versneld door de toevoeging van hoogovenslak. Dit werd ook bevorderd door de aanwezigheid van kalksteenmeel in de binaire mengsels op jonge ouderdom. Echter, de gelijktijdige aanwezigheid van kalksteenmeel en hoogovenslak in ternaire mengsels toont aan dat kalksteenmeel de hydratatie van de aluminaatfasen van het cement belemmert. De hydratatie van cement werd op verschillende wijze versneld door de enkelvoudige toevoeging van hoogovenslak of kalksteenmeel binnen een ouderdom van 91 dagen. De gelijktijdige aanwezigheid van hoogovenslak en kalksteenmeel in ternaire mengsels versnelt de hydratatie van Portland klinker op jonge ouderdom, doch heeft een negatieve invloed op hogere ouderdom (na 14 dagen).

Isotherme hydratatieproeven geven aan dat de toevoeging van kalksteenmeel in samengestelde pasta's een positief effect heeft op de snelheid waarmee de hydratatiewarmte geproduceerd wordt, wat overeenstemt met de verhoogde productie van $Ca(OH)_2$ in samengestelde pasta met kalksteenmeel. Hoogovenslak reduceert de cumulatieve warmteontwikkeling van samengestelde pasta op jonge ouderdom, door de relatief lage reactiviteit van de slak.

De slakreactie was geactiveerd na tenminste 100 uur hydratatie in deze studie. De pH van de poriënoplossing in alle pasta's is hoger dan 13 gedurende de gehele verhardingsperiode, wat voldoende hoog is voor de activatie van de hoogovenslak, zelfs op zeer jonge ouderdom. Bij de hydratatie van hoogovenslak wordt $Ca(OH)_2$ verbruikt, doch het gehalte $Ca(OH)_2$ was voldoende hoog voor de hoogovenslak in de ternaire pasta in dit onderzoek, zelfs na 91 dagen hydratatie. De reactiegraad van de hoogovenslak in het samengestelde cement is ongeveer 8% (massa%) resp. 35% na 1 resp. 91 dagen hydratatie, en is nagenoeg onafhankelijk van de toevoeging van kalksteenmeel. TGA-proeven tonen aan dat een kleine hoeveelheid kalksteenmeel, namelijk ongeveer 2% (massa%) van de totale vaste materialen, reactief was in de pasta, voornamelijk op jonge ouderdom.

De hydratatieproducten van alle pasta's omvatten voornamelijk C-S-H gel, $Ca(OH)_2$, en aluminaatfasen zoals ettringiet, monosulfaat, monocarboaluminaat, hydrogarnet en hydrotalciet. De aanwezigheid van kalksteenmeel leidt tot een verhoging van het gehalte monocarboaluminaat, en tot een vermindering van het gehalte ettringiet en monosulfaat, wat wijst op een verschillend verloop van de reactie van de aluminaatfasen. De vorming van C-S-H gel in samengestelde pasta met hoogovenslak werd sterk gereduceerd door de relatief trage hydratatie van de slak, wat nog meer evident is in het geval van de ternair samengestelde cementpasta. Berekeningen op basis van de experimentele resultaten tonen aan dat het totaal gehalte gebonden water voor een volledige hydratatie van cement en hoogovenslak in dit onderzoek respectievelijk gelijk is aan 40% en 46.8%.

Elektronenmicroscopische opnames tonen aan dat de slakdeeltjes hun originele vorm behouden, en een lage hydratatiegraad vertonen zelfs na 91 dagen hydratatie. De toevoeging van hoogovenslak leidt tot een sterke verbetering van het poriënsysteem van de samengestelde cementpasta, met een gereduceerde totale porositeit en kritieke poriëndiameter na 91 dagen hydratatie. Echter, de toevoeging van kalksteenmeel toont een negatieve invloed op het poriënsysteem. Berekeningen gebaseerd op de resultaten van de kwikporosimetrie geven aan dat de volumetrische expansieratio van de hydratatieproducten van cement en hoogovenslak respectievelijk gelijk zijn aan 2.3 en 3.1. Dit zijn twee belangrijke waarden voor de ontwikkeling van een model voor de hydratatie en microstructuurontwikkeling van ternair samengestelde systemen (cement + hoogovenslak + kalksteenmeel). De druksterkte van samengestelde pasta en mortel met hoogovenslak is zeer laag op jonge ouderdom, maar hoger dan de referentiepasta zonder slak op hogere ouderdom. De enkelvoudige toevoeging van kalksteenmeel leidt tot een sterktevermindering gedurende de hele verhardingsfase, doch leidt tot een sterkteverhoging op jonge ouderdom indien het gecombineerd wordt met slaktoevoeging. Dit wijst op synergetische effecten in ternair samengestelde cementen, en is nog meer uitgesproken merkbaar wanneer de buigtreksterkte bestudeerd wordt.

Modellering van de hydratatie van ternair samengestelde cementpasta’s

Op basis van de experimentele resultaten wordt een theoretisch hydratatiemodel voor (binair en ternair) samengestelde cementpasta voorgesteld, geïnspireerd op het bestaande HYMOSTRUC-model voor Portland cementpasta. Het model beoogt de simulatie van de reactiekinetiek van elke component in het samengestelde systeem. Het geïntegreerde kinetisch algoritme geïmplementeerd in het model vertoont verschillende kenmerken. Het is expliciet gebaseerd op de korrelgrootteverdeling van alle materialen. Elke chemische reactie wordt verondersteld beïnvloed te worden door het fysisch contact tussen de verschillende hydraterende korrels, i.e. interactie tussen reactiekinetiek en microstructurele ontwikkeling. De kern van het algoritme is de berekening van het volume van de deeltjes ingebed in de buitenwaartse hydratatieproducten van elke deeltje. De ingebedde deeltjes induceren een verdere expansie van de buitenwaartse hydratatieproducten, en beïnvloeden zo ook de hoeveelheid water beschikbaar voor de hydratatie. Watertekort in het capillaire poriënsysteem wordt in rekening gebracht in het model. Bovendien worden de invloed van kalksteenmeel op de hydratatie van cement, en het vervangingsniveau van cement door hoogovenslak ook beschouwd in het model.

Het voorgestelde theoretische model werd gekalibreerd op basis van een deel van de experimentele resultaten uit dit onderzoek, en gevalideerd door middel van een ander deel van de experimentele resultaten. De berekeningen uit het model worden geïmplementeerd door middel van MATLAB, resulterend in een goede efficiëntie van het programma, zodat het bruikbaar is voor praktische simulaties. Naast de voorspelde hydratatiegraad van alle componenten in het systeem als voornaamste resultaat van het model, worden ook andere eigenschappen voorspeld zoals de totale porositeit van de pasta in functie van de tijd.

Simulatie geeft aan dat de hydratatie van hoogovenslak op hogere ouderdom (meer dan 91 dagen) nog steeds opmerkelijk is, en finaal een hydratatiegraad van ongeveer 58% bereikt na 2 jaar hydratatie. De simulatie van de hydratatie van ternair samengestelde pasta (Portland cement + hoogovenslak + kalksteenmeel) geeft ook aan dat de beschikbaarheid van water en ruimte in de pasta de potentiële maximale hydratatiegraad limiteren, wat gerelateerd is met de water/poeder-factor.

Contents

Chapter 1

General Introduction

1.1 Research Initiative

Concrete is the most widely used construction material in the world because of its cheap price, adequate quality and large availability. The development of strength of concrete requires the binding material cement that typically generates calcium silicate hydrate (C-S-H) as the main hydration product. As the world is still developing at a high speed, the use of large amount of concrete is consuming huge quantity of cement every year, which makes cement a widely criticized material by the public, as there is a huge total amount of carbon dioxide (CO_2) emission from the cement industry. Though cement has the highest utilization ratio of raw materials comparing with other construction materials such as glass, crude steel and aluminium [1], 60% of the industry's emissions are caused by de-carbonation of limestone during the production process. It is estimated that the production of cement accounts for about 5-8% of the non-natural CO_2 worldwide each year.

When cement is used in construction industry, a certain part of cement is actually wasted or underused. In a sealed condition, the complete hydration of 1 g cement material theoretically requires about 0.42 g water [2]. However, even if the water supply is theoretically sufficient for the complete hydration, there are still at least two main factors hindering the complete hydration of cement in practice. The first is the uneven distribution of water in cement paste or concrete; the second is the limited pore space in the paste for the precipitation of hydration products such as C-S-H gel and $Ca(OH)_2$, because hydration products are expansive compared with the original raw material [3]. Based on these principles, Mills R. H. [4] proposed an empirical formula to predict the ultimate degree of hydration α_u of cement:

$$\alpha_u = \frac{1.031 \times w/c}{0.194 + w/c} \tag{1.1}$$

where w/c is the water to cement ratio of mix (by weight).

If taking a practical water to cement ratio 0.50 as an example, calculated results from E.q. 1.1 show that only 74.3% of cement can be ultimately hydrated given enough curing time, which

Figure 1.1: Slag blended cement used in the foundation of Shanghai Tower of China (top) [8], and fly ash blended cement used in Three Gorges Dam of China (bottom) [9].

means that as high as 25% of the raw cement material that is unreacted act as an **expensive** and **energy-consuming** filler in concrete [5, 6, 7].

In terms of the tendencies in the modern cement industry, the most important are those connected with economical and ecological factors. Over the last decades, Supplementary Cementitious Materials (SCMs) such as fly ash, silica fume and blast-furnace slag have been widely used in construction industry all over the world, because the use of SCMs brings several advantages over Portland cement. First, the cost of SCMs is usually cheaper than Portland cement as they are by-products of industry. Second, the production of SCMs consumes less energy and also reduces CO_2 emission compared to Portland cement. Third, concrete made by SCMs can have better performance such as workability and durability.

SCMs blended cement is a promising route towards the sustainability of cement industry.

For example, cement used in the famous Three Gorges Dam project was replaced by 30-40% fly ash [10] in order to obtain low heat evolution during casting and better durability for the whole service life. In another project in China, the 632 m's high skyscraper Shanghai Tower, over 7,000 tons of slag was used to cast the single huge foundation which consumed 61,000 m^3 concrete and was continuously cast within about 60 hours [11]. This would be almost impossible when using only pure Portland cement, as the heat released during the early hydration would lead to early-age thermal cracking [12] especially in this kind of single large volume foundation.

However, the quantity and availability of SCMs are still limited at least in some parts of the world. Efforts have been paid to the utilization of raw material limestone as a replacement of relatively expensive cement, as it is well known that CO_2 emission occurs in the process of burning limestone to produce cement clinker. If limestone is directly used in cement, its footprint of CO_2 is theoretically nearly zero. A good example is the European Standard EN 197-1 [13], which identifies two types of Portland-limestone cement containing 6-20% limestone (type II/A-L) and 21-35% limestone (type II/B-L), respectively.

Binary blended cements such as cements blended with slag or limestone have long been used for casting concrete, e.g. the domestic market share of CEM II (binary blended cement) in Cembureau (the European Cement Association, its Full Members are the national cement industry associations and cement companies of the European Union (with the exception of Cyprus, Malta and Slovakia) plus Norway, Switzerland and Turkey) countries was 56.1% in the year of 2005 [14]. Research shows that well designed ternary blended cements, e.g. Portland cement blended with slag and limestone powder, have complementary performance [15, 16, 17]. The use of limestone filler in the ternary blend increases the early hydration of cement clinker, while slag contributes to the hydration at later age. This complementary behavior of limestone filler and slag addition permits obtaining concrete with similar strength development of normal Portland cement with much less clinker. As for durability, it is reported [18] that ternary blended cement containing a limited proportion of limestone filler (no more than 12%) and 20 to 30% of slag provides a good resistance to chloride ingress and good performance in sulphate environment of low tricalcium aluminate (C_3A) Portland cement.

Many decades of scientific research have improved the understanding of the relation between "engineering properties", e.g. strength and stiffness, and the microstructure of cement-based material. Nevertheless, the design of concrete mixtures remains to a large extent at an empirical level, in which durability and environmental issues are often neglected. Effective and efficient utilization of blended cementitious materials need fundamental research even after 150 years of concrete research.

Traditional research on cement mainly focuses on experiments which is of course time-consuming. With the development of computer-aided design, numerical modeling of cement hydration is increasingly gaining attention. A reliable modeling of cement hydration on the one hand requires the correct understanding of the real world, which is the key point to mathematically describe the mechanism of the complex process. On the other hand, reliable modeling of cement hydration is able to reduce much experimental work by simulation with different input of materials, which also in turn helps to understand the performance of cement materials and to optimize mix design. Just as K. van Breugel once mentioned, modeling of cement-based systems is the alchemy of cement chemistry [19]. Even for research on durability, "simple lab-based accelerated tests for durability can ever be a successful strategy and we must employ more sophisticated model-based approaches [20]".

Efforts have been paid to the modeling of Portland cement and binary blended cement, such as the original HYMOSTRUC developed by van Breugel [3] and related evolved version by Maruyama et al [21]. The original HYOSTRUC was later extended for binary blended cements, e.g. limestone blended cement [22], slag blended cement [23, 24, 25] and rice husk ash blended cement [26]. Another well known model is CEMHYD3D [27] for hydration of Portland cement, and was later also extended for binary blended cement, e.g. slag blended cement [28] and limestone blended cement [29].

In terms of ternary blended cements, however, quite limited research work has been performed on both experiment and modeling. This is probably due to the relatively actual application of ternary blended cement on the one hand, and the even more complex hydration behavior of ternary blended cement on the other hand. To fill the gap of fundamental research in ternary blended cement especially with high replacement level of cement, a series of systematic experiments, theoretical hydration model and numerical simulation have been carried out in this research.

1.2 Objectives and Strategy of the Research

1.2.1 Objectives of the Research

As such, this work is first intended to experimentally investigate the hydration mechanism and microstructure development of ternary blended cement paste made by Portland cement, slag and limestone powder. Besides the experimental work, the research will also focus on the numerical modeling of the hydration of ternary blended cement paste, which consists of the development, calibration and validation of a numerical model inspired by the existing HYMOSTRUC [3] which is originally for Portland cement.

The materials studied in this research are Portland cement (O**P**C), ground granulated blast-furnace slag (**B**FS) and limestone powder (**L**F). They are mixed into four groups of pastes, including the pure Portland cement (PC, as blank reference), binary limestone blended cement (PL), binary slag blended cement (PB), and ternary blended cement with the three materials (PBL), i.e. Portland cement, slag and limestone powder.

The experimental research aims to investigate the following topics:

1. The kinetics of hydration of each component in the four groups of hydrating pastes.

2. The characterization of hydration products formed at different curing ages.
3. The development of microstructure of the four groups of pastes, including the measurement of mechanical strength at both paste and mortar levels.

Based on the experimental findings, a theoretical hydration model for hydration of blended cement will be proposed, which is inspired by the original HYMOSTRUC model for hydration of pure Portland cement. The objective of this model is able to simulate the hydration process of ternary blended cement paste, predicting two of the most important properties of cementitious materials, i.e. the degree of hydration and the corresponding microstructure.

1.2.2 Research Strategy

The research in this thesis consists mainly of two parts: the first part is experiments, and the second is modeling. The first part is to investigate the hydration by experimental methods, which helps to understand the hydration mechanism of blended cements. The modeling part is the theoretical modeling of experimental findings, which uses the input and output from experiments of PC, PL and PB cements to calibrate the numerical model. The thus obtained model is validated by the experimental results of the ternary blended cement, i.e. PBL paste.

1.3 Outline of the Thesis

As the objective of this research is to investigate the hydration behavior and numerical modeling of ternary blended cement system, the thesis consists of two main parts, experiments and modeling. Besides the *Introduction* (Chapter 1) and the *Conclusions and Recommendations* (Chapter 9) being the first and the last chapter of the thesis, respectively, the main content of the thesis is organized in 7 other chapters, i.e. Chapter 2-8.

- Chapter 2 is a scientific literature review of the research topics in this thesis. The hydration of binary slag blended cement, limestone blended cement and ternary blended cement were summarized, including the hydration kinetics, hydration products and features of microstructure development. Two sets of modeling methods in cement research were introduced. The features of the widely used models were also reviewed. By reviewing the work conducted in this field, the problems and challenges were raised, which are the objectives of this research project.
- In Chapter 3, the reaction kinetics of slag particles activated by $Ca(OH)_2$ solution was investigated by experiment. Slags from two sources were sieved into groups in different sizes. The reaction heat evolution of slag was monitored by isothermal calorimetry method (TAM Air), then the cumulative heat evolution was converted to hydration degree. Based on several assumptions, the penetration speed of the reacting front surface of each

individual slag particle was calculated. Factors governing the reaction kinetics of slag were analyzed. The result was used to simulate slag reaction by the proposed model in Chapter 7 and 8.

- Chapter 4 investigated the hydration kinetics of blended cement paste. The hydration of pastes at early age was monitored by isothermal calorimetry method, aiming to investigate the interaction among Portland cement, slag and limestone powder. The unreacted limestone powder and calcium hydroxide were measured by thermogravimetric analysis (TGA) from the curing age 1 day up to 91 days. The amount of unreacted slag in the hydrating paste was determined by Ethylenediaminetetraacetic acid (EDTA) selective dissolution method, meanwhile, Quantitative X-Ray Diffraction (XRD/Rietveld) was applied to quantify the amount of unhydrated cement clinkers.

- In Chapter 5, the hydration products of all pastes in the study were characterized. The influence of slag and limestone on the formation of hydration products were analyzed. Pore solution of each paste at different curing ages was extracted and analyzed to help understand the hydration behavior. As used in Chapter 4, XRD/Rietveld method was applied to detect and quantify hydration products produced by cement. The content of water and calcium hydroxide ($Ca(OH)_2$) in hydration products were measured by TGA experiment as performed in Chapter 4. Combining the test results of EDTA and XRD/Rietveld, the quantity of amorphous C-S-H gel at each curing age was calculated.

- The microstructure of the hydrating pastes was investigated in Chapter 6. Mercury Intrusion Porosimetry (MIP) technique was applied to analyze the pore system. Different types of density of hydrating pastes were calculated based on MIP. According to the MIP results, bound water and volumetric expansion ratios of hydration products were calculated, of which the latter was used in the model in Chapters 7 and 8. In order to have direct view of the microstructure, Backscattered electron microscopy (BSE) was applied to obtain the images of hydrating microstructure. Besides MIP and BSE techniques investigating the microstructure, the mechanical strength of pastes and mortars were measured, which demonstrates the performance of the materials at macro level.

- Chapter 7 focused mainly on the development of theoretical hydration model for blended cement paste. Based on the experimental findings from aforementioned chapters, a theoretical model for hydration of blended cement paste was proposed, which was inspired by the existing HYMOSTRUC designed for neat Portland cement paste.

- Based on the theoretical model proposed in Chapter 7 and experimental results of this research, Chapter 8 is the calibration and validation part for the model for blended cement paste. The simulation of the hydration model was implemented by computer programming using MATLAB® language. Part of experimental results were used to calibrate the model, while the remaining experimental data was used to validate the model to prove its applicability.

Chapter 2

Literature Review of Research of Blended Cements

2.1 Introduction

This chapter summarizes a scientific literature review on the experimental work on hydration of blended cement as well as the research of modeling. The experimental work mainly covers three topics which are also the research topics of this thesis, i.e. the hydration kinetics, hydration products and the characteristics of microstructure of hydrating blended cement pastes. The review of modeling introduces two main modeling methods as well as some existing models which can simulate the hydration process of blended cement paste.

Since slag and limestone powder are the two materials blended with Portland cement in this thesis, the literature review of blended cements focus mainly on binary cements blended with slag or limestone powder as well as the corresponding ternary blended cement, i.e. Portland cement blended with slag and limestone powder.

2.2 Hydration of Slag Blended Cement

Slag is a widely used construction material. Blast furnace slag is formed from a liquid at 1350-1550 °C during the manufacture of iron. Reaching the bottom of the furnace, the liquid slag generates a layer on top of the molten iron due to its relatively lower density [28]. Being separated from the molten iron and abruptly cooled under 800 °C with large amount of water, the liquid slag has no time to form crystals and thus solidifies as a material with vitreous structure. After grinding to fine powder, the so-called **ground granulated blast furnace slag** (GGBFS) is produced. GGBFS normally contains up to 95% of glass. The glassy material of GGBFS exhibits cementitious properties when mixing with lime, alkalis or Portland cement that destroy the protective layer on top of slag particles, i.e. acting as activators. Unless otherwise stated, the term "slag" in this thesis always denotes GGBFS for the sake of simplicity of expression.

Table 2.1: The specific surface area of slag in some countries (m^2/kg) [32].

	UK	USA	Canada	India
Blaine surface area	375-425	450-550	450	350-450

2.2.1 Factors Governing the Properties of Slag

The properties of slag actually vary over a range of factors that determine the suitability of slag in construction industry. As summarized by [2], these factors mainly include the fineness of grinding, glass content and bulk chemical composition.

Fineness: Like Portland cement, the reaction of slag is influenced by its specific surface area. Increasing specific surface area leads to better strength development but more water requirement. However, the fineness of slag is usually limited by practical conditions such as economic and performance considerations, i.e. setting time and shrinkage. Table 2.1 presents typical fineness data of market slag in several countries, which are generally at the same level compared with Portland cement. [30] stated that slag must be ground to a specific surface of 400-600 m^2/kg to be usable as cement, which generally agrees with conclusion of [31] stating that the optimal fineness range of slag for the production of alkali activated materials is between 400 and 550 m^2/kg.

Glass content: Liquid slag forms glassy and crystalline contents during the cooling process. Practical glass content of slag depends mainly on the cooling rate, i.e. rapid cooling rate results in high glassy content. The main difference between glassy and crystalline content of slag is that the former is of latent hydraulic property, which is an important factor affecting the engineering performance of slag blended cement. Some researchers did obtain a roughly linear relationship between glass content and mechanical strength [33], but there is no well-defined relationship between the glass content and strength of slag cement. For the practical usage, the vitreous phase of slag is required to be 85-95% [30].

As for the relationship between reactivity and glass content, increasing glass content of slag improves its reactivity. However, [34] cited [33]'s data indicating that slag samples with as low as 30-65% glass content are still suitable. Due to this uncertainty, most international standards classify slag reactivity by testing its direct strength rather than regulating the minimum glass content. But from a practical standpoint, the glassy content of slag should exceed 90% to guarantee satisfactory properties.

Chemical composition: Table 2.2 is a collection of chemical compositions of slags from countries worldwide, showing that the main chemical components of slag are CaO, SiO_2, Al_2O_3 and MgO. Compared with Portland cement, slag has lower content of CaO but higher SiO_2, Al_2O_3 and MgO. The variation of chemical compositions leads to different properties as well as the change of hydration products generated from the hydration of slag, e.g. the Ca/Si ratio of C-S-H gel formed by the hydration of slag is generally lower than that formed by Portland cement, though the hydration of slag consumes $Ca(OH)_2$ generated by the hydration of Portland cement.

Table 2.2: A worldwide analysis of chemical compositions (%) of slags [32].

	CaO	SiO_2	Al_2O_3	MgO	Fe_2O_3	MnO	S
UK	40	35	16	6	0.8	0.6	1.7
Canada	40	37	8	10	1.2	0.7	2
France	43	35	12	8	2	0.5	0.9
Germany	42	35	12	7	0.3	0.8	1.6
Japan	43	34	16	5	0.5	0.6	0.9
Russia	39	34	14	9	1.3	1.1	1.1
South Africa	34	33	16	14	1.7	0.5	1
USA	41	34	10	11	0.8	0.5	1.3

Meanwhile, the low Ca/Si ratio of slag blended paste turns its microstructure progressively less fibrillar but more foil-like [2].

From a metallurgical standpoint, slag can be classified as either basic or acidic. The more basic the slag, i.e. higher contents of CaO and MgO but less SiO_2 and Al_2O_3, the greater its hydraulic activity in the presence of alkaline activators [34]. Lea [32] reported that the hydraulic values of slag increase with the increasing CaO/SiO_2 ratio up to a limited value which was not precisely stated. In European Standard EN 197-1 and British Standards, the mass ratio of MgO and CaO to SiO_2 must exceed 1.0 to achieve pH-basic condition [30], by which the high alkalinity is guaranteed otherwise the slag would be hydraulically inactive [35].

With a constant CaO/SiO_2 ratio, the strength of hydrated slag increases with the Al_2O_3 content, and a large amount of Al_2O_3 can compensate the deficiency of CaO. Cited by [2], a further research, by a regression analysis of compressive strength on composition using a wide range of Western European slags, showed that increase in Al_2O_3 content above 13% tended to increase the early strengths but to decrease late strengths. Moreover, the content of Al_2O_3 also influences the sulfate resistance of slag concrete.

Research work by [36] reported that higher Al_2O_3 content of the slag decreased the Mg/Al ratio of hydrotalcite but increased the Al incorporation in the C(-A)-S-H gel and led to the formation of strätlingite. Increasing Al_2O_3 content of slag slowed down the early hydration and a lower compressive strength during the first days. At 28 days and longer, Al_2O_3 content in slag has no observed significant effects on the degree of hydration, the volume of the hydrates, the coarse porosity and the compressive strengths.

The influence of MgO depends on both the basicity and the MgO content of slag. Variations in the MgO content up to 8-10% may have little effect on strength development, but high contents have an adverse effect [32]. However, [37] reported that increasing the MgO content of slag from 8 to 13% resulted in a 50 to 80% increase of compressive strength after 28 days and longer for water glass ($Na_2SiO_3{\cdot}5H_2O$) activated slag pastes due to the faster reaction during the first days. It also reported that MgO in amount up to 11% was quantitatively equivalent to CaO [2]. Frearon and Higgins [38] indicated that the content of MgO should be about 13% to get a satisfactory sulfate resistance.

Many researchers have been attempting to quantify the reactivity of slag by considering the four major components together. Among these results, ratio $\frac{\mathrm{CaO+MgO+Al_2O_3}}{\mathrm{SiO_2}}$ is the simplest and most widely used one. It is observed that the hydraulic activity of slags increases with the increasing contents of CaO, MgO and Al_2O_3 but decreases with the increasing content of SiO_2. Furthermore, minimum values for this ratio have been adopted in some countries' standard specifications, such as 1.0 (Germany), 1.4 (Japan). [34, 39, 40] used the definition **degree of depolymerization** (DP, usually ranges from 1.3 to 1.5, Eq. 2.1) to link the reactivity of slag with its chemical compositions. In the later context, the thesis will cover the influence of chemical compositions of slag on the hydration kinetics on the condition of $Ca(OH)_2$ solution.

$$\mathrm{DP} = \frac{n(\mathrm{CaO}) - 2n(\mathrm{MgO}) - n(\mathrm{Al_2O_3}) - n(\mathrm{SO_3})}{n(\mathrm{SiO_2}) - 2n(\mathrm{MgO}) - 0.5n(\mathrm{Al_2O_3})} \tag{2.1}$$

2.2.2 Hydration Mechanism of Slag

Activation of Slag Hydration

The latent hydraulic property of slag implies that no hydration products could be observed if slag is solely placed in contact with water, though surface analysis using X-ray photoelectron spectrometry showed that the surface of slag was modified as soon as it came into contact with water [32], forming a protective film lacking Ca^{2+} that prevents further reaction which makes slag dissolve to an extremely limited extent. As cited by [41], only 22% reaction degree of a rather coarsely-ground blast furnace slag was reached after 20 years of hydration providing sufficient reactive components for binder gel formation.

The glass network of slag is mainly the cause of its latent hydraulic properties. To be used as cementitious material, it has to be activated. Shi and Day [42] report that all caustic alkalis and alkali compounds whose anions can react with Ca^{2+} to produce Ca-rich compounds which are less soluble than $Ca(OH)_2$ can act as activators for slag.

In the field of alkali activated cement, there are basically two categories of activators used to activate the hydration of slag, i.e. alkali hydroxides and alkali silicates. Provis et al [43] reviewed the features of these two types of activators. Activators such as calcium sulphate and sodium sulphate [44] are also investigated, in which the absence of silicate and relatively low pH include the reaction of slag requiring long curing period and being sensitive to carbonation and frost attack. However, the production of alkali hydroxides and alkali silicates consumes large amount of energy along with high cost of price. In addition, alkali hydroxides may cause efflorescence on the surface of reacted slag paste due to its low reaction degree prior to the material placed into service, and the use of alkali activator brings workers potential occupational health and safety considerations. Therefore, the use of alkali activators is also controversial [41, 30].

Blended with Portland cement, slag can be activated in the presence of a relatively high pH pore solution of blended system that is caused by the hydration product $Ca(OH)_2$ which is one of the main hydration products of C_3S and C_2S in Portland cement. Because of this feature, slag has long been successfully used with Portland cement to produce blended cements (hybrid cements [30]).

As soon as water is added into the slag blended cement system, cement begins to hydrate and a small amount of slag also reacts due to the existence of gypsum in cement. As the hydration of Portland cement proceeds, increasing amount of alkali and $Ca(OH)_2$ is becoming available in the pore solution resulting in a high pH value (e.g. > 13), which efficiently activates the hydration of slag. As the formation of $Ca(OH)_2$ continues due to the further hydration of alite and belite, the hydration of slag proceeds and may consume $Ca(OH)_2$, leading to microstructure development and strength gain of paste. Work of Ye et al [45] reported that the content of $Ca(OH)_2$ in slag blended pastes initially increases and then decreases, showing $Ca(OH)_2$ not only acts as activator for the hydration of slag but also as a reactant, [46] reported similar observations. In the attempt to investigate the kinetics and stoichiometry of slag hydration in the presence of $Ca(OH)_2$, Richardson et al [47, 48] concluded that the hydration of 1 mole of slag consumed 2.6 mol of $Ca(OH)_2$.

It has to be noted that the activation of slag by Portland cement is only feasible with limited proportion of slag blended with cement. If very high proportion of slag is blended without extra activator, the early strength may be markedly reduced due to the slow hydration at early age, which is the major concern for application in construction industry.

Research conducted by F. Bellmann et al [49] shows that activation is possible by lowering the pH to a range between 11.8 and 12.2 by the addition of calcium hydroxide and soluble calcium salts. By the mixture of the two additives, $Ca(OH)_2$ acts as reactant precipitating aluminium in AFm phase, meanwhile, due to its presence, soluble calcium salts can decrease the pH value in pore solution as long as the equilibrium condition of calcium hydroxide is maintained. This kind of method is useful when low pH pore solution in hydrating paste is expected, e.g. alkali silicate reaction.

Hydration Products of Slag Blended Cement

As summarized by [2], X-ray diffraction (XRD) analysis results indicate that the main hydration products of slag blended cement are essentially similar with that of pure Portland cement, except the amounts of $Ca(OH)_2$ are in varying degrees and less than those that would be given by the pure Portland cement constituent if the slag part did not participate in the reaction. The main hydration products of the slag-cement are C-S-H gel, $Ca(OH)_2$, the sulpho aluminate hydrate phases AFt and AFm and a Mg, Al-rich hydroxide phase [50]. In addition, the composition of C-S-H gel shifted towards higher Si and Al contents, whereas that of Ca was lower [51].

In the case of C-S-H, its morphology and composition may be modified by partial accommodation of Mg and Al within the micro- or nanostructure [48], its Ca/Si ratio is then lower (e.g. 1.55) than those formed from alite and belite (e.g. 1.7). Hydrotalcite-like phase could be formed from the MgO of slag.

Microstructure Development of Slag Blended Cement

Similar to Portland cement, the microstructure of slag hydration could also be classified as inner product, which formed within the boundaries of the original anhydrous grains, and outer product that formed in the originally water-filled spaces [50].

Outer product The addition of slag affects the morphology of the microstructure in slag blended cement. In pure Portland cement paste or with low slag replacement level, amorphous C-S-H has a strongly linear directional characteristic being fibrillar in its appearance. As the slag fraction in blended cement paste increases, the fibrillar morphology is gradually replaced by the foil-like one, which may be coarser or finer depending on the space constraints upon the development of C-S-H gel. Although the linear and fibrillar morphology has fine porosity, its inefficient filling of space appears to leave some fairly coarse and interconnected pores, while the more evenly distributed pores of the foil-like C-S-H gel are probably less well interconnected, which may account for the beneficial effects of slag in reducing diffusion rates in blended pastes, thus being largely responsible for the improved durability performance in slag blended cement [50].

Inner product According to the work performed by Richardson [50], the morphology of inner product region from alite or belite in slag blended cement paste is identical to those present in pure Portland cement paste. In mature pastes, fully hydrated small grains of both alite and slag often display a coarse morphology. Generally, inner product in larger grains has a dense homogeneous morphology with very fine porosity, and large slag grains often have a rim of fine textured C-S-H which can exist for many years and merge into outer product C-S-H gel. Mg, Al-rich laths or possibly platelets present within the inner product C-S-H gel, which are oriented either towards the outer boundary of the inner product or randomly even at the outer boundary. It also reported another microstructural feature occurred inner products, i.e. the presence of small, round and poorly crystalline particles, which are rich in iron and aluminum and also often contain significant amount of titanium [50].

The microstructure of hydrating slag blended paste could also be influenced by temperature. [46, 52] reported that the microstructures of the pastes cured at 60 °C showed greater apparent porosity than those cured at 10 °C.

Stoichiometry of Slag Hydration

Taylor [2] proposed a stoichiometry equation of slag hydration in the Portland cement system which can be approximately written as Eq. 2.2.

$$\mathrm{C_{7.86}S_{7.38}M_{3.02}A} + a\mathrm{CH} + b\mathrm{H} \rightarrow l\mathrm{C_nSH_m(M_xA_y)} + k\mathrm{M_5AH_{13}} \tag{2.2}$$

Following the rules suggested by Taylor, Richardson et al [48] proposed a chemical reaction (Eq. 2.3) for the hydration of slag in the sole presence of $\mathrm{Ca(OH)_2}$.

$$C_{7.88}S_{7.39}M_3A + 2.6CH + bH \rightarrow 7.39C_{1.42}SH_mA_{0.043} + 0.66M_{4.6}AH_d \tag{2.3}$$

where $7.39m + 0.66d = b$ excludes other hydrates that may include $\overline{S}$ and M, and the values of m and d influenced by temperature and slag to $Ca(OH)_2$ ratio are determined based on a number of experiments.

It should be noted that the stoichiometry of reaction between slag and $Ca(OH)_2$ is based on the predetermination of C/S and A/S ratios in C-S-H gel. However, the composition of C-S-H is influenced by the replacement level of slag in blended cement [28, 53] apparently due to the different availabilities of Ca^{2+} from cement, which makes the stoichiometry in Eq. 2.3 only applicable to some specific slag/CH ratios.

In the research on the hydration of slag blended cement, Chen [28] proposed several hydration models, which considered various blending proportions and were classified based on different $Ca(OH)_2$ consumptions of the slag reactions.

Among his models, one gives the best agreement with experimental results, which presumed the ratio of C/S less than 1.8 and part of $Ca(OH)_2$ liberated from the hydration of clinker (C_3S and C_2S) entering C-S-H formed from the reaction of slag. In this model, the main hydration phases of slag blended cement consist of C-S-H, $Ca(OH)_2$, hydrotalcite, ettringite and C_4AH_{13}. It is revealed from his research that increasing slag proportion in blended-cement increases the amount of C-S-H and its A/S ratio in the hydration products while the C/S ratio is decreased, which generally agrees with the conclusions of [36, 37].

The Al content of slag is considered as initially combined with Mg to form hydrotalcite and with $\overline{S}$ to form ettringite, then the remaining Al enters C-S-H to substitute for Si. when the maximum degree of Al substitution is reached, the rest Al reacts with C_3A to form AFm phase (C_4AH_{13}). It is claimed the proposed hydration model can successfully predict the compositions of the hydration products and their quantities. However, the proportion of $Ca(OH)_2$ that enters C-S-H from the slag hydration has to be determined by a semi-empirical expression.

The most important phase of slag cement hydration is obviously C-S-H gel, which is also the most complex in the hydration assemblies. In the aforementioned hydration stoichiometry proposed by [48], the Ca/Si ratio is presumed as 1.42. However, as investigated by Richardson [50], the Ca/Si ratios in C-S-H phase vary with the slag loading, i.e. Ca/Si ratio decreases as slag loading increases. In terms of the substitution of Si by Al or Mg in the C-S-H phase, it was revealed that the Al/Ca ratio increases linearly with the increase of Si/Ca ratio according to Eq. 2.4 [54].

$$\mathrm{Si/Ca} = 0.4277 + (2.366 \times \mathrm{Al/Ca}) \tag{2.4}$$

Richardson [50] also reported that there is no distinct difference between the Ca/Si ratios of C-S-H gel in the inner product of alite (or belite), the inner product of slag and the outer product, nor is there any significant change in Ca/Si ratio with the curing age of paste. It is worth noting that there is no marked difference between the Al/Ca ratios of outer product gel and inner product gel formed from cement, but both values are lower than the corresponding value of inner product gel formed from slag, indicating the significant replacement of Si by Al in the inner product of slag hydration.

As for the pore solution of slag blends, the data in the reported literature is rather limited, which may be caused by the difficult process of pore solution extraction in hardening pastes. Research work of Ye [45] revealed that the presence of different proportions of slag in slag blends significantly altered the internal solution chemistry of cement paste, basically, the higher the proportion of slag loading the lower the total ions concentration in the pore solution of blends. It also reported that the loading of slag markedly reduced the content of $Ca(OH)_2$ at all ages and the pozzolanic reaction of slag was delayed and proceeded at low rate, meanwhile, $Ca(OH)_2$ was gradually consumed during the hydration process of slag, making $Ca(OH)_2$ initially increased and then dropped. The rate of $Ca(OH)_2$ formation is markedly reduced when increasing the slag proportion in blends.

2.2.3 Kinetics of Slag Hydration

The hydration kinetics is generally divided into three stages: (1) a nucleation period during which product growth is accelerating, (2) a phase boundary controlled stage, and (3) a diffusion controlled stage [47, 55], which are similar to the stages of Portland cement hydration [3] but the former reacts much more slower.

Factors Influencing the Reaction Kinetics of Slag in Blended Cement

Similar as the factors governing the properties of slag summarized in Section 2.2.1, the reaction of slag in blended cement is influenced by several factors. The main factors affecting the reaction of slag in blended system include the reactivity of slag that could be defined as (C+A+M)/S, the fineness of grinding (specific surface area), the glassy fraction of slag, the replacement level of slag in blended system, the hydration temperature and the water to powder ratio.

According to the work of [34, 56, 57], the rate of reaction of slag decreases with the decreasing water to powder ratio and with increasing proportion of slag in the blend. Higher hydration temperature, glassy content and higher specific surface area (fineness) increase the reactivity of slag. However, the composition of cement and the incorporation of additional gypsum in slag blended cement have no influence on the extent of reaction of slag at ages of 28 days to 1 year.

Methods to Measure the Degree of Reaction of Slag in Blended Cement

It is difficult to quantify the degree of reaction of slag in blended cement using those methods which are successfully applied for Portland cement. Demoulian et al (cited by [58]) described a method based on extraction of the constituents other than unreacted slag with a reagent based on

EDTA (ethylenediaminetetraacetic acid), finding it effective for determining the slag in either unhydrated slag cements or pastes. EDTA selective dissolution method has long been used as a well-known method to measure the reaction degree of slag [45, 57, 58]; however, as stated by Luke et al [57], special care should be paid when applying this method and systematic error may occur due to the residue of hydrotalcite in the extraction of unreacted slag. Lumley et al [57] reported that EDTA selective dissolution method can be used to determine the degree of reaction of slag under certain corrections but the accuracy is poorer at degrees of reaction above 70%.

Besides EDTA selective dissolution method, image analysis based on backscattered electron image could be applied to directly estimate the hydration degree of both plain cement and blended cement paste. This method is based on the fact that cement and slag grains can be easily distinguished from unhydrated clinker and paste matrix. However, it should be bore in mind that using this method may produce an over-estimated result on the reaction degree of slag due to its fine particles [45].

With the aim to find the best method to test the reaction degree of slag in blended cement, Kocaba [59] compared a series of methods testing the amount of unreacted slag in blended cement pastes, including selective dissolution, thermal method, shrinkage, backscattered electron image analysis combined with Mg mapping and isothermal calorimetry. The research claimed that backscattered electron image analysis coupled with Mg mapping gave the best results as expected, however, this method is time-consuming and particularly difficult for samples at young ages, e.g. 1 day.

As for the criticism on selective dissolution method argued by [59], which claimed that the errors introduced by the remaining undissolved phases (in EDTA solution) make it impossible to determine the degree of reaction of slag with any degree of precision, it has to be noted that 1) the prepared EDTA solution used in [59] was different from the one widely used by [45, 57, 58], which makes the contrast less comparable since the right solution is crucial to dissolve materials except unreacted slag. 2) as stated by [57, 58], it is expected to have hydrotalcite in the residue after being dissolved in EDTA solution, therefore, a set of right considerations are necessary to improve the reliability and accuracy of results, which will be covered in the later context of this thesis.

Literature Data on the Degree of Reaction of Slag

Although it is somewhat difficult to measure the degree of reaction of slag in blended cement comparing with Portland cement, many researchers have carried out experiments on this topic. A large body of literature can be found on the kinetics of slag blended cement pastes.

Taylor [2] collected some researchers' data on the reaction degree of slag, as showed in Table 2.3. Other researchers using EDTA or DTA [60] also reported data on this issue under different hydration conditions; Table 2.4 is an uncompleted collection of these data.

By means of EDTA selective dissolution method, Lumley et al [57] focused on the effect of water to solid ratios and the proportions of slag on the degrees of reaction of slag blending with

Table 2.3: Reaction degree of slag in blended cement from literature [2].

As percentage of initial weight of slag (As percentage of total ignited weight of slag)							
%slag	30	40	40	40	67	70	80
Age (days)							
0.25						4(3)	
1				10-20(4-8)		6(5)	
3		17(7)			19(8)	19(13)	8(6)
7		31(12)				23(16)	13(11)
28	42(13)	32(13)	30(12)	30-40(12-16)	13-23(9-15)	29(20)	19(15)
90	40(12)				16-26(11-17)		24(19)
180	40(12)			50-60(20-24)	16-28(11-19)		25(20)
365	64(19)			19-36(13-24)			
540			65(26)				

Table 2.4: Uncompleted data collection of reaction degree of slag blended cements [2].

w/s	%slag	Age (days)	T (°C)	α (%)	Method	Authors
0.5	60	90	-	20-40	Salicylic acid	Kondo et al.
0.6	30	30-180	25	40	EDTA	Luke et al.
0.6	30	180	40/55	60	EDTA	Luke et al.
0.5	-	2	20	detectable	DTA	Hinrichs et al.
0.5	-	28	20	40-60	DTA	Hinrichs et al.
0.5	-	365	20	50-70	DTA	Hinrichs et al.
-	-	3	23	17	EDTA	Battagin
-	-	28	23	35	EDTA	Battagin
-	-	365	23	52	EDTA	Battagin
-	-	5	40	38	EDTA	Battagin
-	-	2	60	38	EDTA	Battagin
-	-	1	80	38	EDTA	Battagin
0.4-0.6	-	28	20	30-55	EDTA	Lumley et al.
0.4-0.6	-	365-730	20	45-75	EDTA	Lumley et al.

Portland cement. It summarized that at water to solids ratios of 0.4-0.6 and 20 °C 30-55% of the slag reacts in 28 days and 45-75% in 1-2 years, for blends containing 92% slag and w/s=0.3, the hydration degree of slag is probably limited to 30%.

Luke and Glasser [58] reported that approximately 40% of the slag in a 30%/70% ratio of slag to Portland cement blend reacted in one month with little change up to 6 months, but over 60% of slag was reacted at the age of 12 months. Their latter study showed similar results with data at 25 °C, 40 °C and 50 °C for times of 0.5 to 24 months.

Quantitative Description of Kinetics of Slag in Blended Cement

The quantitative relationship between the degree of reaction and reaction time of slag in blended system is complex, since plenty of factors may influence it. Nevertheless, researchers have attempted to find solutions on the issue.

By means of experimental and numerical methods, research on cement-based materials conducted by Ye [45] reveals that a logarithmic relationship between the degree of reaction of slag and hydration time was found regardless of slag content. The quantitative relationship was proposed as Eq. 2.5:

$$\alpha_{slag} = k \times ln(t) + b \tag{2.5}$$

where α_{slag} is the degree of reaction of slag at hydration time t, and k is the rate of reactivity of slag derived from the slope of the logarithmic curve of the degree of reaction and curing time. Constant b is a parameter relating to the slag loading in blended cement.

Combining the experimental data of degrees of slag from BSE image analysis and EDTA selective dissolution method, the author made a regression and obtained the average value of k as 9.46 for different slag loadings in blends. However, the author did not give the values of b and nor further data to validate whether the value k is effective to predict the degree of reaction of other slag blended systems.

Research conducted by Biernacki et al [47] reported that the kinetics of hydration for slag in the presence of $Ca(OH)_2$ system are adequately described by Knudsen's parabolic dispersion equation with activation energy between 14 and 22 kJ/ (g.mol).

$$\frac{\alpha}{\alpha_u} = \frac{k(t-t_0)^n}{1+k(t-t_0)^n} \tag{2.6}$$

where $\frac{\alpha}{\alpha_u}$ is the extent of reaction, which is the degree of reaction of slag (α) at time t relative to the maximum value (α_u); k is a rate constant; t_0 is the induction time. n is the reaction exponent, which equals to 0.5 for parabolic behavior and 1 for linear behavior [47].

In order to simulate the hydration process of slag blended cement, fundamental and quantitative relationship between the kinetics (degree of reaction) and material properties is of great importance. Both Ye's and Biernacki's models express the kinetics equation based on the overall hydration process with the constants obtained by regression of experimental data, therefore, these equations are inadequate to link the kinetics with the external factors and intrinsic material properties such as chemical compositions, particle size distribution (PSD).

2.3 Hydration of Limestone Blended Cement

Limestone has long been utilized as a mineral addition in cement industry. The latest European Standard EN 197-1:2000 [13] allows up to 5% limestone as a minor additional constituent, and also identifies four types of Portland limestone cement containing 6-20% limestone (types II/A-L and II/A-LL) and 21-35% limestone (types II/B-L and II/B-LL), respectively. The ASTM Standard C150-04 allows up to 5% of limestone filler. Since the early 1980s, the Canadian cement standard allows the inclusion of up to 5% limestone addition to Portland limestone cement. Similar trend occurs in Latin-American countries such as Argentina, Brazil, and Mexico

Table 2.5: Analysis of chemical composition of several typical limestones (%) [61].

Limestone	A	B	C	D	E
SiO_2	4	13.6	2	12.05	2.96
Al_2O_3	0.77	2.5	0.8	3.19	0.79
Fe_2O_3	0.3	0.9	0.2	1.22	0.3
CaO	51.4	43.4	52.9	43.5	52.3
MgO	1.3	3.2	0.9	1.68	1.3
SO_3	0.1	0.1	0.2	0.56	0.03
LOI	42	35.6	42.5	36.21	42.18
Na_2O	0.01			0.12	0.04
K_2O	0.02	0.6	0.2	0.72	0.23
Total	99.9	99.6	99.7	99.25	100.13

[15]. According to the review of Cement Standards of the World (CEMBUR-EAU 1997), more than 25 countries allow the use of between 1% and 5% limestone in their Portland cement. Some countries even allow up to 35% replacement in Portland composite [61].

2.3.1 Chemical Composition of Limestone Powder

The main chemical composition of limestone is calcium carbonate ($CaCO_3$), with smaller proportion of quartz or amorphous silica and sometimes of dolomite. Table 2.5 is the composition analysis of several typical limestones. Though the Loss On Ignition (LOI) content of limestone is up to 42.5% or even more, limestone must be low in clay minerals and organic matter to guarantee the water demand and setting time [2]. As for the quality requirement, according ASTM Standard C 150, the $CaCO_3$ content calculated from the calcium oxide content should be at least 70% by mass.

Limestone is softer than cement clinker, thus could be ground into finer particles when it is interground with cement clinker. As summarized by [61], addition of finer limestone particles to clinker completes the fine fraction in the particle size distribution curve of cement without an increment on water demand, and improves the cement packing and blocks the capillary pores.

2.3.2 Effects of Limestone Powder on the Hydration of Cement

Physical Effects of Limestone on the Hydration of Cement

Effects of limestone on the hydration of limestone blended cement can be classified into two aspects, i.e. physical effect and chemical effect.

Numerous researchers who investigated Portland limestone cement with high level of limestone addition considered it as inert filler [5, 6, 7, 62], e.g. by means of both thermal analysis and backscatter image analysis, Ye et al. [63] reported that limestone powder blending with

Portland cement did not take part in the chemical reaction at all. The low reactivity of limestone due to its low solubility is the main cause leading to the inert property.

However, even acting as filler, limestone in blended cement can have an apparent hydration acceleration on the hydration of cement clinker especially at early ages [62, 64]. On the one hand, the effective w/c ratio in limestone blended system is increased significantly due to the low reactivity of limestone powder, altering the hydration characteristics of cements and providing more water and space for the hydration of clinker, but as stated by [5, 6], the optimal replacement level of cement by limestone depends on the actual concrete mixture proportions being used in practice. On the other hand, limestone is softer than clinker which could achieve a finer particle size when interground with Portland cement clinker, producing an improved particle size distribution and improving particle packing [65], e.g. for an overall specific Blaine surface area of 420 m^2/kg, the size of 50% of the limestone particles can be smaller than 700 nm, while the corresponding value of clinker is 3 μm [2]. Therefore, a large number of fine limestone particles can act as nucleation sites for the hydration of C_3S (and also C_2S) or offers a favorable surface structure for C-S-H precipitation [66], which then markedly decrease the concentration of Ca and Si ions in the pore solution, promoting the transformation of C_3S phase to the solution phase and accelerating the hydration of C_3S and C_2S.

Chemical Reaction of Limestone with C_3S

The hydration of C_3S can be accelerated in the presence of limestone probably because of the dilution effect, the multiplied nucleation site effect and possible chemical reaction. Jean Péra et al. [67] reported that the total heat resulting from 300 mg of pure C_3S hydration was 145 J while that of the 300 mg of mixture (50 wt. % C_3S + 50 wt. % $CaCO_3$) reached 260 J after 15 h of hydration, and the rate of heat evolution of the later was also constantly higher than the former during the tested 15 h. They concluded that $CaCO_3$ cannot be considered as an inert addition towards C_3S hydration. V.S. Ramachandran's investigation [64] showed that some calcium carbonate was consumed as the hydration of Portland cement proceeded. The product of the reaction of limestone and C_3S is calcium carbosilicate, whose exact type cannot be identified by XRD probably due to its amorphous property and small quantity of formation.

Chemical Reaction of Limestone with C_3A

Besides the reaction with C_3S, limestone can also react with C_3A as well. According to the investigation of Ingram et al. [68] (cited by [61]), for a combination of 2% gypsum, 6% limestone, and 92% clinker, $CaCO_3$ reacts with C_3A in the clinker. The reaction begins with a $C_3A \cdot CaCO_3 \cdot 12H_2O$ product, then forms compounds containing a molar ratio of C_3A to $CaCO_3$ between 0.5 and 0.25. The product later appears to stabilize as $C_3A \cdot xCaCO_3 \cdot 11H_2O$, where x ranges from 0.5 to 0.25.

The transformation of ettringite to monosulfate in the presence of limestone is delayed and reduced due to the formation of monocarboaluminate that is thermodynamically more stable. Bentz [29] proposed a possible chemical reaction stoichiometry equation of this process as follows (Eq. 2.7)

$$\begin{aligned} &3(\mathrm{CaO})_3(\mathrm{Al_2O_3}) \cdot \mathrm{CaSO_4} \cdot 12\mathrm{H_2O} + 2\mathrm{CaCO_3} + 18\mathrm{H_2O} \rightarrow \\ &2(\mathrm{CaO})_3(\mathrm{Al_2O_3}) \cdot \mathrm{CaCO_3} \cdot 11\mathrm{H_2O} + (\mathrm{CaO})_3(\mathrm{Al_2O_3}) \cdot 3\mathrm{CaSO_4} \cdot 32\mathrm{H_2O} \end{aligned} \tag{2.7}$$

G. Kakali et al. [65] concluded that in pastes containing $CaCO_3$, either as a chemical reagent or as a limestone constituent, the transformation of ettringite to monosulfate is delayed, while calcium aluminate monocarbonate is preferably formed instead of monosulfate even at early ages, which agrees with the thermodynamic calculation performed by Lothenbach et al. [69] that the stabilization of monocarboaluminate in the presence of limestone indirectly stabilized ettringite.

It is also reported [64] that the formation of ettringite is accelerated by the addition of limestone at the very beginning of hydration (e.g. 30 min) in the presence of gypsum, corresponding with the accelerated conversion of ettringite to monosulfate due to the incorporation of limestone.

Microstructure Development of Limestone Blended Cement

Though the chemical reaction of the fine particles of limestone in cement paste is rather limited to a low extent due to its low reactivity, the addition of limestone particles has significant effect on the microstructure development of limestone blended cement. Research conducted by Sellevold et al. [70] using MIP method showed that specimens containing 12% $CaCO_3$, which are mainly particles smaller than 0.1 μm, had finer pore structure and somewhat reduced total pore volume. They attribute this observation to the nucleation site effect stating that the introduction of a large number of nucleation sites could result in a more homogeneous distribution of C-S-H and thus a less open pore structure. The effect appears to be in the capillary pore structure rather than in the gel pores [61], as the particle size of limestone particles is at micrometer level rather than nanometer.

The size and distribution of $Ca(OH)_2$ are also influenced by the presence of limestone. In a limestone-filled paste which used 25% limestone, larger regions of $Ca(OH)_2$ were unevenly distributed throughout paste while in the case of Portland cement small regions of $Ca(OH)_2$ were evenly distributed [71]. Their further investigation found that limestone added in amounts of 5% or 25% enhanced the formation of hydration rims of C-S-H surrounding C_3S particles due to the accelerated hydration of C_3S.

Results from image analysis [63] showed that the interface between limestone and hydrates in limestone-filled self-compacting concrete (SCC) is quite porous, while the interface around the unhydrated cement in high performance cement paste is much denser. They offered two possible reasons explaining this distinct difference in microstructure. On the one hand, as the hydration process of cement proceeds, cement particles expand and get connected with each other to form a network, which results in strength gain. However, limestone particles do not expand during the whole hydration process due to its low reactivity, making the porosity of the former become lower than the latter. On the other hand, the addition of limestone may play a negative role in the development of microstructure, because it could block the expansion of hydrating cement, which induces the microstructure of limestone-filled cement paste more porous. It has to be noted that the addition of limestone (> 33%, as applied in self-compacting concrete) in their study is much higher than normal use in traditional concrete.

Research by Pipilikaki et al. [72] showed that limestone used in blended cements changes the pore structure of hardened cement paste. The critical pore size was increased from 20 to 40 nm when using the maximum amount of limestone allowed by the European Standard EN 197-1:2000, i.e. 35%. At the same time, the addition of limestone reduced the threshold diameter of pores (the authors did not mention how the data were calculated) of the paste and presents a more uniform pore size distribution. The authors concluded that this behavior can be attributed to the better packing of particles due to the filling effect of limestone powder, resulting in that chemical species enter the hardened cement more difficult (reduced threshold diameter of pores) but transport easier (increased critical pore size) inside the cement paste due to the pores having approximately the same size. As for gel pores, addition of limestone in cement produces smaller gel pores probably due to the accelerated hydration kinetics.

2.3.3 Quantitative Extent of Reaction of Limestone Powder in Blended Cement

The extent of reaction of limestone with cement clinker is significantly lower than the corresponding values of cement clinker. The probable explanation for this as stated above arises from the low solubility and low reactivity of limestone particles, though other factors such as fineness, particle size distribution do influence its reaction in limestone blended systems.

The Extent of Limestone Reaction from Literature

In experiments of 5% or 15% calcium carbonate reaction with type II cement hydrated up to one year, Klemm and Adams [73] observed that monocarbonate hydrate was formed slower than that of ettringite, and after 129 days hydration, the amount of unreacted $CaCO_3$ was still up to 80-90%. Ramachandran [64] investigated that in mixtures hydrated with 15% and 5% limestone substitution, the amounts of limestone reacted with the hydrating C_3S were 2.38% and 1.34% at the age of 28 days, respectively, and most of $CaCO_3$ was reacted within the first 3 days. A typical simulation performed by Bentz [29] showed that for a 20% by mass fraction substitution of ground limestone for cement, only about 5% of the limestone present reacts during the first 180 days of hydration. Taylor summarized that the maximum quantity of $CaCO_3$ that can react appears to be 2-3% with most cements. A value up to 5.8% has also been reported [2], but the substitution level of limestone in cement was not mentioned.

It is worth noting that limestone being regarded as inert filler always arises from the fact that high levels of limestone are applied. At low substitution level, e.g. using up to 5% limestone, much or perhaps all of the added $CaCO_3$ is reactive with cement [74]. The quantitative relationship between the reactive fractions of limestone and time is still a challenge. No fundamental result is available from literature, besides the fact that limestone is considered as inert filler by many researchers.

2.4 Hydration of Ternary Blended Cements

Compared with the research work performed on binary blended cements such as slag blended cement and limestone blended cement, reports on ternary blended cement are much less from the scientific literature [75].

De Weerdt [76] carried out a series of experiments on a ternary blended cement which was mixed by 65% Portland cement, 35% fly ash and 5% limestone powder. The results show that a small amount of limestone leaded to the formation of hemi- and monocarboaluminate instead of monosulphate, which stopped the decomposition of ettringite. The author concluded that the stable ettringite resulted in higher volume of hydrates and reduced the porosity and increased mechanical strength.

With regard to the advantage of ternary blended cement, the positive effect of limestone is amplified by the addition of fly ash, as the author stated. The effect of limestone powder on Portland cement is limited due to its low aluminate content. When part of the cement is replaced by fly ash, additional aluminate is introduced into the system as it reacts. The addition of fly ash lowers the ratio of SO_3/Al_2O_3 and increases the AFm/AFt ratio and thereby amplifies the impact of limestone powder [77].

Two trends are observed based on the limited reports on research of ternary blended cement. The first is that most of these research work was focused on mechanical properties (i.e. compressive strength) [15, 16, 78, 79] and durability [78, 80, 81, 82, 83]. The second is the adoption of raw materials being applied in these reported studies. Most of reported ternary blended cements more frequently include silica fume, rice husk ash and fly ash [84, 85, 86, 87, 88] compared with the combination of slag and limestone powder. It is important to investigate the mechanical properties and durability of blended cements as in the case of Portland cement, but understanding the hydration mechanism of any type of construction material is the foundation of other research work. As for the adoption of raw materials, the surface area of silica fume and rice husk ash is normally two orders of magnitude larger than that of slag, fly ash, limestone powder and Portland cement, which certainly brings remarkably high reactivity. The addition of silica fume also brings reasonably improvement to the hydration of cement paste. In addition, the price of silica fume is also much higher than cement. Compared with slag, fly ash contains rich aluminate and silicate but lower calcium content, and its reactivity is much lower or needs strong activators. In turn, the use of fly ash in ternary blended cement limits the replacement level [89].

Limestone is a raw material for the production of Portland cement clinker, which is the main source of CO_2 emission of cement production. Adding limestone powder to blended cement implies nearly zero CO_2 emission compared with any other cementitious materials. It also has competitive cost especially compared with silica fume. Slag contains higher content of calcium and is more reactive than fly ash. The higher reactivity and calcium of slag guarantee higher replacement level in ternary blended cement and/or better mechanical strength compared with the use of fly ash. The combination of limestone and slag with Portland cement can replace a high amount of cement and probably without any compromise in terms of the performance at both early age and later age.

2.5 Review of Numerical Modeling of the Hydration of Blended Cements

With the development of computer technology, increasing attention is being paid to the modeling work of cementitious-based materials. Many researchers have been carrying out the research to better simulate the hydration of cement-based materials in the last decades. It is obvious that a reliable model of the hydration of cement-based materials plays a crucial role in construction industry, such as reducing tedious process of trial-and-error when conducting experiments, facilitating the research of durability of concrete from the long term run.

2.5.1 Two Main Approaches to Simulate the Hydration of Cement-based Materials

Many models are already available to simulate the hydration process and the development of microstructure of cement-based materials. Based on different simplification methods [90], two main approaches could be classified, i.e. *continuous approach* (or called vector approach) and *discretization approach*. Due to the complexity of real hardening process of cement-based materials, each model is based on certain assumptions that aim to simplify the calculation of the real cement microstructure and its interactions.

The advantages of *continuous approach* are resolution free and no requirement to divide features of microstructure into smaller elements. Particle shape is normally assumed as spherical, which demands less information to mathematically describe particles compared with other shapes, resulting in the easy and fast calculation of distance between any two particles, e.g. the random distribution of particles in space and the inter-particle overlapping determination. In addition, this method can scale over several orders of magnitude, i.e. from micrometer to millimeter. The kinetics of hydration is usually based on particles with the calculation of spatial interaction of expanding hydration products and chemical reaction. Along with the advantages, the drawback of this approach is that the geometry of microstructure is simplified, since the spherical shape of particles is far from the reality which is even more distinct in the case of slag particles. Furthermore, contrary to the emphasis on kinetics, less attention has been paid on the distribution of hydration products.

The principle of *discretization approach* is similar to *finite element method* (FEM). The entire volume of the microstructure is divided into smaller elements which are placed with their faces in contact. By means of certain algorithms, the development of hydration and microstructure can be simulated. Since the simulation is based on each divided element, this method can locally consider the spatial distribution of each hydration phase, which is different from the continuous approach where only inner and outer products are considered for all particles. The disadvantages of this method are that (1) the calculation of modeling is intensive computing, especially when the size of calculation element is very fine, e.g. 100 nm, the number of elements will exponentially increase, making the practical calculation either time-consuming or impossible. (2) the kinetics of hydration is less straightforward compared with those applied in the continuous approach, thus the accuracy and reliability of simulation depend on the quality of algorithms [90].

2.5.2 Features of Several Existing Models

In the late 1980s, Johnson and Jennings developed a program which was based on the idea that cement hydration is considered as nucleation and growth of spherical particles in three-dimensional space. Van Breugel [3] built HYMOSTRUC for modeling the hydration of Portland cement. This model is based on the assumption that the growth of new layers of hydration products are deposited on the surface of cement particles, resulting in a homogeneous distribution of hydration products. The hydrating cement particles are considered as expanding spheres. In the contact zone, where two expanded hydrating cement particles meet, the overlapping volume of hydration products is redistributed around the two touching particles. In terms of kinetics, the hydration of each particle is divided into two stages, i.e. phase boundary stage and diffusion controlled stage, where the dissolving rate of the reacting front surface obeys a certain of equations.

The HYMOSTRUC model can simulate the development of properties of Portland cement based on real particle size distribution, e.g. the development of hydration kinetics and microstructure, the volume changes and heat evolution of the hardening cement pastes, and the effect of geometrical changes of the microstructure on the creep of the hardening concrete [91]. The advantages of the model are the reasonable prediction of hydration kinetics, the formation of microstructure and related bulk properties, but this model is unable to predict the hydration product phases and their spacial distribution because the hydration products are simply considered as inner product and outer product.

Based on the original HYMOSTRUC model, which was originally proposed to simulate the hydration of Portland cement, Liu et al. [22, 63, 92] extended the model to take account of the addition of limestone and slag [93] into Portland cement individually. Due to large substitution level (33% and 42%) of Portland cement, limestone particles were considered as non-expanding particles and inert filler without participating in the hydration process but accelerating the hydration of Portland cement.

To better represent the accurate microstructure of hardening Portland cement, Pignat el al. developed a model called Integrated Particle Kinetics Model (IPKM) [94]. IPKM assumes that the evolution of C_3S hydration is modeled by the deposition of C-S-H on the surface of C_3S particles but the formation of $Ca(OH)_2$ is assumed to precipitate in pores, which is not considered in the original HYMOSTRUC. As such, it is possible to calculate the interaction between particles and evolution of individual particles, enabling the modeling of the evolution of each particle independently [90]. However, due to the explicit calculation of all possible interactions, simulation using IPKM is rather slow, limiting the simulation to a relatively small number of particles [90].

Similar to IPKM, [90, 95] developed a platform called μic for modeling the hydration of cements. It claimed that the model has improved the performance of the continuous approach enabling simulations with millions of particles within acceptable times typically compared with IPKM. Besides the improved calculation efficiency, the model enables the customization of all aspects of microstructural development of hardening cement paste. The model was applied in modeling the influence of limestone addition on cement hydration [96].

In the field of discretization approach, one of the best known models may be CEMHYD3D which was developed by Bentz et al [97]. This model is used to simulate the development of properties of cement-based materials, e.g. the microstructure development of hardening cement paste, the adiabatic temperature rise of Portland cement as well as silica fume blended concrete [98], and the diffusivity of chloride ions in silica fume blended cement paste [99]. The features of this model are digital image basis, accurate microstructure representation, and rule-based to simulate reaction and diffusion. The drawbacks are that (1) there was little kinetic information corresponding to the hydration process; (2) improving resolution could substantially increase the computation time of a relatively large volume cement paste. As for binary cement, preliminary work was tried to incorporate the reaction of fly ash [100] and slag [48]. However, due to the complexity of the reaction of slag blended cement, more effort is needed for this model to deal with the reaction kinetic constant and activation energy of fly ash and slag, meanwhile, the induction period of slag or fly ash blended cement is not explicitly considered in the model limiting the application of the model in predicting the properties of early-age concrete [100].

Based on CEMHYD3D, Chen [101] extended the model to simulate the hydration and microstructure development of slag blended cement. Some modifications were taken to consolidate the chemical background of the model and eliminate the effect of system resolution on the model predictions, especially the degree of hydration. The model can be used to investigate various stages of hydration of slag cement. As the author stated, the new version model has its own drawbacks, such as the reactivity of slag has not adequately been taken into account, and the role of activator is constrained to the activation from Portland cement.

Maekawa et al. [154] proposed an integrated program named DUCOM (DUrability COncrete Model), which evaluates both the early-age properties of hardening concrete (such as the cement hydration heat and thermal conduction, pore structure formation and moisture equilibrium) and durability of concrete, e.g. chloride ion transport, carbonation, corrosion of steel re-bar and calcium ion leaching. The old version DUCOM model can be used to evaluate the temperature history of slag or fly ash blended concrete. In the latest updated version, the effect of limestone powder and the reaction of silica fume are incorporated. However, DUCOM model does not adequately consider the chemical aspects of the hydration of binary cements. The influence of mineral compositions of fly ash or silica fume on reaction stoichiometry has not been considered in DUCOM model yet. In addition, the evolution of chemical and volumetric composition of silica fume-cement blends or fly ash cement blends cannot be evaluated [102, 103].

De Schutter [104] proposed a kinetics hydration model which is valid for Portland cement and blast furnace slag cement. In this model, the heat evolution of blast furnace slag cement is obtained by the superposition of the heat release from Portland cement reaction (P reaction) and slag reaction (S reaction). The evolution of mechanical properties at early-age concrete is described using functions of the degree of hydration. However, the interactions between the cement hydration and the reaction of mineral admixtures, e.g. the production of $Ca(OH)_2$ by cement hydration and the consumption of $Ca(OH)_2$ by slag reaction, are not considered in this model. In addition, the generalization of the reaction parameters depending on the actual slag replacement ratios is not yet possible [103].

Considering the production of $Ca(OH)_2$ from cement hydration and its consumption in the reaction of mineral admixtures, a numerical hydration model is recently developed by Wang et al. [103]. In this model, the heat evolution rate of fly ash- or slag-blended concrete is determined by the contribution of both cement hydration and the reaction of mineral admixtures, where the total heat generation of fly ash and slag is set as 110 and 50 kcal/kg by the author, respectively. As for $Ca(OH)_2$, it is assumed that the amount of $Ca(OH)_2$ is directly proportional to the degree of hydration of cement, and the reaction of slag is accelerated by the presence of $Ca(OH)_2$ and be dependent on the amount of $Ca(OH)_2$. According to the authors, the prediction of temperature rise from modeling results in blended cement agrees well with the experiment, and the temperature distribution in blended cement is also predicted. However, influence of the chemical compositions of additions on the reaction stoichiometry is not considered in this model, nor are the distribution of hydration products and microstructure development included.

2.6 Problems and Challenges

It is apparent that the hydration of ternary blended cement is much more complex compared with pure Portland cement and even binary blended cements. Not only is the interaction occurring between any two materials, but also the observation methods of experiments lag behind the adequate requirement, e.g. the determination of degree of reaction of slag and cement is more difficult than alkali activated slag and pure Portland cement [105, 106]. This kind of difficulty hinders the understanding of chemical hydration of blended cements. In addition, much less attention has been paid to blended cement compared with pure Portland cement in the research field of cementitious materials. Fortunately, due to the awareness of sustainable construction materials and the urgency of reducing CO_2 emission, increasing research work is being carried out on binary and ternary blended cements is increasing. Results from both experiments and modeling will contribute to the understanding and application of these materials.

However, even the limited available experimental data on hydration of blended cement show no consistency due to the different measurement techniques applied. In terms of ternary blended cements, the replacement level of SCMs is always limited to low ones, which in turn limits the advantage of SCMs since low content of SCMs in concrete makes only little contribution in terms of the cost and environment reservation. Based on the current research on blended cement, this thesis will perform a series of experiments to investigate the hydration process of binary and ternary blended cement pastes as well as pure Portland cement paste. The evolution of hydration of raw materials in the pastes will be measured to investigate the kinetics, and the hydration products at different curing ages will be characterized. Besides, the development of microstructure such as morphology and pore structure will also be investigated.

The modeling of ternary blended cements is more complex than pure Portland cement and binary blended cements. The challenge lies in the possible interaction between any two materials. Furthermore, each material shows different hydration mechanisms. Meanwhile, the hydration mechanisms of ternary blended cement are far from well understood. All these factors are difficult to be investigated. For example, most of current numerical models for blended cement have not solved the theoretical kinetics, instead directly borrow the existing kinetics equations which are applied to Portland cement. A good fitting may be achieved between the simulation results and experimental data especially when given many coefficients, but this does not adequately prove the applicability of the model which is not proposed based on a kinetics relationship bearing strong physical and chemical backgrounds.

It must be admitted that it is almost impossible to develop a model to completely simulate the real hydration of cementitious materials. Nevertheless, this thesis aims to build a hydration model for ternary blended cement paste along with the experimental investigation on blended cement. The model will be based on particle level and real particle size distribution and considering the interaction between each two materials considered. The kinetics equation of SCMs, i.e. slag in this study, will be proposed. The model will be calibrated by a subset of experimental results, while another subset of results will be used to validate the calibrated model. The model will provide an extension to the work of Klaas van Breugel, i.e. HYMOSTRUC.

Chapter 3

The Reaction Kinetics of Slag Activated by $Ca(OH)_2$ Solution

3.1 Introduction

The slag in ternary blended cement in this study is activated by $Ca(OH)_2$ produced by the hydration of cement. This chapter focuses on the reaction of slag activated by $Ca(OH)_2$ solution, aiming to investigate the reactivity of slag at particle level. The result will be used for modeling the reaction of slag in Chapters 7 and 8.

The reactivity of slag is usually estimated by the overall rate or overall kinetics of slag reaction. Investigations of [56, 107] show that the overall reactivity of slag is generally influenced by its glass content chemistry and particle size distribution (surface area). Additionally, process conditions such as the curing temperature, water to solid ratio and the ratio of slag to cement [57] also determine its reactivity.

From the standpoint of overall reaction kinetics, it is obvious that slag made up of fine particles reacts faster than that of coarser particles, since the former has significantly larger specific surface area than the latter. The reaction of a single slag particle takes place by moving the reaction front inwards, thus the rate of thickness increase of the reacting front layer of a single particle is worthwhile to be known. Nevertheless, less attention has been paid to the influence of slag particle size on this topic at particle level. Limited results of Sato et al. [108] and Chen et al. [28] showed that the thickness of the reacting front layer of a slag particle is not significantly influenced by its particle size. It should be noted that the particle sizes of the slag used in their experiments were in a narrow range, i.e. from 3 to 13 μm, while the particle size of slag used in cement industry varies from less than a micrometer to several hundred micrometers. Therefore, it is necessary to investigate the influence of slag particle size on its reaction rate at particle level in a wider size range.

In this chapter [109], two types of slag were separated into different size fractions by sieving, i.e. < 20 μm, 20-40 μm and > 40 μm. For each size fraction, the reaction process in the

Table 3.1: The chemical compositions of slag 1 measured by XRF (wt%).

Name	$< 20\mu m$	$> 20\mu m$	Non-sieved	Error(%)
CaO	38.18	39.61	38.14	0.10
SiO_2	35.87	34.64	35.82	0.10
Al_2O_3	12.07	11.75	12.05	0.09
MgO	9.33	9.24	9.37	0.09
SO_3	1.75	1.70	1.76	0.04
TiO_2	0.97	1.10	1.05	0.02
K_2O	0.48	0.48	0.48	0.02
Fe_2O_3	0.42	0.50	0.41	0.02
MnO	0.45	0.53	0.45	0.02
Na_2O	0.17	0.16	0.16	0.01

Table 3.2: The chemical compositions of slag 2 measured by XRF (wt%).

Name	$< 20\ \mu m$	20-40 μm	$> 40\ \mu m$	Non-sieved	Error (%)
CaO	39.42	41.57	42.09	40.01	0.10
SiO_2	36.14	34.72	34.23	35.75	0.10
Al_2O_3	10.98	10.52	10.32	10.7	0.09
MgO	10.08	9.64	9.64	9.99	0.09
SO_3	1.39	1.37	1.34	1.39	0.04
TiO_2	0.57	0.67	0.66	0.61	0.02
K_2O	0.37	0.37	0.38	0.36	0.02
Fe_2O_3	0.27	0.28	0.4	0.28	0.02
MnO	0.26	0.31	0.34	0.31	0.02
Na_2O	0.21	0.18	0.19	0.23	0.01

presence of $Ca(OH)_2$ solution was monitored up to 84 hours by recording the heat evolution using isothermal calorimetry method. The selection of $Ca(OH)_2$ solution is based on the fact that slag is mainly activated by the hydration products $Ca(OH)_2$ formed by Portland cement in slag blended cement, and the ternary blended cement in this research is mixed by slag, Portland cement and limestone powder.

The measured heat evolution of slag was further used to estimate the overall degree of reaction. Based on the measured particle size distribution and the assumed spherical shape of slag particles, the reaction speed of slag particles was calculated for each size fraction. Moreover, the chemical compositions of each slag size fraction were analyzed by means of X-ray fluorescence (XRF) technique, and the amounts of the crystalline and amorphous phases were quantified by X-ray diffraction analysis combined with Rietveld method.

3.2 Materials and Methods

The first slag (slag 1) was offered by Orcem® company. The second (slag 2) was from Belgian origin. According to the practical fineness, slag 1 was sieved into 3 groups, i.e. particle sizes (diameter) smaller than 20 μm, larger than 20 μm, and the original group (non-sieved). Slag 2

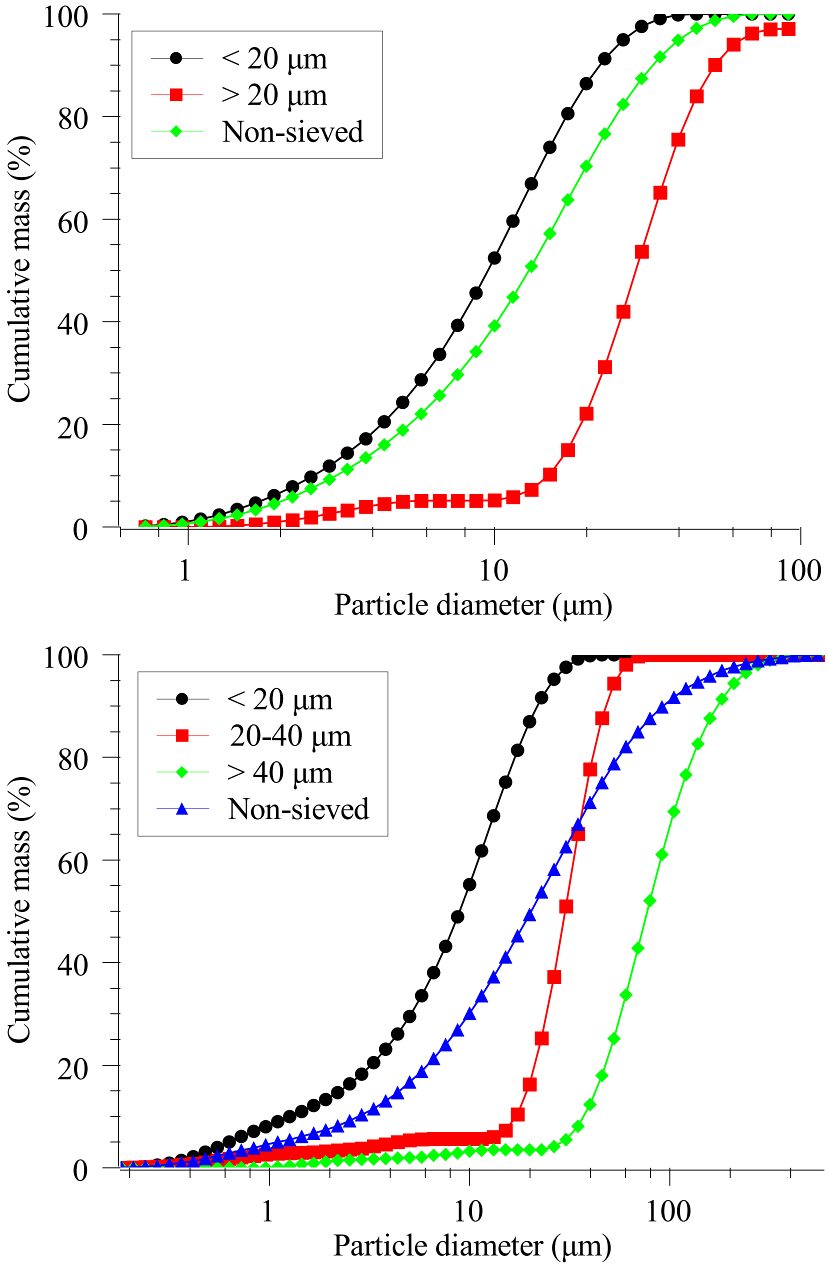

Figure 3.1: The particle size distribution of slag 1 (top) and 2 (bottom).

Table 3.3: Main crystalline phases of slag 1 tested by XRD/Rietveld (wt%, the low content of crystalline phase makes clinkers not detectable).

Name	< 20 μm	> 20 μm	Non-sieved
Akermanite	0.7	0.8	0.9
Calcite	/	/	/
C_2S	/	/	/
C_4AF	/	/	/
C_3A	/	/	/
Quartz	0.5	0.8	1.3
Total Crystalline Content	1.6	1.3	2.2

Table 3.4: Main crystalline phases of slag 2 tested by XRD/Rietveld (wt%).

Name	< 20 μm	20-40 μm	> 40 μm	Non-sieved
Akermanite	/	/	/	/
Calcite	2.2	1.1	0.4	0.5
C_2S	3.4	3.0	3.5	4.1
C_4AF	1.9	1.2	0.4	1.0
C_3A	0.7	1.2	1.4	1.0
Quartz	2.7	2.0	1.7	1.2
Total Crystalline Content	12.7	10.4	9.7	8.7

Table 3.5: Reactivity moduli and Ca/Si (molar) of slag 1.

Name	< 20 μm	> 20 μm	Non-sieved
(C+A+M)/S	1.66	1.75	1.66
(C+M)/S	1.32	1.41	1.33
A/S	0.34	0.34	0.34
(C+M)/(S+A)	0.99	1.05	0.99
Ca/Si	1.14	1.23	1.14

was sieved into 4 groups, i.e. particle sizes smaller than 20 μm, larger than 20 μm but smaller than 40 μm, particle sizes larger than 40 μm, and the original group.

The PSD of the 7 groups of slag was measured by laser diffraction method (Mastersizer 2000). Results are plotted in Fig. 3.1.

The chemical compositions of the slags were analyzed by XRF. For XRF analysis the samples were pressed into powder tablets then the measurements were performed with a Panalytical Axios^{mAX} WDXRF spectrometer. Data evaluation was processed with SuperQ 5.0i/Omnian software. The results are listed in Tables 3.1 and 3.2.

The mineralogy of the slags was determined by quantitative X-ray powder diffraction analysis. Sample preparation, XRD measurement and Rietveld analysis follow the detailed introduction in Section 4.2.3. Results are given in Table 3.3 and 3.4. According to [59], reactivity moduli and Ca/Si molar ratios were calculated based on the obtained chemical compositions as shown in Tables 3.5 and 3.6.

Table 3.6: Reactivity moduli and Ca/Si (molar) of slag 2.

Name	< 20 μm	20-40 μm	> 40 μm	Non-sieved
(C+A+M)/S	1.67	1.78	1.81	1.70
(C+M)/S	1.37	1.48	1.51	1.40
A/S	0.30	0.30	0.30	0.30
(C+M)/(S+A)	1.05	1.13	1.16	1.08
Ca/Si	1.17	1.28	1.32	1.20

3.3 Mix Design and Data Collection

The heat evolution was measured by isothermal heat conduction calorimeter (TAM Air instrument). Each channel of the calorimeter is constructed in twin configuration, of which one side for the test sample and the other for an inert reference (quartz sand). Heat flow sensors are installed under each channel to measure the heat production rate q. The twin principle allows the heat flow from the active sample to be compared with the inactive reference. This comparison enhances the stability and limits the noise within the system.

Data recorded by the isothermal calorimetric measurements were in mV unit and converted to mJ/s after calibration of the test setup. Considering the main active part in the paste was slag, the heat production rate q was expressed in the conventional unit J/gh, in which gh denotes per gram of slag and per hour. The cumulative heat production Q (in J/g) was then calculated as the integral of the heat production rate q over testing time.

Prior to the mixing, the materials were kept at temperature close to the measurement temperature (20 °C) to avoid significant difference between the paste and the isothermal environment. For each calorimetry test, 8.5 g slag taken from each group of slag was manually mixed 2 min in an ampule with 1.5 g $Ca(OH)_2$ powder and 10 g deionized water, so the water to solid ratio was 1:1. The mixed paste was immediately placed in the TAM Air instrument at temperature of 20 °C.

The heat evolution of reaction was recorded every minute up to 84 hours, and each heat release curve was obtained by the average of triplicate samples to achieve statistically stable results. In this study, the ratio of cumulative heat evolution of the slag to its theoretical maximum value is considered as overall degree of reaction. The theoretical maximum heat release of slag reaction is taken as 461 J/g [110].

Since the mixing of pastes occurred outside the calorimeter, the first reaction peak should not be regarded as caused by chemical reaction due to the wetting peak of heat production, which actually amounts to only a few percent of the total heat liberation [107] and is thus discarded in data analysis.

3.4 Calculation Method

3.4.1 Definition of k Value and Calculation Assumptions

Figs. 3.2 and 3.3 show a schematic representation of a reacting slag particle [111]. In this study, the parameter k is defined as *the average rate of thickness increase of the reacting front layer for a single slag particle at a certain time period*. The unit of k is μm/day unless otherwise stated. The k value of a single particle is calculated by linking the overall degree of reaction with the thickness of the reacted layer of all particles. The establishment of this link is based on four assumptions as proposed below.

- The shape of slag particles is assumed as spherical (Fig. 3.2) to facilitate the calculation at particle level, though it is far from the real shape of slag particles [112]. The diameters and size fractions used in calculation were measured by laser diffraction method which also assumes the shape as spherical.
- The first reaction stage is assumed as phase boundary reaction [23], implying the thickness of the reacted layer of a slag particle increases with time following a first order relation (Fig. 3.2 and Eq. 3.1):

$$k = \frac{\delta_{in}(t)}{t} = \frac{d\delta_{in}(t)}{dt} \tag{3.1}$$

  where $\delta_{in}(t)$ is the thickness of the reacting front layer of a slag particle at reaction time t. It has to be noted that in this study k is assumed as an average value of a particle from the start of reaction to the calculation time point t and all slag particles in the same group bear the same k value. The simplification here is for the sake of practical numerical calculation.
- Since there is sufficient space for the expanding volume of each reacting slag particle, it is assumed that no spatial interaction between particles occurs in the reacting system. This simplification is far from the reality at regular water to paste ratios, e.g. 0.5, but it is reasonable in this study because the water to solid ratio used was 1:1.
- Due to sufficient quantity of water and $Ca(OH)_2$ for the reaction of slag, the reaction speed of slag particles in the paste is assumed to be not limited by the shortage of reactant.

3.4.2 The Numerical Calculation of k Value

Based on the above assumptions, the calculation of k is carried out as follows. For each group of slag, 1 g of slag particles is taken to be calculated. The degree of reaction $\alpha_{(r,t)}$ of a single particle at time t is calculated based upon the thickness of the reacted slag layer ($\delta_{in}(t)$),

$$\delta_{in}(t) = k \times t \tag{3.2}$$

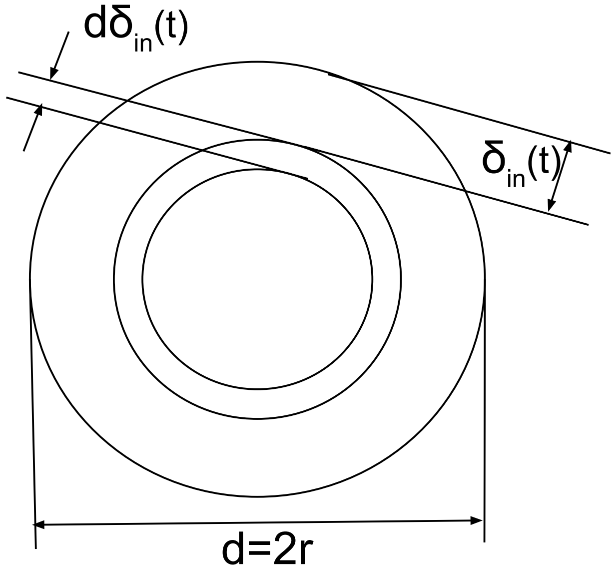

Figure 3.2: Schematic representation of a reacting slag particle: the thickness of the reacting front layer, $2r$ is the original diameter of the particle, $\delta_{in}(t)$ is the thickness of the reacted front layer.

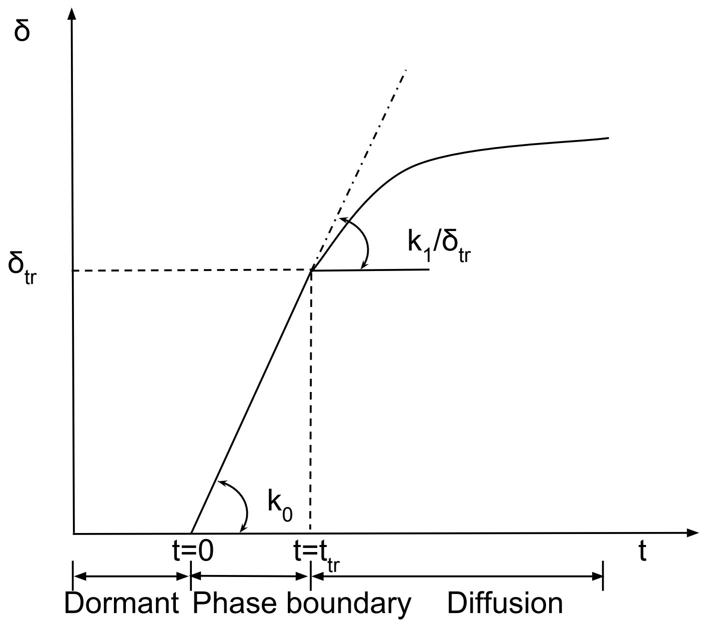

Figure 3.3: Schematic representation of a reacting slag particle: k is a constant in the phase boundary stage, i.e. from $t = 0$ to t_{tr} (the short dormant stage is discarded); the kinetics follows a first order relation [3].

and,

$$\alpha_{(t,r)} = 1 - \left(1 - \frac{\delta_{in}(t)}{r}\right)^3 \tag{3.3}$$

where r is the radius of the slag particle that is obtained from the PSD result.

Since the reaction of all particles in the same size fraction is identical, the degree of reaction ($\alpha_{(total,t,r)}$) of all slag particles with the same size r in 1 g of slag equals to $\alpha_{(t,r)}$ (Eq. 3.4).

$$\alpha_{(total,t,r)} = \alpha_{(t,r)} \tag{3.4}$$

The total degree of reaction $\alpha_{(total,t)}$ of the entire 1 g of slag from the beginning of reaction to time t is thus obtained by summing up all size fractions :

$$\alpha_{(total,t)} = \Sigma_{r_{min}}^{r_{max}} f_r \times \alpha_{(total,t,r)} \tag{3.5}$$

where f_r is the mass fraction of particles with the same size r, which was determined by laser diffraction method (PSD measurement). The parameters r_{max} and r_{min} are the maximum and the minimum radius of particles respectively, which were also obtained from PSD measurement.

Equaling the numerically calculated $\alpha_{(total,t)}$ and the experimentally recorded total degree of reaction $\alpha_{(total,t,e)}$, the value k can be numerically calculated. Note, $\alpha_{(total,t,e)}$ is converted from the calorimetry test, i.e.

$$\alpha_{(total,t,e)} = \frac{\text{measured cumulative heat evolution}}{\text{theoretical maximum cumulative heat evolution, i.e. 461 J/g}} \tag{3.6}$$

For all cases, knowing the experimentally obtained PSD and the overall degree of reaction ($\alpha_{(total,t,e)}$), we can calculate the average rate of thickness increase of the reacting front layer of slag particles for each group, i.e. k value.

3.5 Experimental Results

3.5.1 Heat Evolution Rate and Cumulative Heat

Fig. 3.4 displays the heat evolution rate of each group of slag. The first peak occurred (not shown in the figures) in the first minutes and may have arisen from the physical wetting instead of chemical reaction [113], thus the heat evolution in the first 10 min was discarded. A second peak of heat evolution rate appears after about 10 to 20 hours. Peak values of finer slag particles are as high as 5 times that of the coarse particles, e.g. the second peak of heat evolution rate of slag particles larger than 40 μm (Fig. 3.4 (bottom)) is only 0.12 mW/g when the reaction proceeded 25 hours, while that of the particles smaller than 20 μm is 0.56 mW/g occurring after 17 hours reaction.

Fig. 3.5 shows the cumulative heat evolution of the slag. After the first 10 min that corresponds to the wetting peak, the cumulative heat evolution steadily increases. Coarse particle

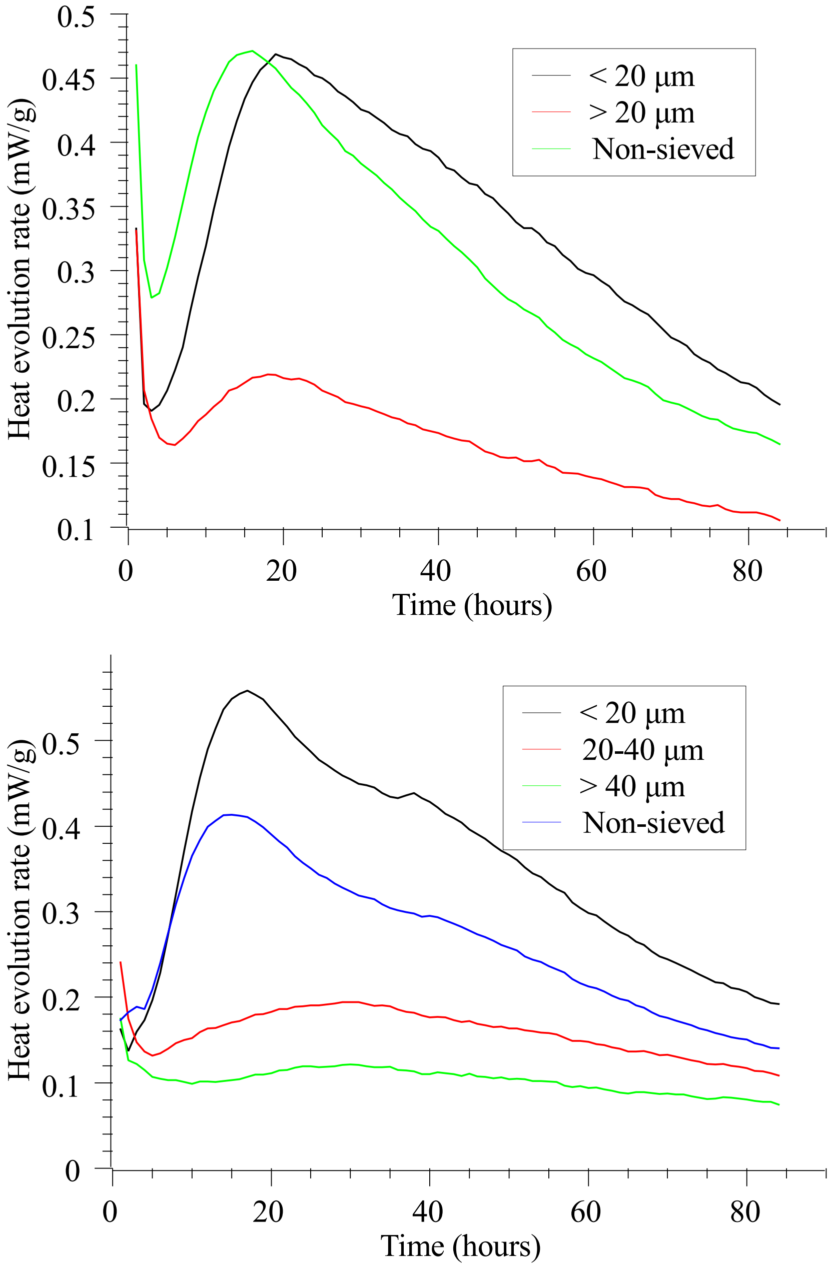

Figure 3.4: Rate of heat evolution of slag 1 (top) and 2 (bottom).

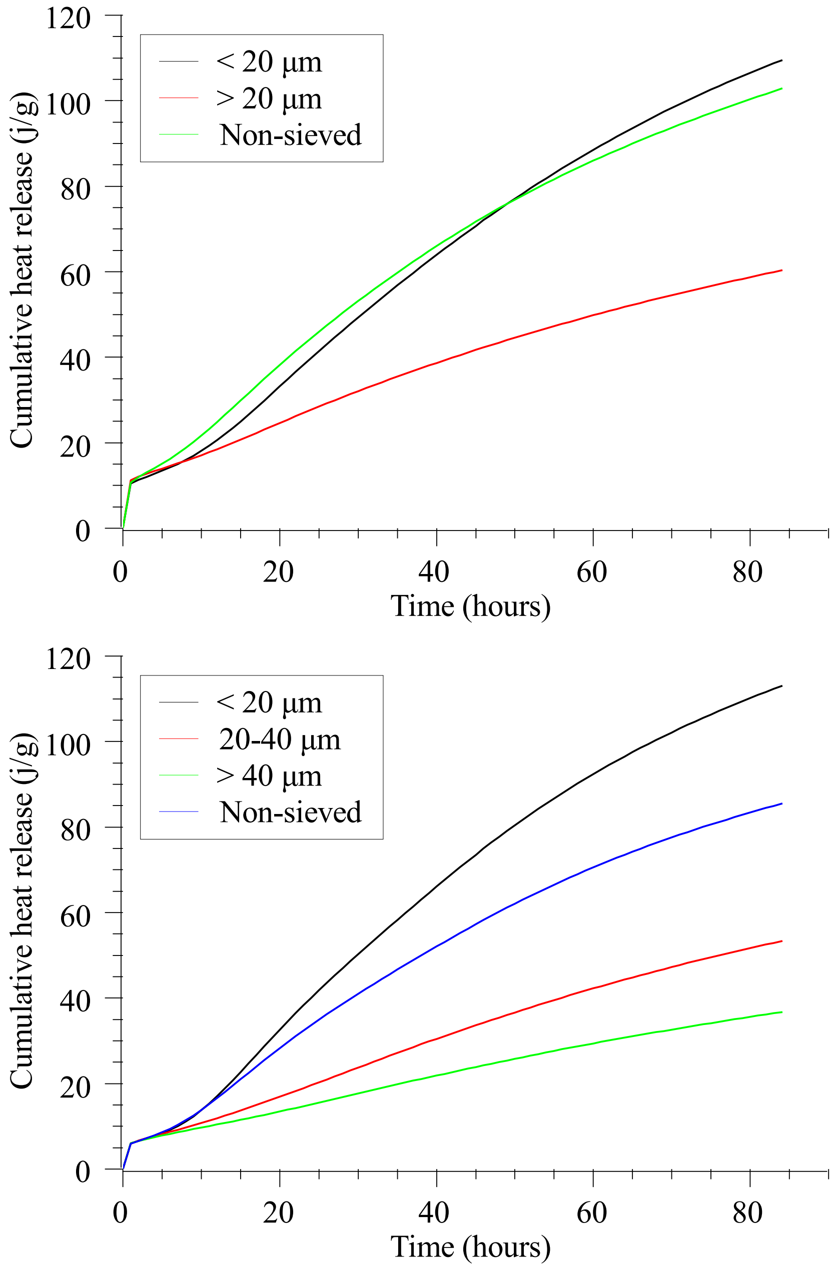

Figure 3.5: Cumulative heat evolution of slag 1 (top) and 2 (bottom).

groups released less heat than fine groups, which was even more distinct at the later stage. It is readily explained by the fact that a group of fine slag has significantly larger specific surface area than that of a coarse group, e.g. specific surface area (or surface area per mass unit) of spherical particles with diameter 1 μm is 10 times that of particles with diameter 10 μm.

3.5.2 Calculated k Values

Based on the aforementioned four assumptions and the calculation method, the k of the slag particles in each group of slag was calculated. The calculated results of k corresponding to each reaction time period t are plotted in Fig. 3.6.

Table 3.7: Calculated average k values of slag 1 after 72 hours reaction (μm/day).

Non-sieved	< 20 μm	> 20 μm
0. 104	0.098	0. 153

Table 3.8: Calculated average k values of slag 2 after 72 hours reaction (μm/day).

Non-sieved	< 20 μm	20-40 μm	> 40 μm
0. 094	0. 066	0. 116	0. 216

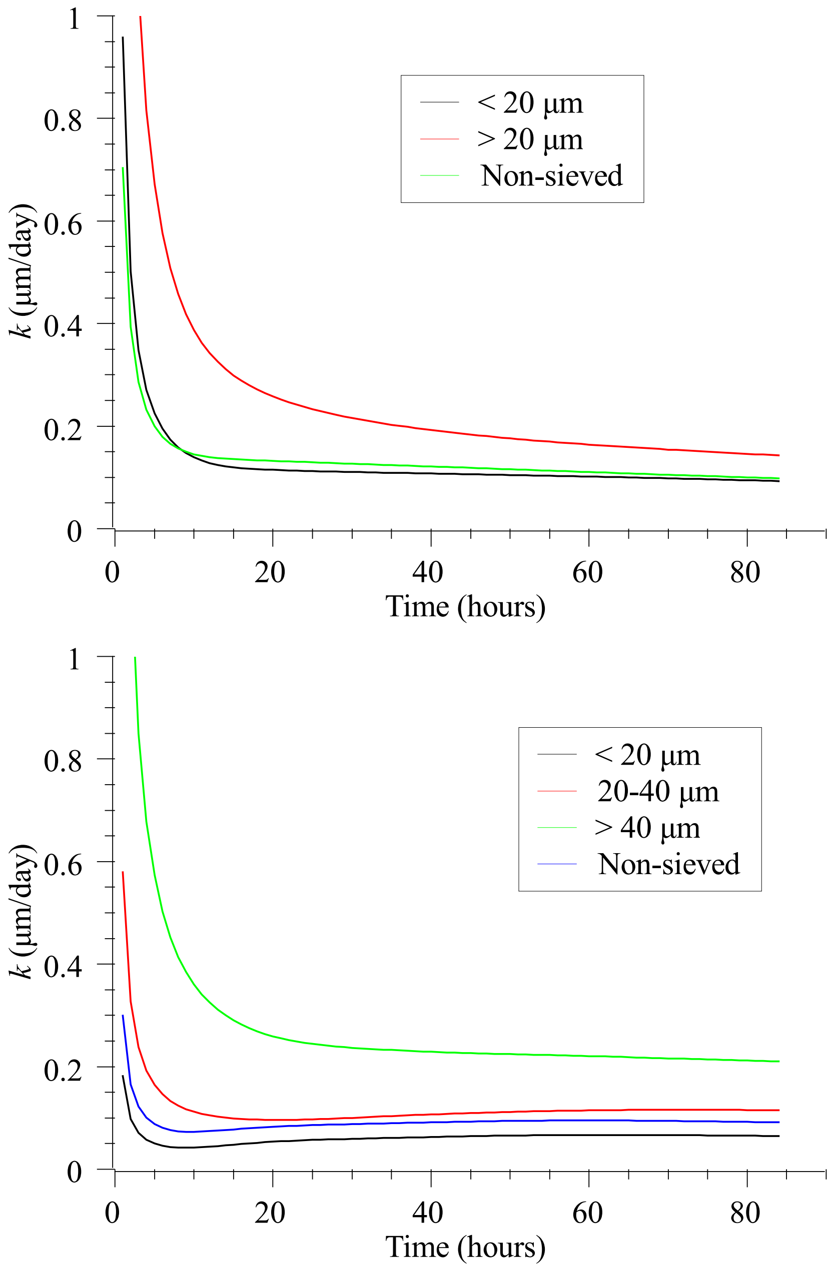

Figure 3.6: Calculated k values of slag 1 (top) and 2 (bottom) based on different reaction time periods.

According to the results, the k value of the coarse slag fraction is always higher than that of fine groups, which means that the rate of thickness increase of the reacting front layer of a single slag particle from coarse group is faster than that from fine group. Additionally, the k value sharply decreased to low values in the first 20 hours of reaction and then steadily reaches relatively stable values, which is in line with the aforementioned assumption that the thickness of the hydrated layer increases with time following a first order relation. It should be noted that the k in the calculation is an average value from the reaction starting point to the calculation time, in other words, the calculated k value in the very early age (several hours) is relatively high since the heat evolution is high. Furthermore, the k in Fig. 3.3 is an average value in the whole period of phase boundary.

Tables 3.7 and 3.8 summarize the calculated average k values of each group of slag after 72 hours of reaction. Among these values, the lowest k value is 0.066 μm/day from particles smaller than 20 μm in slag 2, while the highest is 0.216 μm/day of particles larger than 40 μm in slag 2. Corresponding values of Portland cement particles range from 0.6 to 1.32 μm/day [3]. Compared to Portland cement particles, the lower k value of slag particles explains the slow reaction process of slag.

As [114] reported, the thickness of inner product of slag particle varies between 0.5 μm to > 2μm (150 days), and according to [115] slag particles can gradually react until the thickness of the reaction layer reaches about 0.3 to 0.5 μm, afterwards, the reaction rate may be subsequently hindered by the texture of the reaction products, implying that the further reaction of slag in this investigation was probably switched from phase boundary to diffusion controlled stage after about 72 hours when the thickness of the reacted front layer of slag particles is already 0.3 μm. At later age, the kinetics function for the first stage, i.e. Eq. 3.1, is no longer applicable to calculate k in principle.

3.5.3 The Relationship between k Values and Chemical Compositions

Combining the calculated k values of slags with different size fractions in this study and different reactivity moduli in Tables 3.5 and 3.6, a regression of these data was conducted. It is found that a good relationship exists between k values and the (C+A+M)/S modulus of slag material. Fig. 3.7 shows a distinct trend, showing that the k value becomes higher as (C+A+M)/S increases. Eq. 3.7 is obtained based on the regression result.

$$k_0 = 0.9023 \times \frac{\mathrm{C + A + M}}{\mathrm{S}} - 1.4427 \;\; (\mu\mathrm{m/day}) \tag{3.7}$$

where k_0 denotes the rate of thickness increase of the reacting front layer of slag particles, i.e. k in this chapter, which will be used to estimate the k_0 value of slag according to its chemical compositions for simulation in Chapters 7 and 8.

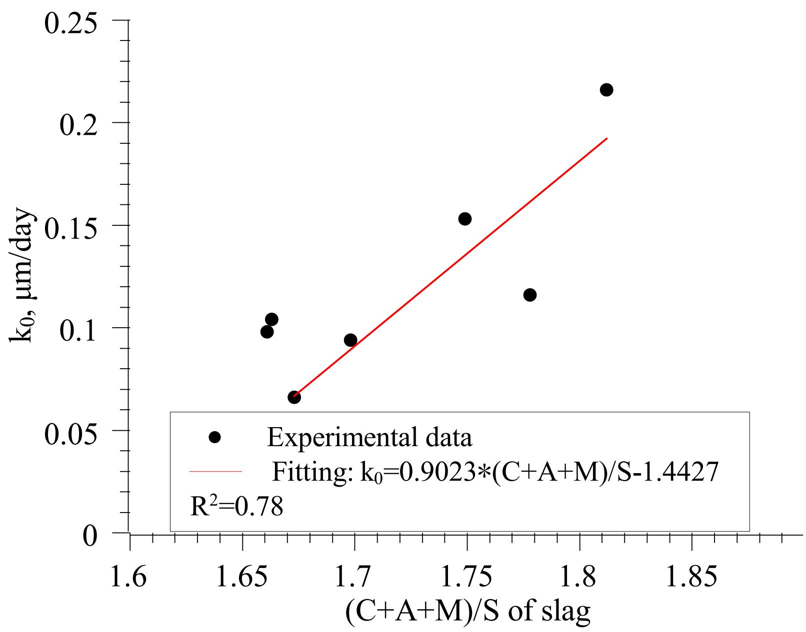

Figure 3.7: The relationship between k values and chemical compositions.

3.6 Discussion

3.6.1 The Simplification of Calculation

The experimental method is of paramount importance to investigate the reaction kinetics of slag. Compared with EDTA selective dissolution method [57], isothermal calorimetry is a continuous way to investigate the reaction process especially at early age. The high accuracy of TAM Air instrument guarantees reliable results of the heat evolution rate during the reaction process.

The maximum heat evolution of the final reaction of slag is taken as 461 J/g based on limited literature data. This value is questionable, but unfortunately there is no formula to calculate the maximum heat evolution of slag reaction, while a large body of data can be used to calculate the maximum heat of hydration of Portland cement. The maximum heat evolution of complete slag reaction is supposed to be a function of chemical composition and its vitreous fraction, which is beyond the scope of this study, therefore, the value 461 J/g is simply applied to convert the heat evolution to degree of reaction.

The shape of slag is assumed as spherical in this study to simplify the numerical calculation. In this way, only the diameter of a particle, which was measured using laser diffraction method, is sufficient to mathematically calculate its volume. However, the spherical shape of slag particles is definitely not realistic. Extensive analysis [116] of geometric characteristics of slag particles using Scanning Electron Microscopy (SEM) shows that the real shape of slag particles is irregular. Therefore, it should be born in mind that the assumption of spherical shape underestimates the specific surface area of slag particles.

As seen from the PSD results, the sieving process adequately separated the slag particles into different sizes. Nevertheless, due to the irregularity of particle shape, some overlap existed to a marginal extent, e.g. a small amount of particles smaller than 20 μm could not be separated into the group smaller than 20 μm, while some particles larger than 20 μm passed through the 20 μm sieve aperture and stayed in the group smaller than 20 μm. This phenomenon also occurred in the case of sieving at 40 μm, as shown by the PSD results in Fig. 3.1. In order to account for the overlapping of sizes, the measured PSD of each group was applied in the calculation. In addition, the amount of these overlapped sizes accounts for only a few percent, so its influence should be minimum upon the calculation of k.

The calculation of k did not consider possible interaction among particles and the influence of varying ion concentration of the pore solution in the paste. This simplification is based on the high water/solid ratio (1:1), because the large amount of water guaranteed enough space for the precipitation of reaction products and a relatively stable ion concentration in the solution.

3.6.2 Influence of Particle Size on Hydration Kinetics of Slag Particle

Based on the measured reaction process of slag with different sizes, the calculated results demonstrate that the rate of thickness increase of the reacting front layer of coarse slag particles is faster than that of fine particles.

The chemical composition analysis of slag by XRF reveals the difference among the 7 slags of different sizes. As the slag size increases, the CaO content slightly increases, while the contents of other oxides such as MgO, Al_2O_3 and SiO_2 decrease. Although the changes are rather small, there is a substantial change in the (C+A+M)/S ratio and thus the reactivity index of slag [117]. The reactivity indices calculated based on the chemical compositions suggest that the coarser slag fraction has higher reactivity, e.g. according to the German standard, the calculated reactivity index (C+A+M)/S (Tables 3.5 and 3.6) of the coarse particle group is higher than that of the fine group, which coincides with the faster rate of thickness increase of the reacting front layer, i.e. higher k value. For example, the k value (0. 216 μm/day) of particles larger than 40 μm is three times higher than those particles smaller than 20 μm (0. 066 μm/day) in slag 2.

Taylor mentioned [2] that small contents of crystalline phases in slag can provide nucleation sites for reaction products, and can thus accelerate the reaction process. The content of crystalline phase of the two types of slag varies significantly, but there is not too much difference in terms of k values of the two non-sieved slags. The content of crystalline phase of each group from the same slag varies as size changes. However, considering the accuracy of XRD/Rietveld and the relatively low content of crystalline phase in this study, it is hard to conclude that the k value is significantly influenced by the crystalline phase, which is also the conclusion of [118] that the amount of glassy phase present in slag is less important for the reactivity than its optimum chemical composition.

The influence of particle size on the rate of thickness increase of the reacting front layer of slag particle investigated in this study is essentially attributed to the chemical compositions which determine its intrinsic reactivity [119, 120]. Slag particles of different sizes are formed during the grinding process. A possible reason accounting for the different sizes when grinding is the different hardness of slag particles, and the hardness is probably determined by the intrinsic chemical compositions as well as other physical properties, e.g. higher CaO content may leads to higher hardness of slag in this study, which of course needs to be further investigated.

Research indicated that amorphous silicate and aluminate phases are the main cementitious phases in slag and mainly exist in the small particles [121]. XRF results in this study also confirm that slag groups of small sizes contain higher content of Al_2O_3 and SiO_2 than the corresponding values of slag groups consisting of large particles.

However, another important property of slag is alkalinity. To assess the activity of steel slag, Mason [122] proposed a method to calculate the alkalinity (denoted as M), which is defined as mass ratio of CaO to SiO_2 and P_2O_5 (Eq. 3.8),

$$\mathrm{M} = \frac{w_{(\mathrm{CaO})}}{w_{(\mathrm{SiO_2})} + w_{(\mathrm{P_2O_5})}} \tag{3.8}$$

Tang et al. [123] also indicated that the major mineral compositions of steel slag depend on its alkalinity. It might be doubtful to directly apply the knowledge from steel slag to GGBFS, but higher Ca/Si ratio of GGBFS with larger size in this study could account for the faster rate of thickness increase of the reacting front layer, i.e. k value.

It is known that the Ca-O and Mg-O bounds are weaker than Al-O and Si-O in the glassy slag surface under the polarization effect of OH^- [113], implying that it is easier to etch the surface of slag particle with more CaO but less SiO_2. Therefore, coarse slag particles with higher content of CaO are more vulnerable to the attack of OH^-, leading to higher k value in this study.

The reaction kinetics of slag particles could also be influenced by the Ca/Si ratio of reaction products. According to the research from Glasser [124], as the Ca/Si ratio declines to less than 1.2-1.3, the electric surface charge of C-S-H gel gradually reverses from positive to negative. The less positive or even negative charges on the surface of C-S-H gel attract Ca^{2+} ions of pore solution moving towards inner reaction products and then reacting with silicate ions, resulting in denser inner product bearing stronger resistance against further ion diffusion. On the contrary, C-S-H gel with a lower Ca/Si ratio has a foil-like morphology rather than fibrillar one, implying the tortuosity of gel pores becomes higher and the path for ion diffusion is elongated. In all, the changed surface charges and morphology of C-S-H gel with lower Ca/Si ratio hamper the reaction front developing inwards.

Since the Si and Ca ion concentrations in pore solution are considerably low (< 20 mmol/L), the Ca/Si ratio of C-S-H gel is mainly determined by that of slag material. The Ca/Si ratio of slag in this study ranges from 1.14 to 1.32 as listed in Tables 3.5 and 3.6. The Ca/Si ratio of fine slag group is lower than coarse group due to its lower content of CaO and higher SiO_2. The lower Ca/Si ratio of fine slag particle results in lower Ca/Si of C-S-H gel, leading to less positive surface charges and foil-like morphology, which accounts for the slower rate of thickness increase of the reacting front layer, i.e. lower k value.

Based on the aforementioned elements, it can be concluded that the Ca/Si of slag is crucial for the reactivity of slag particles at least at early age of reaction. Coarse slag particles in this study have higher Ca/Si ratios, which in turn results in a faster rate of thickness increase of the reacting front layer.

Though the thickness increase rate of the reacting front layer thickness (k value) of fine slag particles is slower than coarse particles, increasing the fineness of slag is still of paramount importance to boost the overall reactivity of slag, and then increase the mechanical strength at both early and later ages [125]. The reason is that k values of fine slag particles and coarse particles are of the same order of magnitude, while the specific surface area of the former is one order of magnitude higher than the latter. Meanwhile, coarse slag particles (e.g. diameter larger than 40 μm) usually make up a relatively small part in slag. The combined effect of particle size and surface area on overall reaction is confirmed by the experimental results that the cumulative heat evolution of the fine slag fraction is always higher than the coarse fraction after the same reaction time, despite the fact that k values of coarse particles are higher than fine particles. This may explain why less attention has been paid to the influence of particle size on the reaction kinetics of slag at particle level.

3.7 Conclusions

In this chapter, the influence of particle size on the rate of thickness increase of the reacting front layer of slag activated by $Ca(OH)_2$ solution was investigated at particle level. The following conclusions are obtained:

1. The overall degree of reaction of slag consisting of fine particles develops faster than that of coarse slag due to its large specific surface area.

2. Particle size of slag has influence on the rate of thickness increase of the reacting front layer of a single slag particle (k value). The k value of coarse particles is higher than fine particles.

3. Slag made up of coarse particles has higher content of CaO but relatively lower content of MgO, Al_2O_3 and SiO_2, resulting in higher reactivity index of (CaO + Al_2O_3 + MgO)/SiO_2. A correlation exists between (CaO + Al_2O_3 + MgO)/SiO_2 and k value.

4. The influence of particle size on the reaction of slag is essentially attributed to the chemical compositions. Higher Ca/Si ratio of slag is crucial for the reactivity of slag particles at least at the early age of reaction.

5. k values of slags were numerically calculated, which will be used for the modeling work in Chapters 7 and 8.

Chapter 4

The Kinetics of Ternary Blended Cement Paste

4.1 Introduction

In Chapter 3, the reaction kinetics of slag activated by $Ca(OH)_2$ solution has been investigated, finding the factors governing the reaction of slag at particle level, i.e. k values of slag particles. Due to the complexity of the hydration process, we assumed and created an ideal environment for the reaction of slag in Chapter 3, offering enough water and unlimited space for the precipitation of hydration products. However, when slag is blended with Portland cement and/or limestone powder, which is the combination in this research, the hydration of the blended paste is much more complex than paste being mixed by any single material. Not only are water and space limited for ongoing hydration, but also the formed hydration products could influence the reaction of other materials. The interactions occurring in blended cement paste make the kinetics complex.

Specifically, in the case of paste mixed by blending cement, slag and limestone powder, hydration product $Ca(OH)_2$ produced by cement hydration firstly activates the hydration of slag and afterwards acts as reactant for reaction of slag. The reaction of slag in turn breaks the balance of cement hydration by consuming limited water and occupying the decreasing space of pore system. Limestone may act at least as nucleation sites for the precipitation of C-S-H gel and other hydration products. In addition, $CaCO_3$ from limestone may participate in a certain limited reaction with aluminate phase given that slag contains a high content of Al_2O_3 compared with cement. The reaction of limestone consumes relatively large amount of water, influencing the hydration of slag and cement.

Most attention has just been paid to the hydration kinetics of binary blended cements such as slag blended cement, limestone blended cement. As for ternary blended cement, systematic investigation on hydration kinetics is extremely limited. Among the few results reported in literature on ternary blended cements by cement, slag and limestone [126, 127, 128], the large

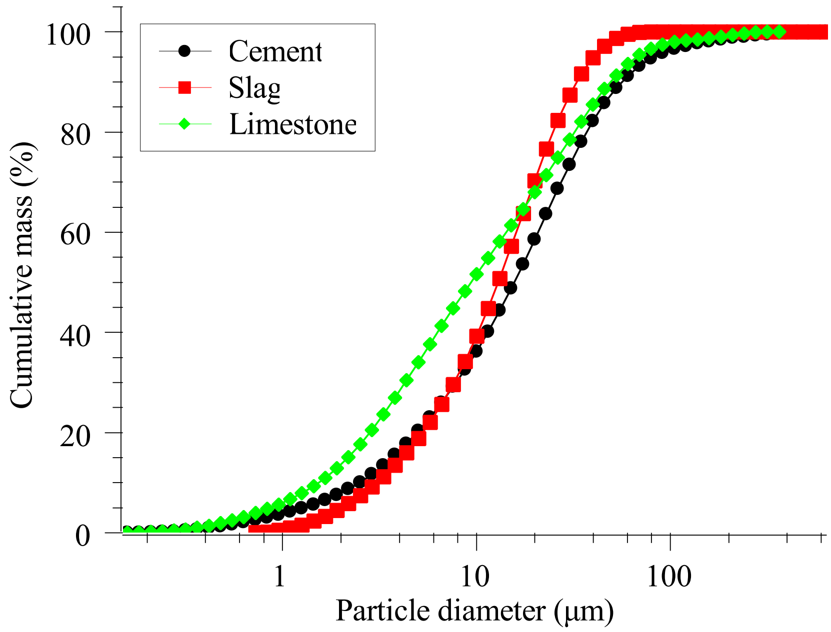

Figure 4.1: Cumulative particle size distribution of cement, slag and limestone powder. Air dispersion and laser scattering techniques were used.

replacement level of limestone (10 wt%) and slag (60 wt% and 70 wt%) in this research makes those conclusions from literature not always applicable. Therefore, the purpose of this chapter is to investigate the hydration kinetics of ternary blended paste with radical mix proportions which also make the mix more economical.

Given the complexity of hydration kinetics in blended cement pastes, a series of experimental methods were applied. For the hydration process in the very early age, isothermal calorimetry method was used, which can precisely record the heat flow of hydration process at early age. For cement, the degree of hydration of cement clinker (C_3S, C_2S, C_3A and C_4AF) from 1 to 91 days was quantified by X-ray diffraction (XRD) test and Rietveld refining analysis since XRD/Rietveld analysis is a promising method for a quantitative study of the phases in cement paste during hydration [126, 129]. As for slag, the degree of reaction of slag was measured by means of EDTA selective dissolution method. In terms of the limited but possible reaction of limestone powder, its content was determined by TGA which is more accurate than differential thermal analysis [130].

4.2 Materials and Methods

4.2.1 Materials

As aforementioned, three materials, i.e. Ordinary **P**ortland cement (OPC, P in short), ground granulated **B**last-furnace slag (B) and **L**imestone power (L), were chosen as the raw materials in this research. OPC was CEM I 52.5 N complying with the European standard EN 197-1 (2000)

Table 4.1: Chemical compositions of materials (wt%). Data of cement and limestone powder is taken from X. Liu [22], data of slag are measured by X-ray fluorescence.

	Cement (P)	Limestone (L)	Slag (B)
CaO	63.95	55.05	38.14
SiO_2	20.29	0.80	35.82
Al_2O_3	4.52	0.17	12.05
Fe_2O_3	2.53	0.10	0.41
MgO	2.22	0.50	9.37
K_2O	0.94	/	0.48
Na_2O	0.20	/	0.16
SO_3	3.35	/	1.76
C_3S	59.00	/	/
C_2S	12.60	/	/
C_3A	8.01	/	/
C_4AF	9.40	/	/

[13]. Slag was essentially the same used in Chapter 3, i.e. slag 1, with a hydraulic modulus ((C + A + M)/S) 1.66 that is higher than the minimum 1.0 according to German specification [2]. Limestone powder was produced from carboniferous limestone with a high purity of 98.3 wt% $CaCO_3$ tested by TGA technique.

The chemical compositions of cement, slag and limestone powder are listed in Table 4.1. Fig. 4.1 shows the cumulative particle size distribution curves of the three materials measured by laser diffraction method. Unless otherwise stated, all experiments in the rest part of this thesis used the same materials as introduced in this section.

4.2.2 Mix Design of Pastes

Mix Proportion, Mixing and Curing

In order to have references of neat Portland cement and binary blended cements, four groups of pastes were designed, which are listed as follows:

1. PC: 100 wt% Portland cement.
2. PL: 10 wt% limestone powder blends with 90 wt% Portland cement.
3. PB: 30 wt% Portland cement blends with 70 wt% slag.
4. PBL: 10 wt% limestone and 60 wt% slag blended with 30 wt% Portland cement.

Detailed mix proportion is listed in Table 4.2. The water to powder ratio (w/p) of the four groups of mixes was constantly fixed at 0.40, meaning 1.00 g solid material(s) mixed with 0.40 g water. Corresponding water to cement ratio was also calculated and listed in the table.

The mixing procedure was taken from European standard EN 196-1:2005 with the consideration of the addition of slag and limestone powder. First, slag and/or limestone powder were/was

Table 4.2: Mix proportion of pastes (in g).

	PC	PL	PB	PBL
CEM I 52.5 N	450	405	135	135
Limestone powder	0	45	0	45
Slag	0	0	315	270
Water	180	180	180	180
Water/Powder ratio	0.40	0.40	0.40	0.40
Water/Cement ratio	0.40	0.44	1.33	1.33

added and mixed at low speed for 2 min to well disperse the slag and/or limestone powder with cement. Later, the mixing procedure was strictly performed as described in EN 196-1:2005. For each sample, the well mixed paste was cast in a sealed plastic cylinder bottle with a volume of 90 cm^3. The sealed paste was rotated at a speed of 2.5 rpm in a curing room with temperature 20 °C for 24 hours to avoid bleeding. Later the sealed sample was cured at the same temperature till each due curing age which was scheduled as 1, 3, 7, 14 and 91 days counted exactly from the start point of casting.

Stopping Hydration, Drying Samples

When each due curing age was reached, the hydrating sample in the sealed plastic bottle was cracked into small pieces (around 1 cm^3) and immediately immersed in liquid nitrogen (-195 °C) for 5 min to stop the ongoing hydration. Later, the frozen sample was placed in a freeze-dryer in which the temperature and vacuum were kept at -20 °C and as low as 10^{-1} Pa, respectively, therefore, passing directly from solid to gaseous state, the free water was sublimed in the process of lyophilization [131]. The water loss during the drying process of each sample was weighed approximately every 24 hours until a stable mass loss of 0.01% per day was reached.

The drying method applied in this research is called low temperature vacuum drying. As stated by [132], the quickly formed ice micro-crystals in the sample by immersion in liquid nitrogen are slowly dried in the low temperature vacuum chamber without much damage to the pore structure of sample. This is the main advantage of this method compared with others such as oven drying and vacuum drying.

4.2.3 Sample Preparation for XRD/Rietveld Test

The procedure of grinding sample for X-ray diffraction measurement was taken from the work of [133]. A representative amount of each dried sample (50-100 g) was crushed by hand in a porcelain mortar, and then passed through a sieve aperture sized at 500 μm. Shock impact was applied when grinding by hand, avoiding shearing stress that may destroy the mineralogical structure of sample. Since grain size smaller than 10 μm is preferred for quantitative X-ray diffraction measurement (Rietveld analysis), the crushed sample was ground further by wet milling in a McCrone® Micronizing mill (Fig. 4.2), which avoids the amorphization of

Figure 4.2: The McCrone® micronizing mill device used in this study.

hydration products during the grinding process. The detailed procedure of sample preparation using McCrone Micronizing mill for XRD/Rietveld test is given as follows:

1. First weigh 2.7 g of sample, then add 0.3 g (10 wt%) of ZnO as internal standard. Note down the exact weight which will be used in the calculation.

2. Micronize the sample in a McCrone® Micronizing mill using 5 ml of hexane as grinding agent and a grinding time of 5 min. Methanol tends to react with some artificial minerals, so hexane is used in this research.

3. After micronizing, recuperate the sample in a porcelain cup. Cover the cup with plastic foil, because recovery of dried powder from the porcelain is difficult. Wash the ground sample with hexane to recuperate as much as possible, then dry the ground sample in the porcelain cup for one or two days under a fume hood.

4. Dried samples are gently disaggregated in an agate mortar and passed through a 250 μm sized sieve aperture, ensuring good mixing of sample and ZnO standard.

5. About 0.5 g ground sample is needed for the X-ray diffraction measurement. Side-loading with frosted glass is recommended to fill the sample holder, preventing preferential orientation of fibrous zeolites (if exists) and clay minerals. Sample holders are gently tapped while filling to ensure good packing of the grains.

XRD/Rietveld Test and Analysis Method

The mineralogy of samples was determined by quantitative X-ray powder diffraction analysis (QXRPD, Philips® PW1830). Diffraction patterns were measured in 2θ range of 10-70° using CuKα radiation of 45 kV and 30 mA, with a 0.02° step size and step time of 2 s. Quantitative results were obtained by adopting the Rietveld method [134, 135], using the "Topas® Academic" software [136]. A fundamental parameter approach was used, meaning that instrumental contributions to the peak shapes were calculated directly [137] and the standard parameters (cell parameters, crystallite size, lattice strain, diffraction optical effects and background) were refined.

The Accuracy of XRD/Rietveld Measurement

The method of X-ray diffraction is usually used for qualitative analysis for crystalline phases. Combined with Rietveld refining method, the X-ray diffraction results are quantified in this research. The accuracy of XRD/Rietveld method may vary from phase to phase. According to the performance of the instrument used in this study, the accuracy varies between $\pm$ 1-2% if there is no overlap of peaks with the neighbor phases. The accuracy is confirmed by the comparison with results obtained from TGA test. For example, XRD/Rietveld result shows that the $CaCO_3$ content in the raw cement is 2.55 wt%, which is slightly higher than 1.97 wt% as measured by the accurate TGA test.

4.2.4 Sample Preparation for EDTA Selective Dissolution Test

The EDTA selective dissolution method applied in this research is taken from [45] based on the work of [57, 58]. The following is a brief introduction of the method used in this research.

1. First, 93.0 g of disodium EDTA $2\,H_2O$ was dissolved in a mixture of 250 ml of triethanolamine and 500 ml of water. The solution was later transferred to a volumetric flask.

2. 173 ml of diethylamine was added into the above solution, then the mixture was made up to 1000 ml with water.

3. For each extraction test, 50 ml of the above solution was pipetted into a beaker and diluted to approximately 800 ml with water.

4. After the diluted solution was brought to a temperature of 20.0 $\pm$ 2 °C, 0.5000 g of dried and ground sample paste (particle size smaller than 90 μm) was weighed to the nearest 0.0001 g, then was sprinkled over the surface of solution.

5. The solution was stirred for 120 $\pm$ 5 min at the stated temperature, then filtered under vacuum through a 90 mm diameter Whatman GF/C filter which had been previously washed with 100 ml of distilled water, dried and weighed.

6. The residue was washed 5 times with 10 ml distilled water, later dried at 105 °C for 1 hour and weighed to the nearest 0.0001 g.

7. The hydration degree of slag was calculated.

Each test was performed three times to obtain statistically stable result.

Calculation of Degree of Reaction of Slag Based on EDTA Selective Dissolution Test

The definition of degree of reaction of slag is mathematically expressed as Eq. 4.1. Therefore, the calculation of reaction degree of slag is theoretically straightforward when knowing the original mass of slag in each sample and its unreacted mass at each due curing age.

$$\alpha_{slag,t} = \frac{\text{weight of slag hydrated at time } t}{\text{original weight of slag}} = \frac{W_{t=0} - W_t}{W_{t=0}} \tag{4.1}$$

where $\alpha_{slag,t}$ is the degree of reaction of slag at curing age t. $W_{t=0}$ is the original weight of slag, while W_t is the weight of unreacted slag at curing age t.

Since the hydration product contains bound water, it should be removed from the sample when calculating the original weight of slag in each test. To solve the issue, we used TGA in this research to quantify the original mass of solid material(s) (also called ignited weight in literature [2]), which was taken as the mass of sample at 900 °C, with the amendment of the escaped CO_2 due to the decomposition of $CaCO_3$. Then the content of each raw material in the sample, e.g cement, slag and limestone in PBL paste, was calculated according to the mix proportion. Detailed results of bound water and mass of original raw material will be introduced in Sections 5.2.2 and 5.3.3 of Chapter 5.

However, the exact quantification of unreacted slag in the sample is complex. The principle of EDTA selective dissolution test is based on the assumption that all materials in the sample except for unreacted slag are dissolved by the EDTA solution, but there are three possible error sources if no proper correction is taken:

1. A minor part of cement and limestone cannot be dissolved by EDTA solution.

2. A few percent of slag is dissolved by EDTA solution.

3. The Mg related hydration product, typically hydrotalcite, does not dissolve but remains in the residue.

In order to eliminate these potential errors, correction for the above three types of errors is of importance to obtain the real weight of unreacted slag in each sample at each curing age. In this research, the following three types of corrections were taken into account to remove the corresponding three possible error sources:

1. Raw materials of cement and limestone powders were dissolved by EDTA solution using the same procedure as for real samples, aiming to find out the exact proportion of undissolved cement and limestone in EDTA solution.

2. Raw material of slag was dissolved by EDTA solution, quantifying the undissolved proportion of slag.

3. In terms of hydrotalcite in the residue, the amount was quantified by XRD/Rietveld experiment when analyzing the hydration products of each paste at different curing ages.

As soon as the original and unreacted mass of slag in a sample is known, the degree of reaction of slag is readily calculated using Eq. 4.1.

4.2.5 Sample Preparation, Test Procedure and Data Analysis of TGA Experiment

The freeze dried samples were first ground to small particles and passed through a sieve with aperture sized at 90 μm. Later, about 40 mg of the ground powder was exposed under an inert atmosphere (N_2) and increasing temperatures, ranging from 20 till 1100 °C at a rate of 10 °C/min (TA Instruments 2950). However, only the data points lower than 900 °C were analyzed in this research due to the crystallization of hydrated compounds occurring at higher temperatures [138]. In addition, the weight of slag is also susceptible to increase at temperature higher than 900 °C. TGA test on raw material slag did show mass increase at high temperature, and even higher than the initial mass, as shown in Fig. 4.3.

Data Analysis of TGA Experiment

Data registered by TGA equipment show the mass change of sample as a function of temperature. The mass loss is caused by the loss of water and the escape of CO_2 decomposed from $CaCO_3$.

From the experimental point of view, water in sample is classified as three types, i.e. free water, evaporable water and non-evaporable water. As mentioned in the procedure of stopping hydration, free water was presumed being removed by freezing drying and low temperature vacuum drying. The content of evaporable and non-evaporable water was measured by TGA. It is assumed in this research that the evaporable water is defined as driven off at temperature lower than 145 °C. Note that the evaporable water contains all physically bound water and partial chemically bound water, as researchers confirmed that adsorbed water can be lost between

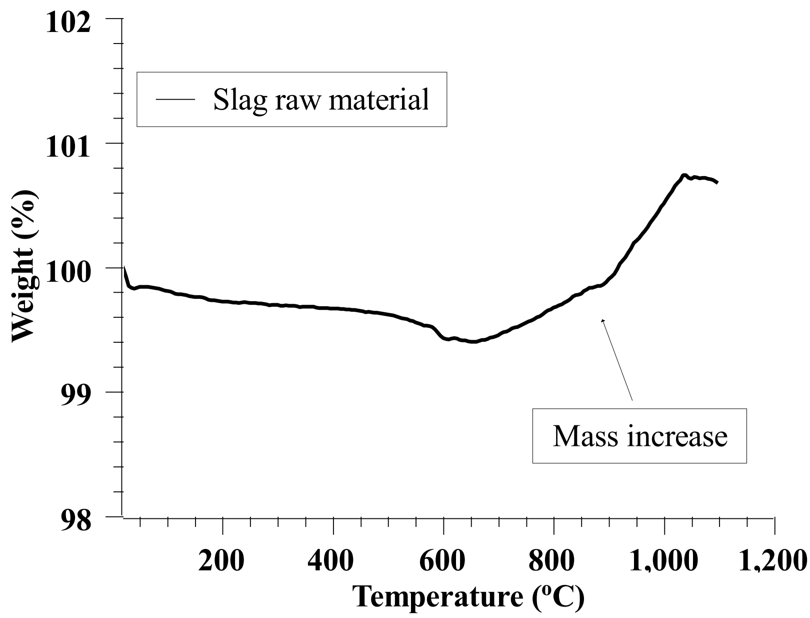

Figure 4.3: Mass of slag increased at high temperature of TGA test.

temperature 105 °C and 145 °C and chemically bound water of hydration products may be lost even at temperature lower than 105 °C [76]. Water loss occurred at temperature higher than 145 °C till 900 °C is thus defined as non-evaporable water.

Mass loss occurred between 450 °C and 550 °C is mainly caused by the decomposition of hydration product $Ca(OH)_2$, while that during the temperature range of 600-850 °C [139] represents the decomposition of $CaCO_3$ that gives out CO_2 (Eq. 4.2).

$$\mathrm{CaCO_3} \longrightarrow \mathrm{CaO} + \mathrm{CO_2} \tag{4.2}$$

The exact temperature ranges of decomposition of $Ca(OH)_2$ and $CaCO_3$ were determined by the corresponding DTG curves that were generated from the TG curves by the instrument, e.g. Fig. 4.4 shows the TG and DTG curves of the binary blended limestone cement sample (PL paste) after 91 days of hydration. The starting and end temperature of $CaCO_3$ decomposition can be easily obtained from the DTG curve, i.e. 704.6 and 759.3 °C corresponding to the starting and end points, respectively.

The correction of water contribution is also necessary to improve the result of TGA test. For example, if there were no $Ca(OH)_2$ between 450 °C and 550 °C in Fig. 4.4, the mass of the sample still decreases due to the loss of chemically bound water from C-S-H gel and other possible hydrates, which is also the case during the decomposition process of $CaCO_3$. In order to exclude the contribution from other phases rather than the targeted, i.e. $Ca(OH)_2$ and $CaCO_3$, a tangent method was applied to analyze the data. As illustrated in Fig. 4.5, the water evaporation rates during the decomposition of $CaCO_3$ are extrapolated from the starting and end of the decomposition. By extending two slope lines from the two points, i.e. the starting

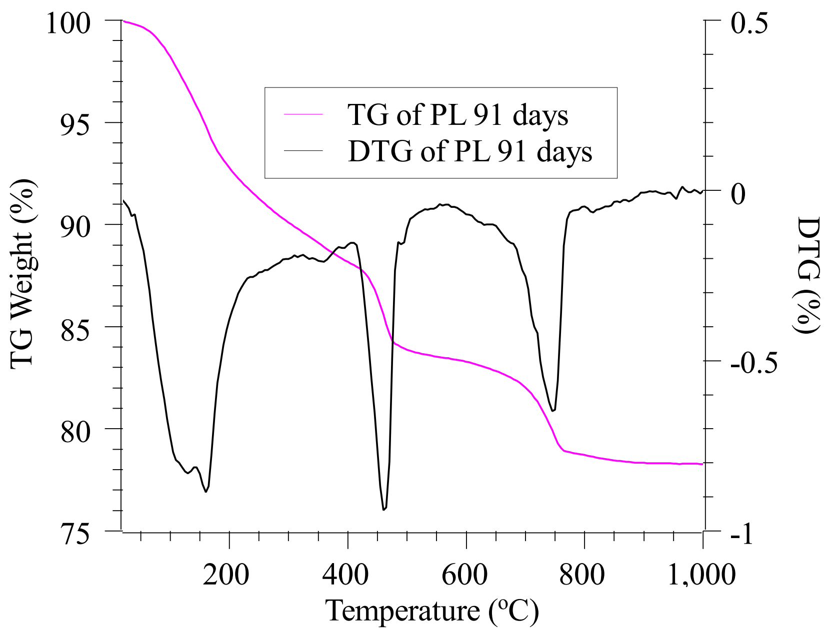

Figure 4.4: TG and DTG curves of limestone blended cement at 91 days.

and end temperature of decomposition of $CaCO_3$, the exact mass loss of $CaCO_3$ decomposition is determined as the weight drop between the slope lines at the position of inflection of the decomposition curve. Detailed introduction of this method can refer to [59]. The practical analysis process in this research was implemented by a so-called MARSH function embedded in the NETZSCH® Proteus Thermal analysis software, which is recommended to use if different reactions cause a total mass loss with non-horizontal start tangent.

When the mass loss of $Ca(OH)_2$ ($w_{\text{loss, 450-550 °C}}$) and $CaCO_3$ ($w_{\text{loss, 600-850 °C}}$) is known, their mass can be easily calculated by the following two equations:

$$w_{\mathrm{Ca(OH)_2}} = w_{\text{loss, 450-550 °C}} \times \frac{74}{18} \tag{4.3}$$

$$w_{\mathrm{CaCO_3}} = w_{\text{loss, 600-850 °C}} \times \frac{100}{44} \tag{4.4}$$

Since $Ca(OH)_2$ is only formed by the hydration of cement, its amount is normalized by the mass of original cement in order to make comparison among the four groups of samples. As already mentioned in the determination of original mass of slag from EDTA test (Section 4.2.4), the original mass of cement in each sample was also quantified by TGA in the same way. TGA measured the total bound water in each hydrating sample, thus the original mass of raw materials in the sample was obtained. According to the mix design, each component can be calculated.

Influence of CO_2 during Sample Preparation on TGA Experiment

As cautioned by [2], cement samples are susceptible to carbonation due to the CO_2 in the air reacting with $Ca(OH)_2$ and C-S-H gel. The sample preparation for TGA test was also performed

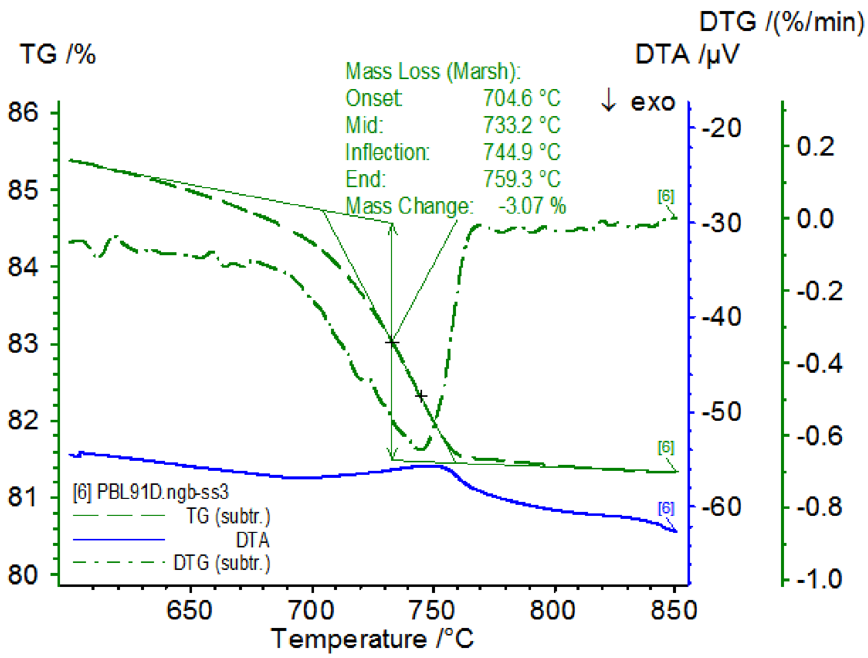

Figure 4.5: Tangent method was applied to analyze the TGA result of limestone blended cement hydrated after 91 days.

in lab with ambient air. To check to what extent the CO_2 in the ambient air influences the sample, a set of comparison experiments was carried out. One part of PBL sample hydrated after 28 days was ground in a glove box filled with N_2, which created a CO_2-free environment, the second part was prepared in the laboratory and exposed to the ambient air for 4 hours and 30 days, respectively. Then the three copies of powder were analyzed by TGA test as aforementioned.

Fig. 4.6 shows the TGA curves of the three samples. It can be seen that there is no difference between the results of samples prepared either in N_2 or air and being exposed for 4 hours. The sample being exposed in ambient air for 30 days indeed shows the mass ratio of $Ca(OH)_2$ in sample decreased from 2.80% to 2.60%. The CO_2 in the lab has no influence on sample preparation within short period, e.g. 4 hours. According to the comparison, we are confident that the samples prepared (grinding) for TGA test in this research were not affected by the CO_2 in the lab, since the grinding process takes only several minutes. Actually, the carbonation of CO_2 with $Ca(OH)_2$ and C-S-H gel needs water, but the samples for TGA test were already freeze dried, implying that no free water was available in the sample. The only source of water for carbonation is from the air humidity. The dry air in the laboratory and short period of grinding made the carbonation hardly to occur. But for long period of exposure to air, the carbonation is still observable, as shown in Fig. 4.6.

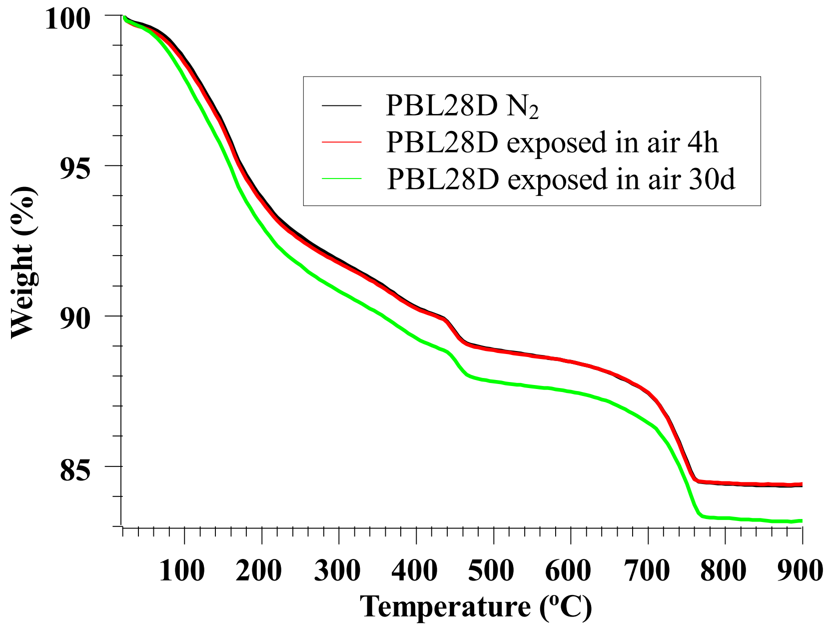

Figure 4.6: The comparison of PBL sample prepared in N_2 and CO_2-free environment and tested by TGA method.

4.2.6 Sample Preparation for Isothermal Calorimetry Test

The method of isothermal calorimetry test in this chapter is the same as applied in the previous chapter that investigated the reaction kinetics of slag activated by $Ca(OH)_2$ solution (Section 3.3). The difference is that for each test an ampule was filled with 14 g paste which was mixed according to the mix design, in addition, isothermal calorimetric tests were performed at 20 °C for 7 days.

4.3 Experimental Results and Discussion

4.3.1 Results of XRD/Rietveld Test

The amount of unhydrated cement clinker of Portland cement in all pastes at different curing ages was quantified by XRD/Rietveld method. Although each phase of clinker, i.e. C_3S, C_2S, C_3A and C_4AF, was quantified individually, it is difficult to compare the content of each phase among different pastes at same curing age due to the following three reasons:

1. The accuracy of XRD/Rietveld analysis is moderate, which is around ± 2%.

2. The content of cement in slag blended paste is low (30 wt%), implying the absolute amount of unreacted clinker in PB and PBL pastes is even less and difficult to be quantified.

3. Possible overlap occurs between peaks of XRD patterns, e.g. it is difficult to distinguish C_3S and C_2S as shown in Fig. 4.7 though quantitative results can be obtained by Rietveld

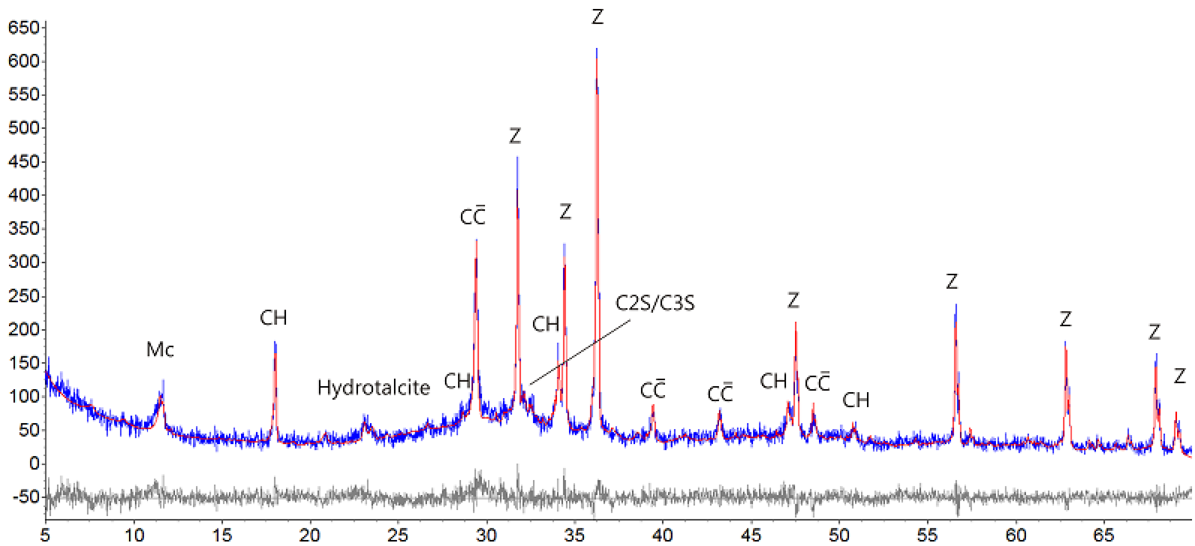

Figure 4.7: XRD patterns of hydrating blended cement paste analyzed by Rietveld method, Z = Zinc oxide, Mc = Monocarboaluminate, CH = $Ca(OH)_2$, $C\overline{C}$ = $CaCO_3$.

refining.

In order to better interpret the XRD/Rietveld results of cement clinker, amounts of C_3S and C_2S were summed up as *calcium silicate phases* and expressed by % of the original mass of cement. In the same way, the amounts of C_3A and C_4AF were summed up as *calcium aluminate phases*.

Kinetics of Calcium Silicate Phases (C_3S + C_2S)

Fig. 4.8 shows the content of calcium silicate phases in samples at different ages relative to the original mass of cement clinker. The hydration of calcium silicate phases in all pastes proceeded considerably fast in the first 7 days, e.g. the original content of C_3S + C_2S in the raw material cement was 74.49%, it decreased to 35.31%, 27.07%, 39.69% and 38.76% after 7 days of hydration in PC, PL, PB and PBL pastes, respectively, while the corresponding values were 20.91%, 18.42%, 30.33% and 32.71% at after 91 days of hydration in PC, PL, PB and PBL, 91 days, respectively.

For cement pastes containing slag, i.e. PB and PBL, the amount of unreacted calcium silicate phases was constantly higher than that of PC and PL pastes during the whole age, showing the relatively slow hydration of calcium silicate phases in PB and PBL pastes, which indicates that the hydration of calcium silicate phases was suppressed by the presence of slag. This is completely different from the observation of Seiichi Hoshino et al. [126], who claimed that the hydration of C_3S in binary (slag:cement:water = 0.4:0.6:0.3, by mass) and ternary (slag:cement:limestone:water = 0.4:0.6:0.04:0.3, by mass) slag blended cement pastes was accelerated by slag up to 28 days of hydration. However, the experimental investigation of

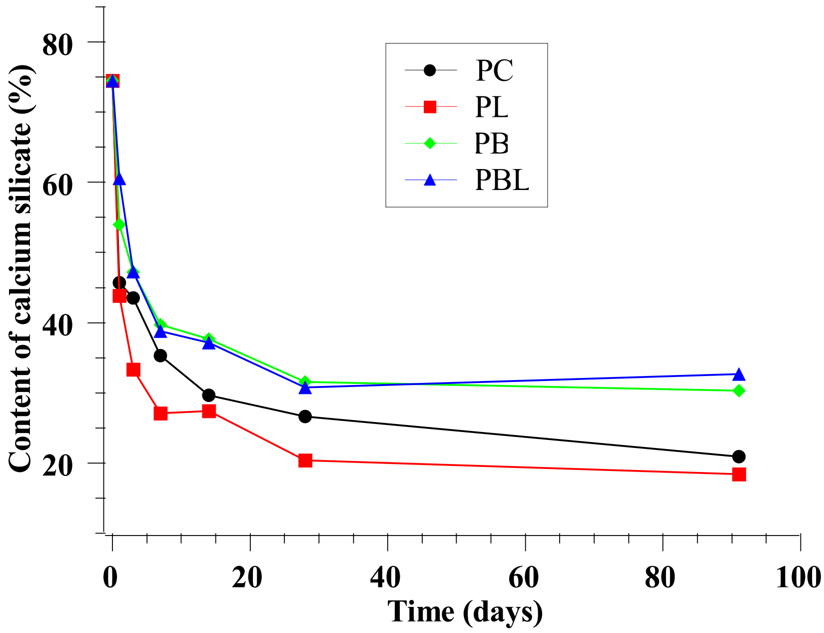

Figure 4.8: Content of calcium silicate phases ($C_3S + C_2S$) of samples at different ages tested by XRD/Rietveld, the content is the mass ratio of $C_3S + C_2S$ to the original cement in each sample.

Kocaba [59] shows that the substitution of cement by slag seems to result in a delay in the hydration of belite in the first days.

Comparing the content of calcium silicate phases in PL paste to that of PC paste, it is clear that the presence of limestone accelerated the hydration of calcium silicate phases at both early and late ages. However, the acceleration effect of limestone on hydration of calcium silicate phases did not occur in PBL paste, since the content of calcium silicate phases in PB and PBL did not show much difference over the whole curing age except for the value at 1 day.

For the combination of limestone and slag in the ternary blended cement paste, i.e. PBL, the hydration of calcium silicate phases was slightly hindered by the presence of limestone at early age (less than 3 days) if compared with PB paste, since there was 53.99 wt% and 60.57 wt% unhydrated calcium silicate phases in PB and PBL pastes at 1 day, respectively. However, the higher content of calcium silicate phases in PBL paste at 1 day than PB paste might be an experiment error or sample variation. Considering the accuracy of XRD/Rietveld analysis, we did not observe distinct difference of kinetics of calcium silicate phases between PB and PBL pastes at later ages, i.e. after 3 days of curing.

Kinetics of Calcium Aluminate Phases ($C_3A + C_4AF$)

Fig. 4.9 demonstrates the amount of calcium aluminate phases of all samples relative to the original amount in each sample from the start of mixing, i.e. prior to hydration, to 91 days of hydration quantified by XRD/Rietveld analysis. Similar to the case of calcium silicate phases, the hydration of calcium aluminate phases proceeded fast during the first 14 days. Calcium aluminate phases in all blended pastes, i.e. PL, PB and PBL pastes, showed faster hydration

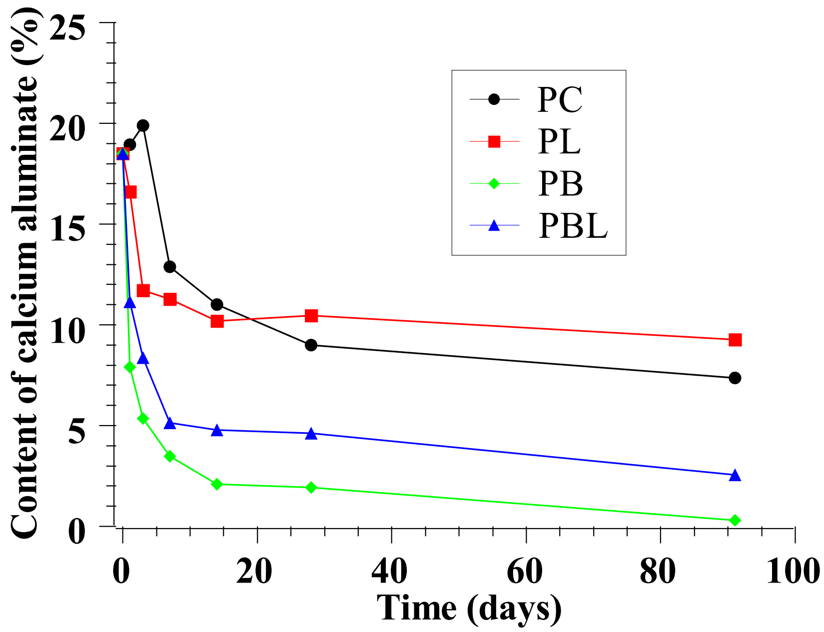

Figure 4.9: Content of calcium aluminate phases (C_3A + C_4AF) of samples at different ages tested by XRD/Rietveld, the content is the mass ratio of C_3A + C_4AF to the original cement in each sample.

kinetics compared with that of neat cement paste (PC) at whole testing ages, with the exception of PL paste after 14 days, as results show the ratio of unreacted calcium aluminate phases in PL paste was constantly higher than PC paste after 14 days of hydration.

The presence of slag significantly enhanced the hydration of calcium aluminate phases at both early and late ages. Although the addition of limestone in PL accelerated the hydration of calcium aluminate phases up to 14 days compared to that of PC paste, the combination of limestone and slag in PBL paste showed distinct negative influence on the hydration kinetics of calcium aluminate phases, as the content of calcium aluminate phases in PBL paste was constantly higher than that in PB paste at all testing ages.

Degree of Hydration of Cement Clinker in all Pastes

The term "degree of hydration of cement" is traditionally defined as *the ratio of the amount of cement that has hydrated at time* ***t*** *relative to the original amount of cement* [3]:

$$\alpha(t) = \frac{\text{amount of cement that has reacted at time } t}{\text{total amount of cement at time } t = 0} \tag{4.5}$$

In this research, the original content of clinker (C_3S + C_2S + C_3A + C_4AF) of cement quantified by XRD/Rietveld analysis was 92.98 wt%. Since the amount of other components of cement was small (7.12 wt%) and difficult to be quantified by XRD/Rietveld, we focused on the hydration of clinker instead of the whole cement. For this reason, we defined a term "degree of hydration of clinker". It is the ratio of reacted amount of clinker at time *t* to the original amount

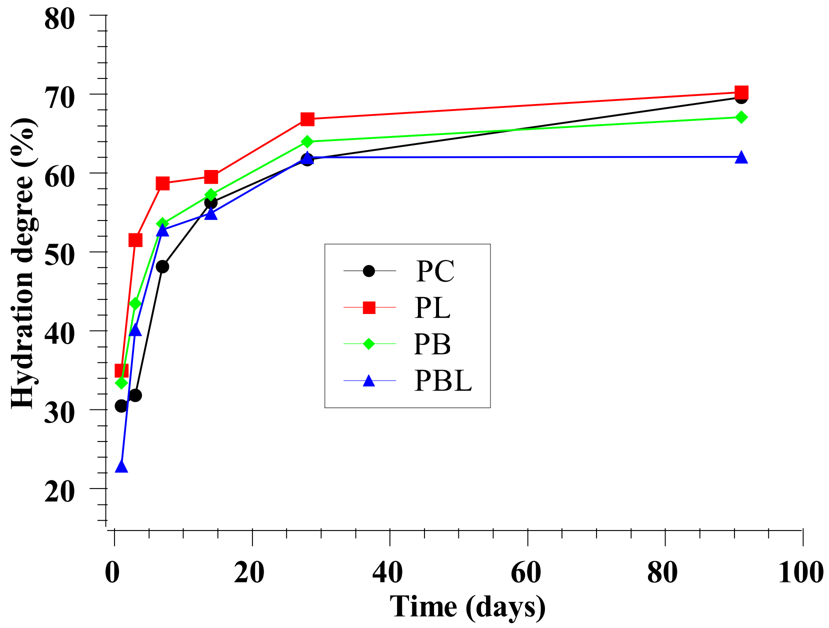

Figure 4.10: Degree of hydration of cement clinker in all samples at different ages measured by XRD/Rietveld.

prior to hydration, which is mathematically expressed as Eq. 4.6. The degree of hydration of clinker approximately represents the degree of hydration of cement if not exactly.

$$\alpha(t) = \frac{\text{amount of clinker that has reacted at time } t}{\text{total amount of clinker at time } t = 0} \tag{4.6}$$

Fig. 4.10 plots the degree of hydration of cement clinker in all samples from 1 day to 91 days of hydration. Most of the hydration of cement occurred at early age, e.g. at least 22 wt% of clinker of PBL paste reacted after 1 day of hydration and as high as 59 wt% of clinker of PL hydrated within 14 days. Hydration of cement clinker in all blended pastes (PL, PB and PBL) after 14 days proceeded noticeably slow compared with the first 14 days.

Hydration of cement clinker at early ages, i.e. less than 14 days, was accelerated by the presence of slag and/or limestone except for the value of PBL at 1 day, but the relatively fast increase of hydration degree of cement clinker in PC at later age shows the relatively slow hydration process of clinker at later age in the three blended cement pastes, i.e. PL, PB and PBL.

It is clear that the single addition of limestone accelerated the hydration of cement clinker over the whole curing age. The acceleration effect was typically significant in the first 14 days, as it is confirmed by the fact that the hydration degree of clinker of PL paste was much higher than the corresponding PC up to 14 days of curing age. However, the hydration degree of cement clinker finally reached almost the same level as PL paste after 91 days of hydration.

Compared with PC paste, the single addition of slag in PB paste, i.e. 70 wt% of cement replaced by slag, exhibited positive influence on the hydration kinetics of cement clinker. The hydration degree of cement clinker in PB paste was constantly higher than that of PC paste at all tested ages except for 91 days, showing the acceleration effect on hydration of cement clinker caused by slag. However, the acceleration effect brought by slag on PB paste was not as strong as that by limestone on PL, as the degree of hydration of cement clinker in PL is always higher than that in PB at all tested ages.

The degree of hydration of cement clinker in PBL paste is complex compared with any other paste in terms of the hydration kinetics of cement clinker. The degree of hydration of cement clinker in PBL paste was the lowest at 1 day among the four pastes. Only 22.88 wt% of clinker in PBL was hydrated at 1 day, which was significantly low than the others. Compared with the acceleration effect on hydration of cement brought by single addition of limestone or slag, i.e. PB or PL paste, the combination of limestone and slag in PBL slightly but clearly hindered the hydration of cement at 1 day, typically hindered the hydration of calcium silicate phases, as shown in Fig. 4.8. A possible reason is that the combination of slag and limestone brought relatively large amount of aluminate phase and $CaCO_3$. The coexistence of aluminate phase and $CaCO_3$ favors the formation of monocarboaluminate hydrates. The monocarboaluminate hydrates may be precipitated on the surface of cement particles, which hindered the hydration of calcium silicate phases to a certain extent.

However, the result shows an obvious acceleration effect on hydration of cement clinker in PBL paste during the curing age from 1 to 14 days, e.g. 40.18 wt% and 52.81 wt% of clinker in PBL paste have reacted after 3 and 7 days of hydration, respectively, which were both higher than the corresponding values of PC even considering the accuracy of XRD/Rietveld analysis. But the hydration of cement clinker in PBL paste had no progress over the curing age from 28 to 91 days, as the hydration degree of clinker only changed from 61.99 wt% to 62.08 wt% at the two ages, while the corresponding values of PC at these two ages increased from 61.68 wt% and 69.59 wt%, respectively. The hydration degree of cement clinker in PBL paste at 91 days is also the lowest compared with the other three types of pastes, i.e. PC, PL, and PB.

Based on the comparison with reference pastes, i.e. PC, PL and PB, the combination of limestone and slag in ternary blended cement paste PBL paste did not show synergistic effect on the hydration kinetics of cement clinker. Instead, the hydration kinetics of cement clinker in PBL was the lowest at both 1 and 91 days comparing with any other type of paste in this research. As revealed in the analysis of hydration of calcium silicate phases (Fig. 4.8) and calcium aluminate phases (Fig. 4.9), the presence of slag hindered the hydration of calcium silicate phases, and the coexistence of slag and limestone impeded the hydration of calcium silicate phases. Therefore, the relatively low hydration degree of cement in PBL is mainly caused by the combination of negative influence brought by slag and limestone on hydration of calcium silicate phases and calcium aluminate phases, respectively.

It should be noted that XRD/Rietveld method has a moderate accuracy and is unable to perform continuous measurement. In order to investigate the hydration behavior at early age, e.g. the first 7 days, isothermal calorimetry method was applied in the later context of this chapter.

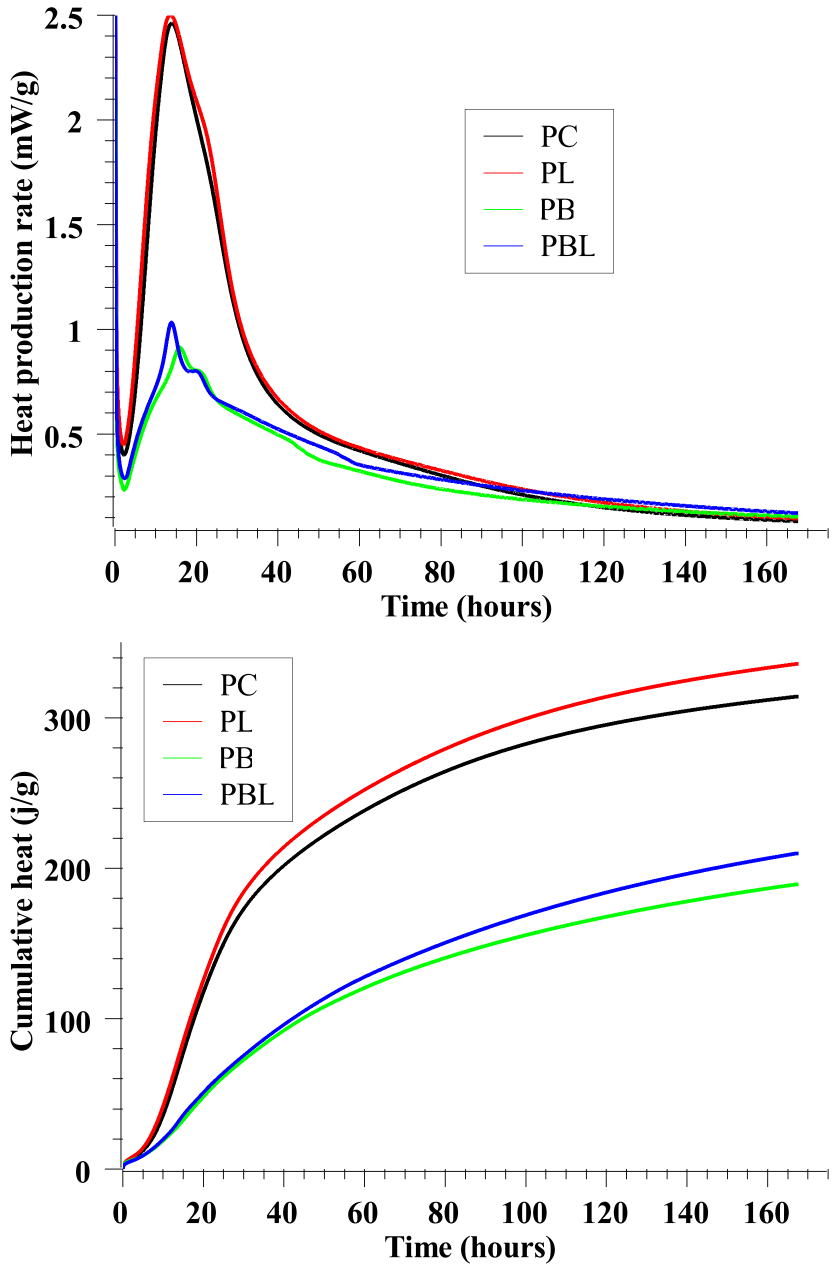

Figure 4.11: Rate of heat evolution (top) and cumulative heat evolution (bottom) of all pastes hydrated up to 168 hours tested by isothermal calorimetry method, data of PC and PL are normalized by the original mass of cement, PB and PBL by the original total mass of cement and slag.

4.3.2 Results of Isothermal Calorimetry Test

Rate of Heat Evolution

Fig. 4.11 presents the rate of heat evolution and cumulative heat evolution of samples recorded up to 168 hours (7 days) of the four types of pastes. The rate in PC and PL pastes is normalized by the original mass of cement. It can be seen that the rate of heat evolution of cement in PL paste was accelerated by the addition of limestone during the whole testing age, as indicated by

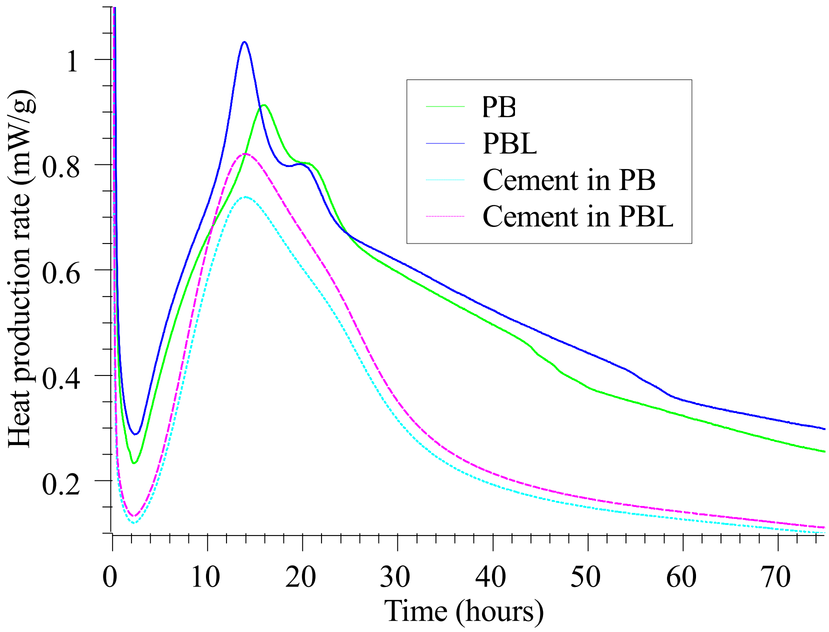

Figure 4.12: Slag and limestone contributed heat release even at early age (the heat rate is normalized by the mass of cementitious materials, i.e. cement + slag), the heat rate of cement in PB and PBL is proportioned from PC paste based on its cement mass ratio.

both peaks in induction and acceleration periods, which agree well with the results of [67] that the addition of limestone increased the heat rate in both C_3S and cement pastes.

It is worth to note that a distinct shoulder peak occurred in PL paste after around 24 hours of hydration, which may be the newly formed ettringite as suggested by [2]. The shoulder in PL paste was apparently enhanced by the addition of limestone probably due to its nucleation site effect which offered sites for the precipitation of crystalline hydration products, i.e. ettringite and $Ca(OH)_2$.

As shown by the results, the heat rates of PB and PBL pastes were much lower than PC and PL pastes in the first 90 hours, apparently caused by the dilution effect by the large amount of slag addition. Two reasons may account for the lower hydration rate of slag blended cement pastes compared to pastes without slag at early age. On the one hand, the latent hydraulic material slag requires the activation of $Ca(OH)_2$ which etches the protective glass layer of slag particles. On the other hand the reaction speed of slag itself is typically slower than cement, as shown by the lower k values of slag particles than cement particles in Chapter 3.

However, detailed analysis shows slag in blended cement contributed heat release even at early age. Fig. 4.12 plots the heat rates of PB and PBL comparing with the proportioned heat rate of cement from PC paste according to the cement mass ratio in PB and PBL pastes, respectively. It can be seen from the comparison that the heat rate of PB and PBL is remarkably higher than the corresponding diluted curves even in the very early age, which implies the positive contribution of slag and limestone to the heat release in both PB and PBL pastes.

Comparing with the results of PC and PL paste, the shoulder of heat rate in the deceleratory period became more recognizable in both PB and PBL pastes. It may be partially explained by the stronger nucleation site effect [63] as it was in PL paste, but it may be mainly caused by the main activation of slag reaction, as Gruyaert [140] stated that this peak is attributed to the reaction of slag that is initiated when the cement hydration has liberated a sufficient amount of $Ca(OH)_2$ and the correct alkalinity is reached. It is hard to link this shoulder with the conversion of ettringite ($\mathrm{C_6A\overline{S}_3H_{32}}$) to calcium monosulphoaluminate hydrate ($\mathrm{C_4A\overline{S}H_{12}}$) with the release of extra heat, because the $CaCO_3$ content in PB paste is quite limited and its content almost did not change as measured by TGA which will be presented in Fig. 4.14.

Another less distinct but noticeable shoulder of heat rate occurred between 40 and 60 hours in PBL paste, which was barely observable in PC and PL pastes. The shoulder in PBL may be caused by the formation of monocarboaluminate ($\mathrm{C_4A\overline{C}H_{11}}$) [69, 141, 142] in the presence of $CaCO_3$ (Eq. 4.7), because monocarboaluminate is thermodynamically more stable than calcium monosulphoaluminate [69]. The reaction in Eq. 4.7 can produce extra heat evolution, resulting in the prolonged second noticeable shoulder in the heat rate curve of PBL paste.

$$\mathrm{3C_4A\overline{S}H_{12} + 2C\overline{C} + 18H \longrightarrow C_6A\overline{S}_3H_{32} + 2C_4A\overline{C}H_{11}} \tag{4.7}$$

As shown in Fig 4.11, the heat rate of slag blended pastes (PB and PBL) surpassed samples containing no slag (PC and PL) after around 90-150 hours of hydration, which was even more evident in the case of PBL paste. The comparable or even higher heat rate of slag blended cement pastes denotes that the hydration of slag was greatly activated and proceeding at least after about 100 hours in this research, which of course does not necessarily mean there was no reaction of slag within the first 100 hours. Work of [113] reports that the accelerated hydration peak of slag reaction activated by various activators appears within the first 48 hours.

Comparing with the result of PB paste, PBL showed higher heat rate during the whole 168 hours, demonstrating the positive contribution of heat caused by the addition of limestone. Moreover, the peak of heat rate in PBL paste during acceleratory period appeared after 13.8 hours of hydration, which was 2.2 hours earlier and significantly higher than that of PB paste, though it is still later than alkali-activated slag [143] (several hours). Compared with the acceleration effect brought by limestone in PL paste, the relatively earlier and higher peak of heat rate that occurred in PBL paste indicates the more pronounced influence of limestone coexisted with slag in ternary blended paste, i.e. PBL. This enhanced influence by the combined slag and limestone agrees with the investigation of [127] which also reported higher heat rate in ternary blended cement paste (cement + slag + limestone) comparing with binary blended systems.

Cumulative Heat Evolution

The cumulative heat evolution of all pastes in the first 168 hours is illustrated in Fig. 4.11. Cumulative heat evolution of PL paste was constantly higher than that of PC, confirming the acceleration effect caused by the presence of limestone, which agrees well with the higher degree of hydration of cement clinker in PL paste compared with PC paste, as shown in Fig. 4.10. The difference between the two sets of cumulative heat curves became even larger as hydration proceeded.

Except for the initial several hours due to a possible strong exothermic wetting process of slag occurred in PB, the cumulative heat evolution of PBL was constantly higher than that of PB paste, showing the positive contribution of heat evolution brought by the addition of limestone as the case in PL paste.

However, unlike PC and PL pastes, it is difficult to conclude that the higher heat rate and cumulative heat evolution in PBL paste was an acceleration effect on the hydration kinetics of cement in the presence of limestone, since the hydration degree of cement clinker in PBL paste was constantly lower than PB paste over the whole age, i.e. from 1 to 91 days, as shown by XRD/Rietveld analysis results in Section 4.3.1.

It can be seen from Fig. 4.11 that the total cumulative heat evolution of slag blended pastes were much lower than that of PC and PL pastes over the whole testing age, e.g. the total heat evolution of PC paste reached 335.9 J/g after 168 hours of hydration, while the corresponding value of PB was only 189.4 J/g, which was the lowest among the four types of pastes. Although the heat evolution rates of PB and PBL exceeded that of PC and PL after around 90 hours of hydration, the lower cumulative heat evolution of slag blended pastes is apparently the result of dilution effect brought by slag and limestone at early age (< 7 days).

In terms of the ternary blended PBL paste, it has to be emphasized that it is still unclear whether the higher cumulative heat evolution of PBL paste than PB was caused by the reaction between limestone and cementitious materials or just the single accelerated hydration according to the isothermal calorimetry result. This question will be discussed in Section 4.3.3 based on the reaction degree of slag at different ages, and will be also covered in Chapter 5 in which the hydration products of all four groups of pastes were investigated.

4.3.3 Degree of Reaction of Slag Tested by EDTA Selective Dissolution Test

Fig. 4.13 presents the reaction degree of slag in slag blended pastes (PB and PBL) tested by EDTA selective dissolution method. The degree of reaction of slag in both PB and PBL pastes was only about 8 wt% and 35 wt% of slag reacted after 1 and 91 days of hydration, respectively, which is generally much lower than that of cement clinker of all pastes at all ages. However, the curves in Fig. 4.13 show an increasing trend of slag hydration at later age for both PB and PBL pastes comparing to the relatively flat curves of cement clinker as shown in Fig. 4.10, which is readily interpreted as that slag is latent cementitious material with the main part of hydration undergone at later age.

The degree of reaction of slag tested by EDTA method in this research agrees well with data from literature [144]. Taylor [2] summarized that at water to solids ratios of 0.4-0.6 and 20

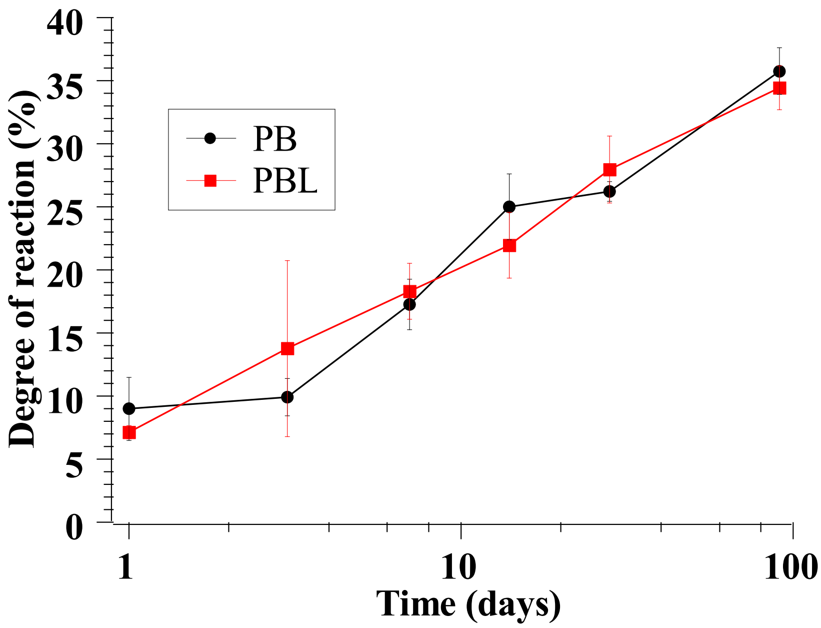

Figure 4.13: Degree of reaction of slag in slag blended cement pastes tested by EDTA method at different ages.

°C 30-55 wt% of the slag reacts in 28 days and 45-75 wt% in 1-2 years. Ye [45] also reported similar results using BSE image analysis and EDTA method.

It is worthwhile to note that there was already a noticeable amount of reacted slag even just after 24 hours of hydration. Using BSE image analysis method, Zhou et al. [145] performed a series of experiments on slag blended cement pastes to quantify the hydration degree of slag. In their results, two slag pastes with same slag replacement level as this research (70 wt% of cement replaced by slag) and two water to powder ratios (0.4 and 0.5) show reaction degree of 8.0 wt% and 7.3 wt% at 1 day, respectively, which agrees very well with the results from this research, showing the reliability of EDTA method on the one hand and confirming a noticeable amount of reacted slag even within 24 hours. In addition, their results reported that the reaction degree of slag at 1 day increases as slag replacement level decreases.

In terms of the influence of limestone addition on reaction kinetics of slag in PBL paste, there was no fixed trend between the reaction degrees of slag in PB and PBL pastes as shown in Fig. 4.13, since the reaction degree of slag in PBL paste was only slightly higher than that of PB paste at the ages of 3 and 28 days. Nevertheless, when considering the errors and accuracy of the data in Fig. 4.13, it is hard to see the difference between them. Limited results of Seiichi et al. [126] showed that 4 wt% of limestone addition did not have significant influence on the hydration kinetics of slag in ternary blended cement paste, in which the paste was mixed at the ratio of cement:slag:limestone:water = 60:40:4:30 and cured at 20 °C.

Section 4.3.2 stated that the cumulative heat evolution in PBL pastes was higher than PB paste measured by TAM Air test (Fig. 4.11). Considering the nearly identical reaction degree of slag and the lower hydration degree of cement clinker in PBL paste compared with PB paste

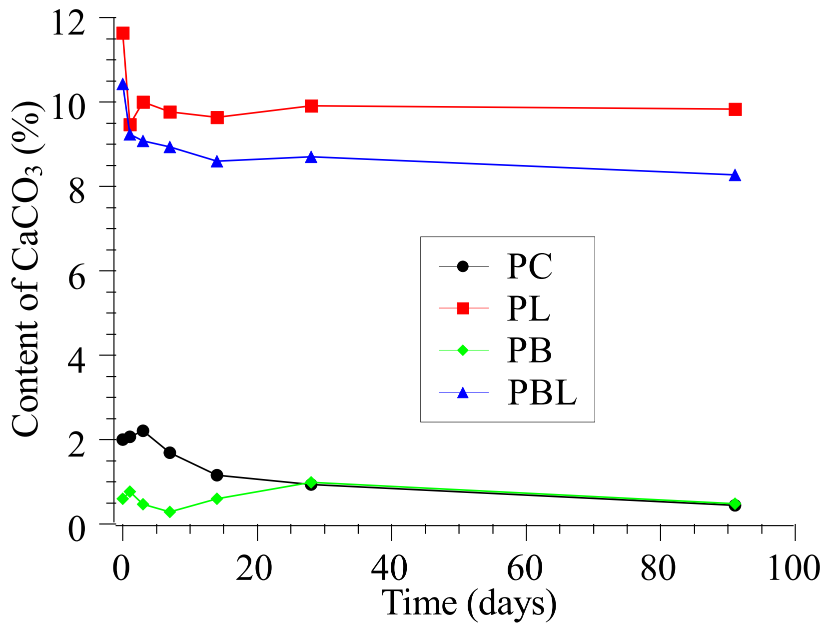

Figure 4.14: Content of $CaCO_3$ in limestone blended cement at different ages tested by TGA method. Data are normalized by the total original mass of samples.

(Fig. 4.10), the higher cumulative heat evolution in PBL paste is unlikely caused by accelerated slag reaction and cement hydration. Therefore, the reaction between limestone and aluminate phase may be responsible to the higher cumulative heat evolution.

4.3.4 Content of $CaCO_3$ Tested by TGA

Figs. A.5 to A.8 show the TG and DTG curves of the four types of samples tested at different curing ages. The mass loss occurring in the temperature range of 600-850 ° in TG and DTG curves clearly show the decomposition of $CaCO_3$ in both PL and PBL pastes, while it was barely distinguishable in PC and PB pastes.

It should be noted that the cement (CEM I 52.5 N) used in this research contained 2.0 wt% $CaCO_3$ measured by TGA. This amount of $CaCO_3$ is allowed according to the European standard [13]. TGA test also shows that 98.3 wt% of limestone in this research was $CaCO_3$. Since the content of $CaCO_3$ in cement is at the same order of magnitude of the limestone that was added in PL and PBL pastes (10 wt%), it definitely should be counted in the content of $CaCO_3$ which was analyzed by TGA test during all testing ages. According to the content of $CaCO_3$ in raw materials, i.e. cement and limestone, the original mass of $CaCO_3$ in PL and PBL pastes was $90\% \times 2.0\% + 10\% \times 98.3\% = 11.63\%$ and $30\% \times 2.0\% + 10\% \times 98.3\% = 10.43\%$ of the total original solid raw materials, respectively.

Based on the TGA measurements, the content of $CaCO_3$ of each paste at different curing ages was calculated. Fig. 4.14 shows the content of $CaCO_3$ in four types of pastes from 0 to 91 days of hydration quantified by TGA experiment.

Comparing with the relatively stable content of $CaCO_3$ in PC paste over the whole curing age, the content of $CaCO_3$ in PL sharply decreased from the original 11.63 wt% of all solid raw materials to 9.47 wt% after 1 day of hydration, and fluctuated afterwards between 9.63-10 wt%. Similar trend of $CaCO_3$ change was also observed in PBL paste. Over the whole curing age of 91 days, the reacted content of $CaCO_3$ was approximately 1.6-2.2 wt% (i.e. 1.6-2.2 g $CaCO_3$ was reacted) of the total solid raw materials except for PB paste which had remarkably low content of $CaCO_3$ in raw materials (0.6 wt%), which generally agrees with the reported data [2, 64] that the maximum quantity of $CaCO_3$ that can react appears to be about 2-3 wt% with most cements.

There is one difference of the limited $CaCO_3$ reaction among PC, PL and PBL pastes. The main part of $CaCO_3$ reaction occurred at the very early age (1 day) in the cases of PL and PBL pastes, which could be caused by the relatively large supply of limestone in PL and PBL pastes, implying larger surface area of limestone particles for the reaction between $CaCO_3$ and aluminate phase. However, the presence of $CaCO_3$ from raw cement in PC also lead to a detectable amount of $CaCO_3$ reacted with clinker within the first 14 days of hydration. Compared with PL and PBL pastes, the less distinct decrease of $CaCO_3$ in PC paste is probably due to its limited content of aluminate phase and $CaCO_3$.

4.4 Conclusions

In this chapter, the hydration kinetics of four groups of pastes, i.e. PC, PL, PB and PBL pastes, were studied by systematic experiments. According to the analyzed results, the main conclusions are drawn as follows.

1. The hydration of calcium silicate phases of cement in ternary blended pastes was enhanced by the presence of limestone powder, but hampered by the addition of slag.

2. The hydration of calcium aluminate phases of cement was greatly accelerated by the addition of slag. It was also enhanced by the presence of limestone powder in binary blended limestone cement paste at early age. However, the coexistence of limestone powder with slag in ternary blended cement paste shows that limestone restrains the hydration of calcium aluminate phases of cement.

3. The degree of hydration of cement clinker is distinctly accelerated by the single addition of slag or limestone powder within 91 days of hydration. The coexistence of slag and limestone in ternary blended cement accelerated the hydration of cement clinker from 1 to 14 days, but lowered the degree of hydration of clinker after 91 days of hydration compared with other pastes.

4. The isothermal calorimetry test indicates the addition of limestone powder in both binary and ternary blended cement pastes had positive effect on the rate of heat evolution of hydration. Slag reduced the cumulative heat evolution of slag blended cement pastes at

early ages due to its low reactivity. The reaction of slag was activated even within the first 24 hours.

5. The degree of reaction of slag in blended cement pastes was about 8 wt% and 35 wt% at 1 and 91 days of curing, respectively, and it was not influenced by the addition of limestone powder.

6. TGA test shows a small amount of limestone, i.e. around 1.6-2.2 g of $CaCO_3$ per 100 g of solid raw materials has reacted, mainly at early age.

Chapter 5

The Hydration Products of Ternary Blended Cement Paste

5.1 Introduction

The hydration kinetics of the four types of pastes was investigated in Chapter 4, which mainly focused on the variation of amounts of raw materials over the hydration process. Apart from the reactants, investigation of the hydration products of cementitious materials is also of paramount importance. The formation of hydration products generates the microstructure which is the source and matrix for mechanical strength on the one hand, and characterizing the hydration products helps understand the chemical reaction mechanism on the other hand.

Similar to a large body of research on hydration products of Portland cement over the development of cement chemistry, much work has been performed on the hydration of binary blended cements such as limestone blended cement, slag bended cement and fly ash blended cement. However, as aforementioned in Section 2.4, limited research work has been performed on the hydration products of ternary blended cements probably because investigation of hydration products on ternary blended systems is complex due to the interaction occurring among each other and the lack of adequate experimental techniques.

In this chapter, the hydration products of the aforementioned four types of pastes, i.e. PC, PL, PB and PBL, were investigated by XRD/Rietveld analysis. The bound water and $Ca(OH)_2$ in hydration products were analyzed by TGA method. In addition, the pore solution of the hydrating pastes was extracted at different ages and analyzed by ion chromatography method, aiming to study the chemistry information of pore solution to better understand the hydration products.

5.2 Materials, Mix Design and Analysis Methods

The materials and mix design used in this chapter were exactly as same as in Chapter 4. Experimental methods of XRD/Rietveld and TGA used in Chapter 4 were also applied in this chapter. Specifically, XRD/Rietveld was used to detect and quantify the types and amount of hydration products formed in each paste at different curing ages, and TGA was used to investigate the amount of water and $Ca(OH)_2$ from hydration products.

5.2.1 Quantification of Calcium Silicate Hydrate

Besides all crystalline phases of hydration products and unreacted clinker phases (Chapter 4) being quantified by XRD/Rietveld method, the total amount of amorphous phases was able to be quantified by XRD/Rietveld method as well, which is mainly regarded as C-S-H gel if no other amorphous phase exists.

However, the slag blended cement pastes (PB and PBL pastes) contained a large amount of slag in this research, so the amorphous phases in these two pastes quantified by XRD/Rietveld definitely included unreacted slag, thus another method was needed to know the amount of unreacted slag at each age, which was implemented by EDTA method as stated in Chapter 4.

Combining the degree of reaction of slag from the EDTA test results and the total amount of amorphous phase by XRD/Rietveld analysis, we calculated the amount of unreacted amorphous slag, thus the amount of C-S-H gel was finally obtained by deducting the content of unreacted slag, though the C-S-H gel is still the total amount formed by the hydration of both cement and slag.

5.2.2 Quantification of Water and $Ca(OH)_2$

The content of evaporable and non-evaporable water (w_n) of hydration products was quantified by TGA method. The sum of evaporable and non-evaporable water was also used to estimate the original amount of raw material in each sample after different hydration time, as aforementioned in Section 4.2.4 of Chapter 4.

In addition, although the content of $Ca(OH)_2$ is able to be quantified by XRD/Rietveld method, the result is probably underestimated because of the carbonation of $Ca(OH)_2$ with CO_2 during the sample preparation for XRD test, i.e. wet grinding. Moreover, the content of $CaCO_3$ (limestone) may be overestimated by XRD/Rietveld method because of the carbonation from $Ca(OH)_2$. In order to obtain more reliable results, the content of $Ca(OH)_2$ in hydration products was quantified by TGA in the same way that quantified the content of $CaCO_3$ in Section 4.2.5 of Chapter 4.

Figure 5.1: The device to extract pore solution of hardened cement paste.

5.2.3 Extraction of Pore Solution and Ion Concentration Analysis

In order to analyze the types and concentrations of ions in the pore solution of hydrating pastes, pore solution was extracted by a steel die method [146]. The setup is shown in Fig. 5.1. The maximum stress applied on extraction was 650 MPa for long aged samples such as cement paste hydrated for 91 days. Except for the solution for pH value test, a drop of 2% HNO_3 was immediately added to the extracted solution to prevent possible precipitation of ions.

The pH value of pore solution was analyzed with a pH electrode. The concentration of Na, K, S, Ca, Si and Al in the pore solution was determined by Dionex Ion Chromatography system (ICS) 3000.

5.3 Experimental Results and Discussion

Similar to Chapter 4, the analysis of hydration kinetics of all pastes was classified as two groups, calcium silicate phases and calcium aluminate phases. Therefore, we also investigate the hydration products from two aspects. The first aspect is products formed from calcium silicate phases and the second from calcium aluminate phases. Typically, main hydration products of calcium silicate phases are $Ca(OH)_2$, C-S-H gel, while that of calcium aluminate phases are ettringite, monosulphate, monocarboaluminate, hydrogarnet and hydrotalcite phases.

Figs. A.1 to A.4 are the main XRD patterns of the four groups of hydrating pastes at different selected curing ages, with common peaks recognized and marked by the corresponding phase names. Using the profile fitting by means of Rietveld method on all measured XRD patterns, the

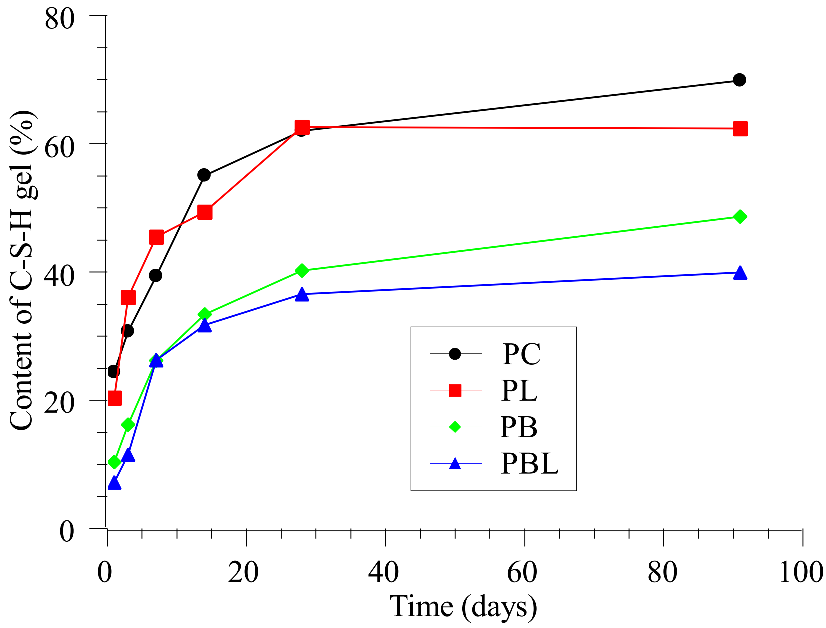

Figure 5.2: Amount of C-S-H gel formed by cementitious materials at different curing ages measured by the combination of XRD/Rietveld analysis and EDTA selective dissolution method. Data are normalized by the original mass of cementitious materials, i.e. cement in PC and PL pastes, cement + slag in PB and PBL pastes, wt%.

amounts of all main phases were quantified and listed in Table A.1. All the results in the table are normalized by the original weight of raw solid material(s) according to the mix design, i.e. cement in PC and PL pastes, cement and slag in PB and PBL pastes.

5.3.1 Calcium Silicate Phase Related Hydration Products

Amount of C-S-H Gel Measured by XRD/Rietveld Analysis

Fig. 5.2 presents the evolution of C-S-H gel generated in the four groups of pastes measured by the combination of XRD/Rietveld analysis and EDTA selective dissolution method. In terms of the contribution to C-S-H gel formation, limestone powder is presumably considered as inert filler.

It should be noted that the result of C-S-H gel quantified by XRD/Rietveld in this research are less reliable than other hydration products. The first reason is the carbonation during the experiment process. The sample preparation for XRD experiment included wet grinding using hexane and the later evaporation of hexane. Both processes were performed in the ambient environment where definitely had CO_2 from the atmosphere, which was far from CO_2-free condition. In addition, the particle sizes of samples prepared for XRD test were generally smaller than 10 μm, which greatly increased the surface area of the sample compared with the powder for TGA measurement. As stated in [2], C-S-H gel may react with CO_2 forming $CaCO_3$, thus contamination by atmospheric CO_2 during the wet grinding process could be serious in laboratory studies. The same contamination may also occur in the case of $Ca(OH)_2$ with CO_2 if measured by similar techniques. The second reason is that the quantification of C-S-H gel in PB and PBL pastes used a combination of XRD/Rietveld and EDTA selective dissolution method, which mathematically amplified the inaccuracy of final result. Therefore, these two factors should be kept in mind when interpreting the amount of C-S-H gel.

As shown in Fig. 5.2, the amount of C-S-H gel formed in PC paste started from 24.4% of original cement mass at 1 day to 69.9% at 91 days. Results indicate that the amount of C-S-H gel of PL was even lower than that of PC paste at 1, 14 and 91 days, respectively, which is probably not the reality given the hydration degree of cement clinker in PL was always higher than that in PC paste, as shown in Fig. 4.10. As aforementioned, the responsible reason could be the carbonation of C-S-H gel with CO_2 during the sample preparation prior to XRD measurement.

The amount of C-S-H gel formed in PB paste was 10.4% and 48.7% of original mass of slag and cement at 1 and 91 days, respectively, while the corresponding values of PBL paste were 7.2% and 40.0%, respectively. The C-S-H gel formed in PBL paste was actually constantly lower than that of PB paste at all testing ages, which actually agrees with the result that the degree of hydration of cement clinker in PBL was constantly lower than that in PB paste (Fig. 4.10).

C-S-H gel in PB and PBL pastes was essentially formed by the hydration of slag and the calcium silicate phases of cement. Considering the hydration kinetics of calcium silicate phases (Fig. 4.8) and slag (Fig. 4.13) investigated in Chapter 4 by XRD/Rietveld analysis and EDTA method, respectively, the slightly lower production of C-S-H gel in PBL paste shows that the addition of limestone in slag blended cement paste had slightly negative influence on the formation of C-S-H gel. Possible reason could be the reaction of limestone with aluminate phase in PBL paste consumed extra water and occupied the limited space, which indirectly restricted the formation of C-S-H gel, as shown in Fig. 4.14 that a certain amount of $CaCO_3$ in PBL paste has reacted at 1 day.

Regardless of the possible carbonation of C-S-H gel in all samples, the difference between the amounts of C-S-H gel of samples with and without slag addition is still enormous. The C-S-H gel in PB and PBL pastes were much lower than that in PC and PL pastes. Apparently two reasons explain this difference. On the one hand, the hydration of calcium silicate phases in PB and PBL pastes was significantly retarded, as shown in Fig. 4.8, leading to less production of calcium containing hydration products, i.e. C-S-H gel and $Ca(OH)_2$. On the other hand, the much lower reaction degree of slag in PB and PBL pastes contributed less C-S-H gel than the counterpart cement in PC and PL pastes, regardless of the difference between the two types of C-S-H gel from hydration of slag and cement, respectively. The dilution effect brought by slag was distinct given that the replacement level of slag in PB and PBL pastes was as high as 70% and 60%, respectively.

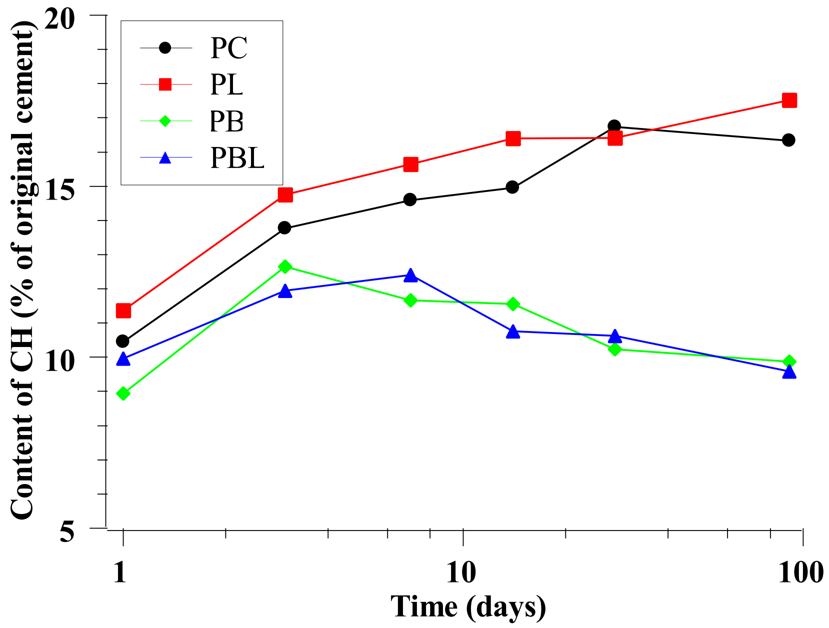

Figure 5.3: The content of $Ca(OH)_2$ in pastes at different ages, data were measured by TGA and normalized by the original mass of cement of each sample.

Amount of $Ca(OH)_2$ Measured by TGA

Fig. 5.3 shows the quantity of $Ca(OH)_2$ formed by the hydration of cement at different curing ages in the four groups of pastes. Values were normalized by the mass of original cement, as cement was the only material that produced $Ca(OH)_2$ during the hydration process.

Except for the value at 28 days that is probably an experimental error, the amount of $Ca(OH)_2$ in PC paste was 10.5% at 1 day and increased to 16.3% at 91 days, while the corresponding values of PL were 11.4% and 17.5%, respectively. The results at 91 days of both PC and PL pastes agree with the values in [2], which summarized that the $Ca(OH)_2$ content found by thermal methods or quantitative X-ray diffraction analysis (QXDA) in Portland cements cured for 3-12 months is typically 15-25% referred to the ignited cement mass.

Since cement was the only source of formation of $Ca(OH)_2$ and $Ca(OH)_2$ may be consumed during the formation of hemicarboaluminate phase in PL paste, as shown in Eq. 5.1 [77], the higher production of $Ca(OH)_2$ in PL paste over the whole curing age compared to PC paste obviously shows that the presence of limestone indeed accelerated the hydration of cement, which coincides with the hydration kinetics of C_3S and C_2S in PC and PL pastes as shown in Fig. 4.8.

$$C_3A + 0.5\,C\overline{C} + 0.5CH + 11.5H \longrightarrow C_4A\overline{C}_{0.5}H_{12} \tag{5.1}$$

The quantity of $Ca(OH)_2$ formed in PB and PBL pastes at all ages did not show fixed trend as in the cases of PC and PL pastes, but generally initially increased and then decreased, showing that the reaction of slag consumed $Ca(OH)_2$. Specifically, the $Ca(OH)_2$ content in PB paste started from 8.9% at 1 day and reached a peak of 12.7% at 3 days, but then gradually decreased to 9.9% at 91 days. The $Ca(OH)_2$ content in PBL paste was marginally higher at 1 day, i.e. 10.0%, and had a slightly lower peak 12.4% at 7 days. Similar and comparable results were also reported by [147], in which the binary blended cement paste shows slightly lower content of $Ca(OH)_2$ due to a relatively high water to powder ratio (0.55). In addition, experimental results of Gruyaert [148] show that there is still a detectable amount of $Ca(OH)_2$ in a cement paste blended with 85% of slag (by mass) after 1 year of hydration.

According to the tiny difference of $Ca(OH)_2$ content between PB and PBL pastes over the whole curing age, it is difficult to reach a conclusion that the addition of limestone had profound influence on the formation of $Ca(OH)_2$ in PBL paste, which is also confirmed by the almost identical hydration kinetics of C_3S and C_2S in PB and PBL pastes as shown in Fig. 4.8. In addition, it is also in line with the almost identical degree of reaction of slag in both PB and PBL pastes, as shown in Fig. 4.13.

However, the amount of $Ca(OH)_2$ formed in pastes without slag addition, i.e. PC and PL, was constantly higher than that with slag addition (PB and PBL) over the whole curing age. The discrepancy between them became even more obvious at later age, i.e. after 3 days of hydration. Based on the relatively low quantity of $Ca(OH)_2$ formed in PB and PBL pastes and the increasing discrepancy compared with that of PC and PL pastes, three conclusions can be drawn as follows:

1. Even at the early age, e.g. after 3 days, $Ca(OH)_2$ was slightly consumed, because the hydration degree of C_3S and C_2S in PB and PBL pastes was very close to that of PC paste at 3 days as shown in Fig. 4.8, while the amount of $Ca(OH)_2$ in PB and PBL pastes started to decline after 3 days of hydration.

2. In this research, the reaction of slag in blended paste did consume $Ca(OH)_2$ that was formed by the hydration of cement clinker, as the amount of $Ca(OH)_2$ in PB and PBL pastes kept decreasing after 3 days, while that in PC and PL pastes still kept increasing over the whole testing age.

3. Even after 91 days of hydration, the content of $Ca(OH)_2$ in both PB and PBL pastes were still as high as about 10% of the original mass of cement clinker, showing the amount of $Ca(OH)_2$ was always sufficient for the reaction of slag, which agrees with the conclusion of [149] that the excess of $Ca(OH)_2$ buffers pH and calcium activities during initial hydration and throughout most of the service lifetime.

The consumption of $Ca(OH)_2$ in PB and PBL paste at early age indicates the reaction of slag occurred at early age, i.e. within 3 days, which agrees with the degree of reaction of slag measured by EDTA selective dissolution method as shown in Fig. 4.13 and the more recognizable shoulder of heat rate in the deceleratory period in both PB and PBL pastes (Fig. 4.11). Apart from the interaction caused by the water consumption in the hydration process of cement and slag, the consumption of $Ca(OH)_2$ in PB and PBL pastes was another interaction

Table 5.1: The content of $Ca(OH)_2$ in pastes. Data were normalized by original mass of hydrated cement clinker at different ages (wt%).

Time (days)	PC	PL	PB	PBL
1	34.2	32.5	26.7	43.6
3	43.3	28.6	29.1	29.7
7	30.3	26.6	21.8	23.5
14	26.6	27.5	20.2	19.6
28	27.1	24.5	16.0	17.1
91	23.5	24.9	14.7	15.4

between the hydration of cement and slag, which will be considered in the theoretical model proposed in Chapter 7 for hydration of cement and slag.

The content of $Ca(OH)_2$ shown in Fig. 5.3 was normalized by the mass of original cement. Since the degree of hydration of cement clinker in each paste was quantified at each curing age, the content of $Ca(OH)_2$ was further normalized by the original mass of hydrated cement clinker, which thus leads to the production of $Ca(OH)_2$ by hydration of each unit of cement clinker.

Table 5.1 is the content of $Ca(OH)_2$ in pastes normalized by hydrated mass of cement clinker at different ages. The results show that the production of PC and PL pastes reached a relatively stable value at around 24% after 91 days of hydration, and the corresponding values in PB and PBL pastes were about 15% which is much lower than in the cases of PC and PL pastes, indicating part of $Ca(OH)_2$ was obviously consumed by the reaction of slag, and as the curing age increased, more $Ca(OH)_2$ was consumed due to the ongoing hydration of slag, which differs with the research result based on binary blended slag cement suggesting that $Ca(OH)_2$ demand of hydrating slag pastes was quite modest [59]. Possible reason could be that the replacement level of cement by slag in this research is higher (60% and 70%), so that the overall lower Ca/Si ratio leads to higher acquisition of Ca from $Ca(OH)_2$.

5.3.2 Calcium Aluminate Phase Related Hydration Products

Calcium Aluminate Phase Related Hydration Products of PC Paste

Fig. 5.4 shows the quantified calcium aluminate phase related hydration products of PC paste at different curing ages. They are mainly ettringite, monosulphate, monocarboaluminate, hydrogarnet, hydrotalcite, as well as gypsum that may be the precipitation of sulphate from pore solution when drying samples. Apparently, XRD/Rietveld failed to quantify the content of sulphate as gypsum in raw material cement (Table 4.1), which could be explained by the fact that gypsum commonly contains significant proportions of such impurities as anhydrite [2].

The amount of ettringite increased sharply at the early age. After reaching the highest (9.2% of raw cement mass) at 3 days, the amount of ettringite quickly decreased in the first 28 days and became almost unnoticeable after 91 days. As ettringite decreased, the amount of monosulphate increased steadily and reached a moderate peak at 28 days. However, both the quantities of

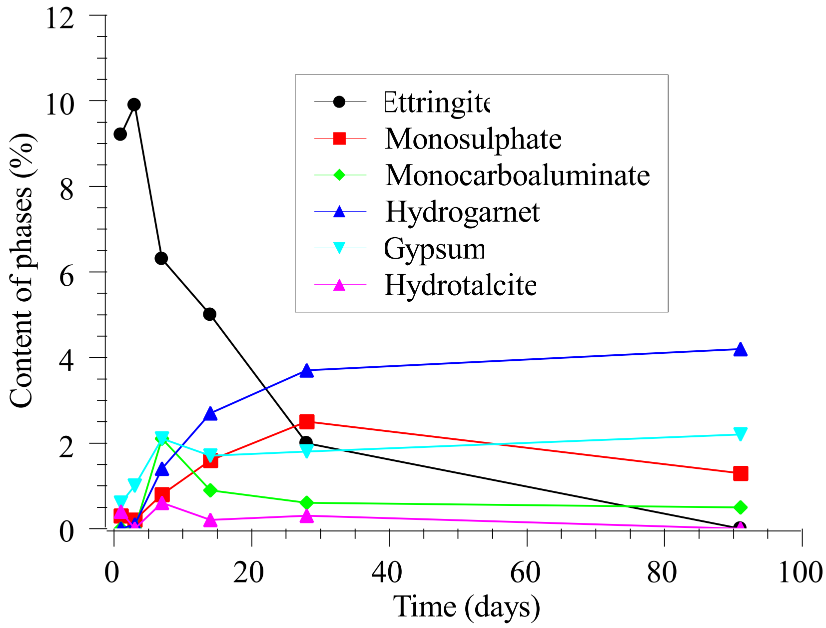

Figure 5.4: Amount of calcium aluminate phase related hydration products of PC paste. Data are normalized by the original mass of raw solid material(s), wt%.

ettringite and monosulphate kept decreasing after 28 days.

Result shows that a relatively higher amount of hydrogarnet was formed when the amount of ettringite was diminishing. The content of hydrogarnet reached 4.2% of original cement mass after 91 days of hydration. Meanwhile, the amount of gypsum quickly reached 2.1% of original cement mass after 7 days of hydration and remained relatively stable afterwards. The presence of appreciable amount of gypsum could be caused by the decrease of ettringite and increase of hydrogarnet, since the dominating phase of hydrogarnet (C_3AH_6) does not contain sulphate, and the amount of monosulphate also slightly decreased as ettringite diminished. Therefore, the probably oversaturated sulphate was precipitated as gypsum when the sample was drying.

The amount of monocarboaluminate sharply increased to 2.1% of original cement mass after 7 days of hydration, and then decreased slightly but still remained detectable. The formation of monocarboaluminate could be caused by the reaction of aluminate phase with a small amount of $CaCO_3$, since the raw material cement contains about 4.52% (Table 4.1) of Al_2O_3 and 2.0% (TGA) $CaCO_3$.

Result also shows a low but noticeable amount of hydrotalcite formed in hydration products of PC paste. The formation of hydrotalcite should be the result of the presence of MgO, as the raw material cement contained 2.22% MgO (Table 4.1).

Calcium Aluminate Phase Related Hydration Products of PL Paste

Fig. 5.5 presents the evolution of calcium aluminate phase related hydration products of PL paste at different curing ages. The main types were the same as those shown in PC paste, with varying quantity of each phase.

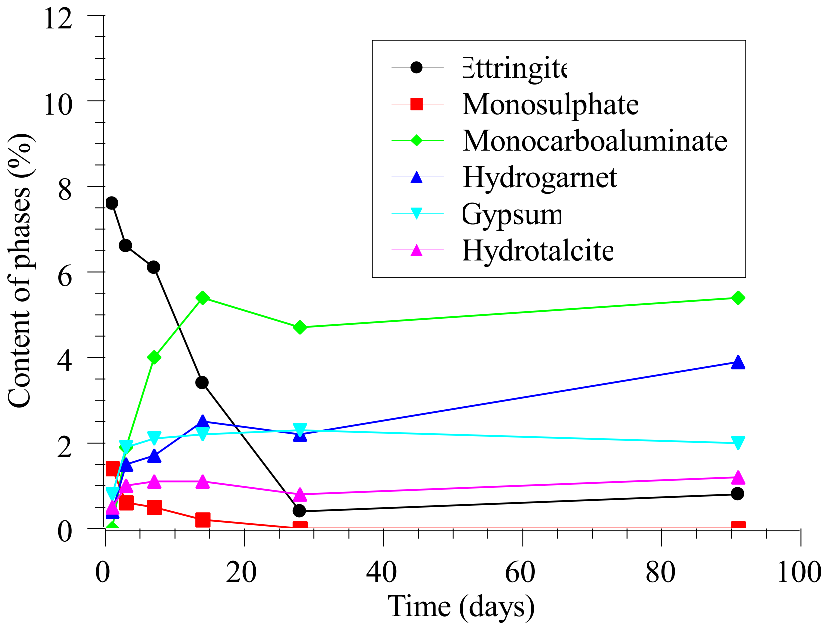

Figure 5.5: Amount of calcium aluminate phase related hydration products of PL paste. Data were normalized by the original mass of raw solid material(s), wt%.

The amount of ettringite immediately reached a maximum value 7.6% of original weight of raw materials (cement and limestone) after 1 day of hydration, which occurred earlier than that in PC paste but slightly lower even considering the dilution of 10% of limestone. The content of ettringite quickly decreased with curing age till 28 days of hydration and remained afterwards at a only detectable level. Similar to the trend of ettringite, the amount of monosulphate also reached a maximum value 1.4% of original weight of raw materials, then quickly decreased to barely traceable till 14 days of hydration, and finally disappeared at later age.

As the amount of ettringite and monosulphate decreased, the formation of monocarboaluminate sharply increased to 5.4% of original weight of raw materials after 14 days of hydration, and stayed relatively stable during the remained curing age. Compared with the case of PC paste, the dominating amount of monocarboaluminate demonstrates that considerable chemical reaction of limestone with the aluminate phase of cement occurred in PL paste within the first 14 days of hydration, which generally agrees with the conclusion of [150] that the presence of limestone inhibits the formation of ettringite and favors the formation of carboaluminate during the first days of hydration.

Besides the increasing amount of monocarboaluminate in the first 14 days, the amounts of hydrogarnet and gypsum also increased to comparable values with that in PC paste, respectively. However, the maximum content of these two phases in PL paste appeared earlier than the counterparts in PC paste regardless of the dilution of 10% of limestone addition, e.g. the amount of hydrogarnet quickly increased to 1.5% of the mass of raw materials (cement and limestone) at 3 days while there was nearly no hydrogarnet in PC paste at the same curing age. The content of gypsum in PL paste was 1.9% of original mass of materials at 3 days, while the corresponding

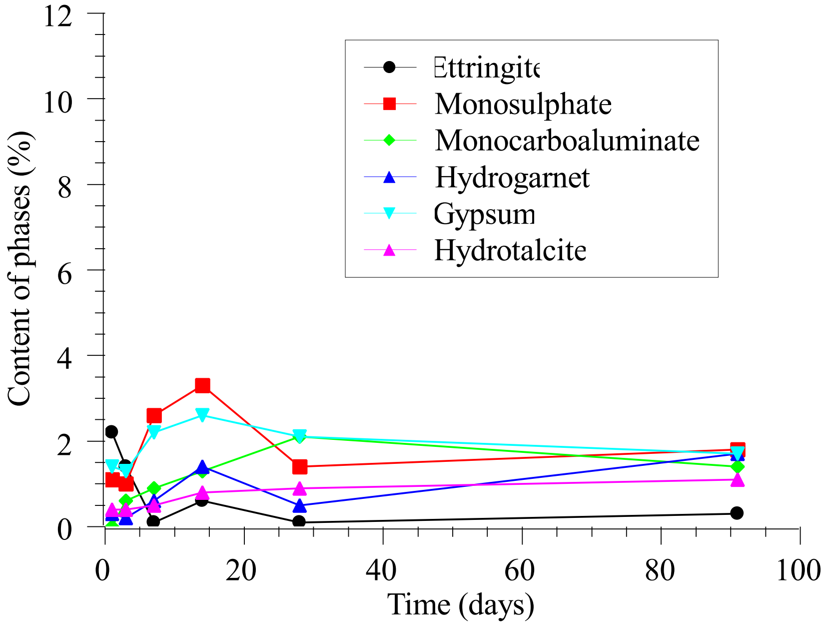

Figure 5.6: Amount of calcium aluminate phase related hydration products of PB paste. Data were normalized by the original mass of raw solid material(s), wt%.

value in PC paste was only 1%.

Combining the decreasing amounts of ettringite and monosulphate and increasing amount of monocarboaluminate over the whole curing age, the earlier appearance of hydrogarnet and gypsum could be caused by the presence of limestone that indeed accelerated the hydration of aluminate phase in PL paste compared with PC paste shown in Fig. 4.9. Compared with ettringite and monosulphate phases, monocarboaluminate contains no sulphate, which probably caused sulphate staying in pore solution and precipitated as gypsum when sample was drying. In addition, the formation of monocarboaluminate also consumed less aluminate phase comparing with ettringite, probably explaining the formation of hydrogarnet phase which contains aluminate phase.

As for the formation of hydrotalcite ($M_6A\overline{C}H_{12}$), its content remained at about 1% of original weight of raw materials after 3 days of hydration, which was higher than the case in PC paste. The slightly higher content of hydrotalcite in PL paste was caused by the presence of limestone which contributed more carbonate than the case of PC paste.

Calcium Aluminate Phase Related Hydration Products of PB Paste

The calcium aluminate phase related hydration products of PB paste are shown in Fig. 5.6. Detected calcium aluminate phase related hydration products were ettringite, monosulphate, monocarboaluminate, hydrogarnet, hydrotalcite and gypsum.

The amount of ettringite reached 2.2% of original weight of cement and slag at 1 day, and then quickly decreased to undetectable after 7 days. Even if the content of ettringite formed in PC paste is divided by 30% that was the amount of cement in PB mix, the maximum production of ettringite in PB paste is still lower than that in PC paste and decreased faster than that in PC paste, while the formation of monosulphate in PB paste was proportionally much higher than that of PC paste at all tested ages, indicating distinct transformation of ettringite to monosulphate compared with the case in PC paste in the first 7 days of hydration, which agrees well with the finding of [151] by means of a series of experimental methods.

Although cement accounted for just 30% of raw materials in PB paste, i.e. less content of $CaCO_3$ from cement, the formation of monocarboaluminate was still comparable compared with PC paste, e.g. the content of monocarboaluminate in PB paste remained higher than 1% after 7 days of hydration. The increased production of monocarboaluminate should be caused by the presence of large amount of aluminate phases from slag material.

The amount of hydrogarnet was lower than that in PC paste, with the highest value being 1.7% at 91 days compared with 4.2% of PC paste, which may be explained by the fact that there were comparable amounts of monosulphate and monocarboaluminate. Corresponded to the low and decreasing amount of ettringite in PB paste, the content of gypsum quickly reached 1.4% of the original weight of cement and slag at 1 day and increased to the highest 2.6% at 14 days, then stayed at around 2%. The production of gypsum was comparable to PC paste, though PB had 70% replacement of cement by slag which reduced the total amount of SO_3 from the raw materials.

Result shows a certain amount of hydrotalcite in PB paste during the whole curing age, which was higher than the case of PC paste and comparable to that in PL paste. Raw material slag contained relatively high amount of MgO than cement, however, the critically low content of $CaCO_3$ in PB paste probably restricted the formation of hydrotalcite.

Calcium Aluminate Phase Related Hydration Products of PBL Paste

As can be seen from Fig. 5.7, the calcium aluminate phase related hydration products of PBL paste were also ettringite, monosulphate, monocarboaluminate, hydrogarnet, hydrotalcite and gypsum, with the quantity significantly being different comparing with PC, PL and PB pastes.

The amount of ettringite phase reached a maximum value at 3 days, which was 2.5% of original weight of solid raw materials, i.e. cement, slag and limestone. This maximum value was higher and occurred later than that in PB paste, showing the influence of limestone on PBL paste. The content of ettringite later decreased to less than 1% after 7 days of hydration. Comparing with PB paste, the amount of monosulphate in PBL paste appeared less than that in PB paste, indicating the addition of limestone did not promote the transformation of ettringite to monosulphate.

After 3 days of hydration, monocarboaluminate became the dominating hydration product related to calcium aluminate phase, with the amount reached 7.3% and 7.8% of original mass of solid materials (cement, slag and limestone) after 14 and 91 days of hydration, respectively. Compared with PL paste, PBL paste produced higher content of monocarboaluminate over the whole curing age, indicating the chemical reaction of limestone with aluminate phase was greatly

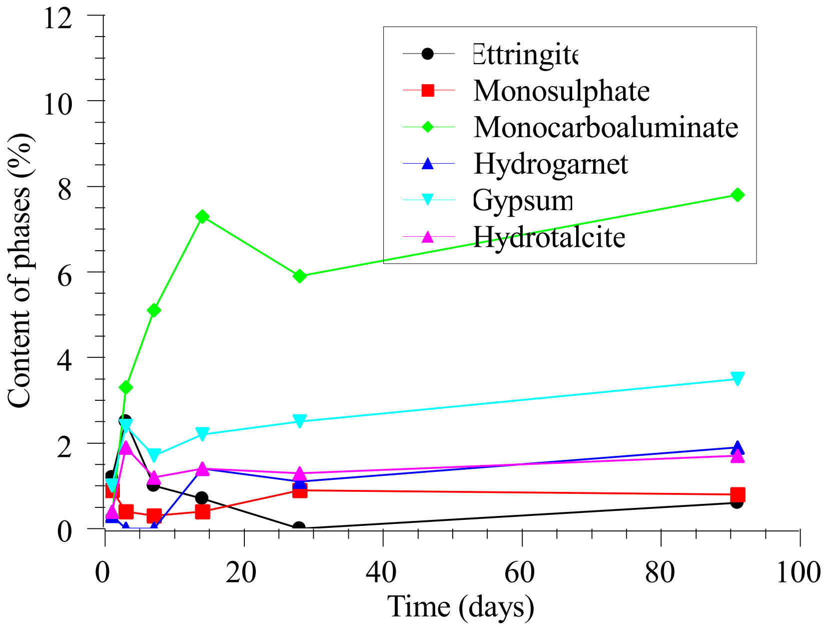

Figure 5.7: Amount of calcium aluminate phase related hydration products of PBL paste. Data were normalized by the original mass of raw solid material(s), wt%.

enhanced in PBL paste, which is readily explained as that slag in PBL paste contained a much higher amount of Al_2O_3 compared with cement.

Besides the dominating formation of monocarboaluminate in PBL paste, gypsum was the second main phase in calcium aluminate phase related hydration products. Result also shows a relatively considerable amount of gypsum appeared in PBL paste, which reached 3.5% of original mass of solid materials after 91 days of hydration. The relatively high production of gypsum coincided with the low content of ettringite and monosulphate that are another two sulphate-rich hydration products in cement paste. As same as in PL paste, the low content of ettringite and monosulphate caused the sulphate probably to exist in pore solution and finally precipitated as gypsum when drying sample.

The formation of hydrotalcite was enhanced in PBL paste. Result shows that the amount of hydrotalcite in PBL paste was systematically higher than any other type of paste, i.e. PC, PL and PB. Comparing with PB paste, the formation hydrotalcite in PBL paste should be promoted by the addition of limestone together with high amount of MgO from slag.

The formation of hydrogarnet became detectable after 14 days of hydration in PBL paste, which was essentially comparable to PB paste.

5.3.3 Total Bound Water and Non-evaporable Water Measured by TGA

As already mentioned in Chapter 4, the ongoing hydration of samples in this research for TGA test was stopped by freeze-drying method. Free water in samples was presumed to be removed by

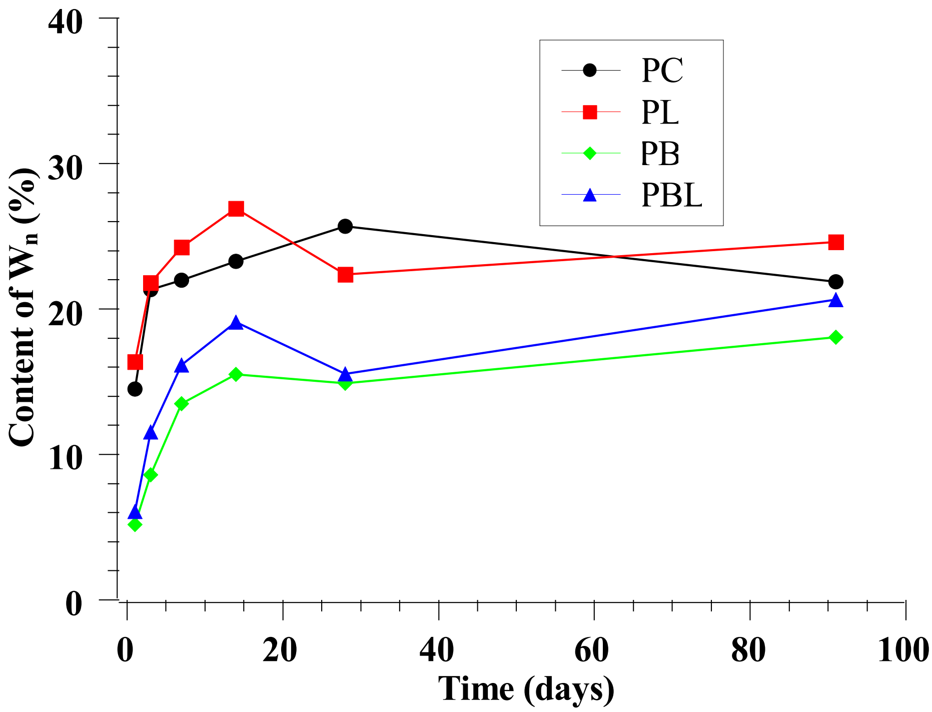

Figure 5.8: The amount of total bound water of pastes tested by TGA at different ages. Data were normalized by the original mass of cementitious material(s).

the freeze-drying procedure, leaving the physically bound water and chemically bound water in the dried sample. From an experimental point of view, it is difficult to measure the exact amount of chemically bound water by experimental methods, e.g. TGA method. This is because on the one hand a certain amount of water can be lost from interlayer spaces under the drying conditions, and on the other hand some hydrates may decompose even under 105 °C that is usually regarded as the temperature threshold for oven-drying to determine the amount of chemically bound water [3].

In this research, we prefer to use another three terms to describe the water retained in samples after freeze-drying: total bound water, non-evaporable water and evaporable water. As free water was removed from prepared samples in this research, the term total bound water is defined as the water removed by heating sample in TGA experiment from temperature 20 to 900 °C, while non-evaporable water is the water removed between temperature 145 to 900 °C. The boundary temperature 145 °C rather than 105 °C is taken based on the suggestion of [2], which will be discussed later in this chapter. Naturally, the discrepancy between bound water and non-evaporable water is defined as evaporable water.

In order to make comparison, the amount of water was normalized by the mass of original cementitious materials, i.e. cement and slag, with the limited reaction of limestone disregarded.

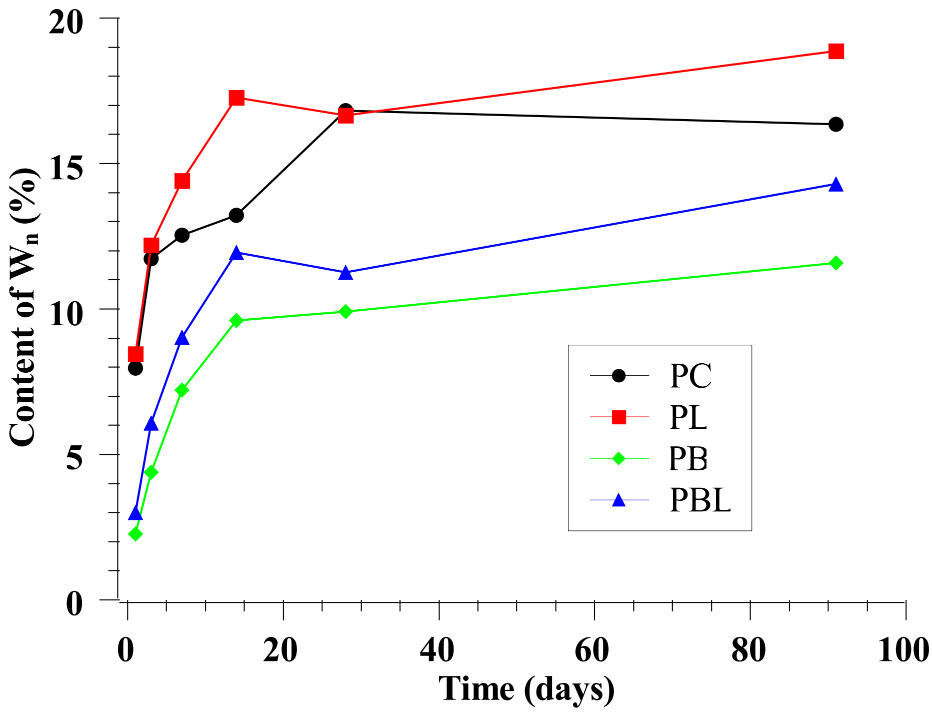

Figure 5.9: The content of non-evaporable water of pastes tested by TGA at different ages. Data are normalized by the mass of original cementitious material(s).

The Amount of Total Bound Water

Fig. 5.8 shows the amount of total bound water of each paste measured by TGA at different ages. Except for the value of PL paste at 28 days, the total amount of bound water in PL paste was higher than that of PC paste. Similar trend was also observed in PB and PBL pastes, i.e. the total amount of bound water in PBL pastes was always higher than PB pastes. This shows that the addition of limestone powder generally resulted in the increased amount of bound water in hydration products. The reason should be that the hydration of C_3S and C_2S in PL paste was accelerated at all ages as shown in Fig. 4.10. In addition, another possible reason could be the enhanced reaction between limestone and aluminate phase at early ages, which consumed more water in hydration process.

Comparing the pastes (PC and PL) to that with slag addition (PB and PBL), results show that less total bound water was measured in pastes with slag addition at all ages, which was apparently caused by lower reaction degree of slag compared with cement clinker in both PB and PBL pastes, as already shown in Section 4.3.1 of Chapter 4.

The Amount of Non-evaporable Water

Fig. 5.9 depicts the content of non-evaporable water of the four groups of pastes at different curing ages. The amount of non-evaporable water in PL paste started from around 8.5% at 1 day and later increased to as high as 18.9% of original mass of cement after 91 days of hydration,

Table 5.2: The amount of total bound water and non-evaporable water for complete hydration. Data were normalized by the mass of reacted cementitious material(s) of each paste measured by TGA (wt%).

Name	PC	PL	PB	PBL	Slag
Total bound water	40.0	38.7	43.1	49.8	46.8
Non-evaporable water	25.1	26.3	26.3	32.0	27.7
Evaporable water	14.9	12.4	16.7	17.8	19.1

which was higher than other pastes at all curing ages except for the value at 28 days for unknown reason.

PB and PBL pastes generally generated lower content of non-evaporable water than the corresponding values of PC and PL paste, which coincides with the lower reaction degree of slag compared with that of clinker in PC and PL pastes. In addition, the content of non-evaporable water in PB paste was constantly the lowest at all curing ages, started from 2.3% to 11.6% of original mass of cement and slag at 1 and 91 days, respectively.

The content of non-evaporable water in PL and PBL pastes is relatively higher than the counterparts without limestone addition (PC and PB pastes), respectively. This difference clearly indicates that the limestone addition increased the amount of non-evaporable water in hydration products. It agrees with the high amounts of monocarboaluminate formed in PL and PBL pastes, as monocarboaluminate contains a high ratio of bound water.

The Amount of Water Required for Complete Hydration

The results of total bound water (Fig. 5.8) and non-evaporable (Fig. 5.9) water measured by TGA were normalized by the mass of original cementitious material(s) for the sake of comparison. However, it is interesting to normalize the content of water by the mass of reacted original cementitious material(s) based on the hydration degree of cement clinker and reaction degree of slag at all ages that were measured in Sections 4.3.1 and 4.3.3. Disregarding the reacted limestone, the water amounts normalized by hydrated amount of cementitious material(s) are essentially the amount of total bound and the amount of non-evaporable water needed for their complete hydration of pastes, respectively.

Table 5.2 lists the calculated results for this purpose. The results are average values of samples from 7 to 91 days. The first two curing ages, i.e. 1 and 3 days, were not considered because of the bad representativity of samples at young age.

The results indicate that the amount of non-evaporable water in each reacted unit (by mass) of cement in PC and PL pastes was 25.1% and 26.3%, respectively. These two values are slightly higher than the widely reported reference values of non-evaporable water of complete cement hydration, i.e. 21-25% [2, 152]. It can be explained by the fact that the results in this research were obtained by a combination of several methods, i.e. XRD/Rietveld, TGA and EDTA. In addition, the water contribution by reacted limestone was ignored, which also leads to the maybe overestimated results. The corresponding values for PB and PBL pastes were 26.3% and 32.0%, respectively. The higher value in PBL paste may be overestimated due to the combined use of experiments, but it indicates that the presence of limestone increased the non-evaporable water required for complete hydration in the PBL paste. The reason could be that the reaction between limestone and aluminate consumed a certain amount of water to form monocarboaluminate as shown in Eq. 5.1.

The amount of total bound water for complete hydration of cement in PC and PL pastes were 40.0% and 38.7% of the original anhydrous cement, respectively, which agree with the data summarized by Brouwers [153], i.e. 39.3%, but lower than the reported values 42-44% from literature [2]. In terms of slag blended pastes, the total amount of water needed for the complete hydration of PB and PBL pastes are 43.1% and 49.8% referred to the total original mass of cement and slag, respectively, implying that the complete hydration of slag consumes more water. Specifically, the coexistence of slag and limestone in ternary blended paste, i.e. PBL, consumed the largest amount of water for complete hydration, which could be caused by the chemical reaction of limestone that consumed relatively large amount of water as shown in Eq. 4.7.

Based on the results of PC in Table 5.2, removing the water bound by cement in PB paste resulted in the water bound by slag. Calculated results show that the complete hydration of each unit of slag needs 46.8% total bound water and 27.7% non-evaporable water. Work of Maekawa [154] (cited by [103]) reported that the chemically bound water and gel water for chemical reaction of slag is 30% and 15% of original mass of slag, respectively. In other words, the total bound water for complete hydration of slag 46.8% in this research is very close to the one of Maekawa's work, which is 45%. It should be emphasized that the definition of chemically bound water is different from non-evaporable water though the two values usually do not differ significantly.

The results in Table 5.2 show that the addition of limestone powder increased the content of non-evaporable water for compete hydration of cement in PL paste, especially when coexisting with slag, i.e. PBL paste. This should be caused by the enhanced formation of aluminate related hydration products in the presence of limestone, as demonstrated by the significantly high production of monocarboaluminate in PL and PBL pastes (Figs. 5.5 and 5.7). Furthermore, the presence of slag in PB paste did not change the content of non-evaporable water normalized by the mass of reacted original cement and slag.

The Amount of Evaporable Water for Complete Hydration

The first two rows of data in Table 5.2 show the amount of total bound water and non-evaporable water normalized by the mass of reacted original cementitious material(s) for PC, PL, PB and PBL pastes (Table 5.2). If the corresponding content of non-evaporable water is deducted from the total bound water, the left part is the content of evaporable water in hydration products.

However, two points should be kept in mind prior to interpretation of the content of evaporable water. The first is the reduced accuracy of the results due to the combination of several methods quantifying reacted cement and slag. The second is that the amount of evaporable water itself is vulnerable to change. The free water in samples was assumed to be removed by freeze-drying in this research, leaving only the total bound water in sample. In the total bound water, the evaporable water contained physically bound water as well as partial chemically bound water in the pore system of the samples.

There are two factors influencing the content of physically bound water in paste. The first is the relative humidity in the pore system. Higher relative humidity greatly increases the thickness of the water layer adsorbed on the surface of hydration products [3]. The second is the surface area of pores in hydration products. Literature [155] suggests that the fibrillar morphology of outer product C-S-H in slag blended cement is gradually replaced by a foil-like morphology as slag loading increased, implying that the pore system of slag blended paste is refined with the increased surface area of pores. As the surface area of pores in slag blended cement increases, the amount of physically bound water should accordingly increase. In addition, the combination of test methods and different pore structures could lead to unstable results of evaporable water with reduced accuracy.

Regardless of the probably reduced accuracy and the variety of amount of evaporable water, the calculated results in Table 5.2 show that the amount of evaporable water of for PC, PL, PB and PBL pastes is 14.9%, 12.4%, 16.7% and 17.8%, respectively, referred to the original mass of reacted cementitious material(s). It can be seen that slag blended cement pastes contain slightly more evaporable water than cement pastes without slag addition, which could have relation with the altered pore system in slag blended pastes. As will be shown in Table 6.3 of Chapter 6, the surface area of pores of slag blended pastes became larger than pastes without slag after 3 days of hydration, and the values of PB and PBL pastes were as high as two times the values for PC and PL pastes after 91 days of hydration. Note that the values of surface area were tested with maximum MIP pressure of 250 MPa, in other words, the surface area of pores of slag blended paste should be even higher than PC and PL tested with pressure higher than 250 MPa, as slag blended pastes contain more fine pores than PC and PL pastes.

5.3.4 Results of Extracted Pore Solution

pH of Extracted Pore Solutions of Pastes

Fig. 5.10 shows the pH values of extracted pore solution of samples at different curing ages. pH value of pore solution in PC increased from 13.56 at 1 day to 13.73 at 91 days, while the corresponding value of PL paste increased from 13.50 to 13.63, respectively. Pore solution in PL paste showed slightly lower pH values especially at young and late ages probably due to the lower content of cement, since 10% of cement in PL paste was replaced by limestone powder. But the pH value of pore solution in PL paste was comparable to that of PC paste during the

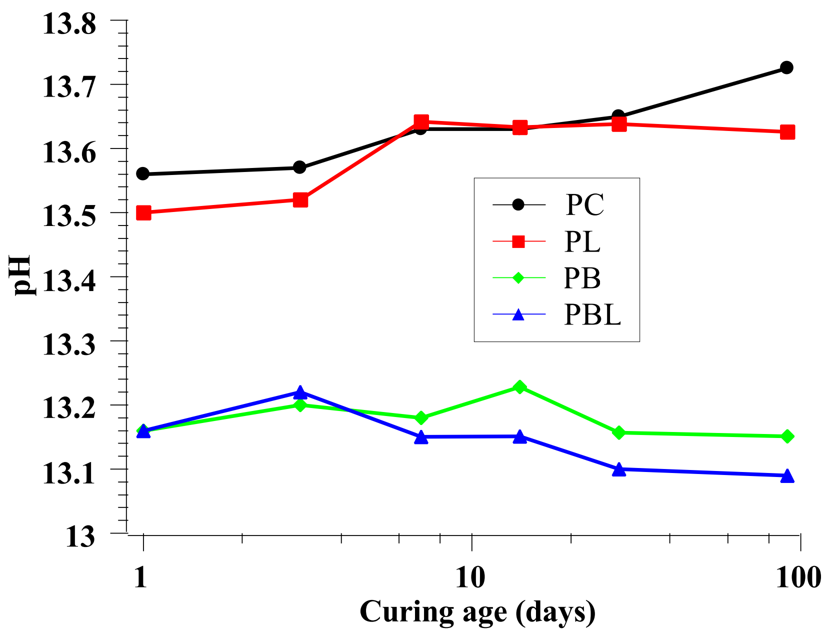

Figure 5.10: The pH of extracted pore solution of samples tested at different curing ages.

curing age of 7 and 28 days, this may be caused by the combination effect of higher production of $Ca(OH)_2$ and less free water in pores of PL paste.

The pH values of solution in PB and PBL pastes varied in the range of 13.09 and 13.23 over the whole curing age, which are systematically lower than that in PC and PL pastes. This is readily explained, since cement accounted for only 30% of solid materials in PB and PBL pastes, and the pH value of pore solution is mainly determined by $Ca(OH)_2$ and the high concentration of alkali ions (K, Na) easily released by cement.

Though the relatively low pH values of pore solution in PB and PBL pastes, they are still high enough for the activation of slag, as literature [156] suggested that the activation of slag occurs at relatively low pH's, e.g. less than 12. It should be noted that even at 1 day the pH was already 13.16 which is high enough to activate slag in paste. This is in line with the considerable reaction degree of slag even after just 24 hours as shown in Fig. 4.13.

Ion Concentrations of Extracted Pore Solutions of Pastes

Table 5.3 presents ion concentrations of extracted pore solutions at different curing ages. For all pastes, the main cations in pore solution were alkali ions, i.e. K and Na. Concentration of alkali ions in pore solution of PC paste increased from 556.3 mmol/l at 1 day to 888.5 mmol/l at 91 days. The equivalent values of PL paste were slightly lower than PC paste, which were probably diluted by the 10% of cement replaced by limestone powder in PL paste.

Fig. 5.11 shows the concentration of total alkali ions in pore solution of slag blended paste, i.e. PB and PBL. The values fluctuated in the range of 180 to 250 mmol/l over the whole curing age, which are relatively more stable but much lower compared with that in PC and PL pastes.

Table 5.3: Ion concentrations of extracted pore solutions (mmol/l, OH^{-a} is calculated from measured pH, OH^{-b} calculated based on charge balance).

Paste	Age (days)	OH^{-a}	OH^{-b}	Si	S	K	Na	Ca	Al
PC	1	363.1	516.3	0.4	20	314.9	241.4	/	/
	3	371.5	574.2	0.6	14.2	329	273.6	/	/
	7	426.6	692.1	0.3	16.5	397.4	327.7	/	/
	14	426.6	775.2	0.4	13.3	440.7	361.1	/	/
	28	446.7	677.4	0.6	24	389.1	336.3	/	/
	91	530.9	859.9	0.9	14.3	502.8	385.7	0.2	0.2
PL	1	316.2	457.7	0.3	11.4	287.9	192.6	/	/
	3	331.1	505.2	0.4	16.3	319.8	218	/	/
	7	438.5	688.1	0.7	20	430.5	297.6	/	/
	14	429.5	705.2	1	14.2	425.2	308.4	/	/
	28	434.5	715.6	0.9	14.2	421.9	322.1	0.3	0.2
	91	422.7	738.8	1	14.2	435.5	331.7	0.2	0.4
PB	1	144.5	182.7	0	0.1	108.3	74.6	/	/
	3	158.5	220.1	0	0.6	124.1	97.2	/	/
	7	151.4	215.7	0.1	0.9	114.7	102.8	/	/
	14	169	220.4	0.6	14.2	128.2	120.6	0.1	0.5
	28	143.5	208.2	0.5	13.8	121.9	113.9	0.1	0.2
	91	141.6	213.3	0.7	13.7	125.3	115.4	0.1	0.6
PBL	1	144.5	185.3	0	0.1	107.2	78.3	/	/
	3	166	204.5	0	0.9	115.1	91.2	/	/
	7	141.3	217.5	0.1	1.4	121.3	99.0	/	/
	14	141.6	202.7	0.7	13.7	118.8	111.3	0.1	0.6
	28	125.9	191.4	0.5	13.7	113.3	105.5	0.2	0.2
	91	123.0	188.7	0.5	13.7	114.1	102.0	0.1	0.2

The low concentration of alkali ions of PB and PBL pastes is readily explained, since the slag addition in PB and PBL pastes was 70% and 60%, respectively, and the content of Na_2O and K_2O in slag are much lower than cement as shown in Table 4.1, thus the concentration of alkali ions in pore solution of PB and PBL pastes was considerably diluted. In addition, there is almost no difference of alkali ions between PB and PBL pastes, given the total amount of cement and sag in PB is 100% while that in PBL is 90%.

Concentrations of ions such as Si, Ca, Al and Mg were found rather low in pore solution of all four types of pastes, similar results were also reported by other researchers [45, 77, 157] for pure Portland cement pastes and blended cement. It should be noted that the results of these ions are less reliable due to the limitation of test method at low concentrations in this research. Moreover, Ca, Al and Mg in most solutions were even unable to be measured due to the background noise caused by the high concentration of alkali ions.

The concentration of Ca in saturated $Ca(OH)_2$ solution is approximately 20 mmol/l according to its solubility, and it is strongly influenced by the pH of solution. As summarized by [3], the concentration of Ca is no more than 5 mmol/l in solution at pH higher than 12 in the first

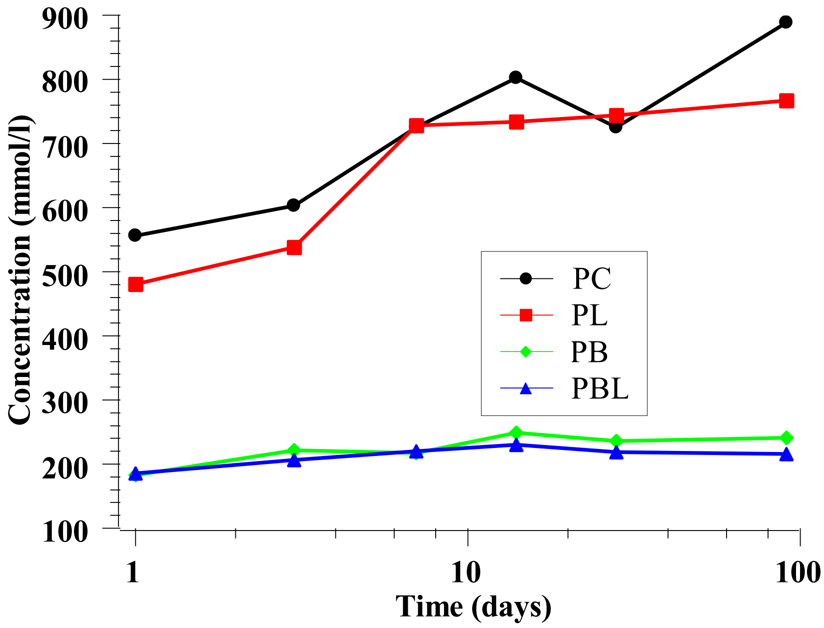

Figure 5.11: Concentrations of alkali ions in pore solution of pastes at different curing ages.

60 hours of hydration. Experiments performed by Weert et al. [77] also show that the Ca concentration in solution of series of neat Portland cement paste, binary and ternary blended cement pastes varies between 0.5 to 2.2 mmol/l. Measured results of Lothenbach [158] also reported low concentration of Ca in pore solution of Portland cement after 26 hours of hydration. Using inductively coupled plasma spectroscopy, [159] measured the ion concentrations of Si, Ca, Al and Mg in alkali activated slag pastes, showing the concentration of Si and Al increased with the pH, whereas those of Ca and Mg decreased. Based on the theoretical analysis and literature results, we estimate that the Ca concentration of pore solution in this research is probably less than 1 mmol/l except for the initial hours of hydration [45].

It has to be noted that the absolute concentrations of species such as Ca and Si are low, but the equilibration in the pore solutions is fast, so these ions are still available in solution for the precipitation of related hydration products.

OH^{-} was the dominating anion in all extracted pore solutions at all ages. It should be noted that the OH^{-} concentration calculated based on the measured pH values of pore solution as indicated in Fig. 5.10 are lower than the ones calculated based on the charge balance between anions and cations. Since the precision of alkali ions concentration is much higher than that of pH measurement in this research, the OH^{-} concentration determined based on charge balance is more reliable. As the OH^{-} in pore solution determines pH, the measured pH in this research was underestimated, though the concentration of alkali ions and pH show similar patterns in Fig. 5.10 (pH) and Fig. 5.11 (alkali ions).

Besides OH^{-}, another main anion in pore solution is $\overline{S}$. The $\overline{S}$ concentration in pore solution of PC and PL pastes varied between 11 to 20 mmol/l over the whole testing age, while that in PB and PBL pastes were rather low in the first 7 days of curing, which could be on the one hand

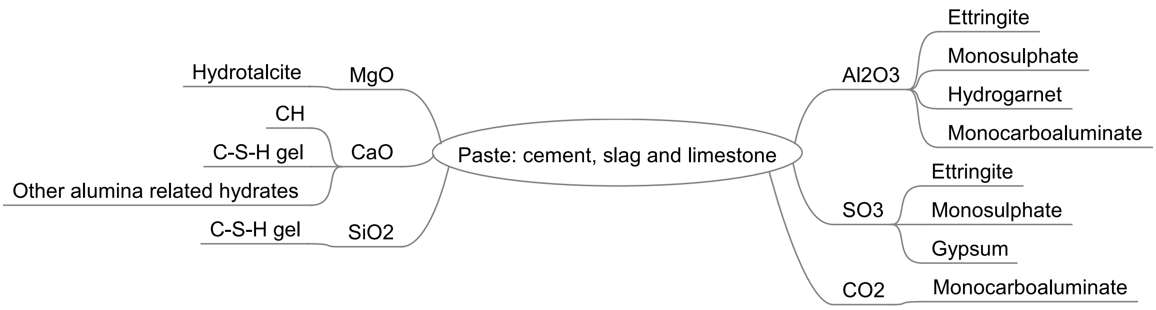

Figure 5.12: The trace of main elements from raw material in hydration products, Mg, Al in C-S-H were not considered.

caused by the low content of cement in PB and PBL pastes thus reduced the total amount of SO_3, and on the other hand the released $\overline{S}$ was greatly consumed by the reaction of large amount of aluminate phase in PB and PBL pastes forming ettringite and monosulphate phases, as slag in PB and PBL pastes indeed brought high content of Al_2O_3 compared with cement and the reaction of aluminate phase of cement was enhanced even at early age that is confirmed in Fig. 4.9.

However, the $\overline{S}$ concentration of slag bended pastes increased to comparable level compared with pastes without slag after 7 days of curing, which agree well with the considerable presence of gypsum in hydration products of PB and PBL pastes after the initial days as shown in Figs. 5.6 and 5.7. The possible reason should be the disappearance of ettringite and monosulphate phases and the formation of monocarboaluminate and hydrogarnet in hydration products of PB and PBL pastes as hydration of slag and cement proceeded. The disappearance of ettringite and monosulphate released sulphate to pore solution while the formation of monocarboaluminate and hydrogarnet consumed no sulphate. This was particularly obvious in ternary blended paste, i.e. PBL, the total amount of ettringite and monosulphate was very low while that of monocarboaluminate considerably high in the presence of limestone, as shown in Fig. 5.7 tested by XRD/Rietveld method.

Furthermore, from the viewpoint of raw material, it was also less likely to form ettringite from the long-term run. The content of Al_2O_3 and SO_3 in cement was 4.52% and 3.52%, respectively, which means the molar ratio between Al_2O_3 and SO_3 is 1.06:1. This value is much larger than the ratio 1:3 in ettringite ($C_6A\overline{S}_3H_{32}$). Considering the large amount of Al_2O_3 in raw material slag, the ratio in total raw materials in PB and PBL pastes is even larger. As illustrated in Fig. 5.12, there are mainly three possibilities of the trace of $\overline{S}$ elements in the hydrating pastes, i.e. ettringite, monosulphate and gypsum. The insufficient supply of sulphate lowered the possibility to form ettringite, while the presence of limestone favors the formation of thermodynamically stable monocarboaluminate instead of monosulphate, which probably led to the relatively high concentration of $\overline{S}$ in pore solution and the presence of gypsum in hydrating pastes when the samples were dried. The absence of ettringite and the presence of gypsum in limestone blended cement pastes (PL and PBL pastes) in this research is completely different from the claimed thermodynamic calculation of [74] that sulphate liberated from sulphoaluminate in the course of carbonation reacts with water and $Ca(OH)_2$ forming ettringite.

5.4 Conclusions

The hydration products of all pastes were investigated in this chapter. Based on the experimental investigation, several conclusions are reached as below:

1. The hydration products of all pastes are mainly C-S-H gel, $Ca(OH)_2$, and aluminate related assemblages such as ettringite, monosulphate, monocarboaluminate, hydrogarnet and hydrotalcite. The presence of limestone powder greatly increased the amount of monocarboaluminate, while decreased the content of ettringite and monosulphate, showing distinct reaction with aluminate phases from slag and cement.

2. In all pastes, remarkable content of hydrogarnet and gypsum was observed, showing the trace of aluminate phase and sulphate.

3. The formation of C-S-H gel in slag blended cements is largely reduced due to the relatively slow reaction of slag, which was even distinct in the case of ternary blended cement paste.

4. The acceleration effect of limestone powder on hydration of cement is confirmed by the increased production of $Ca(OH)_2$ in PL paste.

5. The hydration of slag consumed $Ca(OH)_2$, but $Ca(OH)_2$ is sufficient for the reaction of slag in the PBL paste of this research even after 91 days of hydration.

6. Calculation based on experimental results shows the total amount of bound water for complete hydration of cement and slag in this research was 40% and 46.8%, respectively.

7. The pH of pore solution from all pastes was higher than 13 over the whole curing age, which is sufficiently high for the activation of slag even at the very early age of hydration.

8. The ion species in pore solution were dominated by alkali ions. Other cations such as Ca, Mg, Al and Si were almost not detectable. Concentration of $\overline{\mathrm{S}}$ was constantly high in cement pastes containing no slag, while it occurred at later age in the case of slag blended cement pastes (PB and PBL).

Chapter 6

The Microstructure and Mechanical Strength of Ternary Blended Cement Paste

6.1 Introduction

The foregoing two chapters investigated the hydration kinetics and products of four groups of cement pastes. An important property of construction materials is the features of microstructure. On the one hand, the microstructure of hydrating cementitious material determines the mechanical strength that is the most important interest for structural engineers. On the other hand, characteristics of microstructure of cementitious materials, e.g. porosity and pore size distribution, have strong relationship with the durability of construction materials that is a key topic for construction material engineers. The addition of supplementary cementitious materials (e.g. slag in this research) and mineral materials (e.g. limestone powder in this research) into cement paste definitely modifies the microstructure and mechanical strength.

By means of Mercury Intrusion Porosimetry, BSE image acquisition and mechanical strength tests, this chapter investigated the microstructure of the hardening pastes and mortars, i.e. PC, PL, PB and PBL from micro-level to macro-level, aiming to find the influence of slag and limestone on the development of microstructure and mechanical strength.

6.2 Materials and Methods

6.2.1 Materials and Mix Design for MIP Test and BSE Image Acquisition

Materials and mix design for MIP test and BSE image acquisition were the same as used in Chapter 4. In the process of obtaining dried samples at each curing age for MIP and BSE experiments, the method of stopping ongoing hydration of pastes and freeze-drying were also the same as that used in Chapter 4.

6.2.2 Principle, Sample Preparation and Testing Procedure of MIP Test

Mercury intrusion porosimetry measurements were performed using a Pascal® instrument. Detailed description of the principle of MIP method can be referred to [132]. The Washburn equation and relevant parameters applied in this research are introduced in Eqs. 6.1 and 6.2, which convert the measured pressure to the corresponding pore size.

$$r = -\frac{2\gamma cos\theta}{P_c} \tag{6.1}$$

where r is the radius of the pore size in nm, θ is the contact angle (taken as 140 °). γ is the surface tension of pure mercury (taken as 480 dyne/cm), P_c is the applied pressure of mercury expressed in MPa. Based on the taken parameters, Eq. 6.1 is further simplified to Eq. 6.2 as follows:

$$r = \frac{735.403}{P_c} \tag{6.2}$$

The instrument in this research is capable of generating as high as 400 MPa mercury intrusion pressure, enabling it to determine pore size as fine as 3.68 nm (diameter). It consists of a low-pressure chamber and a high-pressure chamber. A measurement was carried out in two stages: an automatic low pressure running from 0 to 0.2 MPa and a high pressure from 0.2 to 400 MPa. All measured data were automatically collected and handled by dedicated computer program (control module).

An important step is the determination of the mass for each MIP test. After the freeze drying process, the mass of a sample for MIP test was basically determined according to the capacity of the stem volume of MIP instrument. Since the stem of the instrument used in this research has a maximum volume of 500 mm^3, which is the maximum volume of mercury that can be intruded into a sample, e.g. if a sample has a bulk density of 1.6 g/cm^3 and estimated total porosity 35%, then the maximum mass of the sample should not be larger than $(500/1000)/35\% \times 1.6 = 2.28$ g. As curing age and water to powder ratio change, the bulk density and total porosity also change accordingly due to the changing amount of hydration products, thus the maximum mass of the sample for each MIP test should be accordingly estimated each time. Generally, the maximum mass of a sample for MIP test increases as curing age increases due to the decreasing total porosity. Detailed introduction of determination of the maximum mass for each sample can be referred to [132].

As soon as the mass of a sample was determined, it was placed in the right dilatometer of the MIP instrument and underwent the test that includes both the low and high pressure stages.

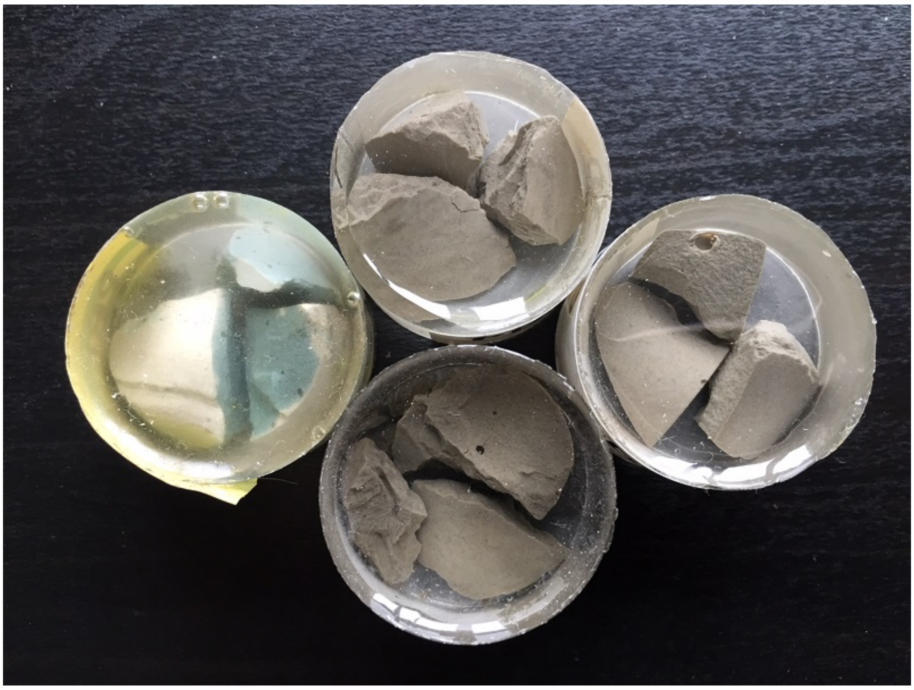

Figure 6.1: Samples after epoxy impregnation processing.

Considering the possible damage to the fine pore system at high pressure [2], we applied only 250 MPa as the maximum pressure for all samples in this research. This pressure corresponds to a pore size 5.88 nm (diameter).

6.2.3 Sample Preparation and Testing Procedure of BSE Image Acquisition

The BSE images were acquired by Environmental Scanning Electrical Microscopic (ESEM) method with a split quadrant backscattered electrons detector. Detailed introduction of the principle of ESEM can be referred to [132, 160]. The method applied in this research aims to observe the microstructure of the pastes at different curing ages, offering visible images of inner structure at micro-level.

Following the procedure introduced in Section 4.2.2, after the hydrating pastes were crushed into pieces at each due curing age, the ongoing hydration was stopped by immersing in liquid nitrogen, and then the free water was removed by freeze drying. However, Samples for BSE image acquisition need to be prepared by additional steps, i.e. epoxy impregnation, cutting, grinding and polishing as well as image acquisition.

Epoxy Impregnation

The first step is epoxy impregnation. Around 20 g of paste pieces (more than 3 pieces and each is smaller than half of the mold size, Fig. 6.1) were collected into a plastic mold to make one sample. The mold was then placed into a vacuum chamber which was later evacuated at 30

Table 6.1: Mix properties of mortars for mechanical strength test (in g).

	PC	PL	PB	PBL
CEM I 52.5 N	450	405	135	135
Limestone powder	0	45	0	45
Slag	0	0	315	270
Water	225	225	225	225
Standard sand	1350	1350	1350	1350
Water/Cement ratio	0.50	0.56	1.67	1.67
Water/Powder ratio	0.50	0.50	0.50	0.50

mBar for 2 hours. At the end of evacuation, low viscosity epoxy-resin was fed to the top of the sample through a rubber tube from a cup outside. The upper face of the sample was thus covered by liquid epoxy. After 10 min, the vacuum chamber was gradually open to let the air fill the space. Due to the pressure difference between the outside and inside of the chamber, epoxy on the surface of sample was pushed into the pore system of the sample. The impregnated sample was cured at atmospheric pressure and ambient temperature for about 24 hours, then it was ready for the cutting and polishing processes.

Cutting, Grinding and Polishing

The cured sample was first cut by a 1 mm thick diamond saw, and then carefully ground by hand at moderate pressure on the moderate speed lap wheel with P320, P500 and P1200 sand papers. The ground sample was later polished on the same wheel lap with 6, 3, 1 and 0.25 μm diamond paste for 2 min, respectively. After the polishing using diamond paste, a final polishing step was performed on the wheel lap covered with a low-relief polishing cloth. The sample was finally ready for BSE image acquisition.

Image Acquisition

The images were acquired using a BSE detector in the water vapor mode and at low acceleration voltage of 10$\sim$20 KV. All technical operating parameters, i.e. contrast, brightness, magnification and spot size were kept constant for all samples for the sake of good comparison.

6.2.4 Mix Design and Specimen Casting for Mechanical Strength Test

The mix design for pastes was also exactly the same as used in Chapter 4, i.e. PC, PL, PB and PBL with w/p=0.4 as listed in Table 4.2. After the mixing procedure, the paste was cast in the mold as described in EN 196-1:2005 [161]. The curing conditions and strength measurement was carried out according to EN 196-1:2005. The scheduled curing age was 1, 3, 7, 14, 28 and 91 days, as also applied in Chapter 4.

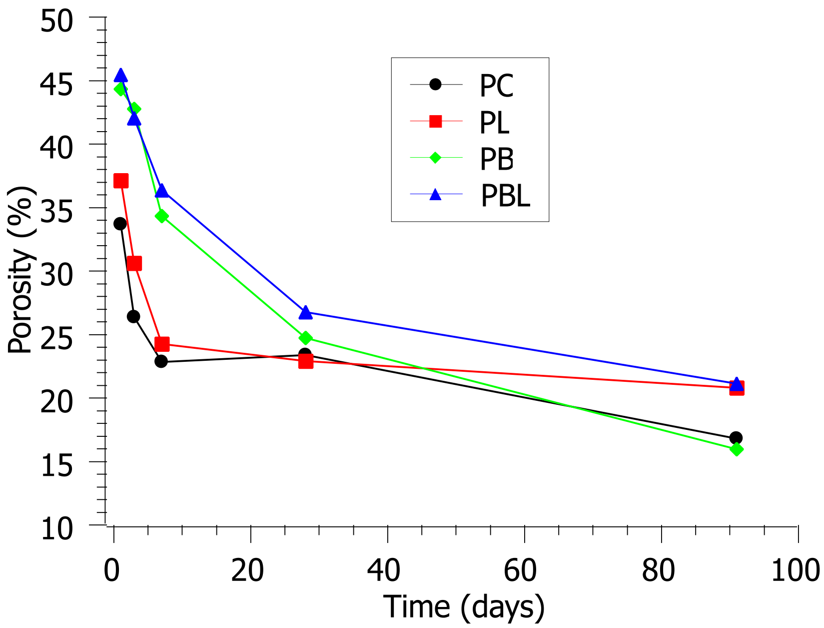

Figure 6.2: Porosity of pastes at different ages tested by MIP.

Besides mechanical strength of pastes, batches of mortars with same replacement ratio of slag and/or limestone powder were also cast to test the mechanical strength. The mixture design of mortars was strictly carried out according to the European standard EN 196-1:2005. The mix proportions of four groups of mortars, i.e. Portland cement (PC), Portland cement blended with limestone (PL), Portland cement blended with slag (PB) and Portland cement blended with slag and limestone (PBL), are listed in Table 6.1.

It should to be noted that EN 196-1:2005 is designed for cement mortars. However, slag and limestone powder were added into mortars in this research, thus two minor changes were adopted. The first is that the blended powders were first mixed at low speed for 2 min in order to well disperse slag and/or limestone powder in cement. After the pre-mixing of blended cements, the rest mixing procedure was performed as described in EN 196-1:2005 [161]. The second change is the curing environment. The modified part in this research was that all demolded mortar prisms ($40\times40\times160$ mm^3) were cured in saturated lime solution instead of pure water, considering the leaching of calcium from samples to pure water may influence the hydration of slag in blended cements. The strength of mortars was tested at curing ages of 1, 3, 7, 14, 91 and 180 days according to the standard.

6.3 Experimental Results and Discussion

6.3.1 Results of MIP

Total Porosity

Figs. A.9 to A.12 present the curves of cumulative volumes and the corresponding differential volume of the first intruded mercury at different mercury pressures from MIP experiments. Note that the mercury pressure in the figures was transfered to pore size according to Eq. 6.2. Fig. 6.2 shows the measured porosity of pastes at different curing ages.

For all types of pastes, the total porosity expectedly decreased as curing age increased. This is apparently because the increasing amount of hydration products filled the space which was originally occupied by water. Most of pore sizes (diameter) were smaller than 100 nm at least after 7 days of hydration.

Pure Portland cement paste, i.e. PC, had the lowest porosity 33.7% after 1 day of hydration. Porosity of PL paste was constantly higher than PC except for the curing age 28 days, but the porosity of PC at 28 days may be slightly overestimated given certain variation of sample preparation.

The higher porosity of PL paste could be caused by the addition of limestone that reduced the total amount of hydration products due to the dilution effect. Although the hydration degree of clinker in PL was higher than that of PC, 10% of cement in PL paste was replaced by limestone powder. The limestone powder in PL paste remained almost unchanged after 1 day of hydration as confirmed by TGA test, thus it did not produce enough expansive hydration products to fill the capillary pores as in the case of PC paste, leading to higher total porosity in PL paste at all ages. Similar observation was also reported by [63].

Porosity of slag blended cement paste, i.e. PB and PBL pastes, was significantly higher than that of PC and PL pastes in the first 28 days, e.g. the porosity of PB and PBL pastes was 44.3% and 45.4% at 1 day, respectively, while the corresponding values of PC and PL pastes was 33.7% and 37.1%, respectively. The higher porosity of slag blended pastes is caused by the relatively slow hydration process of slag at early age. After 91 days of hydration in this research, however, the porosity of PB paste was only 16.0%, which is slightly lower than that of PC (16.8%); meanwhile, the porosity of PBL is 21.1% at 91 days, which is almost equivalent to the value of PL (20.8%).

Comparing the porosity of PB and PBL to that of PC and PL, respectively, i.e. PB vs. PC, PBL vs. PL, we can see that the volume of hydration products produced by slag is comparable to that of cement after 28 days of hydration, though the reaction degree of slag was still lower than that of cement even at later ages. In other words, the expansion ratio of hydration products of slag is higher than that of cement clinker, which will be quantitatively investigated in Section 6.3.1.

As for the influence of limestone on porosity of slag blended cement paste, i.e. PB and PBL

Table 6.2: Critical pore sizes of samples at different curing ages (nm).

Time (days)	PC	PL	PB	PBL
1	95.68	117.37	583.41	656.31
3	56.96	65.10	442.86	491.67
7	44.09	64.73	15.94	76.00
28	79.32	50.11	14.40	32.66
91	51.75	52.02	< 5.88	19.70

pastes, it can be seen from the results that porosity of PBL was comparable to that of PB at the early ages (< 7 days) but the difference became larger as curing age increased. Being compared to PB paste, the higher porosity of PBL paste at later age is the result of addition of 10% of limestone which contributed quite limited expansive volume of hydration products filling the capillary pores.

Critical Pore Size

As shown in Figs. A.9 to A.12, the differential curves of MIP cumulative volume provide additional information to analyze the pore size distribution in samples. Table 6.2 lists the sizes corresponding to the first peak of differential curves. The first peak is defined as the first critical pore diameter that denotes the physical meaning that pores whose diameter is greater than this value cannot form connected path through the sample [132].

Table 6.2 lists the measured first critical pore size of all pastes at different curing ages. The first critical pore size of sample decreases as curing age increases, indicating the critical pore size to form an inter-connected pore system became fine as more hydration products were available to fill the pores. PB and PBL pastes at certain curing ages, e.g. 3 days, showed two peaks in the differential curves, implying two pore systems were formed, i.e. the first peak shows the critical pore size of capillary pores while the second corresponds to that of gel pores.

Except for a possible experimental error in the sample PC at 28 days, the addition of limestone powder in PL paste just had slight influence on the critical pore size at early age. The critical pore size of PC and PL did not change too much after 28 days of hydration and shows comparable values, i.e. the critical pore size of PC at 91 days was 51.75 nm and that of PL paste was 52.02 nm, which are slightly larger than the results reported by [72] that critical pore size of about 30 nm was measured in the binary limestone blended cement paste (cement:limestone:water=0.85:0.15:0.425, by mass) hydrated after 6 months. The relatively stable critical pore size of PC and PL pastes at later age coincides with their slowly decreasing porosity, which should be caused by the slow development of hydration degree of clinker as shown in Fig. 4.10. Since clinker was the only source forming hydration products in PC and PL paste over the whole curing ages, the slow hydration process of PC and PL pastes at later age contributed less hydration products to reduce the porosity.

The first critical pore sizes of PB and PBL pastes were significantly large within the first 3

Table 6.3: Surface area of pores in samples at different ages tested by MIP (m^2/g, tested at maximum MIP pressure of 250 MPa).

Time (days)	PC	PL	PB	PBL
1	21.17	17.83	11.86	10.10
3	20.18	18.72	21.39	22.19
7	20.55	17.97	38.06	32.98
28	17.15	22.05	49.61	38.07
91	17.16	21.00	43.04	40.13

days of hydration due to the slow hydration of slag at early age. However, the critical pore sizes of PB and PBL sharply decreased after 3 days of hydration, e.g. value of PB paste was as large as 442.86 nm at 3 days but soon decreased to just 15.94 nm after 7 days of hydration. The latter was much smaller than the corresponding values of PC and PL pastes. Even at the age later than 7 days, the critical pore size of PB and PBL continued decreasing remarkably compared with the cases of PC and PL pastes, and the values of PB and PBL pastes were much finer than that of PC and PL pastes after 28 days of hydration, e.g. critical pore size of PBL was just 19.70 nm, and that of PB was even smaller than 5.88 nm. These results demonstrate that slag improved the pore system in this research, which can improve the durability.

Surface Area of Pores and Average Pore Size

Based on the assumption that the shape of pore in hardening paste is cylindrical, the total surface area of pores S_{pore} (m^2/m) was calculated based on MIP results according to the calculation method of [162]:

$$S_{pore} = \frac{\int_0^{P_{max}} P dV_{mercury}}{\gamma \times cos(\theta)} \tag{6.3}$$

where γ is surface tension of mercury, P is the mercury pressure corresponding incremental intruded mercury volume $dV_{mercury}$, θ is the contact angle of mercury with sample. Values of θ and r used in this research are 140° and 0.48 N/m, respectively.

Table 6.3 shows the calculated results of surface area of pores of pastes at different curing ages. The surface area of pores in slag blended pastes is smaller than PC and PL pastes at early ages and soon exceeded after 3 days of hydration. They were approximately two times higher than that of PC and PL pastes after 91 days of hydration, generally indicating the fine pore system in slag blended pastes.

It is worthwhile to link the total porosity with the surface area of pores, which mathematically leads to the average pore diameter. The average pore diameter d_{ave} is calculated using Eq. 6.4:

$$d_{ave} = 4 \times \frac{V_{mercury}}{S_{pore}} \tag{6.4}$$

where $V_{mercury}$ is the total intruded mercury (cm^3/cm^3) directly measured by MIP test.

Table 6.4: Average pore sizes of samples at different curing ages (nm, tested with maximum MIP pressure 250 MPa).

Time (days)	PC	PL	PB	PBL
1	39.18	54.40	102.36	126.15
3	29.51	40.67	55.26	51.97
7	24.84	31.04	22.90	29.51
28	31.27	23.70	12.57	17.87
91	21.79	22.56	8.90	12.85

Table 6.4 lists the average pore diameter of pastes at different curing ages. Average pore diameter of all pastes decreased as curing age increases. PC paste showed the smallest average pore diameter during the first week, and slag blended cement pastes (PB and PBL) had coarse average pore size in the first 3 days, but they soon decreased to comparable values of PC and PL pastes after 7 days of hydration. The average pore sizes of PB and PBL pastes were much smaller than that of PC and PL pastes at later age, e.g. values of PB and PBL after 91 days of hydration were 7.59 nm and 10.77 nm, respectively, while the corresponding values of PC and PL pastes were 19.23 and 20.50 nm, respectively. The smaller average pore diameter of PB and PBL confirms the positive contribution of slag to the pore system, making the pore system finer than that in PC and PL pastes.

In terms of the influence of limestone powder on the average pore diameter, it can be seen from the results (Table 6.4) that limestone did coarsen the average pore size of both PL and PBL pastes compared with the counterparts during the whole curing age, i.e. PL vs. PC, PBL vs. PB. The influence is even more distinct in slag blended pastes. The coarsened average pore in limestone blended pastes is readily explained by the fact that very limited reaction of limestone occurred in pastes thus hardly contributing to expansive hydration product.

According to the generally accepted classification, two different pore systems exist in cement paste. The first is capillary pore system with average pore diameter larger than 10 nm. The second is gel pore system with average pore diameter smaller than 10 nm [72, 132, 163]. It is clear in Table 6.4 that pore system of PB was transformed to gel pore system after 28 days of hydration, which also approximately occurred after 91 days of hydration in the case of PBL paste, but the pore system in PC and PL pastes still remained as capillary pores, since the average pore size in PC and PL pastes at 91 days was 21.79 and 22.56 nm, respectively. The refined pore system in PB and PBL pastes definitely lead to better transport property and durability.

Bulk Density

The bulk density of paste is defined as the mass m_{sample} (g) of dried sample relative to its bulk volume V_{bulk} (cm^3):

$$\rho_{bulk} = \frac{m_{sample}}{V_{bulk}} \tag{6.5}$$

Table 6.5: Bulk density (g/cm^3. Time ∞ assumes all water being bound in hydration products).

Time (days)	PC	PL	PB	PBL
0	1.3839	1.3748	1.3547	1.3500
1	1.6236	1.5315	1.4615	1.4271
3	1.7705	1.6086	1.447	1.4589
7	1.7888	1.7399	1.5758	1.4951
28	1.7434	1.7530	1.5874	1.5741
91	1.7981	1.7558	1.6649	1.6371
∞	1.9375	1.9248	1.8966	1.8901

Regardless of the shrinkage of bulk volume, ρ_{bulk} is just a function of m_{sample}. Since free water was removed by freeze-drying in this research, m_{sample} is the mass of all solid raw material(s) and total bound water.

Table 6.5 lists the bulk density of all pastes at different curing ages. It should be mentioned that the bulk density at 0 day of pastes (prior to hydration) was calculated based on the initial mixing state (with density of cement, slag, limestone and water being 3.1000, 2.9000, 2.7000 and 1.000 g/cm^3, respectively), which means no bound water at all in the mass of sample m_{sample}. The values of ∞ time means that the density is calculated based on the assumption that all water is converted to bound water in hydration products.

The bulk density of paste generally increased as hydration proceeded, which is essentially the result of water being gradually bound in hydration products. According to the calculated theoretic maximum bulk density (∞ time) and the experimentally measured results, the bulk density of all pastes in this research was less than 2.0 g/cm^3, while overestimated result as high as 2.2 g/cm^3 for similar pastes was also reported in literature [164], which is probably caused either by misunderstood definition of bulk density or misused calculation method.

Total Bound Water Calculated from Bulk Density

According to the definition by Eq. 6.5, the total bound water can be calculated from the measured bulk density, assuming that the shrinkage of bulk volume in the process of hydration is ignored. For example, the bulk density of PBL paste at 0 and 91 days is 1.3500 and 1.6371 g/cm^3 (Table 6.5), respectively, which means there is initially 1.3500 g solid materials (cement, slag and limestone) and 1.3500 $\times$ 90%=1.2150 g cement and slag. The mass of total bound water in 1 cm^3 of paste after 91 days of hydration is 1.6371-1.3500=0.2871 g, thus at 91 days the mass ratio of total bound water relative to original cementitious materials is 0.2871/1.2150=23.6% in PBL paste.

Table 6.6 lists the calculated mass ratio of total bound water relative to original cementitious material(s) (cement or cement and slag) based on the measured bulk density.

It should be emphasized that the results in Table 6.6 cannot be directly compared with Fig. 5.8, though the two results denote the same ratio, i.e. total bound water relative to original cementitious material(s). The results calculated based on bulk density in Table 6.6 are essentially

Table 6.6: The mass ratio of total bound water relative to original cementitious material(s) calculated from bulk density (%).

Time (days)	PC	PL	PB	PBL
0	0	0	0	0
1	17.3	12.7	7.9	6.3
3	27.9	18.9	6.8	9.0
7	29.3	29.5	16.3	11.9
28	26.0	30.6	17.2	18.4
91	29.9	30.8	22.9	23.6
∞	40.0	44.5	40.0	44.5

Table 6.7: Apparent density at pressure 250 MPa (g/cm^3).

Time (days)	PC	PL	PB	PBL
0	3.1000	3.0547	2.9572	2.9351
1	2.4478	2.4365	2.6257	2.6164
3	2.4040	2.3183	2.5274	2.5177
7	2.3180	2.2972	2.3998	2.3497
28	2.2754	2.2736	2.1092	2.1494
91	2.1614	2.2169	1.9808	2.0752

much less accurate compared with that tested by TGA in Fig. 5.8. The reason is that the shrinkage of bulk volume of each paste was ignored in the calculation based on bulk density. As analyzed by [165], the shrinkage of bulk volume of cement paste can reaches as high as 7% for a Portland cement paste with w/c ratio 0.33. However, as the volume change of different pastes at the same age does not differ much, the results in Table 6.6 still bear information of the hydration process of pastes.

The mass ratio of total bound water relative to cementitious material(s) increased as curing age increased, which was the result of increasing hydration as more water is consumed and converted to bound water. Slag blended pastes, i.e. PB and PBL pastes, showed lower ratio of total bound water compared with that of PC and PL pastes, which was caused by the low hydration degree of slag at each same curing age compared with that of cement clinkers as confirmed by XRD/Rietveld and EDTA measurements. The ratio of total bound water in limestone blended cements became slightly higher than the counterpart pastes without limestone at later age, e.g. 1 g of cement bound 0.295 g water in PL paste after 7 days of hydration, while the corresponding value in PC paste was 0.293 g, same trend also appeared at curing age of 28 days in the case of PB and PBL pastes, which agrees with the trend investigated by TGA in Section 5.3.3. The increased mass ratio of total bound water relative to raw cementitious material(s) at later age could be the result of limited reaction of limestone with aluminate phase, i.e. the formation of monocarboaluminate.

Apparent Density

Apparent density (g/cm^3, also called skeleton density $\rho_{apparent}$) is defined as the mass (m_{sample}) of a sample divided by its skeleton volume ($V_{skeleton}$):

$$\rho_{apparent} = \frac{m_{sample}}{V_{skeleton}} \tag{6.6}$$

The skeleton volume is obtained from the bulk volume of a sample minus the volume of pores. Due to the limitation of practical maximum pressure in MIP test, mercury of MIP can just reach a certain size of pore, i.e. 5.88 nm corresponding to 250 MPa applied in this research, thus the practical skeleton volume is obtained from the bulk volume of a sample minus the maximum volume of intruded mercury.

Table 6.7 lists the apparent density of all pastes from curing ages of 1 day to 91 days at the maximum MIP pressure 250 MPa. Values at 0 day were calculated from the initial stage of raw material(s) without water at all. Results show apparent density of all pastes decreased as curing age increased, which is readily explained by the fact that hydration products of all pastes are expansive.

Volumetric Expansion Ratio (ν)

As used in HYMOSTRUC [3], the volumetric expansion ratio ν is defined as the proportion of the volume of hydration products after hydration relative to the corresponding original volume of reacted raw cementitious material(s), which is mathematically described as Eq. 6.7:

$$\nu = \frac{V_{\text{after hydration}}}{V_{\text{original raw cementitious material(s)}}} \tag{6.7}$$

According to the definition, it can be calculated from measured porosity and hydration degree of cementitious material(s) based on certain assumptions. For example, the porosity of PBL sample at 91 days is 21.11%, and the hydration degree of cement and the reaction degree of slag in PBL at 91 days is 62.08% and 34.18%, respectively. The density of materials and mix proportion are the same as aforementioned, therefore, the bulk volume of the PBL paste mixed by 1 g of raw materials and 0.4 g water is as follows:

$$V_{bulk,PBL} = \frac{0.3}{3.1} + \frac{0.6}{2.9} + \frac{0.1}{2.7} + \frac{0.4}{1.0} = 0.7407\ cm^3 \tag{6.8}$$

In this 1.4 g paste, the original volume of solid materials (0 day) is:

$$V_{solid,0d} = \frac{0.3}{3.1} + \frac{0.6}{2.9} + \frac{0.1}{2.7} = 0.3407\ cm^3 \tag{6.9}$$

And volume of solid phase (hydration products and unreacted raw materials) in PBL paste at 91 days is:

$$V_{solid,91d} = V_{bulk,PBL} \times (1 - porosity) = 0.7407 \times (1 - 21.11\%) = 0.5843\ cm^3 \tag{6.10}$$

Table 6.8: Volumetric expansion ratio calculated from MIP test.

Time (days)	PC	PL	PB	PBL
1	2.59	2.28	2.35	2.70
3	3.04	2.18	2.28	2.30
7	2.51	2.31	2.57	2.48
28	2.16	2.20	2.72	2.70
91	2.24	2.22	2.86	2.86

So the increased volume of solid phase in the paste is:

$$\Delta V = V_{solid,91d} - V_{solid,0\ d} = 0.5855 - 0.3421 = 0.2436\ cm^3 \tag{6.11}$$

And, the total original volume of reacted cement and slag is calculated based on their hydration degree and original weight:

$$V_{reacted\ solid} = 62.08\% \times \frac{0.3}{3.1} + 34.18\% \times \frac{0.6}{2.9} = 0.1308\ cm^3 \tag{6.12}$$

Therefore, the volumetric expansion ratio of hydration products relative to the original raw materials is obtained:

$$\nu_{PBL,91d} = \frac{\Delta V + V_{reacted\ solid}}{V_{reacted\ solid}} = \frac{0.2434 + 0.1308}{0.1308} = 2.86 \tag{6.13}$$

The following four assumptions should be noted:

1. The volumetric expansion ratio is the overall value of both cementitious materials, i.e. cement and slag in this case;
2. Limited volume expansion contributed by limestone reaction was not considered.
3. Shrinkage of bulk volume were not considered.
4. The porosity was measured at maximum MIP pressure 250 MPa in this research, which means finer pores smaller than 5.88 nm (diameter) existing in hydration products were considered as the "volume" of hydration products.

Table 6.8 lists the calculated expansion ratios of hydration products of each paste at all ages. Except for the abnormal value of PC paste at 3 days, calculated values are generally higher than the reference value 2.2 used in HYMOSTRUC for Portland cement. Values at later age, e.g. 91 days, are more accurate than those at early ages due to the relatively higher variation of samples for MIP, XRD/Rietveld and EDTA tests at early age when only limited cement and slag were reacted.

As shown in Table 6.8, the volumetric expansion ratios of PC and PL pastes are systematically lower than that of PB and PBL pastes, which is in agreement with the lower apparent density of slag blended cement pastes, indicating the better pore filling effect of slag hydration products.

Furthermore, the value ν of PC is theoretically identical to that of PL paste because limestone is assumed to contribute in a quite limited way to expansive hydration products, which is also the case in PB and PBL pastes.

The expansion ratio of hydration products is an important parameter for the hydration model proposed in Chapter 7. It is one of the key material properties for calculating and building the microstructure of hydrating cement paste. The average volumetric expansion ratio of PC hydration products calculated from the last three ages (i.e. 14, 28, 91 days) is 2.30, slightly higher than the value 2.20 theoretically calculated in [2] and applied in HYMOSTRUC. It is also higher than 2.15 that was used in [166].

Combining the average volumetric expansion ratio 2.30 of PC hydration products and the hydration/reaction degree of cement and slag at each age, we can also calculate the individual volumetric expansion ratio of slag hydration products. The calculated results show that the average volumetric expansion ratio of slag hydration products in PB and PBL pastes is 3.06 and 3.11, respectively. As for the case of PC paste, the first two ages, i.e. 1 and 3 days, were not included in the calculation of average volumetric expansion ratio of slag hydration products due to the variation of samples at early age.

According to the two calculated volumetric expansion ratios, 2.30 of cement vs. 3.10 of slag, it can be seen that the hydration products of slag is more expansive than that of cement. The calculated volumetric expansion ratios will be used in developing the theoretical hydration model of blended cement in Chapter 7 and the calibration and validation work in Chapter 8.

6.3.2 Results of BSE Image Observation

Fig. 6.3 presents the BSE images of PC, PL, PB and PBL pastes hydrated after 7 and 91 days, respectively, showing direct views of inner microstructure of hydrating pastes. Although the porosity of PL paste at 7 days is slightly higher than that of PC paste as shown by MIP, the BSE image at 7 days shows that there was less unreacted fine cement particles in PL paste, which is quantitatively confirmed by the higher degree of hydration of clinkers in PL paste using XRD/Rietveld analysis in Chapter 4. As shown by BSE images of PC and PL pastes after 91 days of hydration, a certain amount of large cement particles still remained unreacted. Limestone particles still can be seen in image of PL paste at 91 days. Unlike the hydration products precipitated on the front surface of unhydrated cement particles, some limestone particles in PL are not fully covered by hydration products, resulting in the porous microstructure in the neighborhood of limestone particle, which is in agreement with the observation of [63].

It can be seen that the microstructure of slag blended cement pastes at 7 days is more porous than that of PC and PL. Large pores in the size of several micrometers exist in PB and PBL pastes at 7 days. After 91 days of hydration, the microstructure of slag blended cement pastes was greatly improved with pores filled by hydration products. Although small cement particles are not visible in images of 91 days, some large cement particles as well as few large pores

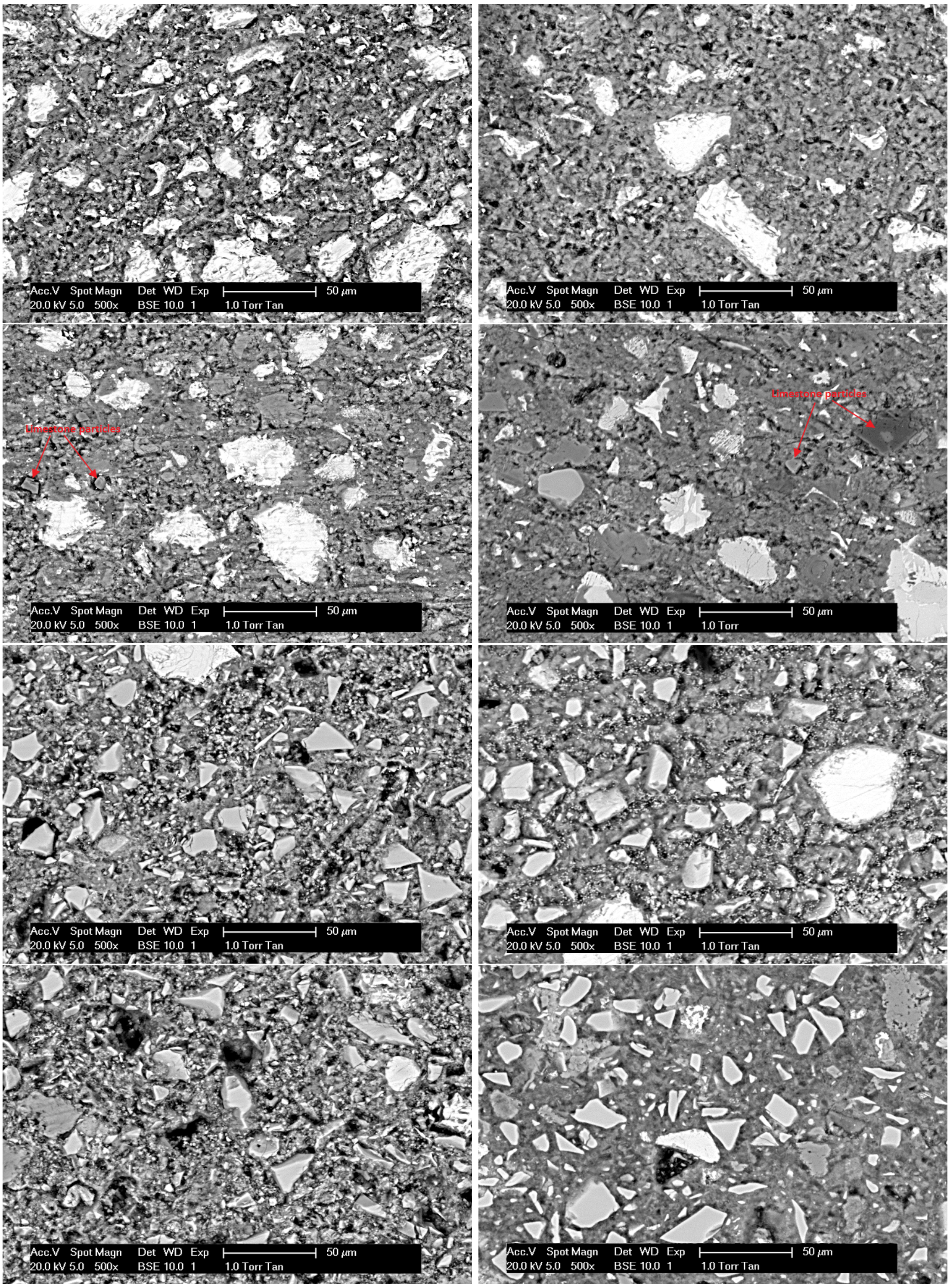

Figure 6.3: BSE images of microstructure of hydrating pastes. From top to bottom: PC, PL, PB and PBL, the left pictures are for 7 days, the right ones are for 91 days.

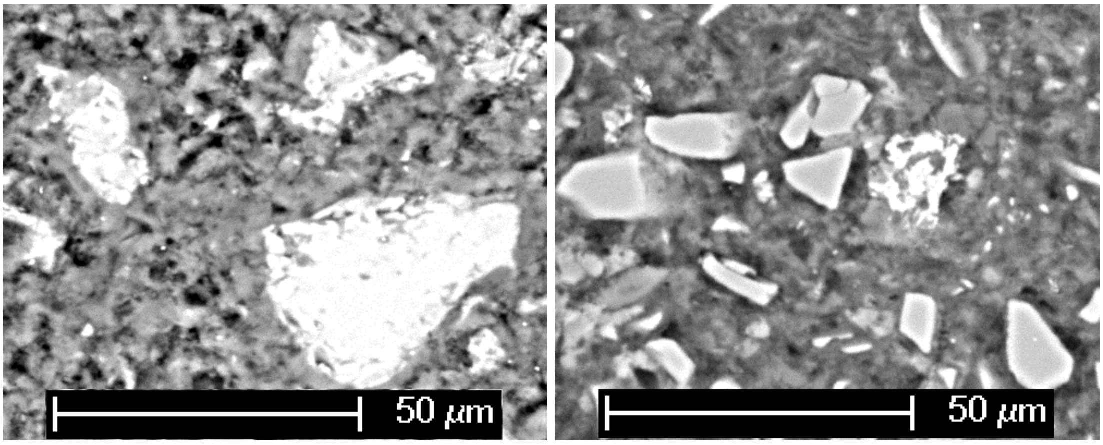

Figure 6.4: No distinct reaction rim of slag particle was observed in BSE images. The left is PC paste at 91 days, and the right is PBL paste at 91 days.

still exist in slag blended cement pastes. Contrary to the image of PL paste at 91 days, the microstructure in the vicinity of limestone particles in PBL paste is evidently enhanced by the filling of hydration products, which could be caused by the higher expandability of slag hydration products as confirmed by its calculated higher volumetric expansion ratio ν. A remarkable amount of slag particles including large and small sizes remained unreacted even after 91 days as indicated by BSE images, which is in agreement with the low reaction degrees of slag at 91 days as tested by EDTA experiment in Section 4.3.3.

Another feature of slag in ESEM image is that no distinct reaction rim of slag particle was observed (Fig. 6.4), which usually occurs in the hydration of cement particle as shown in the case of PC. In terms of microstructure, the hydration products of cement are usually classified as inner product and outer product by researchers. The inner product layer is typically shown as a reaction rim in the BSE image of hydrating cement paste. Compared with the reported distinct reaction rim in alkali-activated slag pastes [36, 37], the absence of reaction rim of slag particle in PB and PBL pastes could be caused by two reasons: (1) lower reaction degree of slag makes the depth of reaction rim of a slag particle thinner than the case of cement particle, and (2) the slow reaction process of slag particle allows hydration products being precipitated at remote positions thus results in less distinct inner product layer. SEM-BSE pictures of slag blended cement paste in Kocaba's work [59] also show the absence of reaction rim on the front surface of slag particles.

It appears in BSE images that microstructure of slag blended cement pastes has less pores, however, it is difficult to quantitatively assess the pore system of pastes by BSE images obtained in this research. Due to the limited resolution of BSE applied in this research (each pixel represents 0.178 μm), the pore size revealed by BSE images is not at the same order of magnitude with that measured by MIP experiment which measured the pore size as fine as 5.86 nm (diameter). Meanwhile, the moderate quality of BSE images in this research makes gray levels of different phases hard to be distinguished, thus quantitative BSE image analysis was not carried

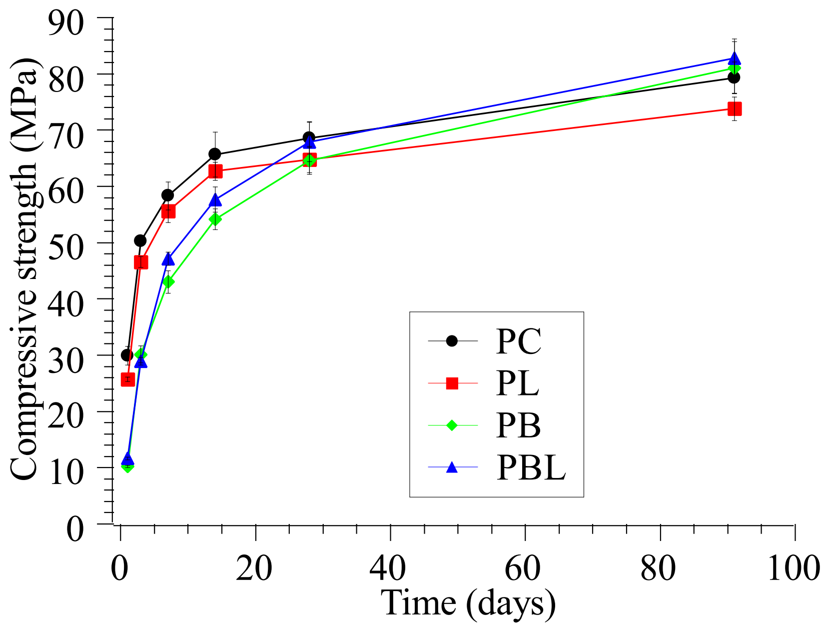

Figure 6.5: Compressive strength of paste prisms from 1 to 91 days of curing.

out in this research.

6.3.3 Results of Mechanical Strength

Compressive Strength of Paste

Fig. 6.5 shows the compressive strength results of pastes tested from 1 to 91 days of curing. The strength of all pastes developed fast in the first 14 days of curing, which is in line with the hydration kinetics of cementitious materials as discussed in Chapter 4. The compressive strength of PC and PL pastes was higher than PB and PBL pastes in the first 28 days of curing, showing the dilution effect of slag on compressive strength due to its slow hydration progress at early age. However, compressive strength of PB and PBL pastes surpassed PC and PL pastes after 91 days of curing. This indicates that the hydration products produced by slag blended cements have stronger compressive strength, as the hydration degrees of cement clinker in all pastes are comparable but the reaction degrees of slag in PB and PBL pastes are much lower.

The single addition of limestone powder into cement (PL paste) showed negative influence on its compressive strength, as the compressive strength of PL paste was constantly lower than that of PC paste over the whole curing age, which could be caused by the fact that limestone powder acts as inert filler due to its limited chemical reaction. However, in the ternary blended cement i.e. PBL pastes, the addition of limestone powder showed a positive effect on the compressive strength. As shown by all tested results, the compressive strength of PBL grows from 11.64 MPa at 1 day to 82.75 MPa at 91 days, while the corresponding values of PB was 10.25 and 81.07 MPa, respectively. Except for the value of 3 days, the compressive strength of PBL paste was systematically higher than that of PB paste. Contrary to the influence of limestone in PL

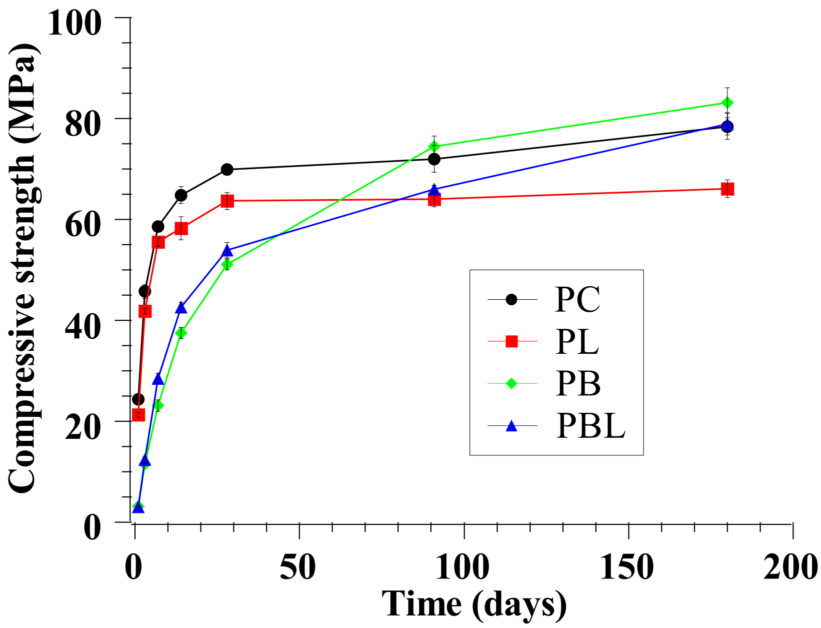

Figure 6.6: Compressive strength of mortar prisms from 1 to 180 days of curing.

paste, it can be concluded that the combination of limestone and slag in cement paste brought a synergistic effect on compressive strength. A possible explanation is that the inert limestone filler acted as a kind of micro-aggregate for the more expansive hydration products of slag.

Compressive Strength of Mortar

The tested compressive and flexural strengths of mortar samples cured from 1 to 180 days are plotted in Figs. 6.6 and 6.7. Compressive strength of all mortar samples developed fast in the first 28 days of curing. Results show that the replacement of cement by slag reduced the compressive strength in the first 91 days, e.g. the compressive strength of PC mortar was always higher than PB mortar till 91 days of curing, which also occurred if comparing PL to PBL mortar within the 91 days of curing. The reduced compressive strength of slag blended cement mortars at early age is mainly the result of relatively slow hydration process of slag. However, the compressive strength of slag blended mortars exceeded the counterparts containing no slag after 91 days of curing, i.e. PBL vs. PL and PB vs. PC. The compressive strength of PBL mortar (78.95 MPa) was even slightly higher than that of PC mortar (78.42 MPa) after 180 days of curing.

Similar to the influence of limestone powder in paste, the single addition of limestone powder into mortar reduced the compressive strength, as shown by the constantly lower compressive strength of PL mortar compared with PC mortar at the same curing age. The difference of compressive strength between PC and PL mortars became larger as curing age increased. The reduced compressive strength of PL mortar indicates that the addition of limestone powder had negative influence on compressive strength due to its dilution effect [127], though other researchers [167] reported that as high as 18% of cement was replaced by limestone powder

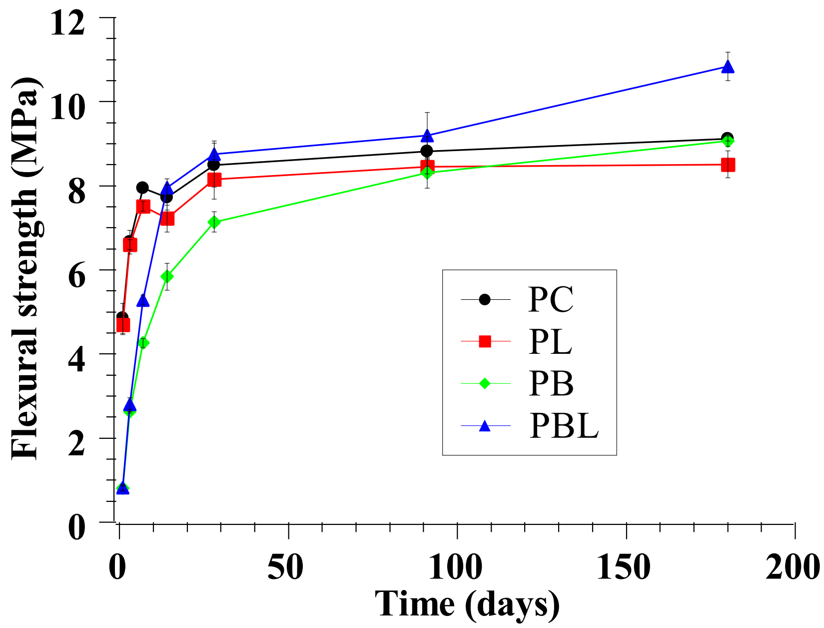

Figure 6.7: Flexural strength of mortar prisms from 1 to 180 days of curing.

with median size 5 μm (diameter) in concrete resulted in higher 28-day compressive strength than the corresponding reference.

However, the addition of limestone powder in slag blended mortar, i.e. PBL mortar, showed a positive influence on the compressive strength within the first 28 days of curing age [168], which also occurred in PBL paste. Tested results suggest that the compressive strength of PBL mortar increased from 3.08 MPa at 1 day to 53.95 MPa after 28 days of curing, which was constantly higher than the corresponding values of PB mortar except for the value at 1 day. The compressive strength of PB mortar finally exceeded PBL mortar after 28 days of curing, which could be explained by that the dilution of cementitious materials by limestone surpassed its positive contribution (nucleation site effect [127]) to compressive strength at later age, i.e. after 28 days. Contrary to the performance of limestone in PL mortar, the so called synergistic effect brought by the combination of limestone and slag also occurred in PBL mortar in the first 28 days in this research.

Flexural Strength of Mortar

Fig. 6.7 displays the flexural strength of mortar samples from the curing age 1 to 180 days. Flexural strength of PL mortar was constantly lower than PC mortar over the whole curing age and the difference became larger as curing age increased, indicating the dilution effect of limestone in PL mortar. Flexural strength of PB was the lowest among the four groups of mortars within the first 91 days of curing, but it finally exceeded the value of PL mortar after 180 days of curing and reached comparable flexural strength of PC mortar. As for PBL mortar, its flexural strength was always stronger than PB mortar at all ages. Compared with PC and PL mortars, PBL showed the strongest flexural strength after 14 days of curing. Considering the distinct influence brought by limestone in PL and PBL on flexural strength, we can see the significant synergistic effect caused by the combination of slag and limestone in ternary blended mortar, which was stronger and lasted longer comparing with the same effect on compressive strength. The increased flexural strength in PBL mortar is probably caused by the strong bond between the interface of slag and limestone particles due to their special shapes and surface textures.

Similar to the experiment testing mechanical strength of mortar in this research, Weerdt [169] tested the mechanical strength of two batches of mortars, one is 65% CEM I+ 35% fly ash and the other 65% CEM I+25% fly ash +10% limestone powders. It was reported that the compressive and flexural strength of ternary blended mortar from 1 to 140 days of curing was slightly higher than that of binary blended system, showing synergistic effect brought by the combination of limestone and fly ash.

6.4 Conclusions

This chapter investigated the microstructure of hydrating pastes and mechanical strength of pastes and mortars. Conclusions can be summarized as follows.

1. The addition of slag greatly improved the pore system of blended cement paste, reducing both the total porosity and critical pore size after 91 days of hydration, while the presence of limestone powder had negative influence on the pore system.

2. Calculation based on MIP results indicates the volumetric expansion ratio of hydration products of cement and slag is 2.3 and 3.1, respectively, which will be used to develop, calibrate and validate the hydration and microstructure model of ternary cementitious system in the next chapters.

3. BSE images reveal that the slag particle still maintains its original shape, showing low degree of hydration even after 91 days of hydration.

4. Compressive strength of slag blended cement paste and mortar was low at early age but superior to that containing no slag at later age. The single addition of limestone powder in cement reduced the compressive strength over the whole curing age, but improved the compressive strength at least at early age when coexisting with slag, showing synergistic effect in ternary blended cement, which is even more distinct in the case of flexural strength of mortar.

Chapter 7

The Simulation Model of Hydration of Ternary Blended Cement Paste

7.1 Introduction

In this chapter, a model to simulate the hydration of ternary blended system is proposed based on the existing HYMOSTRUC proposed by van Breugel [3] which is originally dedicated to modeling the hydration process of pure Portland cement.

7.2 Spatial Model for Ternary Blended System Based on HYMOSTRUC

7.2.1 Particle Size Distribution

The shape of all particles is assumed as spherical. The particle size distribution of the three components, i.e. Portland cement (with c as subscript), blast furnace slag (s) and limestone powder (l), are considered as obeying the Rosin-Rammler function that is expressed with two constants, i.e. $b_{(\cdot)}$ and $n_{(\cdot)}$.

$$G_c(x) = 1 - exp(-b_c \times x^{n_c}) \;\; [g] \; (x \; in \; \mu m) \tag{7.1}$$

$$G_s(x) = 1 - exp(-b_s \times x^{n_s}) \;\; [g] \; (x \; in \; \mu m) \tag{7.2}$$

$$G_l(x) = 1 - exp(-b_l \times x^{n_l}) \;\; [g] \; (x \; in \; \mu m) \tag{7.3}$$

where x denotes the diameter of a material particle, $n_{(\cdot)}$ and $b_{(\cdot)}$ ($b_{(\cdot)} > 0$) are two constants of each material. $G_{(\cdot)}(x)$ is the cumulative mass of particles that is not larger than x in 1 gram same material. The maximum particle size x_{max} in the 1 g of material is defined as the particle with no more than 0.01 g oversize weight, i.e.

$$G(x_{max}) = 0.99 \;\; g \tag{7.4}$$

The minimum size x_{min} of each component is determined by realistic value that depends on its fineness, so particles less than x_{min} or larger than x_{max} are disregarded. To meet the physical consistency of the above equations, a correction factor $\gamma_{(\cdot)}$ for each material is needed, e.g. for cement, γ_c follows from:

$$\gamma_c = \frac{G_c(x=\infty)}{G_c(x_{max}) - G_c(x_{min})} = \frac{1}{G_c(x_{max}) - G_c(x_{min})} \tag{7.5}$$

From HYMOSTRUC, two equations are used to calculate the two constants $n_{(\cdot)}$ and $b_{(\cdot)}$ for Rosin-Rammler function:

$$n = -3.1 \times 10^{-4} \times \text{fineness} + 1.2 \tag{7.6}$$

$$b = 1.74 \times 10^{-4} \times \text{fineness} - 0.0290 \tag{7.7}$$

other source (NIST):

$$n = -8.333 \times 10^{-4} \times \text{fineness} + 1.1175 \tag{7.8}$$

$$b = 7.54 \times 10^{-4} \times \text{fineness} - 0.143 \tag{7.9}$$

where *fineness* is the specific surface area of particles (in m^2/kg).

It is obvious the above equations have relationship with the granular characteristics of material, even for Portland cement, different types of cement have varied b and n.

Using the above equations, values of n and b of each kind of material can be calculated. However, when particle size distributions of materials are available. e.g. measured by laser diffraction method, the values of n and b can be obtained by least squares fitting based on the Rosin-Rammler function Eqs. 7.1 - 7.3.

The mass $W_{(\cdot),x}$ of each material belonging to the particle size fraction F_x is obtained by differentiating Eqs. 7.1, 7.2 and 7.3 with respect to x:

$$W_{c,x} = \gamma_c \times b_c \times n_c \times x^{n_c - 1} \times exp(-b_c \times x_c^{n_c}) \;\; [g] \tag{7.10}$$

$$W_{s,x} = \gamma_s \times b_s \times n_s \times x^{n_s - 1} \times exp(-b_s \times x_s^{n_s}) \;\; [g] \tag{7.11}$$

$$W_{l,x} = \gamma_l \times b_l \times n_l \times x^{n_l - 1} \times exp(-b_l \times x_l^{n_l}) \;\; [g] \tag{7.12}$$

The volume V_x of all particles of each component in size fraction F_x is obtained by:

$$V_{c,x} = \frac{W_{c,x}}{\rho_c} \ \ [cm^3] \tag{7.13}$$

$$V_{s,x} = \frac{W_{s,x}}{\rho_s} \ \ [cm^3] \tag{7.14}$$

$$V_{l,x} = \frac{W_{l,x}}{\rho_l} \ \ [cm^3] \tag{7.15}$$

where $\rho_{(\cdot)}$ is the specific mass (or density) of each material.

The particle number $N_{(\cdot),x}$ in size fraction F_x of 1 gram of material is calculated by dividing the volume $V_{(\cdot),x}$ of fraction F_x by the volume of a single particle v_x:

$$N_{c,x} = \frac{V_{c,x}}{v_{c,x}} = \frac{\gamma_c \times b_c \times n_c \times x^{n_c-1} \times e^{-b_c \times x_c^{n_c}}}{\dfrac{\pi \times x^3}{6} \times \rho_c \times 10^{-12}} \tag{7.16}$$

$$N_{s,x} = \frac{V_{s,x}}{v_{s,x}} = \frac{\gamma_s \times b_s \times n_s \times x^{n_s-1} \times e^{-b_s \times x_s^{n_s}}}{\dfrac{\pi \times x^3}{6} \times \rho_s \times 10^{-12}} \tag{7.17}$$

$$N_{l,x} = \frac{V_{l,x}}{v_{l,x}} = \frac{\gamma_l \times b_l \times n_l \times x^{n_l-1} \times e^{-b_l \times x_l^{n_l}}}{\dfrac{\pi \times x^3}{6} \times \rho_l \times 10^{-12}} \tag{7.18}$$

Supposing the mixing proportion of cement, slag and limestone powder in the paste is m_c, m_s and m_l ($m_c + m_s + m_l = 100\%$), respectively, and the rib size of the cube in the model is l_{cube} = 100 μm, the water to binder ratio is w_b (w/b) (the exact w/c can be calculated as w_0), then the particle numbers of cement, slag and limestone with different size x in the cube can be calculated respectively according to the above equations in this chapter. The total number N_x of all particles is used to randomly distribute the particles in the cube at the beginning of hydration (Fig. 7.1) and later to calculate the degree of hydration/reaction evolving with curing age.

7.2.2 Specific Surface Area

For the specific surface area S_x of a spherical particle with diameter x (in μm), it holds:

$$S_x = \pi \times x^2 \ \ [\mu m^2] \tag{7.19}$$

thus for the total surface area of all particles in fraction F_x holds that:

$$S_{F_x} = N_x \times S_x \ \ [\mu m^2] \tag{7.20}$$

For the total particle surface area of all particles with diameters $x_{min} \leq x \leq x_{max}$, it holds that:

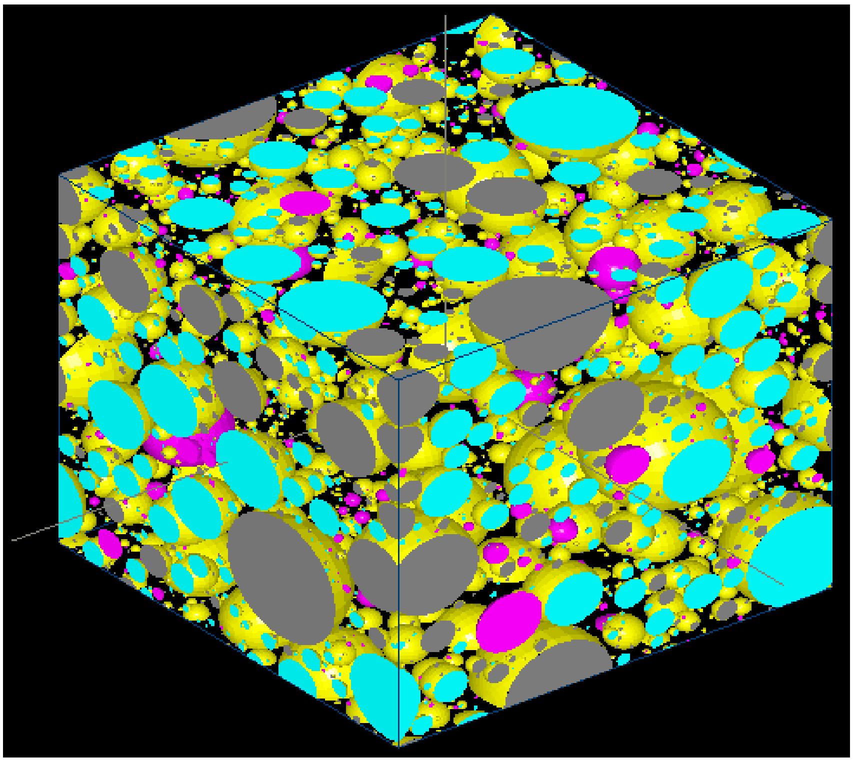

Figure 7.1: Randomly distributed particles in the cubic cell (100 $\times$ 100 $\times$ 100 μm^3) of a ternary blended paste, initial state i.e. prior to hydration (Color match: gray = cement, turquoise = slag, magenta = limestone).

$$S_{\leq x_m} = \sum_{x=x_{min}}^{x_{max}} S_{F_x} \;\; [\mu m^2] \tag{7.21}$$

The specific surface of the material made of all particles is obtained as follows:

$$S = \sum_{x=x_{min}}^{x_{max}} S_{F_x} \;\; [\mu m^2/g] \tag{7.22}$$

It has to be noted that the method to calculate the specific surface area works for all materials.

7.2.3 Paste Characteristics

For a paste mixed by the three components with water to powder ratio w_p = w/p, the specific mass ρ_{pa} is calculated as follows (air content is ignored):

$$\rho_{pa} = \frac{1 + w_p}{\dfrac{m_c}{\rho_c} + \dfrac{m_s}{\rho_s} + \dfrac{m_l}{\rho_l} + \dfrac{w_p}{\rho_w}} \;\; [g/cm^3] \tag{7.23}$$

The volumetric paste density of binders ξ_{pa} is defined as the volume of solid relative to that of the whole fresh paste:

$$\xi_{pa} = \frac{\dfrac{m_c}{\rho_c} + \dfrac{m_s}{\rho_s} + \dfrac{m_l}{\rho_l}}{\dfrac{m_c}{\rho_c} + \dfrac{m_s}{\rho_s} + \dfrac{m_l}{\rho_l} + \dfrac{w_p}{\rho_w}} \tag{7.24}$$

Similarly, the volumetric paste density of each individual material, i.e. ξ_{pa}^c, ξ_{pa}^s and ξ_{pa}^l, follows:

$$\xi_{pa}^c = \frac{\dfrac{m_c}{\rho_c}}{\dfrac{m_c}{\rho_c} + \dfrac{m_s}{\rho_s} + \dfrac{m_l}{\rho_l} + \dfrac{w_p}{\rho_w}} \tag{7.25}$$

$$\xi_{pa}^s = \frac{\dfrac{m_s}{\rho_s}}{\dfrac{m_c}{\rho_c} + \dfrac{m_s}{\rho_s} + \dfrac{m_l}{\rho_l} + \dfrac{w_p}{\rho_w}} \tag{7.26}$$

$$\xi_{pa}^l = \frac{\dfrac{m_l}{\rho_l}}{\dfrac{m_c}{\rho_c} + \dfrac{m_s}{\rho_s} + \dfrac{m_l}{\rho_l} + \dfrac{w_p}{\rho_w}} \tag{7.27}$$

7.2.4 Cell Definition, Cell Volume and Shell Density

To model the hydrating microstructure of the ternary blended paste, we need to define a spatial cell as a calculation space unit. Similar to the way applied in HYMOSTRUC, the definition of cell $I_x^{(\cdot)}$ belonging to a particle with diameter x is proposed as follows:

Apart from the particle x itself the cubic space only contains $\frac{1}{m_{(\cdot)} \times N_{(\cdot),x}}$ times the volume of particles smaller than x and $\frac{1}{m_{(\cdot)} \times N_{(\cdot),x}}$ times original water volume.

Based on the above definition, the cell I_x^c, I_x^s and I_x^l of cement, slag and limestone particle x is expressed in equations below, respectively:

$$I_x^c = \frac{\dfrac{m_c \times G_c(x)}{\rho_c} + \dfrac{m_s \times G_s(x-1)}{\rho_s} + \dfrac{m_l \times G_l(x-1)}{\rho_l} + \dfrac{w_p}{\rho_w}}{m_c \times N_{c,x}} \quad [cm^3] \tag{7.28}$$

$$I_x^s = \frac{\dfrac{m_c \times G_c(x-1)}{\rho_c} + \dfrac{m_s \times G_s(x)}{\rho_s} + \dfrac{m_l \times G_l(x-1)}{\rho_l} + \dfrac{w_p}{\rho_w}}{m_s \times N_{s,x}} \quad [cm^3] \tag{7.29}$$

$$I_x^l = \frac{\dfrac{m_c \times G_c(x-1)}{\rho_c} + \dfrac{m_s \times G_s(x-1)}{\rho_s} + \dfrac{m_l \times G_l(x)}{\rho_l} + \dfrac{w_p}{\rho_w}}{m_l \times N_{l,x}} \quad [cm^3] \tag{7.30}$$

where $(x-1)$ is the biggest particle size that is just 1 μm smaller than x given that the size step is 1 μm in this study.

Since $I_x^{(\cdot)}$ is the volume of the cell, the rib size $L_x^{(\cdot)}$ (μm) of the cubic cell can be calculated, which is as follows for cement, slag and limestone, respectively:

$$L_x^c = [I_x^c \times 10^{12}]^{\frac{1}{3}} \;\; [\mu m] \tag{7.31}$$

$$L_x^s = [I_x^s \times 10^{12}]^{\frac{1}{3}} \;\; [\mu m] \tag{7.32}$$

$$L_x^l = [I_x^l \times 10^{12}]^{\frac{1}{3}} \;\; [\mu m] \tag{7.33}$$

It is obvious that the rib size $L_x^{(\cdot)}$ is the mean center-to-center distance between two center particles x of any two neighboring cells.

$$L_x^c = [I_x^c \times 10^{12}]^{\frac{1}{3}} \;\; [\mu m] \tag{7.34}$$

For the sake of mathematic calculation, the cubic cell is converted to a spherical cell, in which the radius $r_x^{\cdot}$ holds:

$$r_x^c = [\frac{3 \times I_x^c \times 10^{12}}{4\pi}]^{\frac{1}{3}} \;\; [\mu m] \tag{7.35}$$

$$r_x^s = [\frac{3 \times I_x^s \times 10^{12}}{4\pi}]^{\frac{1}{3}} \;\; [\mu m] \tag{7.36}$$

$$r_x^l = [\frac{3 \times I_x^l \times 10^{12}}{4\pi}]^{\frac{1}{3}} \;\; [\mu m] \tag{7.37}$$

7.2.5 Cell Density

In analogy to the definition of volumetric paste density, cell density of each material is also defined as follows:

$$\xi_x^{\cdot} = \frac{\text{volume of material in cell } I_x^{\cdot}}{\text{cell volume } I_x^{\cdot}} \tag{7.38}$$

Taking the cell I_x^c as an example, the volumetric cell density of cement $\xi_x^{c,c}$ in I_x^c is thus expressed by the following equation:

$$\xi_x^{c,c} = \frac{\frac{\frac{m_c \times G_c(x)}{\rho_c}}{m_c \times N_{c,\ x}}}{\frac{\frac{m_c \times G_c(x)}{\rho_c} + \frac{m_s \times G_s(x-1)}{\rho_s} + \frac{m_l \times G_l(x-1)}{\rho_l} + \frac{w_p}{\rho_w}}{m_c \times N_{c,\ x}}} \tag{7.39}$$

or,

$$\xi_x^{c,c} = \frac{\frac{m_c \times G_c(x)}{\rho_c}}{\frac{m_c \times G_c(x)}{\rho_c} + \frac{m_s \times G_s(x-1)}{\rho_s} + \frac{m_l \times G_l(x-1)}{\rho_l} + \frac{w_p}{\rho_w}} \tag{7.40}$$

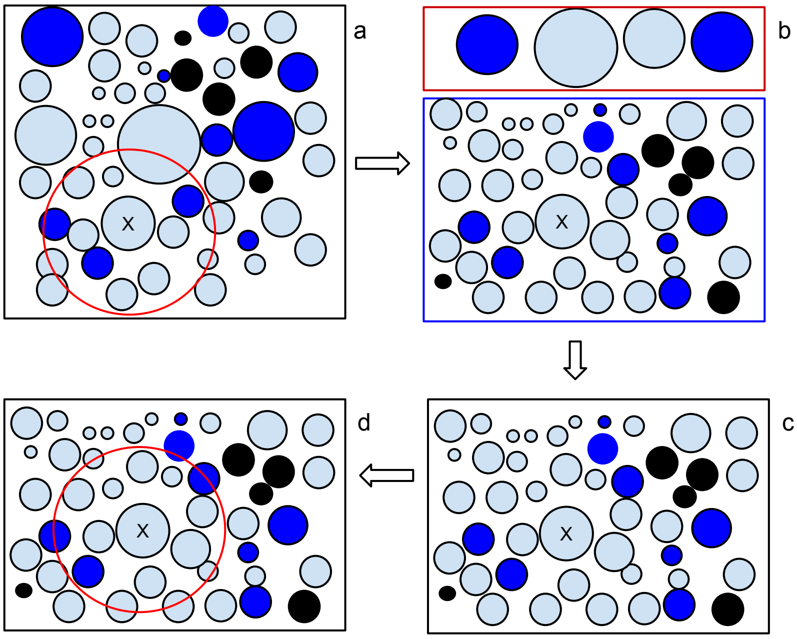

Figure 7.2: Schematic presentation of shell density, three colors represent three materials.

Similarly, the volumetric cell density of slag $\xi_x^{s,c}$ and limestone $\xi_x^{l,c}$ in I_x^c is obtained as follows, respectively:

$$\xi_x^{s,c} = \frac{\frac{m_s \times G_s(x-1)}{\rho_s}}{\dfrac{m_c \times G_c(x)}{\rho_c} + \dfrac{m_s \times G_s(x-1)}{\rho_s} + \dfrac{m_l \times G_l(x-1)}{\rho_l} + \dfrac{w_p}{\rho_w}} \tag{7.41}$$

$$\xi_x^{l,c} = \frac{\frac{m_l \times G_l(x-1)}{\rho_l}}{\dfrac{m_c \times G_c(x)}{\rho_c} + \dfrac{m_s \times G_s(x-1)}{\rho_s} + \dfrac{m_l \times G_l(x-1)}{\rho_l} + \dfrac{w_p}{\rho_w}} \tag{7.42}$$

7.2.6 Shell Density

The definition of cell density, e.g. $\xi_x^{c,c}$, includes the center particle x which is not the content in the shell of cell I_x^c. We define the shell density of cement particles in cell I_x^c as the ratio of cement volume in the shell to the total shell volume (Fig. 7.2):

$$\xi_{x,sh}^{c,c} = \frac{\text{cement volume in the shell of } I_x^c}{\text{total shell volume of } I_x^c} \tag{7.43}$$

in mathematical equation:

$$\xi_{x,sh}^{c,c} = \frac{\frac{\frac{m_c \times G_c(x)}{\rho_c}}{m_c \times N_{c,x}} - v_x^c}{\frac{\frac{m_c \times G_c(x)}{\rho_c} + \frac{m_s \times G_s(x-1)}{\rho_s} + \frac{m_l \times G_l(x-1)}{\rho_l} + \frac{w_p}{\rho_w}}{m_c \times N_{c,x}} - v_x^c} \tag{7.44}$$

where v_x^c is the volume of the center cement particle x. It follows:

$$v_x^c = \frac{G_c(x) - G_c(x-1)}{\rho_c \times N_{c,x}} \tag{7.45}$$

The simplified Eq. 7.44 by inserting v_x^c (Eq. 7.45) is as follows:

$$\xi_{x,sh}^{c,c} = \frac{\frac{m_c \times G_c(x-1)}{\rho_c}}{\frac{m_c \times G_c(x-1)}{\rho_c} + \frac{m_s \times G_s(x-1)}{\rho_s} + \frac{m_l \times G_l(x-1)}{\rho_l} + \frac{w_p}{\rho_w}} \tag{7.46}$$

Similarly, the shell densities of slag $\xi_{x,sh}^{s,c}$ and limestone $\xi_{x,sh}^{l,c}$ in the cell I_x^c are as follows, respectively:

$$\xi_{x,sh}^{s,c} = \frac{\frac{m_s \times G_s(x-1)}{\rho_s}}{\frac{m_c \times G_c(x-1)}{\rho_c} + \frac{m_s \times G_s(x-1)}{\rho_s} + \frac{m_l \times G_l(x-1)}{\rho_l} + \frac{w_p}{\rho_w}} \tag{7.47}$$

$$\xi_{x,sh}^{l,c} = \frac{\frac{m_l \times G_l(x-1)}{\rho_l}}{\frac{m_c \times G_c(x-1)}{\rho_c} + \frac{m_s \times G_s(x-1)}{\rho_s} + \frac{m_l \times G_l(x-1)}{\rho_l} + \frac{w_p}{\rho_w}} \tag{7.48}$$

From the equations of shell density (Eqs. 7.46 - 7.48), it can be seen that shell density is only a function of the particle size x and has nothing to do with the material type of the center particle x in the cell, in other words, the shell density of cement particles ($\xi_{x,sh}^{c,c}$) in the cell of cement particle x (I_x^c) is identical to that ($\xi_{x,sh}^{c,s}$) in the cell of slag particle x (I_x^s), and also to that ($\xi_{x,sh}^{c,l}$) in the cell of limestone particle (I_x^l), which means:

$$\xi_{x,sh}^{c,c} = \xi_{x,sh}^{c,s} = \xi_{x,sh}^{c,l} = \xi_{x,sh}^{c} \tag{7.49}$$

The above conclusion also applies to shell density of slag and limestone particle in all cells:

$$\xi_{x,sh}^{s,c} = \xi_{x,sh}^{s,s} = \xi_{x,sh}^{s,l} = \xi_{x,sh}^{s} \tag{7.50}$$

$$\xi_{x,sh}^{l,c} = \xi_{x,sh}^{l,s} = \xi_{x,sh}^{l,l} = \xi_{x,sh}^{l} \tag{7.51}$$

where $\xi_{x,sh}^{c}$, $\xi_{x,sh}^{s}$ and $\xi_{x,sh}^{l}$ denote the shell density of cement, slag and limestone particles in all cells, respectively.

The definition of shell density greatly facilitates the calculation of spatial interaction when the adjacent particles are embedded in the outer product of a given center particle.

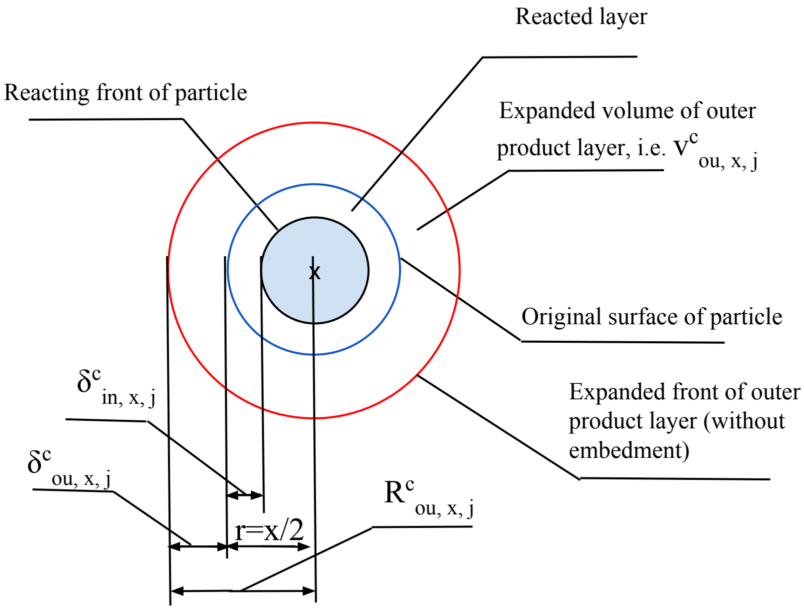

Figure 7.3: Schematic representation of a single hydrating cement particle, no embedded particles.

7.2.7 Particle Expansion during Hydration

Cement Particle x

For each particle sized x, as the progress of hydration proceeds the associated expansion of hydration products of the particle x will be followed. For example, at a given stage, i.e. at time step $t = t_j$, the hydration degree of cement particle x is $\alpha^c_{x,j}$, the corresponding *penetration thickness* $\delta^c_{in,x,j}$ of the reacted front layer is obtained by:

$$\delta^c_{in,x,j} = \frac{x}{2} \times [1 - (1 - \alpha^c_{x,j})^{\frac{1}{3}}] \ \ [\mu m] \tag{7.52}$$

The volume of the outer product layer $v^c_{ou,x,j}$ that corresponds to the degree of hydration $\alpha^c_{x,j}$ is obtained as follows:

$$v^c_{ou,x,j} = (\nu^c - 1) \times \alpha^c_{x,j} \times \frac{\pi x^3}{6} \ \ [\mu m^3] \tag{7.53}$$

where ν^c is the volume expansion ratio of hydration products to hydrated cement. As shown in Fig. 7.3, absence of particles in the outer product layer (shell) surrounding the particle x would lead to free expansion of hydration products. As a result, the radius $R^c_{ou,x,j}$ of the expanded central particle x, which consists of anhydrous core, inner and outer products, would be:

$$R^c_{ou,x,j} = \left[\frac{v^c_{ou,x,j}}{\frac{4\pi}{3}} + (\frac{x}{2})^3 \right]^{\frac{1}{3}} \ \ [\mu m] \tag{7.54}$$

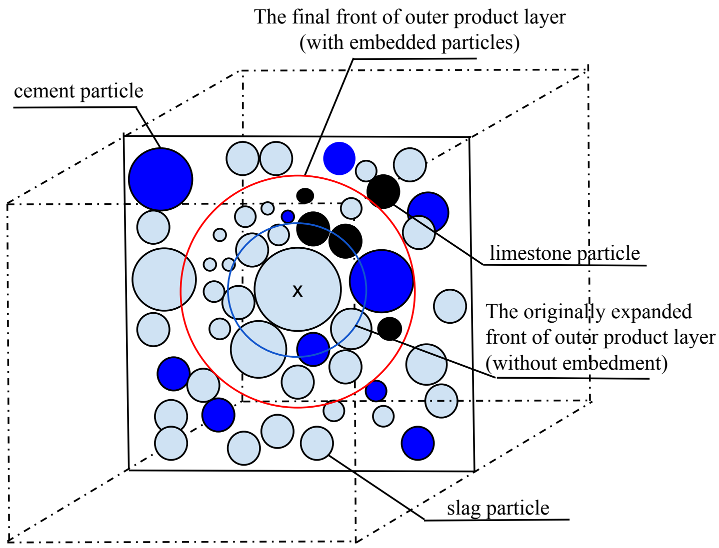

Figure 7.4: The schematic cubic cell of a ternary blended paste.

The thickness $\delta^c_{ou,x,j}$ of the outer product layer is obtained as follows:

$$\delta^c_{ou,x,j} = R^c_{ou,x,j} - \frac{x}{2} \ \ [\mu m] \tag{7.55}$$

However, the reality is that the outer product layer partly embeds other particles, i.e. cement, slag and limestone powder. Meanwhile, those embedded particles in the outer product layer also undergo hydration, which indirectly increases the depth of the outer product layer. The increased depth of outer product layer further embeds particles again, and the newly embedded particles also hydrate. This process at time step t_j finally reaches an equilibrium.

For the sake of modeling, the key point is to know the final depth of the outer product layer $\delta^{c'}_{ou,x,j}$ at the end of this time step $t = t_j$, i.e. the position of the final front of outer product layer as shown in Fig. 7.4. To solve this issue, we use the principle *volume balance* to calculate. It is based on the fact that the volume $v^{c'}_{ou,x,j}$ of the final outer layer of particle x equals to the volume of all embedded particles and the expanded volume of all hydrated materials in this outer layer, which is mathematically expressed by the following equation:

$$\begin{aligned} v^{c'}_{ou,x,j} = {} & \alpha^c_{x,j} \times \frac{\pi x^3}{6} \times (\nu^c - 1) \\ & + v^{c'}_{ou,x,j} \times \xi^c_{x,sh} \times [\alpha^c_{<x,j} \times (\nu^c - 1) + 1] \\ & + v^{c'}_{ou,x,j} \times \xi^s_{x,sh} \times [\alpha^s_{<x,j} \times (\nu^s - 1) + 1] \\ & + v^{c'}_{ou,x,j} \times \xi^l_{x,sh} \times [\alpha^l_{<x,j} \times (\nu^l - 1) + 1] \ \ [\mu m^3] \end{aligned} \tag{7.56}$$

where $\alpha^c_{x,j}$ is the overall hydration degree of cement particle x at time t_j, $\alpha^c_{<x,j}$, $\alpha^s_{<x,j}$ and $\alpha^l_{<x,j}$ are hydration degrees at this time of all particles smaller than x of each individual material,

i.e. cement, slag and limestone, respectively. ν^c, ν^s and ν^l are volumetric expansion ratios of hydration products of cement, slag and limestone, respectively. Typically, ν^s was investigated in Section 6.3.1.

At the right side of Eq. 7.56, the first part is the net expanded volume of the reacted layer ($\delta^c_{in,x,j}$) of cement particle x, the second, third and last part are the total volume (i.e. unreacted, reacted and expanded volume) of reacting embedded cement, slag and limestone particles, respectively.

Since there is only one unknown (i.e. $v^{c'}_{ou,x,j}$) in Eq. 7.56, the function can be easily solved with definite answer:

$$v^{c'}_{ou,x,j} = \frac{\alpha^c_{x,j} \times \frac{\pi x^3}{6} \times (\nu^c - 1)}{1 - \xi^c_{x,sh}[\alpha^c_{<x,j}(\nu^c - 1) + 1] - \xi^s_{x,sh}[\alpha^s_{<x,j}(\nu^s - 1) + 1] - \xi^l_{x,sh}[\alpha^l_{<x,j}(\nu^l - 1) + 1]} \ [\mu m^3] \tag{7.57}$$

Now the final radius $R^{c'}_{ou,x,j}$ of expanded cement particle x at the end of time step t_j can be calculated using Eq. 7.54 as follows:

$$R^{c'}_{ou,x,j} = \left[\frac{v^{c'}_{ou,x,j}}{\frac{4\pi}{3}} + (\frac{x}{2})^3 \right]^{\frac{1}{3}} \quad [\mu m] \tag{7.58}$$

and the final depth of the outer product layer $\delta^{c'}_{ou,x,j}$ of cement particle x is

$$\delta^{c'}_{ou,x,j} = R^{c'}_{ou,x,j} - \frac{x}{2} \ \ [\mu m] \tag{7.59}$$

With Eqs. 7.52 and 7.59, the total thickness $\delta^c_{x,j}$ at time t_j of the product layer that includes inner and outer products surrounding the shrinking anhydrous core is:

$$\delta^c_{x,j} = \delta^{c'}_{ou,x,j} + \delta^c_{in,x,j} \ \ [\mu m] \tag{7.60}$$

The total embedded cement volume $v^{c,c}_{em,x,j}$ in the outer product layer of cement particle x at time t_j is:

$$v^{c,c}_{em,x,j} = v^{c'}_{ou,x,j} \times \xi^c_{x,sh} \ \ [\mu m^3] \tag{7.61}$$

Similarly, the total embedded slag volume $v^{s,c}_{em,x,j}$ is obtained as follows:

$$v^{s,c}_{em,x,j} = v^{c'}_{ou,x,j} \times \xi^s_{x,sh} \ \ [\mu m^3] \tag{7.62}$$

and the total embedded limestone volume $v^{l,c}_{em,x,j}$ is obtained as follows:

$$v^{l,c}_{em,x,j} = v^{c'}_{ou,x,j} \times \xi^l_{x,sh} \ \ [\mu m^3] \tag{7.63}$$

The above results are the calculation for the cell with the center cement particle x. The purpose is to calculate the thickness of the expanded layer at time step j. The layer embeds other smaller particles (cement, slag and limestone), meanwhile, the embedded particles are also hydrating.

The method for cement particle x also applies to calculating the final thickness of product layer of slag particle x and limestone particle x.

Slag Particle x

For the cell I_x^s with the center slag particle x at the end of time step t_j, its volume of final outer layer follows:

$$v_{ou,x,j}^{s'} = \frac{\alpha_{x,j}^s \times \frac{\pi x^3}{6} \times (\nu^s - 1)}{1 - \xi_{x,sh}^c[\alpha_{<x,j}^c(\nu^c - 1) + 1] - \xi_{x,sh}^s[\alpha_{<x,j}^s(\nu^s - 1) + 1] - \xi_{x,sh}^l[\alpha_{<x,j}^l(\nu^l - 1) + 1]} \ [\mu m^3] \tag{7.64}$$

Thus the final radius of the expanded particle:

$$R_{ou,x,j}^{s'} = \left[\frac{v_{ou,x,j}^{s'}}{\frac{4\pi}{3}} + (\frac{x}{2})^3\right]^{\frac{1}{3}} \quad [\mu m] \tag{7.65}$$

and the final thickness of the outer product layer $\delta_{ou,x,j}^{s'}$ of slag particle x is

$$\delta_{ou,x,j}^{s'} = R_{ou,x,j}^{s'} - \frac{x}{2} \ \ [\mu m] \tag{7.66}$$

The total thickness $\delta_{x,j}^s$ of the product layer (including inner and outer products) surrounding the shrinking anhydrous slag particle core is

$$\delta_{x,j}^s = \delta_{ou,x,j}^{s'} + \delta_{in,x,j}^s \ \ [\mu m] \tag{7.67}$$

where $\delta_{in,x,j}^s$ is the depth of total hydrated layer of the original slag particle x till time t_j.

With the known volume of final outer layer of slag particle x, the total volume of embedded cement ($v_{em,x,j}^{c,s}$), slag ($v_{em,x,j}^{s,s}$) and limestone ($v_{em,x,j}^{l,s}$) particles in the expanded outer product layer of slag particle x at time t_j is as follows, respectively:

$$v_{em,x,j}^{c,s} = v_{ou,x,j}^{s'} \times \xi_{x,sh}^c \ \ [\mu m^3] \tag{7.68}$$

$$v_{em,x,j}^{s,s} = v_{ou,x,j}^{s'} \times \xi_{x,sh}^s \ \ [\mu m^3] \tag{7.69}$$

$$v_{em,x,j}^{l,s} = v_{ou,x,j}^{s'} \times \xi_{x,sh}^l \ \ [\mu m^3] \tag{7.70}$$

Limestone Particle x

Similarly, the volume of final outer layer at the end of time t_j of limestone particle x:

$$v^{l'}_{ou,x,j} = \frac{\alpha^l_{x,j} \times \frac{\pi x^3}{6} \times (\nu^l - 1)}{1 - \xi^c_{x,sh}[\alpha^c_{<x,j}(\nu^c - 1) + 1] - \xi^s_{x,sh}[\alpha^s_{<x,j}(\nu^s - 1) + 1] - \xi^l_{x,sh}[\alpha^l_{<x,j}(\nu^l - 1) + 1]} \ [\mu m^3] \tag{7.71}$$

The final radius of the expanded particle:

$$R^{l'}_{ou,x,j} = \left[\frac{v^{l'}_{ou,x,j}}{\frac{4\pi}{3}} + (\frac{x}{2})^3\right]^{\frac{1}{3}} \quad [\mu m] \tag{7.72}$$

The thickness of the expanded outer product layer:

$$\delta^{l'}_{ou,x,j} = R^{l'}_{ou,x,j} - \frac{x}{2} \ \ [\mu m] \tag{7.73}$$

The total thickness $\delta^s_{x,j}$ of the product layer (including inner and outer products) that surrounds the shrinking anhydrous core of limestone particle x:

$$\delta^l_{x,j} = \delta^{l'}_{ou,x,j} + \delta^l_{in,x,j} \ \ [\mu m] \tag{7.74}$$

The total volume of embedded cement particles $v^{c,l}_{em,x,j}$ in the outer product layer of limestone particle x at time t_j is:

$$v^{c,l}_{em,x,j} = v^{l'}_{ou,x,j} \times \xi^c_{x,sh} \ \ [\mu m^3] \tag{7.75}$$

The total volume of embedded slag particles $v^{s,l}_{em,x,j}$ in the outer product layer of limestone particle x:

$$v^{s,l}_{em,x,j} = v^{l'}_{ou,x,j} \times \xi^s_{x,sh} \ \ [\mu m^3] \tag{7.76}$$

The total volume of embedded limestone particles $v^{l,l}_{em,x,j}$ in the outer product layer of limestone particle x:

$$v^{l,l}_{em,x,j} = v^{l'}_{ou,x,j} \times \xi^l_{x,sh} \ \ [\mu m^3] \tag{7.77}$$

7.3 Basic Penetration Rate of Particle Hydration

7.3.1 Cement Particle

To determine the incremental increase of penetration depth $\Delta\delta^c_{in,x,j+1}$ of cement particle x during time increment $\Delta t_{j+1} = t_{j+1} - t_j$, the formula of basic penetration rate based on the original HYMOSTRUC is modified to account for ternary blended system.

Experimental results in Chapter 4 show the acceleration effect of limestone powder on the hydration of cement. As within the method used by Bentz in [29], the addition of limestone in this study is considered as offering extra nucleation sites for the precipitation of hydration products of cement particles [61]. In this study, the modification of the basic penetration rate equation of cement particle is mathematically implemented by adding a factor ω_l, which denotes the acceleration effect of limestone powder on the kinetics of cement hydration.

It is assumed that ω_l works only during the phase boundary stage of cement hydration. On the one hand, as the penetration depth of the hydrating layer increases, the hydration kinetics of cement particle decreases and is gradually transformed to diffusion controlled stage, and hydration products are already precipitated on the surface of limestone particles. Therefore, the acceleration effect caused by offering extra nucleation sites is less significant in diffusion controlled stage. The detailed mechanism needs further investigation, but it is unfortunately not the topic in this study. On the other hand, the reaction kinetics of slag is greatly slower than cement at early age, thus the acceleration effect of limestone on reaction of slag is ignored. In addition, the possible nucleation site effect of slag on cement is not considered, as experimental results in Fig. 4.10 provides no evidence.

The factor is mathematically expressed by the following equation:

$$\omega_l = 1 + \frac{S_l}{S_c}(1 - \frac{\delta^c_{in,x,j}}{\delta^c_{tr}}) \tag{7.78}$$

where S_l and S_c are the surface area of all original limestone and cement particles, respectively, and δ^c_{tr} is the transition thickness of cement particle while $\delta^c_{in,x,j}$ is the thickness of the hydrated cement particle layer at time t_j. Apparently, the value of Eq. 7.78 ends at 1 when $\delta^c_{in,x,j}$ reaches δ^c_{tr}, implying the end of phase boundary stage of cement hydration.

By introducing the factor ω_l, the basic penetration rate of cement particle hydration is extended:

$$\frac{\Delta\delta^c_{in,x,j+1}}{\Delta t_{j+1}} = \frac{\omega_l \times k^c_i(\alpha^c_j) \times F_1(\cdot) \times [F_2(\cdot)]^\lambda \times \phi^c_1(x, \alpha_{x,j}) \times \phi_2(\cdot)}{\{(\delta^c_{in,x,j})^\lambda\}^{\beta_c}} \tag{7.79}$$

where:

- $k^c_i(\alpha^c_j)$ = rate constant, depending on the rate-controlling mechanism, cement composition and hydration degree.
  i = 0 phase boundary reaction, i.e. $\delta^c_{in,x,j} < \delta^c_{tr,j}$ (transition thickness), [μm/h]
  i = 1 diffusion controlled reaction i.e. $\delta^c_{in,x,j} > \delta^c_{tr,j}$ [μm/h]
- $F_1(\cdot)$ = temperature function, accounting for the effect of curing temperture on the kinetics.
- $F_2(\cdot)$ = temperature function, accounting for the effect of temperature on morphology.
- $\phi^c_1(x, \alpha^c_{x,j})$ = reduction factor, accounting for water withdrawal effect due to the hydration of embedded particles in the outer product layer of cement particle x.

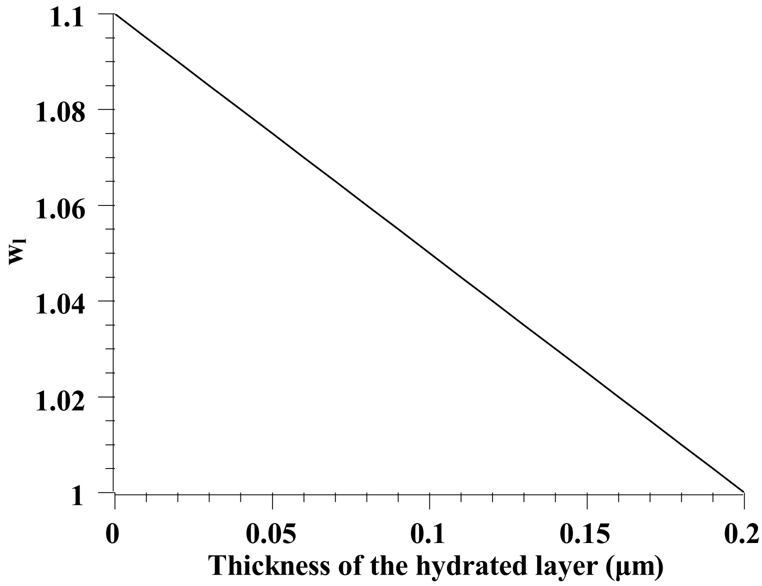

Figure 7.5: The factor ω_l is proposed to linearly decrease with increasing thickness of hydrated layer of cement particle (assuming $\frac{S_l}{S_c} = 0.1$, δ^c_{tr} = 0.2 μm).

- $\phi_2(\cdot)$ = reduction factor, accounting for the water shortage in the pore system.
- λ = factor, depending on the hydration mechanism.
  λ = 0 for phase boundary reaction
  λ = 1 for diffusion controlled reaction
- β_c = a constant, determined by tests (calibration).
- $\delta^c_{in,x,j}$ = total thickness of inner product layer of cement particle x at the end of time step Δt_{j+1}.

Detailed calculation of these factors will be discussed in the later context of this chapter.

7.3.2 Slag Particle

The hydration kinetics of slag particle is similar to the form of cement particle, with a different rate constant k. Although the reaction of slag needs the activation caused by the hydration of cement in this study (Portland cement blends with slag and limestone), experimental results show that the slag already reacts even within the first 24 hours, therefore, the dormant period of slag reaction waiting for breaking its glass layer is ignored. This simplification would theoretically overestimate the hydration of slag in the very early age.

Generally, the hydration process of slag is divided into two stages, i.e. phase-boundary and diffusion-controlled.

$$\frac{\Delta\delta^s_{in,x,j+1}}{\Delta t_{j+1}} = \frac{k^s_i(\alpha^s_j) \times F_1(\cdot) \times [F_2(\cdot)]^\lambda \times \phi^s_1(x, \alpha^s_{x,j}) \times \phi_2(\cdot)}{\{(\delta^s_{x,j})^\lambda\}^{\beta_s}} \tag{7.80}$$

The factors in this equation bear the same physical meanings as that in the kinetics equation of cement (Eq. 7.79). The only difference is changing the material type from cement to slag. Specifically, the rate constant of slag, i.e. k value of slag, is taken from Chapter 3, which is based on the chemical compositions of raw material (Eq. 3.7).

7.3.3 Limestone Particle

The hydration of limestone is found very slow due to its low solubility. However, in order to make the new model work for any ternary blended system, a theoretic hydration model of limestone is also proposed as follow:

$$\frac{\Delta\delta^{l}_{in,x,j+1}}{\Delta t_{j+1}} = \frac{k^{l}_{i}(\alpha^{l}_{j}) \times F_1(\cdot) \times [F_2(\cdot)]^{\lambda} \times \phi^{l}_{1}(x, \alpha_{x,j}) \times \phi_2(\cdot)}{\{(\delta^{l}_{x,j})^{\lambda}\}^{\beta_l}} \tag{7.81}$$

Except changing material from cement to limestone, all the factors bear the same physical meanings as that in cement (Eq. 7.79).

Particularly, the rate constant of limestone k_l in this study is assigned a tiny value based on the fact that the extent of reaction of limestone is quite limited, which results in an extremely low value of the practical depth of reacting layer.

It is worth noting that for other material than limestone, e.g. fly ash, applying the corresponding value of k_l and relevant factors in Eq. 7.81 is necessary for the practical simulation as shown in Section 8.2.1. In other words, the model proposed in this study is not limited to cement, slag and limestone ternary blended paste.

7.3.4 Interaction between Particles

It is needless to say that the interaction among particles makes numerical modeling of hydration of blended cement complex. As soon as the hydration in blended cement paste commences, e.g. the ternary blended cement paste: PBL in this research, the interaction between cement and slag starts. In this model, the issue is considered from two aspects: water and $Ca(OH)_2$. The hydration of cement and slag needs water, and the hydration product $Ca(OH)_2$ from hydration of cement acts as the reactant of slag hydration as well as the activator at early age.

The first interaction, i.e. water related, is solved by the two factors ϕ_1 and ϕ_2. ϕ_1 accounts for the water partially consumed by the embedded particles (cement and slag), while ϕ_2 calculates the overall shortage of water in pore system, which is also the interaction caused by water between the hydration of cement and slag particles.

In terms of the interaction caused by $Ca(OH)_2$ of cement, experimental results in Chapter 5 show that there is no shortage of $Ca(OH)_2$ in both PB and PBL pastes even after 91 days of hydration. However, different replacement level of cement by slag indeed influence the overall hydration degree of each other [55], which is confirmed by experimental results [45, 57]. The intensive experimental results of Zhou et al. [145] show that the overall hydration degree of

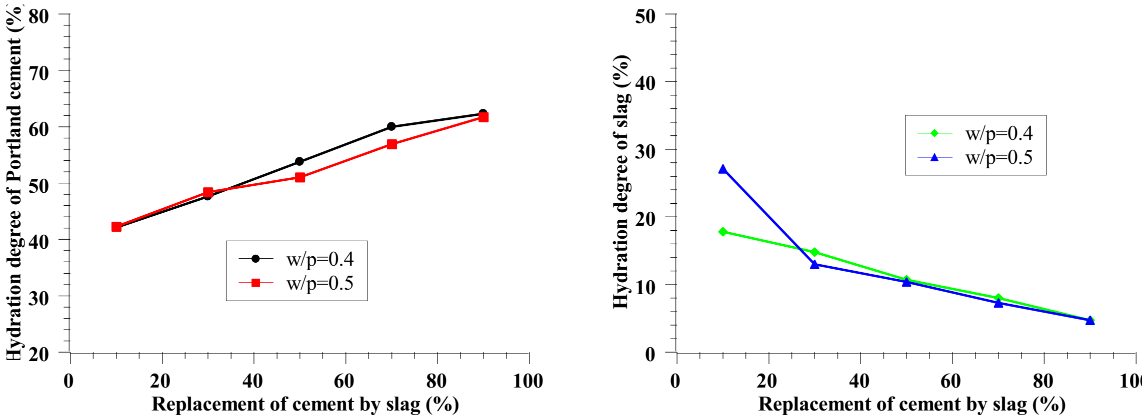

Figure 7.6: The relationship between the replacement level of cement/slag in paste and degree of hydration of cement.

both cement and slag is linearly influenced by the replacement level of cement by slag (Fig. 7.6) at the very early age. Regression analysis on results in Fig. 7.6 indicates each 10% of cement replaced by slag lead to 2.5% increase on the overall degree of hydration of cement and 1.5% decrease on overall degree of hydration of slag. As for the long-term age, results of [56] and [57] reported a consistent decrease in reactivity of slag with increased content of slag in blended cement pastes.

Two possible reasons account for the influence of replacement level of cement by slag on the degree of hydration of cement. On the one hand, as more cement is replaced by slag, the essential water for the hydration of cement is increased due to the slow reaction of slag at least at early age, and $Ca(OH)_2$ produced by cement is also quickly consumed by the reaction of increasing slag, therefore, the overall degree of hydration of cement is increased. On the other hand, the increased consumption of water by cement makes the water less accessible for the reaction of slag, which proceeds along with the less $Ca(OH)_2$ available for slag since $Ca(OH)_2$ should be dissolved in water to react with slag. Less supply of water and $Ca(OH)_2$ reduces the overall degree of reaction of slag.

As aforementioned, the Ca^{2+} concentration in pore solution is very low after the first several hours, actually the dissolution of blast furnace slag type glasses is reduced only by increasing Ca^{2+} concentration [120], and the observed $Ca(OH)_2$ in hydration products also shows that the supply of Ca^{2+} in pore solution is guaranteed in the paste even with only 30% cement after 91 days of hydration (PB and PBL pastes in Chapter 5). Another factor is the pH of pore solution, since the corrosion of glassy phase in slag needs the attacking of OH^{-} as illustrated by Eq. 7.82 [28, 170]. As experimental results show, the alkalinity environment (pH) in pore solution is constantly higher than 13 even in the ternary blended paste PBL, which is much higher than the minimum requirement pH 12 [156]. Based on the experimental results, it can be concluded that the influence of replacement level of cement by slag on hydration of slag and cement is essentially related to water, which is actually considered in the two factors ϕ_1 and ϕ_2 of the proposed model in this research.

$$\equiv\mathrm{Si{-}O{-}Si}\equiv + \mathrm{H_2O} \xrightleftharpoons{OH^-} 2 \equiv\mathrm{Si{-}OH} \tag{7.82}$$

In terms of the influence of limestone powder on hydration of cement, it is considered by factor ω_l as aforementioned. However, the influence of limestone on the reaction of slag is not considered in this model, based on the fact that no significant difference cased by the addition of limestone was observed in experiment. The influence of slag and cement on limestone is ignored because limestone is assumed as inert filler in the proposed simulation model, though a very small amount of limestone participates in the reaction with aluminate phases.

7.4 Degree of Hydration. Particle -, Cell -, and Overall Hydration

By the help of the proposed spatial model and basic penetration rate of all particles, hydration degree of each material at different levels, i.e. particle, cell, and overall hydration, can be obtained.

7.4.1 Degree of Hydration. Particle Level

For an arbitrary particle with diameter x at the end of time step t_j, its degree of hydration $\alpha_{x,j}$ is determined by the thickness $\delta_{in,x,j}$ of the hydrated layer of particle x, for which holds,

$$\delta_{in,x,j} = \delta_{in,x,j-1} + \Delta\delta_{in,x,j} \tag{7.83}$$

where $\delta_{in,x,j-1}$ is the thickness of hydrated layer of the particle at the end of time t_{j-1}, and $\Delta\delta_{in,x,j}$ is the incremental thickness of the hydrated layer during time step Δt_j.

With the obtained $\delta_{in,x,j}$, the hydration degree of the particle is as follows:

$$\alpha_{x,j} = 1 - \left(1 - \frac{2 \times \delta_{in,x,j}}{x}\right)^3 \tag{7.84}$$

The incremental hydration degree of particle x in time step Δt_j is given by:

$$\Delta\alpha_{x,j} = \alpha_{x,j} - \alpha_{x,j-1} \tag{7.85}$$

7.4.2 Degree of Hydration. Cell Level

The hydration degree of a cell I_x is easily obtained by summing up the hydration degrees of all particles of the same material not larger than the center particle x in the cell:

$$\alpha_{\leq x,j} = \frac{1}{G(x)} \sum_{z=x_{min}}^{x} \alpha_{z,j} \times W(z) \tag{7.86}$$

7.4.3 Degree of Hydration. Overall Level

According to the hydration degree at cell level, assigning the particle size x as x_{max} result in the overall hydration degree. It holds,

$$\alpha = \frac{1}{G(x_{max})} \sum_{z=x_{min}}^{x_{max}} \alpha_{z,j} \times W(z) \tag{7.87}$$

It has to be indicated that the calculation of hydration degree at all levels does not specify the type of material, which means it is an universal method for all three materials in the model.

7.5 Calculation of Factors of the Model for Ternary Blended System

Although the basic penetration rate equations of particles, i.e. cement, slag and limestone, are almost as same as that of pure Portland cement in HYMOSTRUC, the factors in the equations of this model are fundamentally modified to account for the influence of interaction among different materials.

The modification mainly considers the changing amount of water and temperature effect in the hydrating paste.

7.5.1 Calculation of ϕ_1 of Each Particle: Water Availability in the Outer Product Layer

Cement Particle x: $\phi^c_{1,x,j+1}$

The factor ϕ_1 considers the water consumed by embedded particles in the outer product layer. Since there are cement, slag and limestone embedded in the outer product layer of cement particle (Fig. 7.4), the water consumed by these particles also consists of three parts, which is calculated as follows.

1. Water consumed by the hydration of embedded cement particles:

$$\Delta w^{c,c}_{em,x,j} = 0.40 \times v^{c,c}_{em,x,j} \times \frac{\rho_c}{\rho_w} \times \{\alpha_{c,<x,j} - \alpha_{c,<x,j-1}\} \tag{7.88}$$

2. Water consumed by the hydration of embedded slag particles:

$$\Delta w^{s,c}_{em,x,j} = 0.45 \times v^{s,c}_{em,x,j} \times \frac{\rho_s}{\rho_w} \times \{\alpha_{s,<x,j} - \alpha_{s,<x,j-1}\} \tag{7.89}$$

3. Water consumed by the hydration of embedded limestone particles:

$$\Delta w^{l,c}_{em,x,j} = 1.62 \times v^{l,c}_{em,x,j} \times \frac{\rho_l}{\rho_w} \times \{\alpha_{l,<x,j} - \alpha_{l,<x,j-1}\} \tag{7.90}$$

where $\alpha_{(\cdot),<x,j}$ is the total hydration degree of all particles smaller than x of the same material at time t_j, and the amount of water for complete hydration of 1 g slag is assumed as 0.45, which is taken from [103], while that of 1 g limestone is taken as 1.62 g according to [141].

The calculation of the reduction $\phi^c_{1,x,j+1}$ in the time step Δt_{j+1} is defined as follows:

$$\phi^c_{1,x,j+1} = \frac{\Delta w^c_{x,j}}{\Delta w^c_{x,j} + \Delta w^{c,c}_{em,x,j} + \Delta w^{s,c}_{em,x,j} + \Delta w^{l,c}_{em,x,j}} \tag{7.91}$$

where $\Delta w^c_{x,j}$ is the water consumed by the hydration of cement particle x in the time step t_j:

$$\Delta w^c_{x,j} = 0.40 \times \Delta\alpha^c_{x,j} \times (v^c_x \times \frac{\rho_c}{\rho_w}) \tag{7.92}$$

Slag Particle x: $\phi^s_{1,x,j+1}$

As the same way of calculation of $\phi^c_{1,x,j+1}$, the calculation of ϕ^s_1 as follows:

1. Water consumed by the hydration of embedded cement particles in the outer product layer of slag particle x:

$$\Delta w^{c,s}_{em,x,j} = 0.40 \times v^{c,s}_{em,x,j} \times \frac{\rho_c}{\rho_w} \times \{\alpha_{c,<x,j} - \alpha_{c,<x,j-1}\} \tag{7.93}$$

2. Water consumed by the hydration of embedded slag particles:

$$\Delta w^{s,s}_{em,x,j} = 0.45 \times v^{s,s}_{em,x,j} \times \frac{\rho_s}{\rho_w} \times \{\alpha_{s,<x,j} - \alpha_{s,<x,j-1}\} \tag{7.94}$$

3. Water consumed by the hydration of embedded limestone particles:

$$\Delta w^{l,s}_{em,x,j} = 1.62 \times v^{l,s}_{em,x,j} \times \frac{\rho_l}{\rho_w} \times \{\alpha_{l,<x,j} - \alpha_{l,<x,j-1}\} \tag{7.95}$$

The calculation of the reduction $\phi^s_{1,x,j+1}$ in the time step Δt_{j+1} is defined as follows:

$$\phi^s_{1,x,j+1} = \frac{\Delta w^s_{x,j}}{\Delta w^s_{x,j} + \Delta w^{c,s}_{em,x,j} + \Delta w^{s,s}_{em,x,j} + \Delta w^{l,s}_{em,x,j}} \tag{7.96}$$

where $\Delta w^s_{x,j}$ is the water consumed by the reaction of slag particle x in the time step t_j:

$$\Delta w^s_{x,j} = 0.45 \times \Delta\alpha^s_{x,j} \times (v^s_x \times \frac{\rho_s}{\rho_w}) \tag{7.97}$$

Limestone Particle x: $\phi^{l}_{1,x,j+1}$

Similarly, the $\phi^{l}_{1,x,j+1}$ of limestone particles x is calculated as follows.

1. Water consumed by the hydration of embedded cement particles in the outer product layer of limestone particle x is as follows:

$$\Delta w^{c,l}_{em,x,j} = 0.40 \times v^{c,l}_{em,x,j} \times \frac{\rho_c}{\rho_w} \times \{\alpha_{c,<x,j} - \alpha_{c,<x,j-1}\} \tag{7.98}$$

2. Water consumed by the hydration of embedded slag particles:

$$\Delta w^{s,l}_{em,x,j} = 0.45 \times v^{s,l}_{em,x,j} \times \frac{\rho_s}{\rho_w} \times \{\alpha_{s,<x,j} - \alpha_{s,<x,j-1}\} \tag{7.99}$$

3. Water consumed by the hydration of embedded limestone particles:

$$\Delta w^{l,l}_{em,x,j} = 1.62 \times v^{l,l}_{em,x,j} \times \frac{\rho_l}{\rho_w} \times \{\alpha_{l,<x,j} - \alpha_{l,<x,j-1}\} \tag{7.100}$$

The calculation of the reduction $\phi^{l}_{1,x,j+1}$ in the time step Δt_{j+1} is defined as follows:

$$\phi^{l}_{1,x,j+1} = \frac{\Delta w^{l}_{x,j}}{\Delta w^{l}_{x,j} + \Delta w^{c,l}_{em,x,j} + \Delta w^{s,l}_{em,x,j} + \Delta w^{l,l}_{em,x,j}} \tag{7.101}$$

where $\Delta w^{l}_{x,j}$ is the water consumed by the reaction of limestone particle x in the time step t_j:

$$\Delta w^{l}_{x,j} = 1.62 \times \Delta\alpha^{l}_{x,j} \times (v^{l}_{x} \times \frac{\rho_l}{\rho_w}) \tag{7.102}$$

7.5.2 Calculation of ϕ_2: Water Availability in the Pore System due to Shrinkage

The factor ϕ_2 denotes the shortage of water in the pore system. When paste is initially mixed, there are theoretically no pores (void) in the paste. However, as the hydration process proceeds, the void space in the hardening system appears and increases. This phenomena is caused by chemical shrinkage, which is because the volume of hydration products is smaller than that of the original reacted cementitious materials and the consumed water [165, 171], this also occurs in limestone blended cement paste [172] and slag blended cement paste [173].

The calculation of ϕ_2 in ternary blended system, which is of course influenced by the added slag and limestone in this study, is implemented by considering the water consumption of cement, slag and limestone and their corresponding chemical shrinkage.

The content of water consumed by hydration can be divided into two parts, one is called chemically bound water, the other physically bound water or gel water. Both chemically and

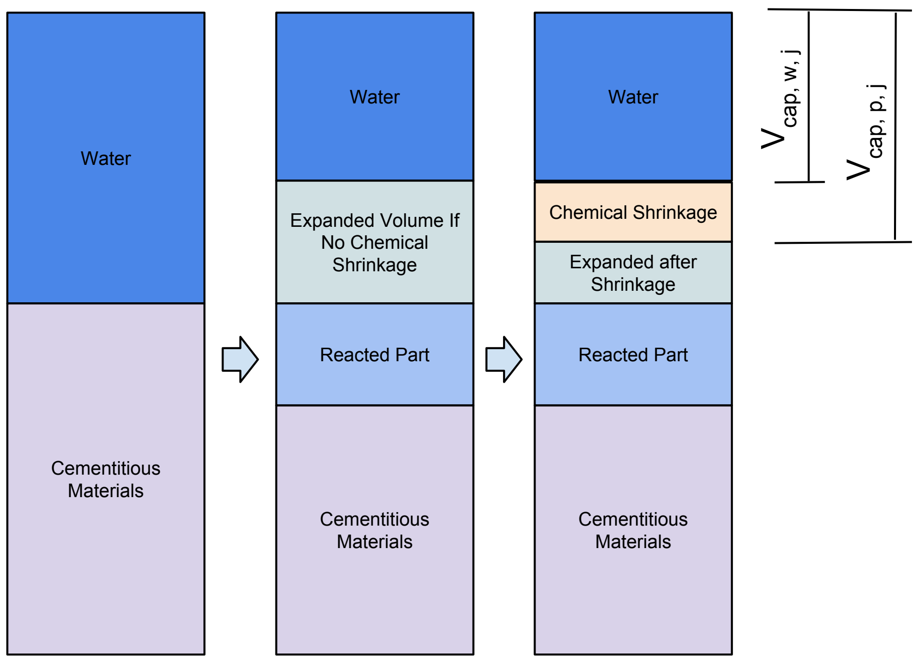

Figure 7.7: Schematic presentation of water shortage in the pore system ϕ_2 (The picture is similar to that in [174]).

physically bound water stay in the hydration products. The left water is called capillary water and stays in the capillary pores. If there is no chemical shrinkage, the pore system should be fully filled by the left capillary water and serves for further hydration.

However, as illustrated in Fig. 7.7, the appearance of chemical shrinkage offering extra space in the paste for capillary water, therefore, the capillary pores are not completely covered by water, which hampers the hydration of particles because of the limited access of water for the hydrating particles. In this study, the factor ϕ_2 is defined as the ratio of the volume of capillary water to the available capillary space (Fig. 7.7), obtained by the following equation:

$$\phi_{2,j} = \frac{V_{cap,w,j}}{V_{cap,p,j}} \tag{7.103}$$

where $V_{cap,w,j}$ and $V_{cap,p,j}$ are the volume of capillary water and available space of capillary pore at time step j, respectively.

The volume of capillary water $V_{cap,w,j}$ at time t_j is the amount of water after consumption by the hydration of all particles:

$$V_{cap,w,j} = \frac{w_p - (0.40 \times m_c \times \alpha_{c,j} + 0.45 \times m_s \times \alpha_{s,j} + 1.60 \times m_l \times \alpha_{l,j})}{\rho_w} \tag{7.104}$$

$V_{cap,p,j}$ is the sum of capillary water and chemical shrinkage of hydration products at time t_j. The amount of chemical shrinkage $V_{sh,j}$ in this research is taken as 25% of chemically bound water that is 25% of the hydrated original material (by mass). This value is estimated from the result of [171], though the exact two values need further investigation, which is not the focus in this study. Based on the assumption, $V_{cap,p,j}$ is calculated as follows:

$$V_{cap,p,j} = V_{cap,w,j} + V_{sh,j} \tag{7.105}$$

or,

$$\begin{aligned} V_{cap,p,j} =& \frac{w_p - (0.40 \times m_c \times \alpha_{c,j} + 0.45 \times m_s \times \alpha_{s,j} + 1.60 \times m_l \times \alpha_{l,j})}{\rho_w} \\ &+ \frac{0.25 \times 0.25 \times (m_c \times \alpha_{c,j} + m_s \times \alpha_{s,j} + m_l \times \alpha_{l,j})}{\rho_w} \\ =& \frac{w_p - (0.3375 \times m_c \times \alpha_{c,j} + 0.3875 \times m_s \times \alpha_{s,j} + 1.5375 \times m_l \times \alpha_{l,j})}{\rho_w} \end{aligned} \tag{7.106}$$

Therefore,

$$\phi_{2,j} = \frac{w_p - (0.40 \times m_c \times \alpha_{c,j} + 0.45 \times m_s \times \alpha_{s,j} + 1.60 \times m_l \times \alpha_{l,j})}{w_p - (0.3375 \times m_c \times \alpha_{c,j} + 0.3875 \times m_s \times \alpha_{s,j} + 1.5375 \times m_l \times \alpha_{l,j})} \tag{7.107}$$

According to Eq. 7.107, $\phi_{2,j}$ is never larger than 1 and could be mathematically a negative value when there is insufficient water for further hydration, i.e. $w_p - (0.40 \times m_c \times \alpha_{c,j} + 0.45 \times m_s \times \alpha_{s,j} + 1.60 \times m_l \times \alpha_{l,j}) < 0$, which is impractical as the shortage of water in pore system means no further hydration.

Indicative Values of ϕ_2

To illustrate the relationship between ϕ_2 and water to powder ratio (w/p), mixing proportion, two sets of pastes are chosen to demonstrate the comparison.

Fig. 7.8 shows that ϕ_2 changes with hydration degree at different w_p (0.4 and 0.5). It can be concluded from the two curves that ϕ_2 decreases sharply when the hydration degree is high, e.g. $\alpha > 0.5$, which is even more distinct at low w_p. This is because the overall chemical shrinkage at high hydration degree is high and low w_p means that the water shortage in the capillary pore system is even severer. In a paste with low w_p, the ratio of capillary pore filled with water to the overall capillary pore is much lower than the case of high w_p.

Fig. 7.9 indicates the difference between two sets of mixing proportions at a moderate w_p. Although ϕ_2 decreases faster as hydration degree increases, the variation of mixing proportion does not have much effect on ϕ_2, which should result from the assumption that the water consumption and chemical shrinkage rate of slag are approximately the same as that of cement in this study.

7.5.3 Temperature Function $F_1(\cdot)$

Factor $F_1(\cdot)$ refers to the net temperature effect on the rate of reaction and process from the morphology and structure related components [3].

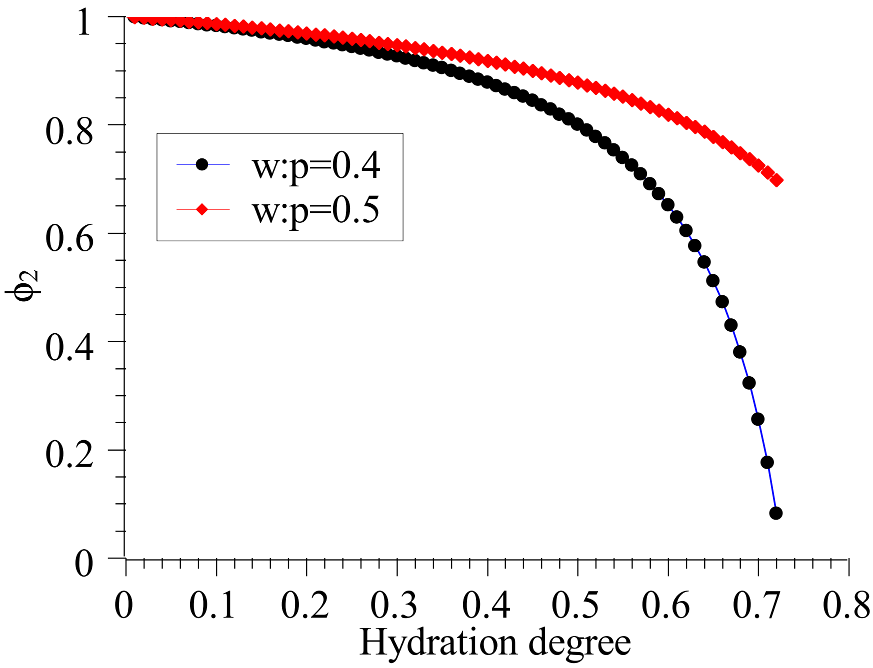

Figure 7.8: ϕ_2 decreases with increasing hydration degree (cement:slag:limestone = 0.3:0.6:0.1).

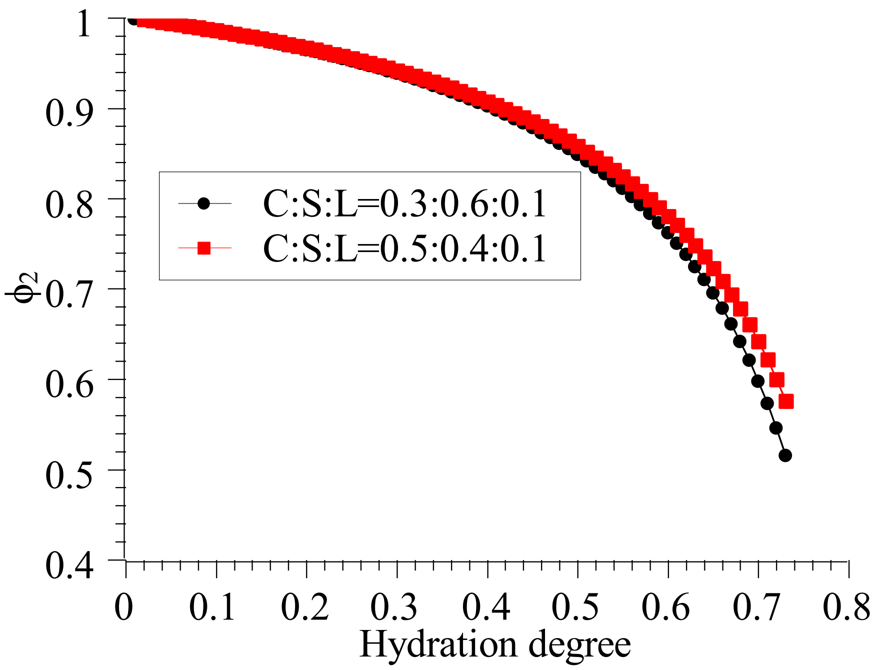

Figure 7.9: ϕ_2 decreases with increasing hydration degree (w/p = 0.45).

Table 7.1: Apparent activation energies of GGBFS mortars (Ea, kJ/mol) [175].

% GGBS	High w/b	Intermediate w/b	Low w/b
0	34.8	35.1	32.9
20	36.6	35.2	36.8
35	47.1	47.0	46.8
50	54.6	48.0	52.6
70	58.8	62.1	57.9

Implementation of Temperature function $F_1(\cdot)$ for Blended Paste in the Model

The implementation of $F_1(\cdot)$ in blended systems is achieved by the Arrhenius function as the case of pure Portland cement in HYMOSTRUC.

$$F_1(\cdot) = A \times e^{\frac{AE}{R \times (273+T)}} \tag{7.108}$$

where R is the gas constant (8.31×10^3 kJ/mol·K), and AE is the activation energy of the mixed paste and obtained from literature references [175]. A is a constant and determined by defining $F_1(\cdot)$ as 1 at temperature T = 20 °C (Celsius degree) that means a *neutral* temperature effect:

$$\frac{1}{A} = e^{\frac{AE(T_{20^\circ C})}{R \times (273+20)}} \tag{7.109}$$

Table 7.1 lists limited data for slag blended cement mortars by [175]. For the sake of mathematic calculation, a linear regression equation of AE and replacement level of slag is proposed based on these data as shown by Eq. 7.110. This is an overall apparent activation energy of slag blended paste, which is different from the individual apparent activation energy of slag and cement proposed by [148] based on experimental results.

$$AE(\text{slag}\%) = 32.4 + 0.4 \times slag\% \tag{7.110}$$

where slag$\%$ is the replacement level of cement by slag.

7.5.4 Temperature Function $F_2(\cdot)$

The factor $F_2(\cdot)$ accounts for the effect of temperature on morphological and structure changes, i.e. $\nu_{(\cdot)}$ is a function of the curing temperature. Detailed discussion of this topic is given in [3]. Compared to pure Portland cement, the relationship between $\nu_{(\cdot)}$ of blended system and temperature is far more complex. Research on this issue is badly needed.

Due to the lack of detailed and reliable information on this subject, the implementation of $F_2(\cdot)$ in this model for blended cements has no change compared with that of pure Portland cement. The mathematical expression of $\nu(T)$ at temperature T (Celsius degree) is as follows:

$$\nu(T) = 2.2 \times e^{-2.8 \times 10^{-5} \times T^2} \tag{7.111}$$

The method solving the temperature history of a hydrating paste is fully proposed by [3].

With the proposed equation of $\nu(T)$ (Eq. 7.111), temperature induced densification in the diffusion layer (hydration products) is considered by the reduction factor $F_2(\cdot)$ of the basic penetration rate according to:

$$F_2(T) = \left(\frac{\nu(\overline{T})}{\nu_{20}}\right)^{\beta_2} \tag{7.112}$$

where β_2 is a constant calibrated from experiment.

At the transition point of hydration process, disregarding other factors ($\phi_1(\cdot)$, $\phi_2(\cdot)$ and $F_1(\cdot)$, giving them the value 1), then:

$$k_0 \times \Delta t = k_1 \frac{1}{(\delta_{tr,20^\circ})^{\beta_1}} \times \Delta t \tag{7.113}$$

thus,

$$k_1 = k_0 \times (\delta_{tr,20^\circ})^{\beta_1} \tag{7.114}$$

7.6 Summary

A model inspired by the existing HYMOSTRUC is proposed in this chapter to simulate the hydration process of ternary blended system. By the help of cell definition and shell density, the spatial interaction of the randomly distributed particles can be calculated, aiming to solve the interaction during hydration process on the one hand and build the developing microstructure on the other hand. The method applied in this model is similar to "finite element method". The hydration is considered based on the size of each particle, and the whole hydration duration is divided by each time step, with the kinetics solved within each time step. Accumulating the hydration of all particles and all time steps, the overall hydration kinetics and microstructure are thus simulated.

The parameters in the basic penetration equation are modified and even fundamentally altered to simulate the factors influencing the hydration process, i.e. $\phi_1(\cdot)$ accounts for the water consumed by the embedded particles in the outer product layer, and $\phi_2(\cdot)$ for the water shortage in the capillary pore caused by chemical shrinkage. The former factor is essentially solving the interaction with the neighborhood particles via water consumption, which also solves the influence of reactant such as $Ca(OH)_2$ in the pore solution. In addition, The influence calculated by $\phi_1(\cdot)$ is at particle level, specifically, $\phi_1(\cdot)$ is a function of each particle and the reaction time. While $\phi_2(\cdot)$ is a factor that considers the water shortage due to the enlarged pore volume during the hydration process. This is an influence factor for the whole calculated paste, i.e. overall level.

It should be noted that the three different materials in this model are by no means limited to cement, slag and limestone powder, which are the three types of materials in this research.

Given the corresponding input such as the proper k values, particle size distribution, chemical shrinkage ratio of hydration products, water amount for complete hydration, and the accordingly modified calculation of the interaction between different materials, the model has the potential to work for other ternary blended systems.

Chapter 8

Implementation of the Model: Calibration and Validation

8.1 Introduction

A theoretical model for simulating the hydration process of ternary blended cement was proposed in Chapter 7. The model needs calibration and validation, making sure the right output is produced by the model based on the right input, which proves the applicability of the model. For this purpose, this chapter is to cover the calibration and validation of the model, linking the model to experimental observations of this research.

The calibration and validation of the model is implemented on computer using the powerful programming language MATLAB which is an easy-to-use scientific program with the strong capability of processing large scale vector and matrix. The calculated results are visualized in HYMOSTRUC by a newly developed module from the work of Gao [160]. The experimental results of pure Portland cement paste (PC) and binary slag blended cement paste (PB) are used for calibration, obtaining the corresponding parameters, i.e. β_c, β_s and β_l, then the calibrated model is validated by the results of binary limestone blended cement paste (PL) and ternary blended cement paste (PBL).

Fig. 8.1 is a brief flowchart of modeling based on the model proposed in Chapter 7. Apparently, the calculation is performed at two vectors, one is the size step which starts from the smallest, the other is time step, from the initial stage to designated curing age.

8.2 Input and Output of the Model

As introduced in Chapter 7, the proposed model includes two parts, the first part is the building of the calculation cell, in which particles are randomly distributed. The spacial characteristics such as paste density of each material, shell density of each particle are then calculated. The second part is the calculation of hydration kinetics. The basic hydration of each material is governed by

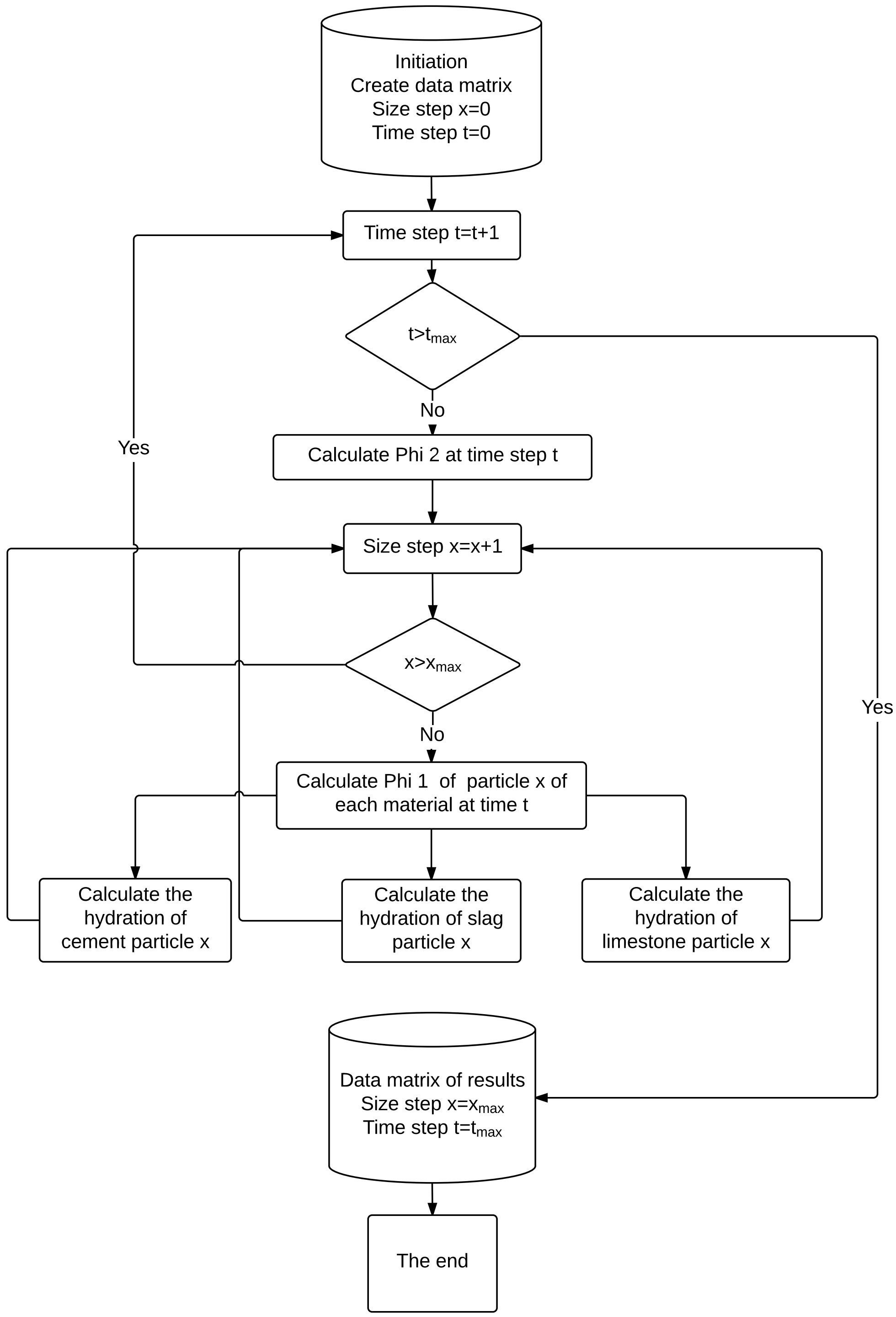

Figure 8.1: The main flowchart of modeling.

Table 8.1: Input for the calibration and validation of the model.

Name	Parameter	Value used
Water to powder ratio	w/s	0.4
Mix proportion	P:B:L	Section 4.2.2
Temperature	T	20 °C
Particle size distribution	n, b	Regression from Fig. 4.1
Chemical composition of slag	(C + A + M)/S	1.66 cf. Table 4.1
Chemical composition of cement	C_3S, C_2S, C_3A, C_4AF	Table 4.1
Density of raw materials	ρ_c, ρ_s, ρ_l	3.1, 2.9, 2.7 g/cm^3
Volumetric expansion ratio	ν_c, ν_s, ν_l	2.2, 3.1, 2.2
Basic penetration rate at 20 °C	$k_{0,c}$, $k_{0,s}$, $k_{0,l}$	0.0430, 0.0042, 0.0002 μm/h
Transition thickness	$\delta_{tr,c,20°C}$, $\delta_{tr,s,20°C}$, $\delta_{tr,l,20°C}$	2.6, 0.3, 0.3 μm
Apparent energy of each material	AE_c, AE_s, AE_l	T = 20 °C, AE not necessary

its own rate constant, i.e. $k_{0,(\cdot)}$, which are quantified based on experiment or reference. The main work is simulating the interaction between different particles. It is implemented by calculating the embedded volume of each material in the outer product layer of each particle at each time step, which uses the shell densities and *volume balance* (Section 7.2.7). Obtaining the spatial interaction, the water accessibility in paste ($\phi_1^{(\cdot)}$ and ϕ_2) for hydration of each particle at each time step is quantified, which then influences the hydration kinetics at next time step.

8.2.1 Input for the Model

Prior to the calibration and validation, the right set of input for each simulation needs to be clearly known. According to the proposed model in Chapter 7, the list of input is illustrated in Table 8.1.

There are mainly two types of input for the model, which are also two types of influences on the kinetics of hydration of each component. The first is intrinsically determined by the properties of the materials, such as chemical composition of material, density of material, volumetric expansion ratio of hydration products, the basic penetration rate of particle, apparent energy of material, transition thickness of particle. The extrinsic influences are from the hydration environment, including water to powder ratio, mix proportion, and curing temperature. Meanwhile, the influence from other factors, such as the nucleation effect of limestone addition and the replacement level of cement by slag as introduced in Chapter 7, are essentially considered by combination of the aforementioned input.

The values of materials in Table 8.1 are obtained by experiments in this research, such as w/s, P:B:L, T, n, b, chemical compositions and density of materials. The values of $\delta_{tr,c,20°C}$, ν_c, 20 °C and AE_c for cement are determined by the original HYMOSTRUC, while $A_{E,s}$ and $\delta_{tr,s,20°C}$ for slag are obtained from and literature [175] and [114, 115], respectively. $k_{0,s}$ is determined according to the results of Chapter 3. Limestone is given a very small $k_{0,l}$ that is about 1/20 of slag.

It should be noted that the actual value of $F_1(\cdot)$ and $F_2(\cdot)$ for modeling of all four types of pastes in this research are 1, since the curing temperature of these pastes were exactly 20 °C over the whole hydration process. Therefore, apart from the input listed in Table 8.1 for the model, there is only one parameter to be calibrated by experimental data, i.e. β_c and β_s for cement and slag, respectively, comparing with sets of parameters to be calibrated in other models [131, 103], less parameter to be calibrated in this proposed model of this research also demonstrates its simplicity, as stated by van Breugel [3]:

Models with more than three free parameters might be strong in being able to fit almost any hydration curve, but become increasingly weak in proving the correctness of the assumed hydration mechanisms.

8.2.2 Output of Simulation

Using the input and the calibrated parameters, i.e. β_c and $\beta_s$of cement and slag, respectively, the first output of the model is the thickness of the reacted front layer of each particle at each time point, which is the most important value of hydration in this model. As soon as this value of each particle is obtained, the degree of hydration/reaction at different level is thus calculated, which is the main output of the model, furthermore, other related results such as water remained in the pore solution and the total volume of pore system in the paste are also accordingly calculated, since all these values are mathematically related to the degree of hydration.

8.3 Cases for Calibration and Validation

8.3.1 Calibration of β_c Based on Experimental Results of PC Paste

The calibration of β_c in the model uses the input and output from experiment of pure Portland cement paste, i.e. PC, which is reported in Chapter 4. The input of PC is as listed in Table 8.1, while the output is mainly the hydration degree of cement measured by XRD/Rietveld.

After several times of fitting, the calibration result of PC paste shows that the parameter β_c of cement in this model is 2.3, which is slightly higher than the default value 2.0 in the original HYMOSTRUC. The simulated degree of hydration of cement using this value is averagely 4.2% higher than the experimental results. Fig. 8.2 demonstrates the hydration degree of cement determined by experiment and modeling, respectively.

8.3.2 Validation of β_c Based on Experimental Results of PL Paste

Using the calibrated β_c, we used the model to simulate the hydration of PL paste that was measured in Chapter 4 by experiment. As shown in Fig. 8.3, the degree of hydration of cement in PL paste simulated by the model generally agrees well with the result of experiment, though the

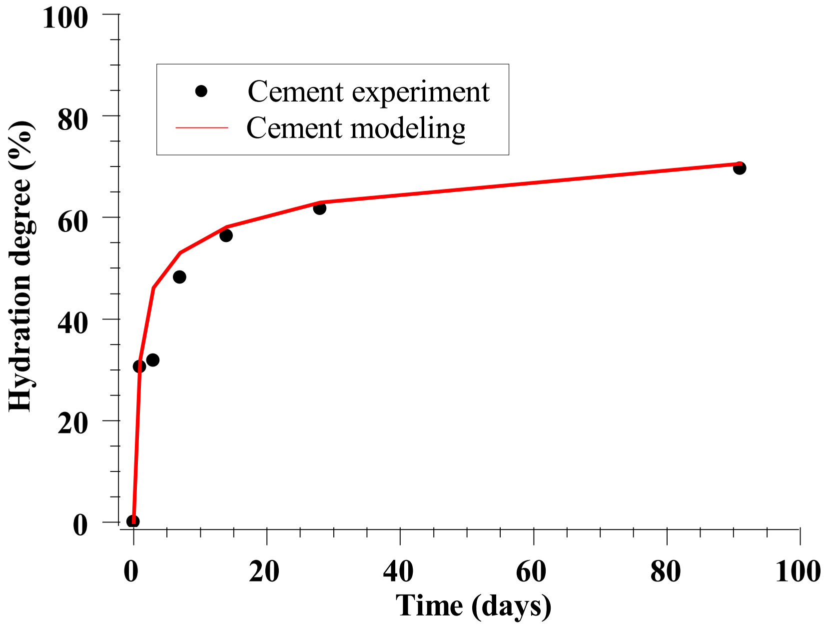

Figure 8.2: Calibration of β_c: hydration degree of cement in PC paste simulation and experimental results.

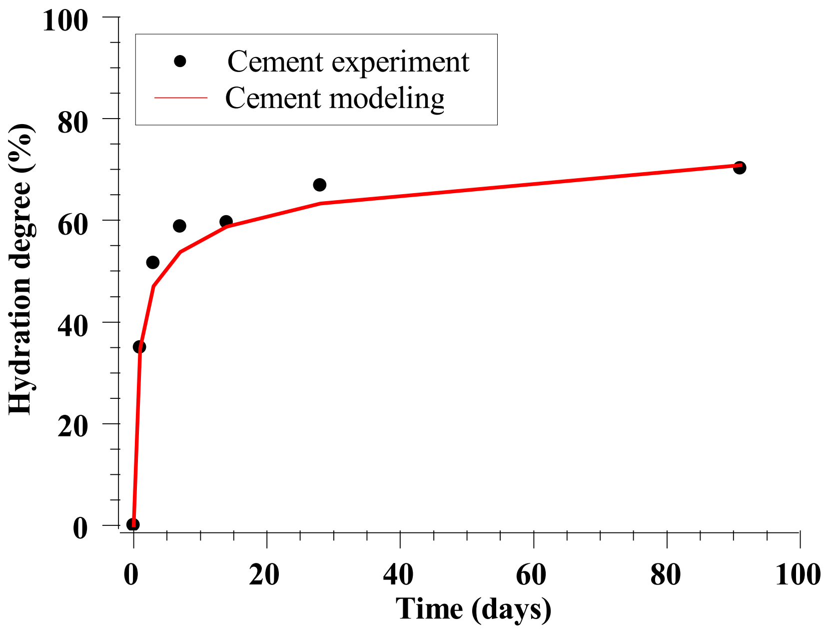

Figure 8.3: Validation of β_c: hydration degree of cement in PL paste from simulation and experimental results.

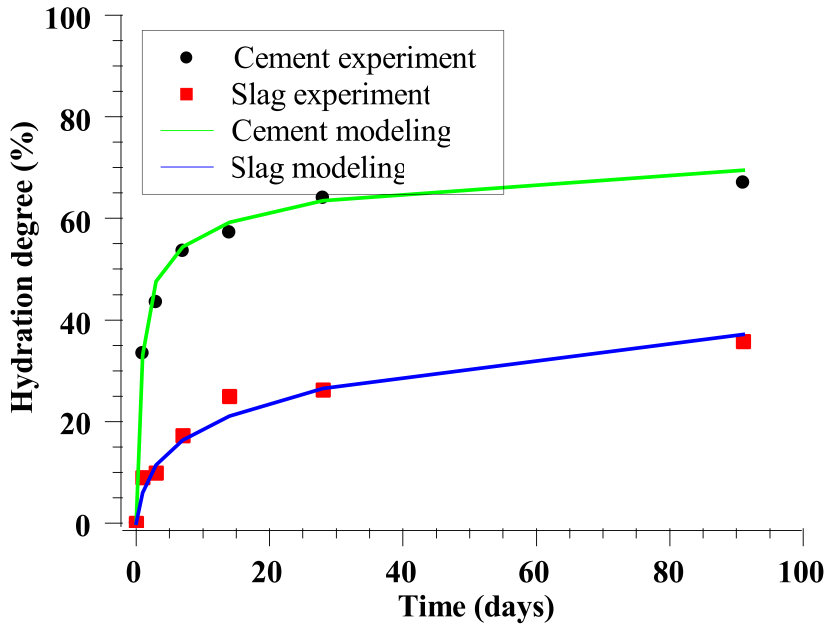

Figure 8.4: Calibration of β_s: hydration degree of cement and slag in PB paste simulation and experimental results.

simulated degree of hydration of cement is slightly underestimated compared with the measured results at 3, 7 and 28 days, which could be explained by the assumption that the nucleation effect of limestone on cement is only considered during the phase boundary stage of hydration. However, due to the limited accuracy of XRD/Rietveld analysis which quantified the hydration degree of cement in this research, the overall performance of the validation is acceptable, as the simulated hydration degree of cement at 1, 14 and 91 days, which represent the early, middle and late ages of hydration in this research, agree very well with the experimental results. The validation of the model demonstrates the rightness and reliability of the proposed model to numerically simulate the hydration of cement and binary blended limestone cement.

8.3.3 Calibration of β_s Based on Experimental Results of PB Paste

The calibration of β_s is based on experimental results of PB paste and the validated β_c. With the input of PB paste and the measured degree of hydration of cement and slag, the value of β_s is calibrated as 1.3, which is smaller than that of cement, i.e. 2.3. Fig. 8.4 presents the simulated and measured degree of hydration of cement and slag, showing a good fitting between the calibrated and tested results.

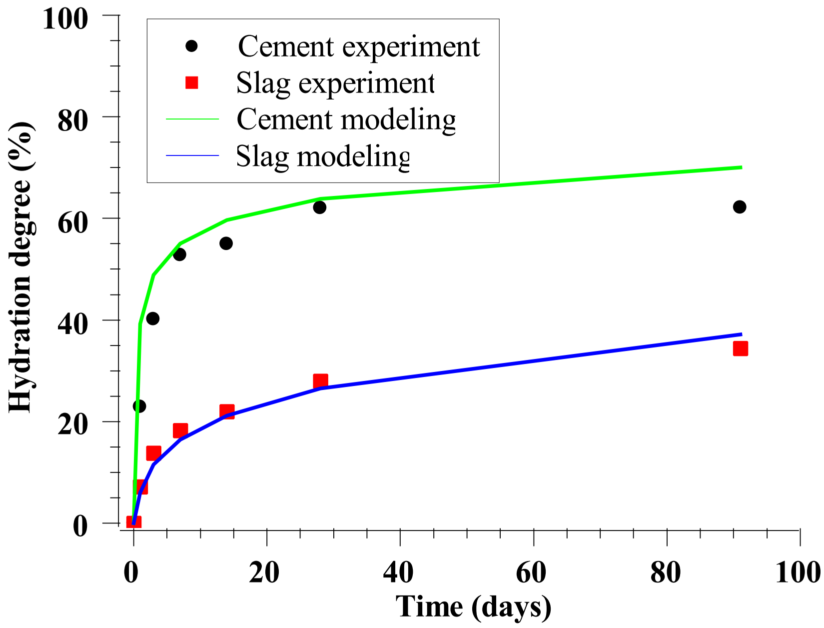

Figure 8.5: Validation of β_s: hydration degree of cement and slag in PBL paste from simulation and experimental results.

8.3.4 Validation of β_s Based on Experimental Results of PBL Paste

Based on the validated β_c and calibrated β_s, we use the proposed model to simulate the hydration of ternary blended cement paste, i.e. PBL paste. By comparing the degree of hydration/reaction of cement and slag from simulation and experiment, the proposed model is validated for ternary blended cement.

Fig. 8.5 presents the simulated and tested degree of hydration/reaction of cement and slag. As shown by the results, the degree of hydration of slag is well predicted by the model during the whole curing age from 1 to 91 days. The degree of hydration of cement predicted by simulation generally agrees with the experimental results. However, the degree of hydration of cement from experiment is lower than the values of simulation, especially at the curing age of 1 and 91 days. The reason could be that the acceleration effect of limestone powder on hydration of cement is probably overestimated at the early age, which also implies the nucleation effect of limestone needs a better mathematical expression rather than the simplified linear equation Eq. 7.78. Considering the complex hydration process in ternary blended cement paste, we believe that the performance of simulation in PBL paste validates the reliability of the proposed model.

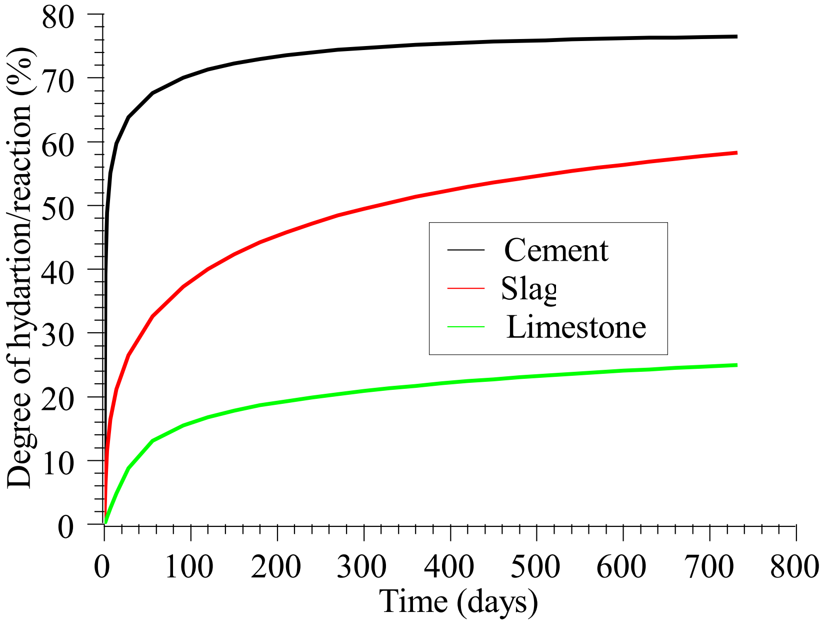

Figure 8.6: Long-term prediction of hydration degree of cement and slag in PBL paste simulated by the model.

8.4 Analysis Based on the Validated Model

8.4.1 Hydration of PBL Paste over Long-term, Case Study

Degree of Hydration/Reaction

Using the calibrated and validated β_c and β_s of the model, it is easily to simulate the hydration of PBL paste in this research over long term. Fig. 8.6 shows the simulated degree of hydration of cement and slag in ternary blended cement paste from 0 to 730 days (2 years).

The predicted degree of hydration/reaction of cement and slag after 730 days of hydration is 76.48% and 58.24%, respectively, while the corresponding values at 91 days are 70.05% and 37.15%. There is only 6.43% of cement hydrated after 91 days till two years, in contrast, another 21.08% of slag in this ternary blended cement paste, i.e. PBL, is hydrated after 3 months till 2 years. This shows the potential hydration of slag even at the very late curing age.

Considering the comparable compressive strength of PC and PBL pastes and mortars after 91 days of curing, it is confident to predict that the compressive strength of PBL paste (Fig. 6.5) and mortar (Fig. 6.6) will be much higher than PC after two years of curing.

It has to be noted that about 15% of limestone reacted after 91 days of curing at the assumed $k_{0,l} = 0.0002$ μm/hour and $\delta_{tr,l,20°C} = 0.3$ μm and $\beta_l = 2$, which shows about 1.5 g of limestone reacted in the 10 g of blended limestone of each 100 g of cement + slag + limestone. The value agrees with the experimental results tested by TGA, as shown in Fig. 4.14.

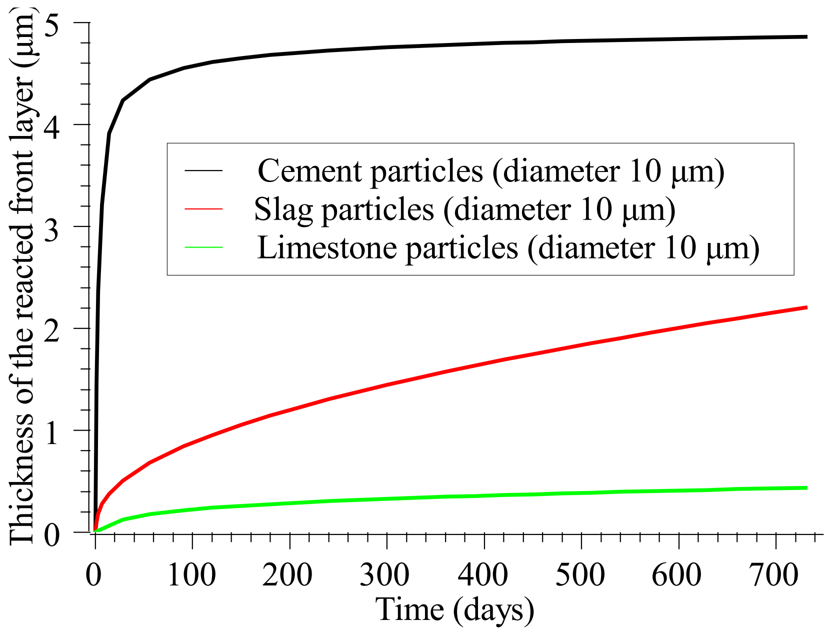

Figure 8.7: The penetration thickness of the reacted front layer of particles with diameter 10 μm at different curing ages.

The Penetration Thickness of Reacted Front Layer of Particles

Fig. 8.7 presents the penetration thickness (i.e. $\delta^{c}_{in,x,j}$, $\delta^{s}_{in,x,j}$ and $\delta^{l}_{in,x,j}$, see E.q. 7.52) of the reacted front layer of particles with diameter 10 μm at different curing ages from the simulation. Particle size 10 μm is a good representative size because most of particles are sized smaller or around this size.

The modeled results of cement, slag and limestone particles are 4.86, 2.20, 0.44 μm, respectively. The main part of development of cement particles occurs within the first 28 days (4.24 μm at 28 days). The total penetration thickness of slag particles with diameter 10 μm is much lower than that of the equivalent cement particles, but it shows significant evolution even at later age, which in turn contributes to the strength development of slag blended cement at later age. The penetration thickness of limestone particles with diameter 10 μ is generally small, which is apparently the result of the tiny penetration rate, i.e. $k_{0,l}$, but it also shows that the particles can undergo a certain amount of reaction even at a very low penetration rate.

Fig. 8.8 shows the penetration thickness of the reacted front layer of particles with diameter from 1 to 80 μm after 2 years of hydration/reaction from the simulation. The maximum values of cement, slag and limestone particles are 7.09, 2.76 and 0.67 μm, respectively, with the corresponding diameter of the three materials are 19, 6, and 2 μm. The simulated results indicate only particles with diameter several micrometers can completely reacted/hydrated, while large particles (i.e. diameters larger than 20 μm) have relatively thinner reacted front layer. The simulated results from this specific ternary blended cement paste also imply that fine particles play an important role in the hydration/reaction. It is straightforward to know that cementitious

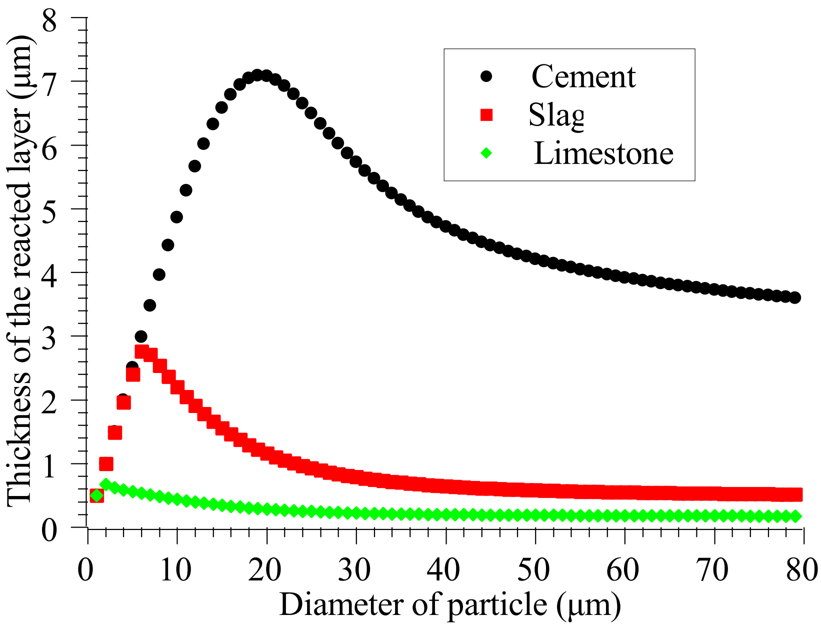

Figure 8.8: The penetration thickness of the reacted front layer of particles with diameter from 1 to 80 μm after 2 years of reaction.

Table 8.2: Simulated amount of total bound water in PBL paste at different ages, normalized by 1 g of solid raw material, i.e. cement + slag + limestone, and the original water is 0.4 g.

Time (Days)	1	3	7	14	28	91	365	730
W_b	0.064	0.091	0.114	0.136	0.162	0.209	0.264	0.289

materials consisting of fine particles bear large specific surface area, but the simulated results demonstrate that fine particles can have higher penetration thickness of the reacted front layer.

Total Bound Water

Based on the simulated degree of hydration, the amount of total bound water of PBL paste at different ages is calculated according to the model. Table 8.2 is the total bound water in PBL paste at different ages, normalized by 1 g of solid raw material, i.e cement + slag + cement. The water to powder ratio is 0.4, meaning the original water is 0.4 g.

Table 8.3 shows the simulated and measured amount of total bound water normalized by cementitious materials, i.e. cement + slag. Comparing with the experimental results, the simulated results are slightly underestimated in the early and late age, but overestimated in the middle age. However, a fact that should be kept in mind is that the amount of total bound water tested by TGA (Fig. 5.8) is subject to vary due to the evaporable water sensitive to the relative humidity, as already discussed in Section 5.3.3. Even under the condition that the simulated amount of total bound water is overestimated, implying the water consumed by hydration is overestimated, the simulated results indicates only 0.289 g of water is consumed after two years of hydration, leaving 0.111 g of water for unreacted materials, which demonstrates that the water

Table 8.3: Simulated and measured amount of total bound water in PBL paste at different ages, normalized by 1 g of cementitious materials, i.e. cement and slag. (%).

Time (Days)	1	3	7	14	28	91	365	730
W_b Mod.	7.08	10.17	12.71	15.15	18.02	23.24	29.34	32.10
W_b Exp. (Fig. 5.8)	6.08	11.53	16.16	19.10	15.54	20.63	/	/

in this PBL paste is still available for further hydration of materials, in other words, water is not a handicap for further hydration.

Total Porosity from Simulated Results

Based on the simulated degree of hydration/reaction of cement and slag (also a limited reacted amount of limestone), the expanded volume in hydration products is calculated with the volumetric expansion ratio of each material. Therefore, the total porosity is obtained. The simulated porosity is used to validate the volume change of the hydration system, partially checking the feasibility of the developed microstructure.

Fig. 8.9 shows the measured total porosity of PBL paste by MIP and calculated according to the simulated degree of hydration/reaction at different curing ages, respectively. The modeled total porosity agrees very well with the experimental results from 1 to 91 days of hydration. The predicted total porosity of PBL by simulation is 10.72% and 6.35% after one and two years of hydration, respectively. Despite the complete hydration of cement and slag, the maximum volume for all hydration products and water required is not enough in this PBL paste. However, the simulated results of water and space show that the space and water is still available after 730 days of hydration.

Availability of Water in the Hydrating PBL Paste ϕ_1 and ϕ_2

Figs. 8.10 and 8.11 show the evolution of two water related factors: ϕ_1 and ϕ_2. As proposed in Section 7.5.1, the factor ϕ_1 in the model is calculating the water consumed by the embedded particles in the outer product layer, the lower the value, the less the water is available for the hydration of the center particle. It changes with particle size, curing time and the type of material in a given paste. The diameter of cement and slag particles in Fig. 8.10 is 80 μm, representing the large particle which still needs to be reacted in the paste.

The simulation results show that ϕ_1 value of both cement and slag particles quickly decrease to 0.5 and become almost less than 0.1 after one year. The low values of ϕ_1 at late ages indicate that high ratio of water is consumed by the embedded particles at later ages, though there is still water available in the pore system. This is probably the reason why the overall hydration/reaction degree of cement and slag proceeds very slow at late age. The water availability has a strong influence on large slag particle at late age, since the most part of hydration of cement is finished at early age, while most of reaction of slag proceeds during the late age.

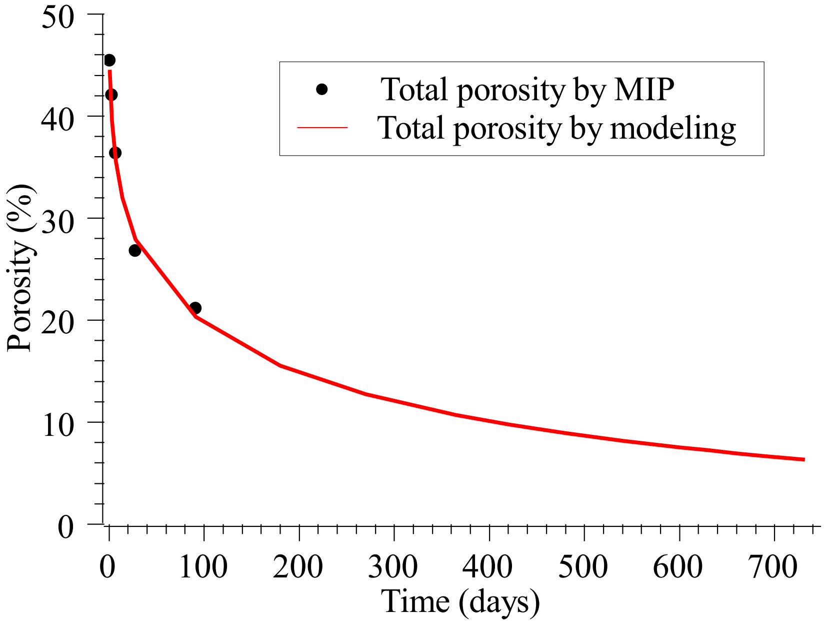

Figure 8.9: Total porosity of PBL paste simulated by the model and measured from MIP experiment (for the modeling curve, only data at 1, 3, 7, 14, 28, 91, 180, 365 and 730 day(s) are plotted in the figure).

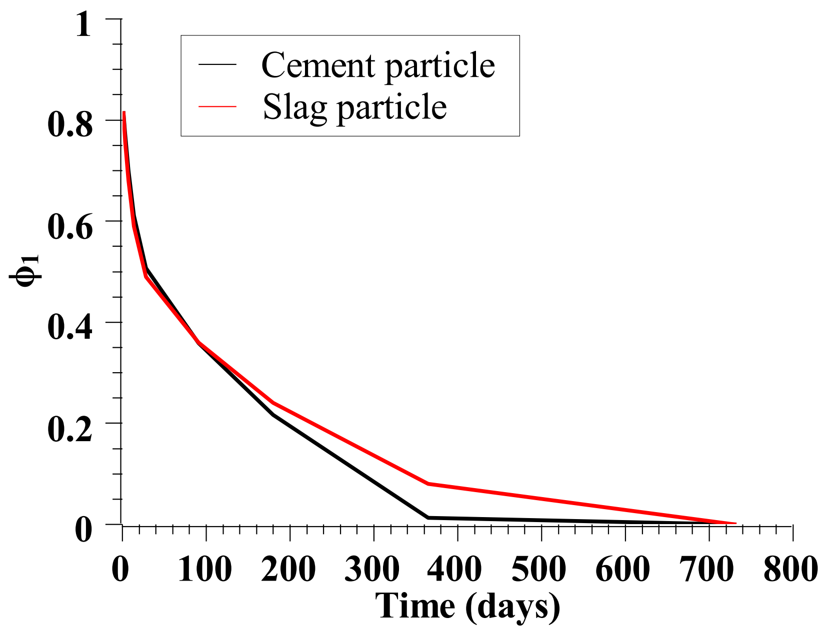

Figure 8.10: The evolution of ϕ_1 of cement and slag particle (diameter = 50 μm) in PBL paste from 1 to 730 days (only data at 1, 3, 7, 14, 28, 91, 180, 365 and 730 day(s) are plotted in the figure).

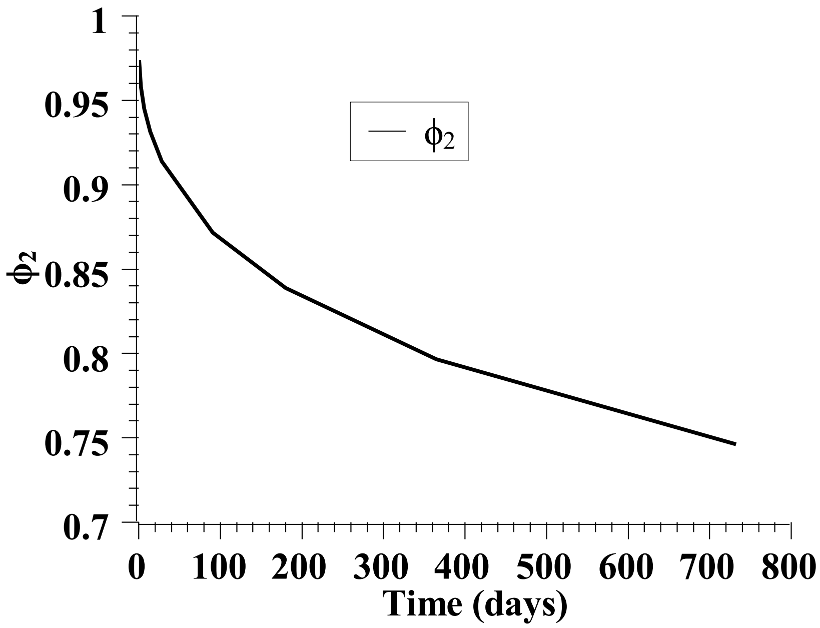

Figure 8.11: The evolution of ϕ_2 of the PBL paste from 1 to 730 days (only data at 1, 3, 7, 14, 28, 91, 180, 365 and 730 day(s) are plotted in the figure).

According to Section 7.5.2, the factor ϕ_2 is proposed to estimate the water distribution in the whole system due to the shrinkage. In other words, ϕ_2 judges the total distribution of water in the pore system for all particles. As shown in Fig. 8.11, the simulated values of ϕ_2 in paste PBL decrease from 0.973 at 1 day to 0.746 after two years, which indicates particles in the paste can get access to the remaining water. This is readily explained by the simulated result that there is still 0.111 g water relative to the original 0.4 g for unreacted materials after two years of hydration.

Comparing with the simulated values of ϕ_1 and ϕ_2, we can conclude that it is the accessibility of water for large particles at later age that determines the hydration in this PBL paste.

The hydration of cementitious material is actually intrinsically determined by the chemical composition and also possibly inner structure. Although the hydration kinetics of cement and slag is closely determined by the basic and intrinsic penetration rate $k_{0,c}$ and $k_{0,s}$ as well as extrinsic factors such as temperature, as soon as the thickness of reacted layer exceeds the transition thickness, i.e. $\delta_{tr,c,20^\circ C}$ of cement and $\delta_{tr,s,20^\circ C}$ of slag, the water and space in the system limit the potential degree of hydration/reaction, which is of course closely related to the water to powder ratio.

Fig. 8.12 presents the simulated degree of hydration/reaction of cement and slag in PBL paste hydrated under water to powder ratios, i.e. 0.2, 0.4 and 0.6 from 1 to 91 days. The hydration of slag and cement in the PBL paste is strongly influenced by the water to powder ratio, which is even more distinct in the case of cement at later age.

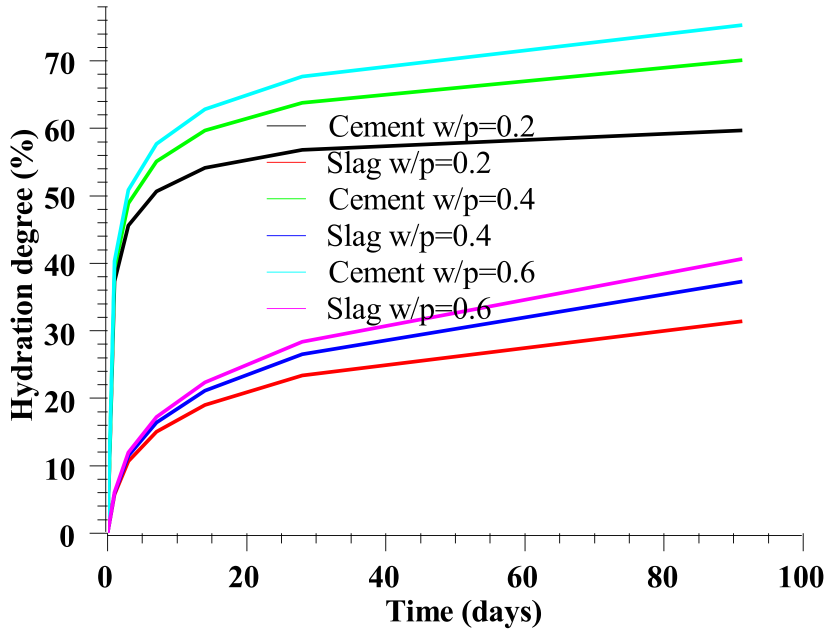

Figure 8.12: The simulated degree of hydration of PBL paste hydrated under different water to powder ratios from 1 to 91 days (only data at 1, 3, 7, 14, 28 and 91 day(s) are plotted in the figure).

Visualized Three-dimensional Microstructure

Fig. 8.13 is the visualized three-dimensional microstructure of PBL paste prior to hydration and after 2 yeas of hydration, respectively. As shown in the microstructure, most of cement particles except for few large particles are completely hydrated after two years of hydration, but there are still many particles including moderate size remaining unreacted. The modeled results actually show that slag particles smaller than 5 μm (diameter) are completely reacted after two years, while the corresponding value of cement particle is 13 μm. Limestone particles generally maintain the original sizes, acting mainly as inert filler as assumed in the model. However, a thin product layer (inner and outer products) is observable, which is due to the low reactivity ($k_{0,l}$) of limestone particles over long curing age.

8.4.2 Calculation Efficiency of the Model

As introduced in the beginning of this chapter, the proposed model for simulating the hydration of blended cement is implemented in Matlab language. Simulating the hydration of 1.4 g of PBL paste for two years takes less than 30 min on an average desktop computer (the hardware specification is shown in Fig. 8.14). The total number of particles is about 1.64×10^{10} in the 1.4 g of paste. Therefore, the calculation efficiency of the model is acceptable for normal numerical simulation.

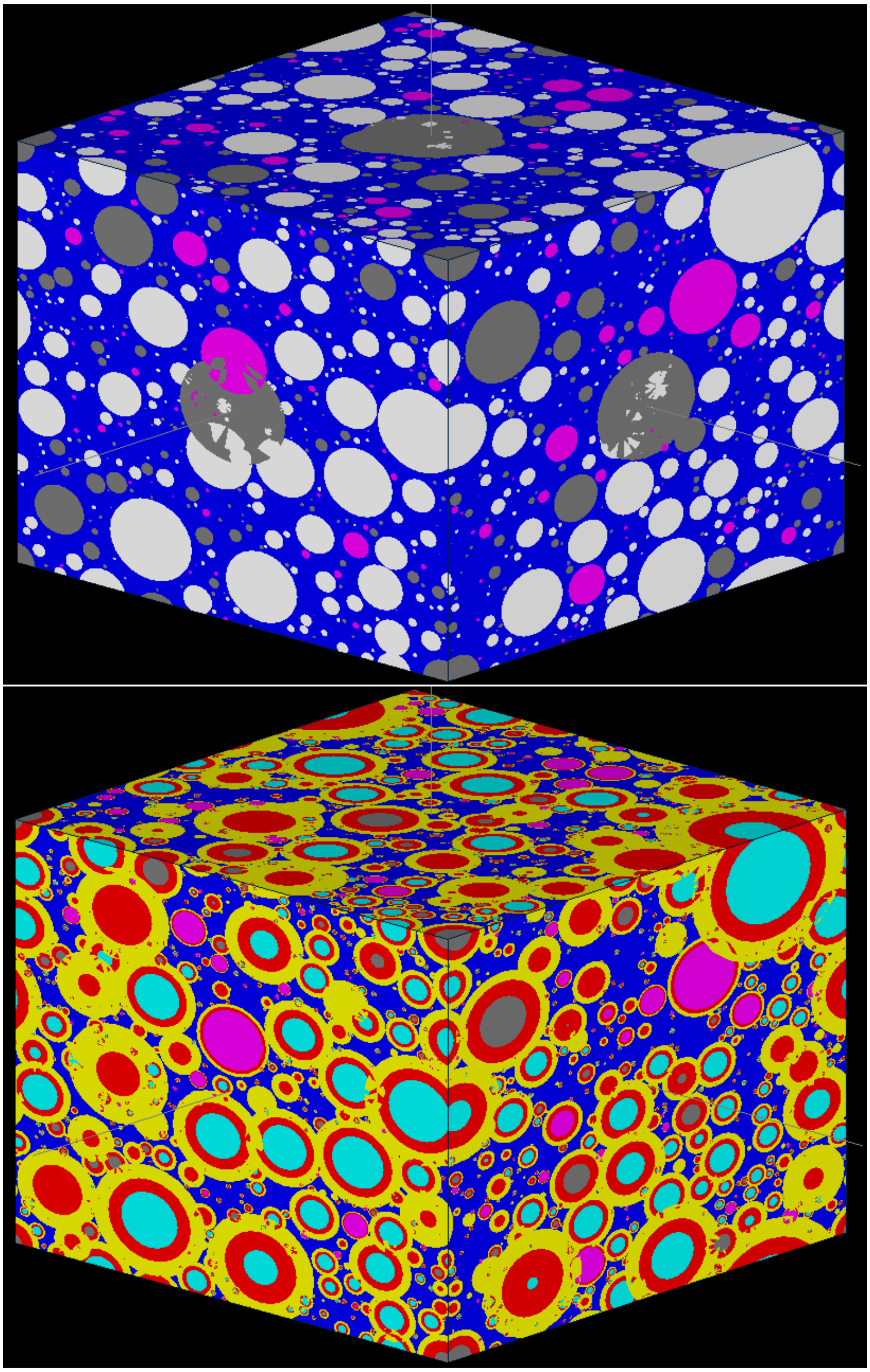

Figure 8.13: The visualized microstructure of PBL paste prior to (top) hydration and after two years of hydration (bottom) (29,371 particles in the $100 \times 100 \times 100$ μm^3 box, color match: gray = cement, turquoise & white = slag, magenta = limestone, blue = water, red = layer of inner products, yellow = layer of outer product).

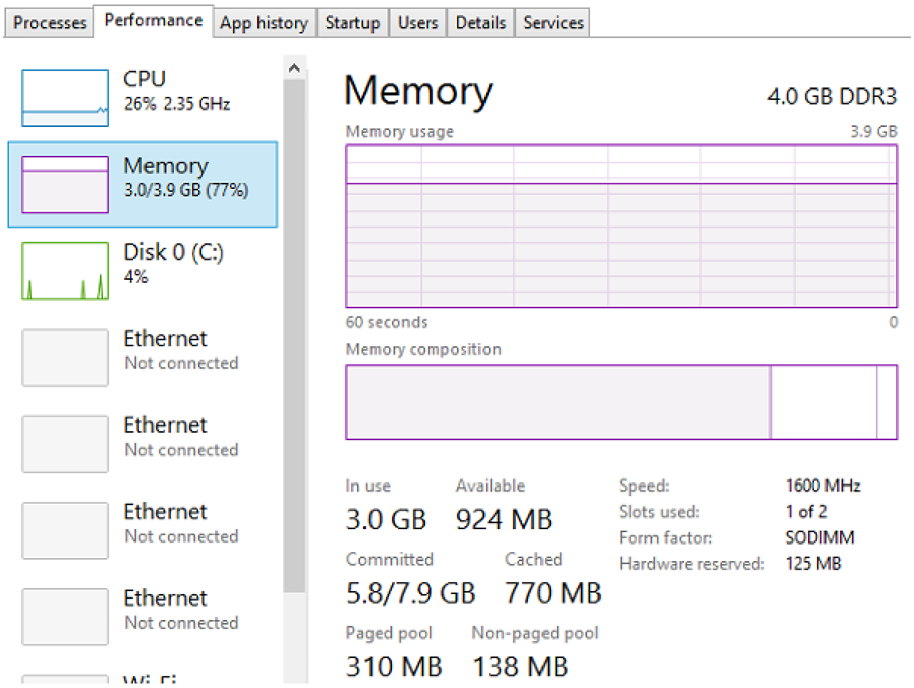

Figure 8.14: The hardware specifications used in the modeling of this study.

8.5 Summary

This chapter calibrated the proposed model for hydration of ternary blended cement based on the input and output of experimental results of PC and PB pastes. The calibrated model was then validated by the experimental results of PL and PBL pastes. The model can simulate the degree of hydration of binary and ternary blended cement pastes hydrated at 20 °C.

The case study using the validated model shows that the hydration of slag at late age (later than 91 days) is still remarkable. The simulation of hydration of PBL paste also indicates that the water and space in the paste limits the potential evolution of hydration degree, which is related to the water to powder ratio.

Chapter 9

Conclusions and Recommendations

9.1 Conclusions

The research work presented in this thesis systematically investigated the hydration of blended cement by both experimental means and numerical modeling, specifically Portland cement, slag and limestone powder ternary blended cement. The thesis consists of two parts. The first part is mainly focused on experiment. Chapters 3-5 studied the reaction kinetics of slag activated by $Ca(OH)_2$ solution, hydration kinetics and products of blended cement pastes. Chapter 6 investigated the microstructure and mechanical strength. The second part of the thesis is modeling. Chapter 7 proposed a theoretical model for simulating the hydration kinetics of ternary blended cement. The model is greatly inspired by the original HYMOSTRUC but developed a new algorithm dealing with the spatial interaction between different particles. In addition, the water availability in pore system was considered. In Chapter 8, the model was calibrated and validated based on the experimental results obtained in this research.

Detailed conclusions are listed at the end of each individual chapter of the thesis. However, summarizing the work conducted in this research, the author would like to highlight the main conclusions as follows.

1. Specific surface area of slag plays an important role in the overall reaction. The overall reaction degree of slag consisting of fine particles develops faster than that of coarse slag. However, coarse slag particles in this study have higher content of CaO but relatively lower content of MgO, Al_2O_3 and SiO_2, resulting in higher reactivity index of (CaO + Al_2O_3 + MgO)/SiO_2, implying higher reactivity at particle level. Calculation shows that the rate of increase of the front reacting layer thickness (k value) of a coarse slag particle is higher than that of fine particles. It is also found that higher Ca/Si ratio of slag is crucial for the reactivity of slag particles at least at the early age of reaction.

2. The hydration of calcium silicate phases of cement in ternary blended pastes was enhanced by the presence of limestone powder, but hampered by the addition of slag. The hydration of calcium alumina phases of cement was greatly accelerated by the addition of slag. It

was also enhanced by the presence of limestone in binary blended limestone cement paste at early age. However, the coexistence of limestone with slag in ternary blended cement paste shows that limestone restrained the hydration of calcium alumina phases of cement.

3. The hydration of cement clinker was distinctly accelerated by the single addition of slag or limestone within 91 days of hydration. The coexistence of slag and limestone in ternary blended cement accelerated the hydration of cement clinker at early age but showed negative influence at later age (after 14 days).

4. Results from isothermal calorimetry test indicates that the addition of limestone in blended pastes had positive effect on the rate of heat evolution of hydration, which is also confirmed by the increased production of $Ca(OH)_2$ in PL paste. Slag reduced the rate of heat evolution of hydration of cement pastes at early age due to its low reactivity.

5. The reaction of slag was activated within 24 h of hydration in this study. The pH of pore solution from all pastes was higher than 13 over the whole curing age, which is sufficiently high for the activation of slag even at the very early age of hydration. The reaction of slag consumed $Ca(OH)_2$, but $Ca(OH)_2$ was sufficiently available for slag in the PBL paste of this research even after 91 days of hydration.

6. The degree of reaction of slag in blended cement pastes was about 8% and 35% at 1 and 91 days of curing, respectively. It was almost not influenced by the addition of limestone powder.

7. Results of TGA show that a small amount of limestone, i.e. around 1.6-2.2 g of $CaCO_3$ per 100 g of solid raw materials has reacted in pastes, mainly at early age.

8. The hydration products of all pastes are mainly C-S-H gel, $Ca(OH)_2$, and aluminate related assemblages such as ettringite, monosulphate, monocarboaluminate, hydrogarnet and hydrotalcite phases. The presence of limestone increased the amount of monocarboaluminate, but decreased the content of ettringite and monosulphate, showing distinct reaction with aluminate phases from slag and cement. The formation of C-S-H in slag blended cements is largely reduced due to the relatively slow reaction of slag, which is more distinct in the case of ternary blended cement paste. Calculation based on experimental results show that the total amount of bound water for complete hydration of cement and slag in this research is 40 wt% and 46.8 wt% relative to the raw material, respectively.

9. BSE images reveal that the slag particles still maintain their original shapes, showing low degree of reaction even after 91 days of hydration. The addition of slag greatly improved the pore system of blended cement paste, reducing both the total porosity and critical pore size after 91 days of hydration, while the presence of limestone powder had negative influence on the pore system.

10. Calculation based on MIP results indicates the volumetric expansion ratio of hydration products of cement and slag is 2.3 and 3.1, respectively, which are two important values for developing hydration and microstructure model for ternary blended cementitious system.

11. Compressive strength of slag blended cement paste and mortar was low at early age but superior to that containing no slag at later age. The single addition of limestone powder in cement reduced the compressive strength over the whole curing age, but improved the compressive strength at least at early age when coexisting with slag, showing synergistic effect in ternary blended cement, which is even more remarkable in the case of flexure strength of mortar.

12. A model inspired by the idea of HYMOSTRUC is proposed to simulate the hydration process of ternary blended system. By the help of cell definition and shell density, the spatial interaction of the randomly distributed particles can be calculated, aiming to solve the interaction during hydration process and to build the developing microstructure.

13. Influence of water on hydration kinetics in this model is implemented by two aspects. The first is the water consumed by the embedded particles in the outer product layer. The second is the water shortage in the capillary pore caused by chemical shrinkage.

14. The proposed model for hydration of ternary blended cement was calibrated based on the input and output of experimental results of PC and PB pastes. The calibrated model was then validated by the experimental results of PL and PBL pastes. The model can simulate the degree of hydration of binary and ternary blended cement paste hydrated at 20 °C.

15. Simulation indicates that the reaction of slag at late age (later than 91 days) is still remarkable. The simulation of hydration of PBL paste also reveals that water and space in the paste limit the final potential degree of hydration, which is related to the water to powder ratio.

9.2 Future Research

No matter from the viewpoint of experimental or modeling, it is a challenge to explore the world of ternary blended cementitious materials, including but not limited to Portland cement, blast furnace slag and limestone powder. However, the sustainability of development of construction materials demands cement researcher to pay attention to this field.

Experimental work related to cement research is always time-consuming and sometimes tedious. It should be kept in mind that agreement between theoretical and experimental data does not necessarily prove the correctness of model, but merely fails to eliminate the possible model [3], therefore, modeling in cement research relies on the adequate understanding of the real world and efficient calculation algorithm to implement the simulation. In terms of the relation between experiment and modeling, on the one hand, experiments are the foundation and starting point for modeling work. Reliable experimental results help to calibrate and validate theoretical model. On the other hand, robust modeling work in turn helps reduce the tedious experimental work, predicting the properties of cementitious materials when any condition of the materials changes.

The research in this thesis paid efforts to investigate the hydration of ternary blended cement from both experimental and modeling methods, which are presented in Chapters 3 - 8. However, there are more challenges than achieved results on these topics. The author would like to list them below as prospects for future research.

1. Experimental work covering more mix designs of ternary blended cement is necessary. The mix design for ternary blended cement in this research is made up by 30 wt% Portland cement, 60 wt% blast furnace slag and 10 wt% limestone powder, and the water to powder ratio is fixed at 0.4. Experimental and simulation results indicate that a quite limited amount of limestone powder has reacted and most of it acted as inert filler. According to the simulation results over two years, the water to powder ratio 0.4 would not cause water shortage in pore system but the water availability in the outer product layer of particles is extremely limited. Systematic experimental results help calibrate and validate the model at a broader context.

2. The hydration of slag is temperature sensitive. High curing temperature can reduce the apparent energy and thus speed up the kinetics of slag reaction in blended cement. The experimental work in this research is fixed at 20 °C. More experimental work focusing on the varying temperature in slag blended cement will benefit the modeling work, especially the quantitative apparent energy of slag material.

3. Construction material functions in the environment. Research attention is worthwhile to be paid to the response of material to environment deterioration. Thus transport properties of ternary blended cement based on modeling results is the next step, which helps the durability related research.

4. The main purpose of the proposed model in this research is simulating the hydration kinetics of each component. The model for the moment is unable and not meant to deal with the phase assemblage. In terms of this issue, thermodynamic modeling based on the simulated kinetics may be a promising way to predict the quantities of all possible hydration products.

5. The current research is mainly focused on paste level. It may be worthwhile to go up scale to mortar and concrete levels for the applicability of ternary blended cements. In particular, as the addition of limestone powder can improve the workability of concrete, fundamental research work on rheology (i.e. yield stress and plastic viscosity) of ternary

blended cement is also valuable, which benefit the field work of these materials, e.g. pumping and setting.

Appendix A

Additional Figures and Tables

Table A.1: Content of phases in hydration products quantified by XRD/Rietveld analysis (normalized by the weight of raw solid materials, %, $Ca(OH)_2$ and cement clinker not included), Ett. = Ettringite, Hyrt. = Hydrotalcite, $M\bar{c}$ = Monocarboaluminate, CH = $Ca(OH)_2$, $C\overline{C}$ = $CaCO_3$, Ms = Monosulphate, Qua. = Quartz, Gyp. = Gypsum, Hydrg. = Hydrogarnet, Tob. = Tobermorite, Dol. = Dolemite.

Name	Time (days)	Ett.	Ms	$M\bar{c}$	Hyrt.	Hydrg.	Gyp.	Tob.	Dol.	$C\overline{C}$	Qua.
PC	1	9.2	0.3	0	0.4	0	0.6	0.5	0	2.4	1.8
	3	9.9	0.2	0	0	0.1	1.0	1.6	0	2.2	2.1
	7	6.3	0.8	2.1	0.6	1.4	2.1	0.6	0	2.5	0.5
	14	5.0	1.6	0.9	0.2	2.7	1.7	1.9	0	0.8	0
	28	2.0	2.5	0.6	0.3	3.7	1.8	1.4	0	0.7	2.0
	91	0	1.3	0.5	0	4.2	2.2	1.6	0	1.1	0.1
PL	1	7.6	1.4	0	0.5	0.4	0.8	1.3	2.1	15.7	0.8
	3	6.6	0.6	1.9	1.0	1.5	1.9	1.4	1.9	12.7	2.4
	7	6.1	0.5	4.0	1.1	1.7	2.1	0.7	2.6	12.0	1.1
	14	3.4	0.2	5.4	1.1	2.5	2.2	0.4	2.4	11.6	0.5
	28	0.4	0	4.7	0.8	2.2	2.3	1.2	1.5	10.1	0.5
	91	0.8	0	5.4	1.2	3.9	2.0	2.3	2.3	10.9	0.1
PB	1	2.2	1.1	0	0.4	0.3	1.4	0.7	0	3.5	0.2
	3	1.4	1.0	0.6	0.4	0.2	1.3	0	0	1.6	0.4
	7	0.1	2.6	0.9	0.5	0.6	2.2	0.9	2.8	0	0.4
	14	0.6	3.3	1.3	0.8	1.4	2.6	2.2	1.7	0	0.2
	28	0.1	1.4	2.1	0.9	0.5	2.1	1.9	2.1	0	0.6
	91	0.3	1.8	1.4	1.1	1.7	1.7	7.8	0	1.8	0.6
PBL	1	1.2	0.9	0.3	0.4	0.3	1.0	0.9	0.4	12.4	0
	3	2.5	0.4	3.3	1.9	0	2.4	1.3	0.7	13.9	0.6
	7	1.0	0.3	5.1	1.2	0	1.7	0.8	0.6	11.8	0
	14	0.7	0.4	7.3	1.4	1.4	2.2	1.0	0.6	10.5	0.3
	28	0	0.9	5.9	1.3	1.1	2.5	2.0	0.5	10.8	0.2
	91	0.6	0.8	7.8	1.7	1.9	3.5	1.7	0.8	11.1	0

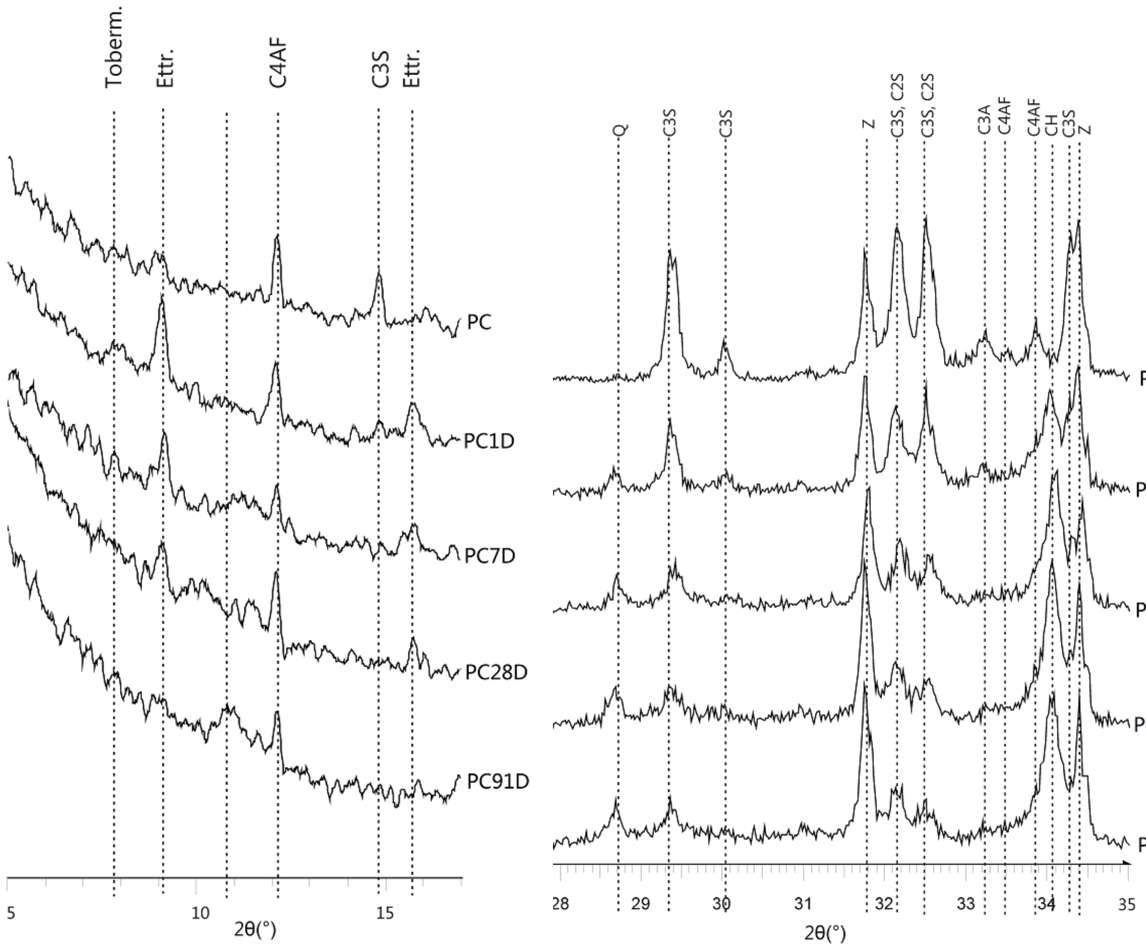

Figure A.1: XRD patterns of PC paste at different ages, Ettr. = Ettringite, Hydrotalc. = Hydrotalcite, Z = Zinc oxide, monocarb. = Monocarboaluminate, CH = $Ca(OH)_2$, CC = $CaCO_3$, Monos. = Monosulphate, Q = Quartz.

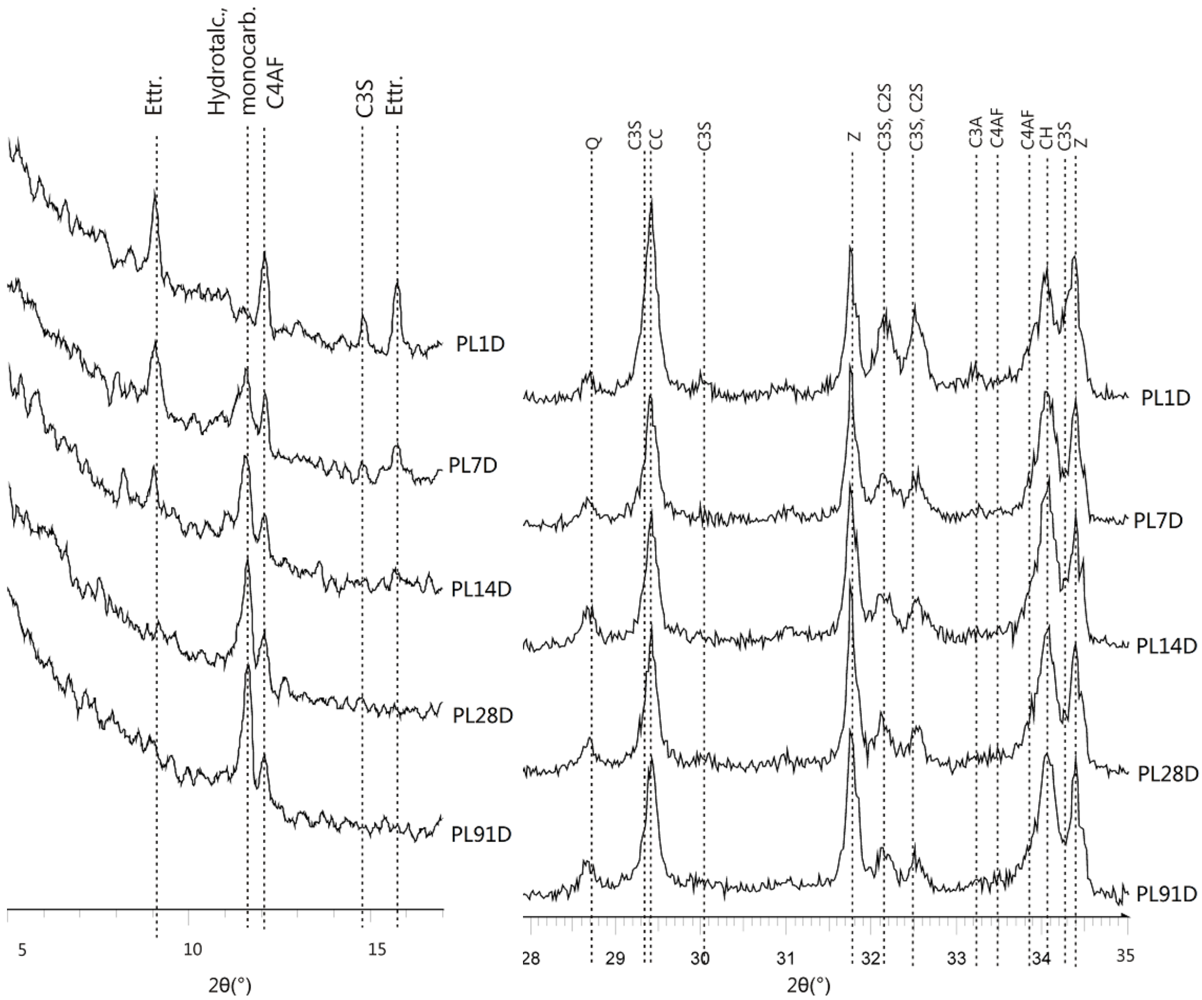

Figure A.2: XRD patterns of PL, Ettr. = Ettringite, Hydrotalc. = Hydrotalcite, Z = Zinc oxide, monocarb. = Monocarboaluminate, CH = $Ca(OH)_2$, CC = $CaCO_3$, Monos. = Monosulphate, Q = Quartz.

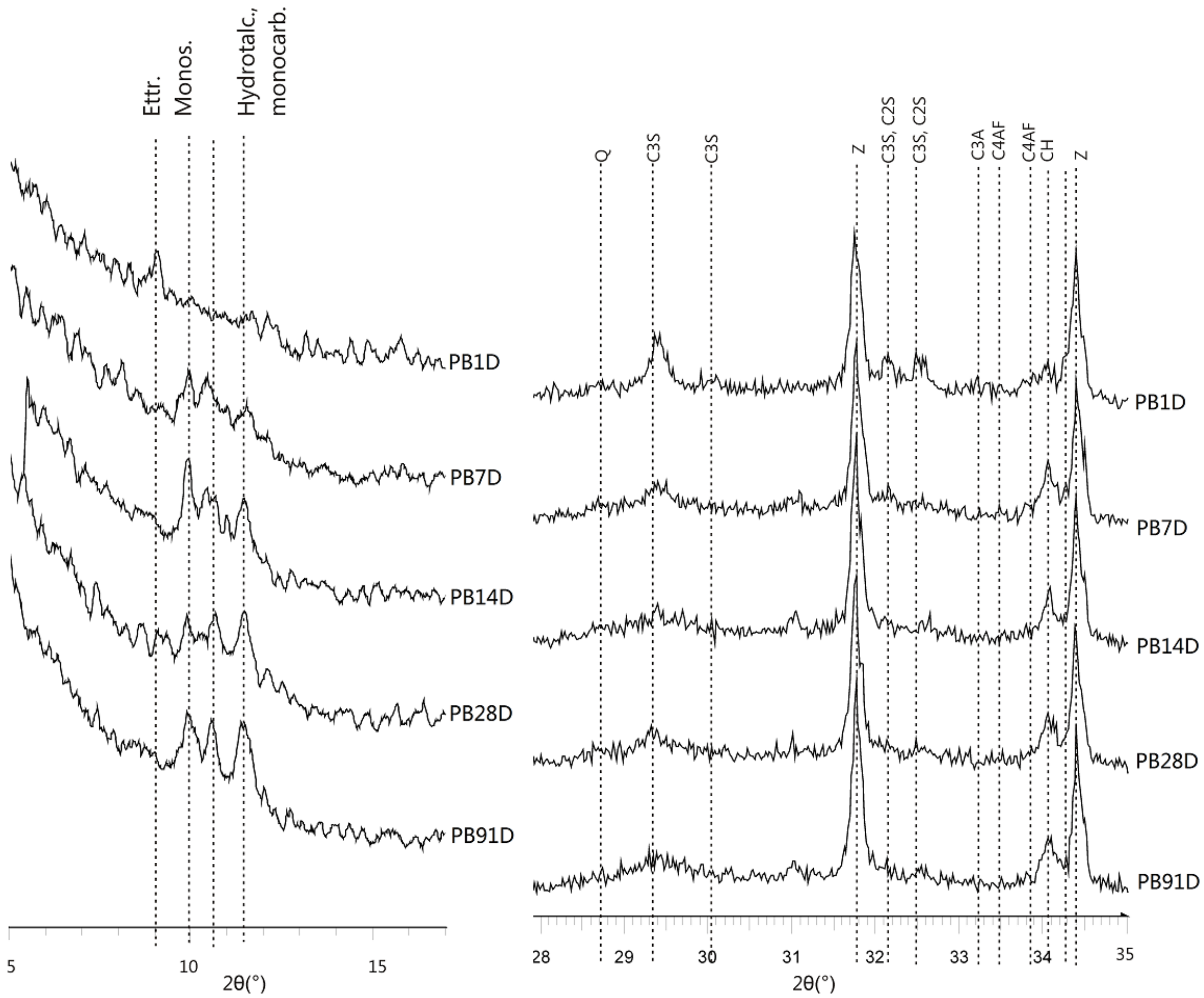

Figure A.3: XRD patterns of PB paste at different ages, Ettr. = Ettringite, Hydrotalc. = Hydrotalcite, Z = Zinc oxide, monocarb. = Monocarboaluminate, CH = $Ca(OH)_2$, CC = $CaCO_3$, Monos. = Monosulphate, Q = Quartz.

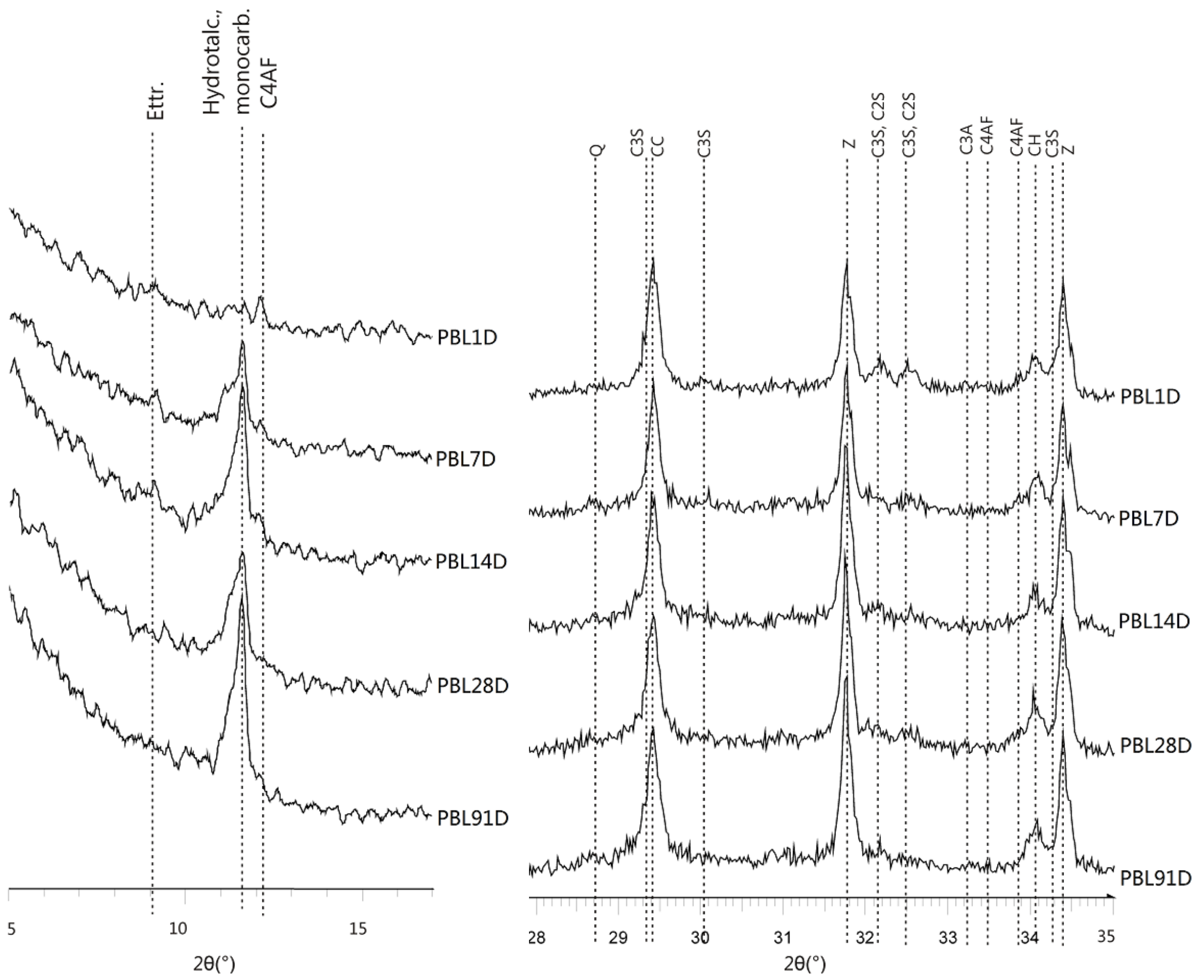

Figure A.4: XRD patterns of PBL paste at different ages, Ettr. = Ettringite, Hydrotalc. = Hydrotalcite, Z = Zinc oxide, monocarb. = Monocarboaluminate, CH = $Ca(OH)_2$, CC = $CaCO_3$, Monos. = Monosulphate, Q = Quartz.

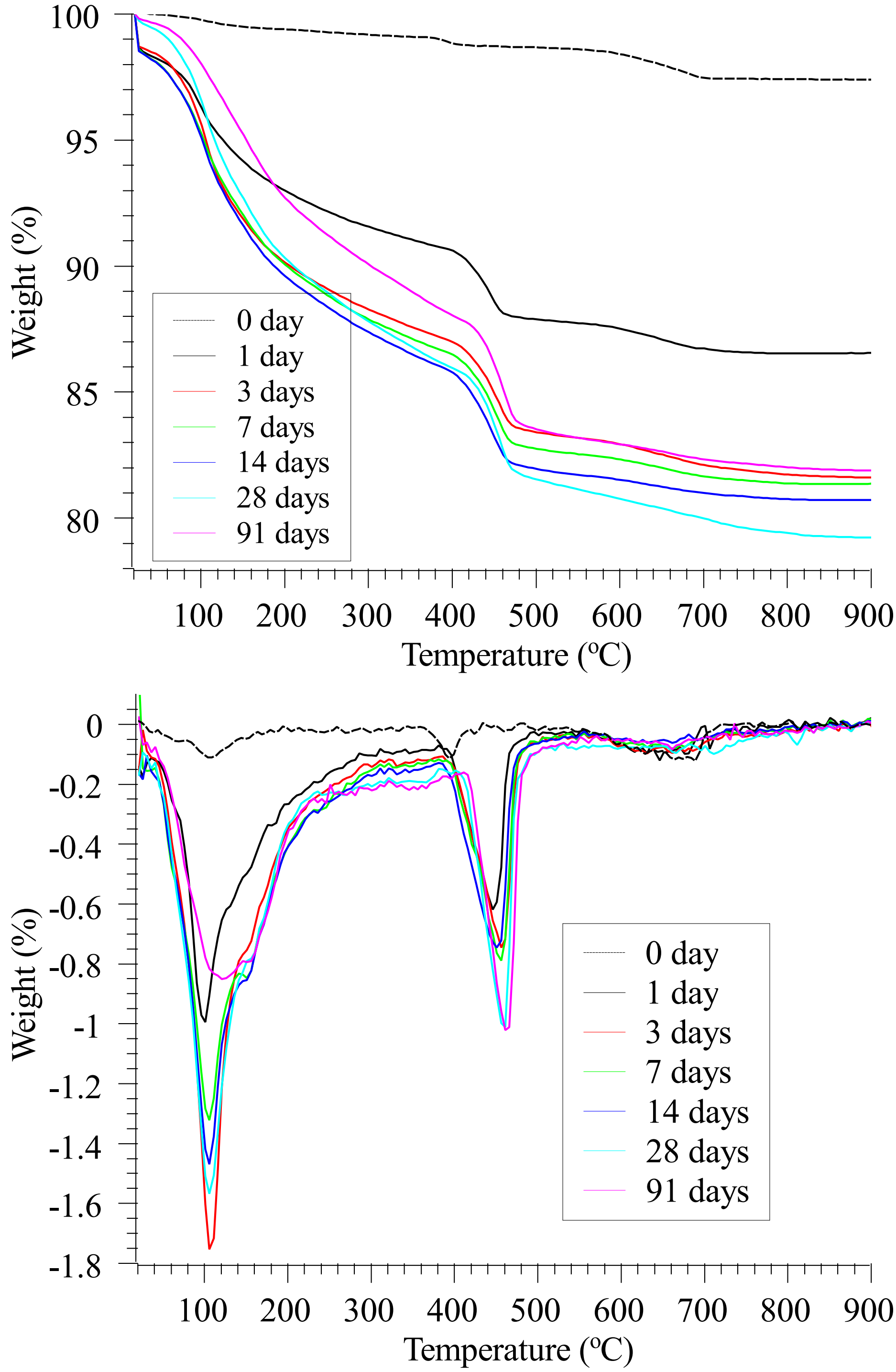

Figure A.5: TG and DTG curves of PL pastes at different curing ages tested by TGA method.

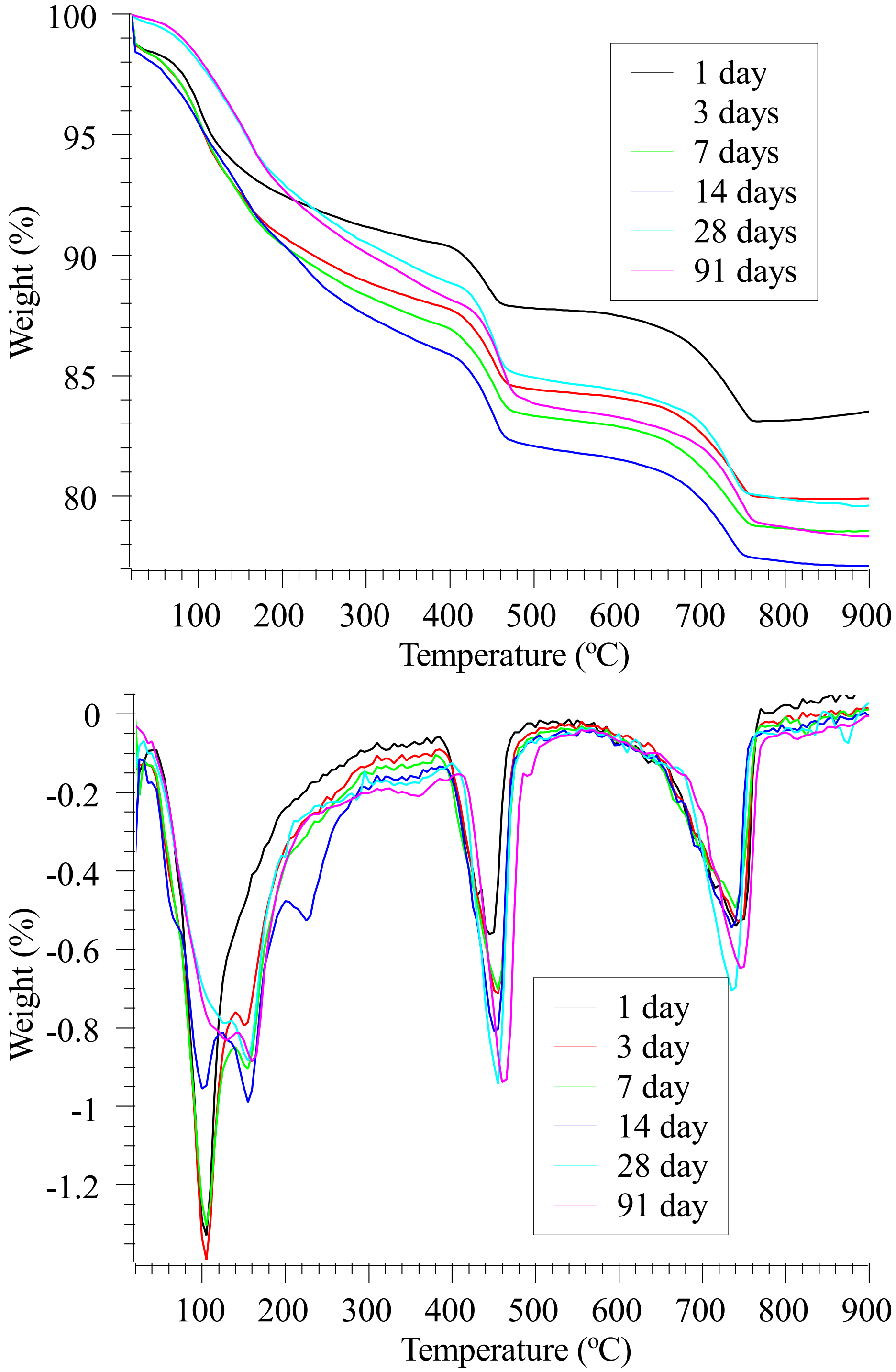

Figure A.6: TG and DTG curves of PB pastes at different curing ages tested by TGA method.

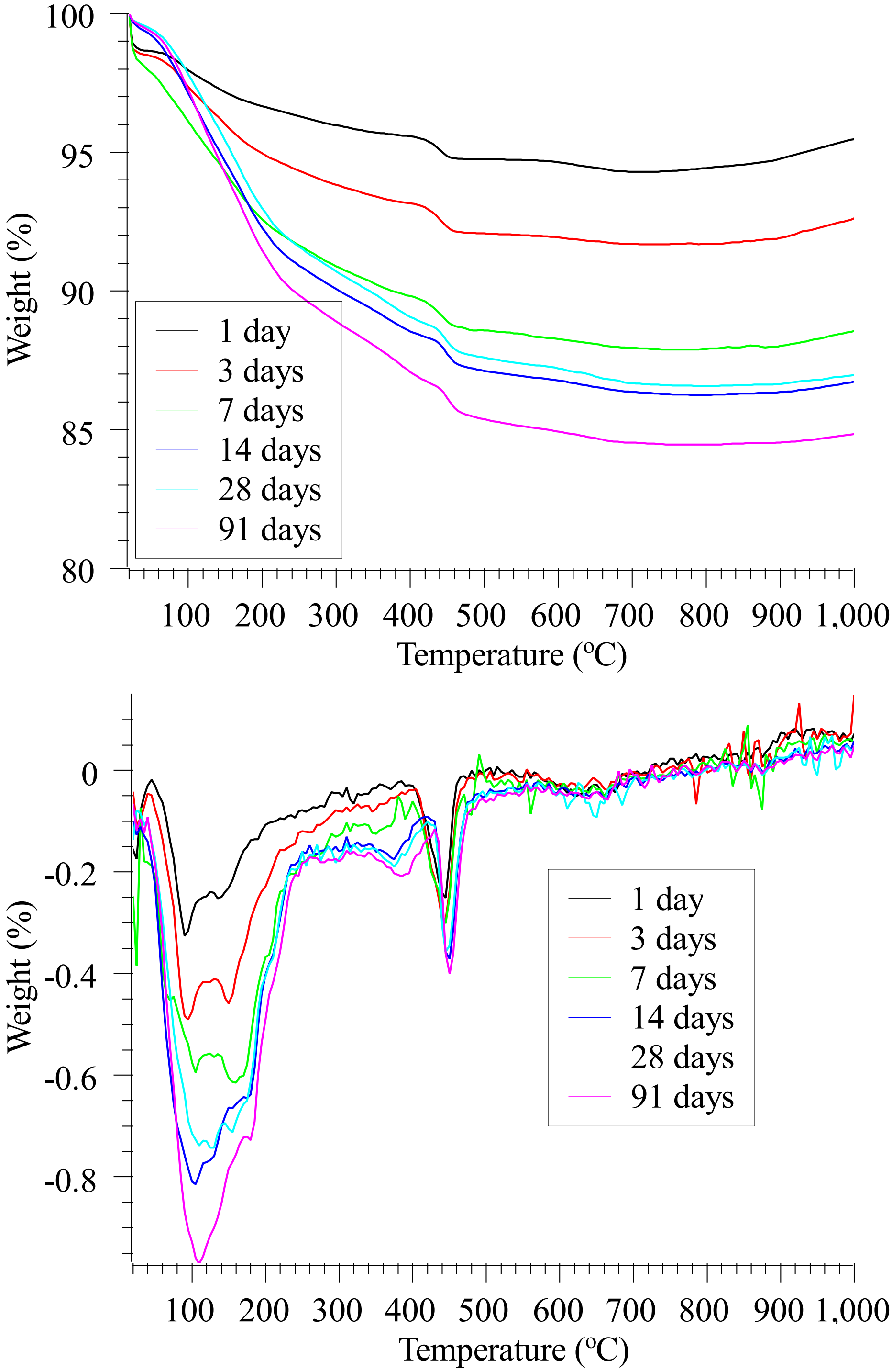

Figure A.7: TG and DTG curves of PBL pastes at different curing ages tested by TGA method.

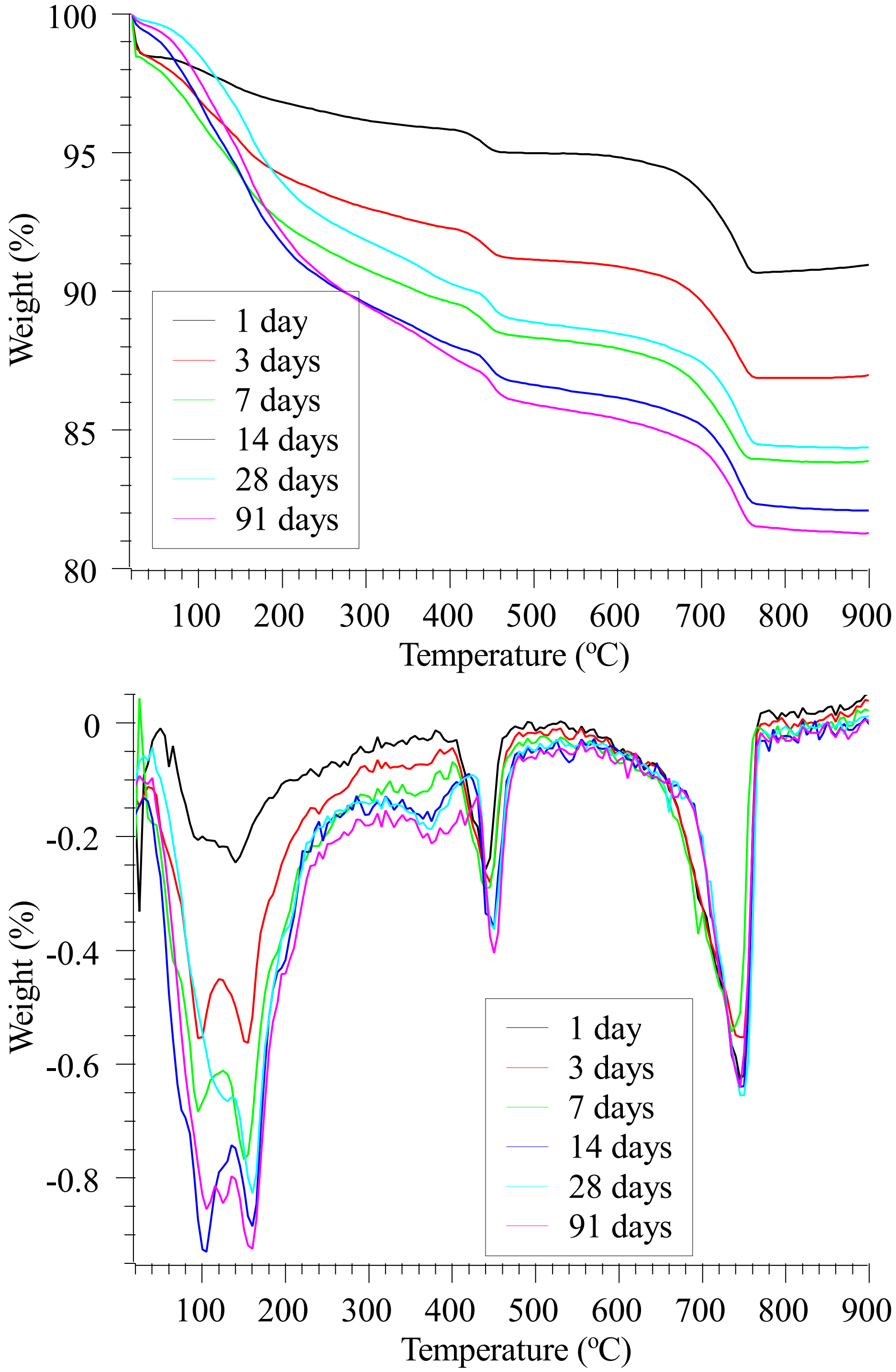

Figure A.8: TG and DTG curves of PBL pastes at different curing ages tested by TGA method.

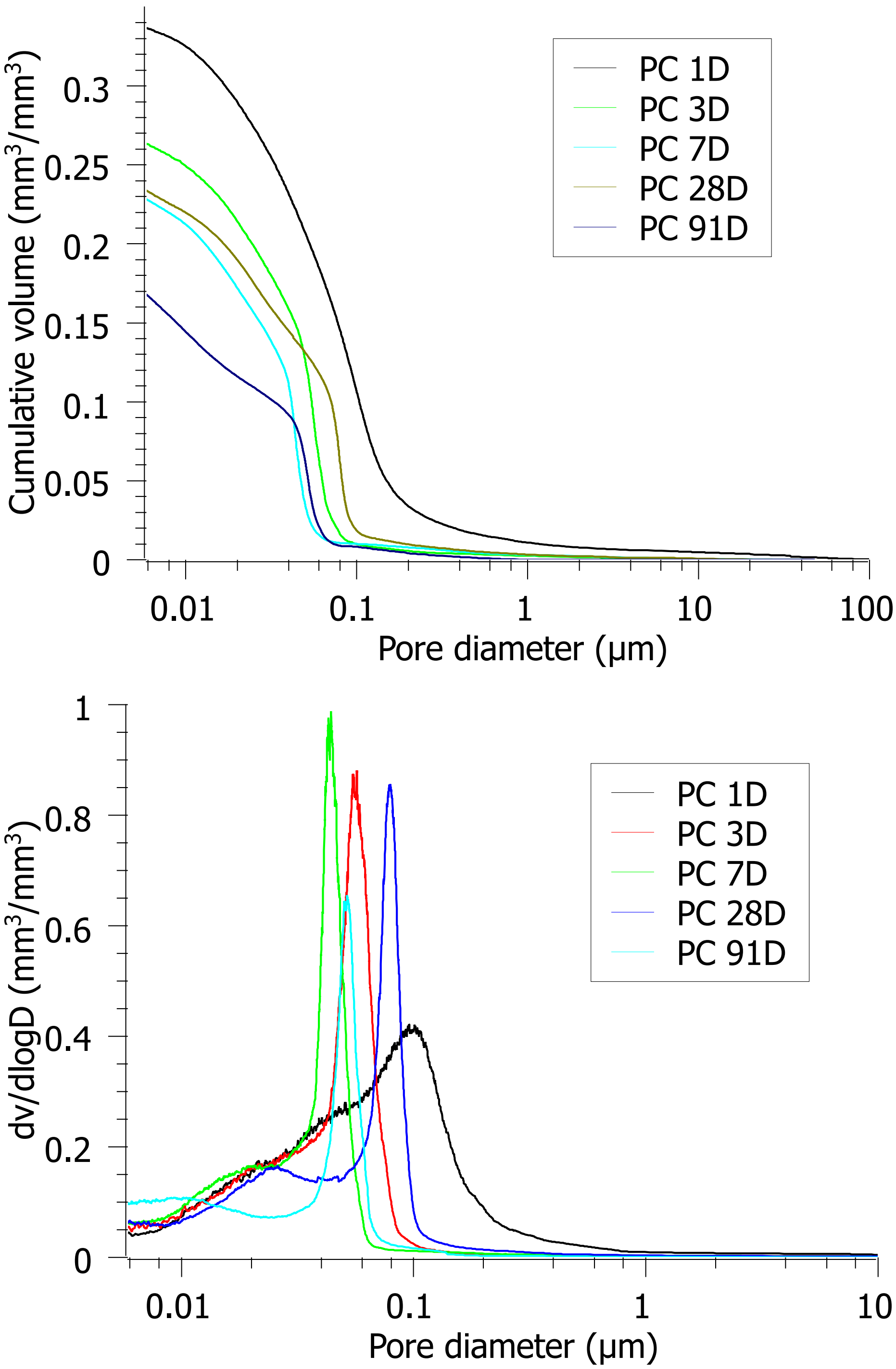

Figure A.9: MIP curves of PC pastes at different ages.

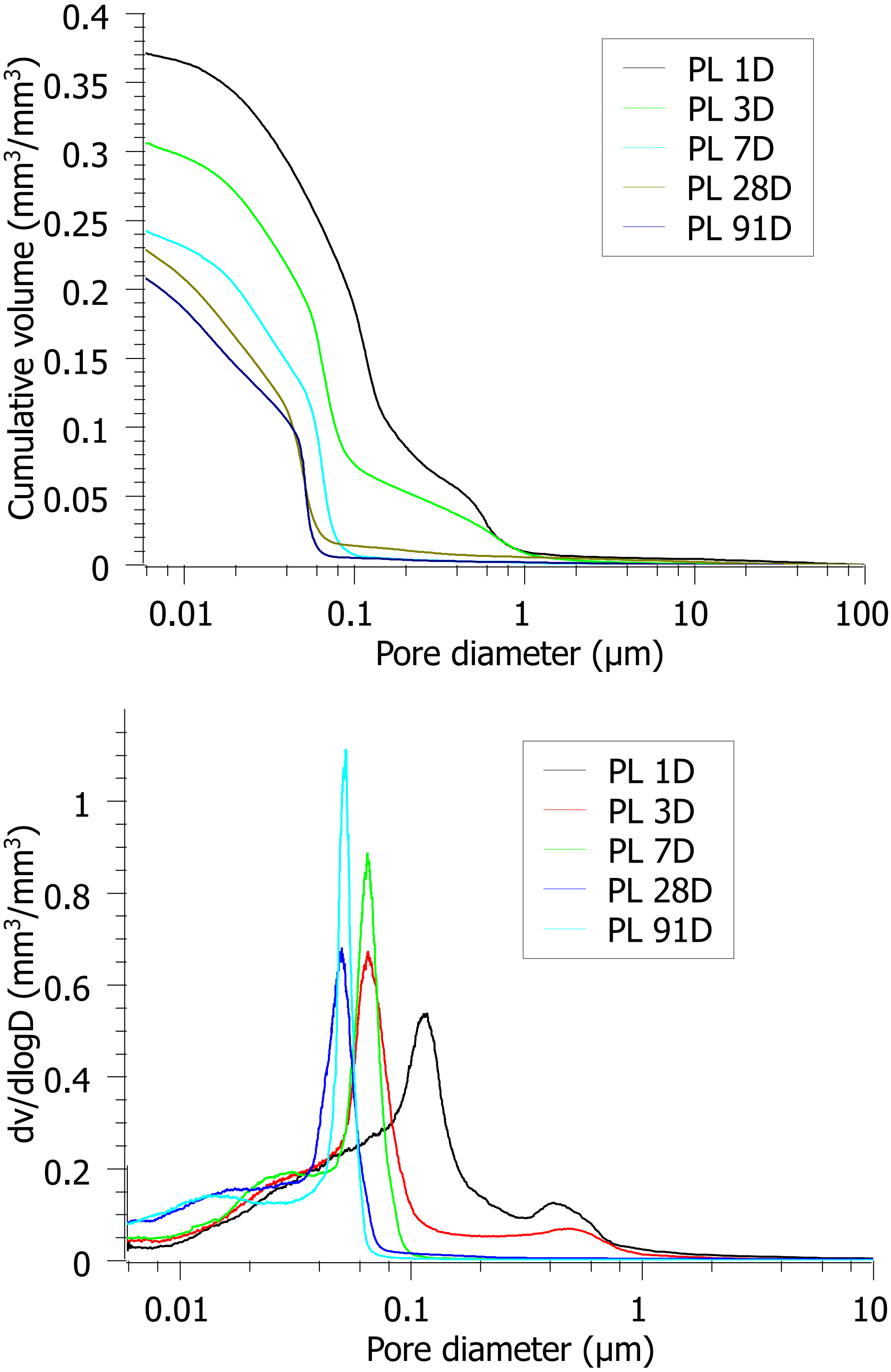

Figure A.10: MIP curves of PL pastes at different ages.

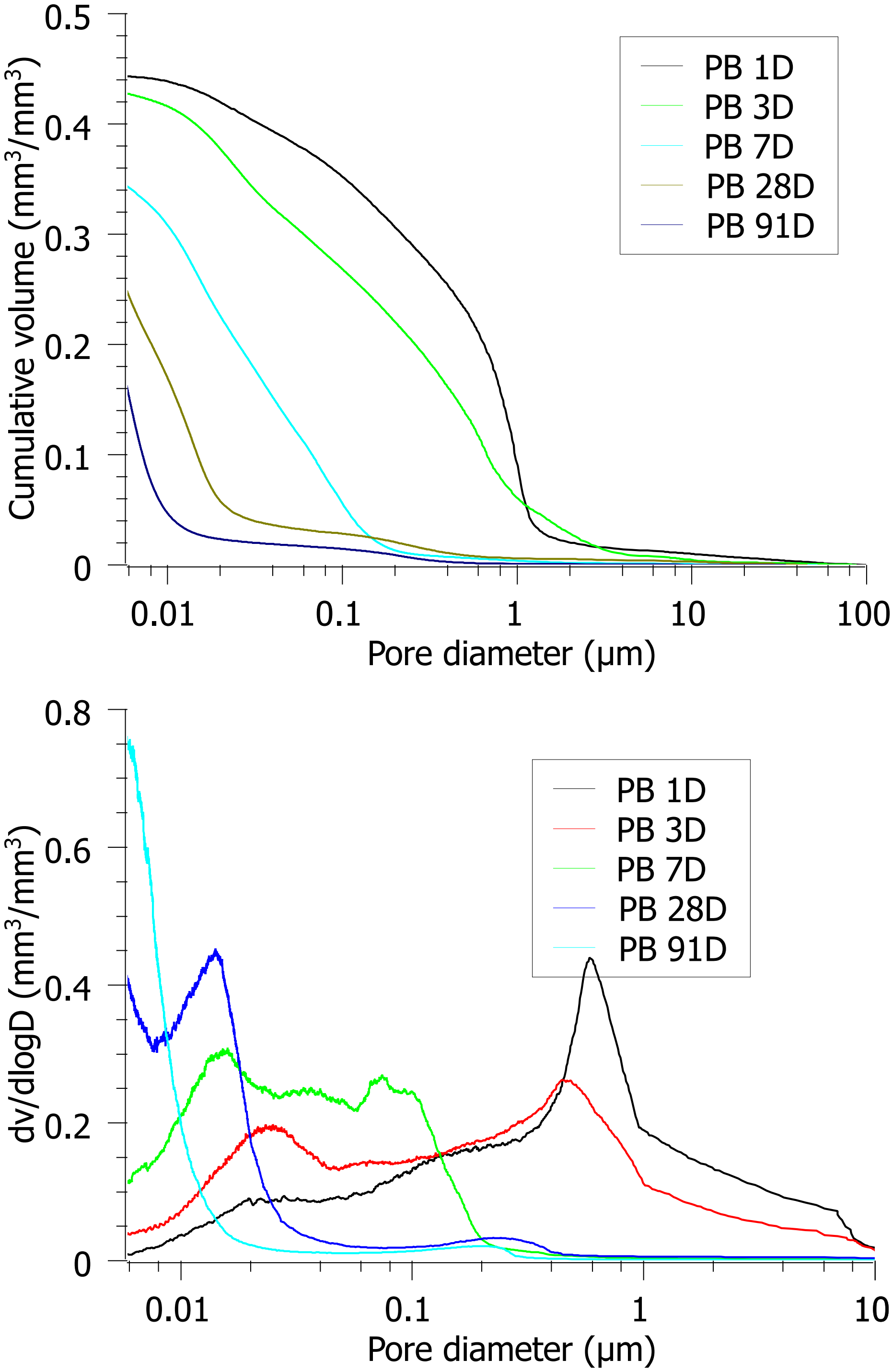

Figure A.11: MIP curves of PB pastes at different ages.

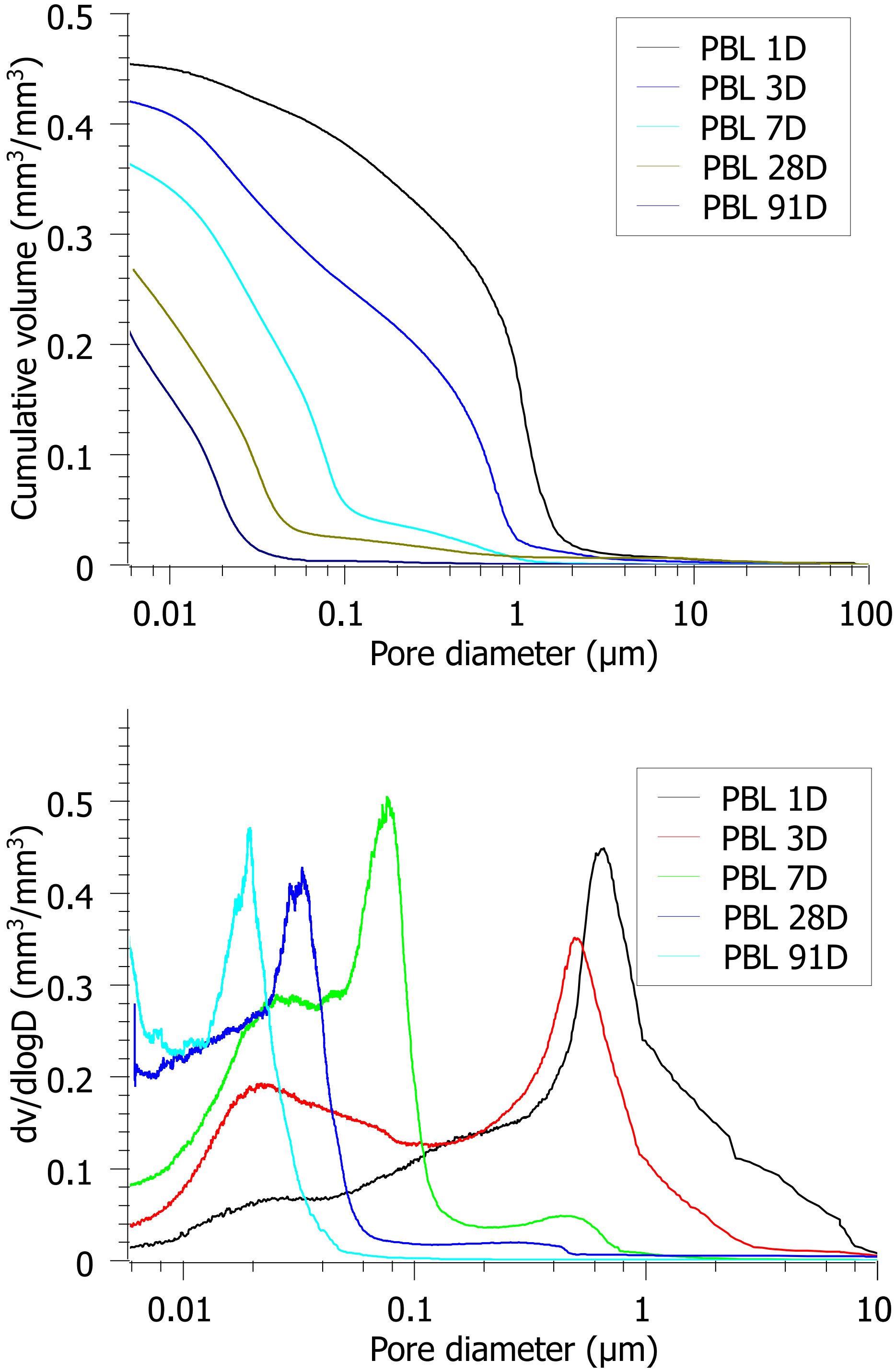

Figure A.12: MIP curves of PBL pastes at different ages.

Appendix B

Publications Related to the Project

Publications Related to This Project

- Zhijun Tan, Guang Ye, Yun Gao, Lieven Machiels, Els Bruneel, Geert De Schutter. Experimental investigation of hydration of ternary blended cement paste. 14^{th} International Congress on the Chemistry of Cement (ICCC 2015). Beijing, China. October, 2015.

- Zhijun Tan, Guang Ye, Kai Wu, Geert De Schutter. Investigation of pore system of ternary blended cement consisting of limestone filler, blast furnace slag and Portland cement. 35^{th} CEMENT & CONCRETE SCIENCE CONFERENCE (CCSC35). Aberdeen, Scotland (UK). August, 2015.

- Zhijun Tan, Geert De Schutter, Guang Ye, Yun Gao, and Lieven Machiels. Influence of particle size on the early hydration of slag particle activated by $Ca(OH)_2$ solution. Construction and Building Materials, 52:488--493, 2014.

- Yun Gao, Geert De Schutter, Guang Ye, Zhijun Tan, and Kai Wu. The ITZ microstructure, thickness and porosity in blended cementitious composite: Effects of curing age, 155 water to binder ratio and aggregate content. Composites Part B: Engineering, 60(0):1 -- 13, 2014.

- Zhijun Tan, Geert De Schutter, Guang Ye, Yun Gao, Lieven Machiels. Hydration simulation of ternary blended cement. In The Fourth RILEM Symposium on Concrete Modelling (CONMOD 2014). Beijing, China. October 2014.

- Zhijun Tan, Geert De Schutter, Guang Ye, and Yun Gao. The effect of limestone powder addition on strength of slag blended cement. In Concrete under Severe Conditions: Environment and Loading (CONSEC-2013), volume 2, pages 1888--1898. RILEM Publications SA. RL. Nanjing, China. September, 2013.

- Yun Gao, Geert De Schutter, Guang Ye, Zhuqing Yu, Zhijun Tan, and Kai Wu. A microscopic study on ternary blended cement based composites. Construction and Building Materials, 46:28--38, 2013.
- Yun Gao, Geert De Schutter, Guang Ye, Haoliang Huang, Zhijun Tan, and Kai Wu. Characterization of ITZ in ternary blended cementitious composites: experiment and simulation. Construction and building Materials, 41:742--750, 2013.
- Yun Gao, Geert De Schutter, Guang Ye, Haoliang Huang, Zhijun Tan, and Kai Wu. Porosity characterization of itz in cementitious composites: Concentric expansion and overflow criterion. Construction and Building Materials, 38:1051--1057, 2013.
- Zhijun Tan, Geert De Schutter, Guang Ye, and Yun Gao. A reaction kinetics model of blast-furnace slag in binary blended cement. In International Congress on Durability of Concrete (ICDC-2012), pages 1--12. Trondheim, Norway. June, 2012.

Bibliography

[1] Delong Xu, Yuansheng Cui, Hui Li, Kang Yang, Wen Xu, and Yanxin Chen. On the future of Chinese cement industry. *Cement and Concrete Research*, 2015.

[2] H. F. W. Taylor. *Cement Chemistry*. Thomas Telford, 1997.

[3] Klass van Breugel. *Simulation of hydration and formation of structure in hardening cement-based materials*. PhD thesis, Delft University of Technology, 1997.

[4] R. H. Mills. Factors Influencing the Cessation of Hydration in Water Cured Pastes. In *Symposium on structure of Portland cement paste and concrete*, 90, pages 406--424. Highway Research Board (HRB), Washington, DC, USA, Highway Research Board, 1966.

[5] DP Bentz and JT Conway. Computer modeling of the replacement of "coarse" cement particles by inert fillers in low w/c ratio concretes: hydration and strength. *Cement and Concrete Research*, 31(3):503--506, 2001.

[6] D.P. Bentz. Replacement of "coarse" cement particles by inert fillers in low w/c ratio concretes. *Cement and Concrete Research*, 35(1):185--188, January 2005.

[7] G. Menéndez O. Cabrera E.F. Irassar V. Bonavetti, H. Donza. Limestone filler cement in low w/c concrete: A rational use of energy. *Cement and Concrete Research*, 33(6):865--871, June 2003.

[8] Shanghai Tower Construction & Development Cooperation Ltd. Shanghai Tower Finishs the Casting of Foundation. *http://www.shanghaitower.com.cn/*, 2010.

[9] Wikipedia. Three Gorges Dam. *http://www.wikipedia.org/*, 2014.

[10] Chen Wenyao and Li Wenwei. The technical measures for the mix design of the concretedam in Three Gorges Project. *Journal of Hydraulic Engineering*, 2000.

[11] Baosteel Group Corporation. Baosteel Supplies Material for Shanghai Tower, No.1 High-rise under Construction in China to Lay the Foundation. Technical report, Baosteel Group Corporation, 2010.

[12] D. P. Bentz. A review of early-age properties of cement-based materials. *Cement and Concrete Research*, 38(2):196--204, 2008.

[13] European Committee for Standardization. European standards EN 197-1: Cement - Part 1: Composition, specifications and conformity criteria for common cements, institution = European Committee for Standardization, organization = European Committee for Standardization, address = Central Secretariat: rue de Stassart, 36 B-1050 Brussels, May 2000.

[14] Christoph Müller. Use of cement in concrete according to European standard EN 206-1. *HBRC Journal*, 8(1):1--7, 2012.

[15] G Menéndez, V Bonavetti, and EF Irassar. Strength development of ternary blended cement with limestone filler and blast-furnace slag. *Cement and Concrete Composites*, 25(1):61--67, 2003.

[16] L Bagel. Strength and pore structure of ternary blended cement mortars containing blast furnace slag and silica fume. *Cement and Concrete Research*, 28(7):1011--1022, 1998.

[17] M. F. Carrasco, G. Menéndez, V. Bonavetti, and E. F. Irassar. Strength optimization of "tailor-made cement" with limestone filler and blast furnace slag. *Cement and Concrete Research*, 35(7):1324--1331, 2005.

[18] E F Irassar, V L Bonavetti, G Menéndez, H Donza, and M F Carrasco. Durability of Ternary Blended Cements Containing Limestone Filler and GBFS. pages 327--346.

[19] K. van Breugel. Modelling of cement-based systems - the alchemy of cement chemistry. *Cement and Concrete Research*, 34(9):1661--1668, 2004.

[20] J Francis Young. Looking ahead from the past: The heritage of cement chemistry. *Cement and Concrete Research*, 38(2):111--114, 2008.

[21] I Maruyama, T Matsushita, and T Noguchi. Numerical modeling of Portland cement hydration based on particle kinetic model and multi-component concept. *Proc. of Int. Cong. on Chem. of Cem., TH1-08.3*, 2007.

[22] Xian Liu. *Microstructure investigation of self-compacting concrete and high-performance ceoncrete during hydration and after exposure to high temperature*. PhD thesis, Ghent University, 2006.

[23] K. van Breugel G. Ye. Microstructure simulation of Portland cement blended with blast furnace slag. In *International RILEM Symposium on Concrete Modeling*, pages 791--800, Delft, the Netherlands, 2008.

[24] Guang Ye and Klaas Van Breugel. Simulation of connectivity of capillary porosity in hardening cement-based systems made of blended materials. 54(2):163--184, 2009.

[25] Neven Ukrainczyk, Eduard AB Koenders, and K van Breugel. Simulation of Pozzolan Blended cement hydration. In *Proceedings of the First International Conference on Concrete Sustainability*, pages 27--29, 2013.

[26] VT Nguyen. *Rice husk ash as a mineral admixture for Ultra High Performance Concrete*. PhD thesis, PhD Thesis, Delft University of Technology, 2011.

[27] Dale P Bentz. CEMHYD3D: A three-dimensional cement hydration and microstructure development modelling package. Version 2.0. *National Institute of Standards and Technology Interagency Report*, 7232, 2000.

[28] Wei Chen. *Hydration of slag cement: Theory, Modeling and Application*. PhD thesis, University of Twente, 2007.

[29] D.P. Bentz. Modeling the influence of limestone filler on cement hydration using CEMHYD3D. *Cement and Concrete Composites*, 28(2):124--129, February 2006.

[30] Fernando Pacheco-Torgal, João Labrincha, C Leonelli, A Palomo, and P Chindaprasit. *Handbook of Alkali-Activated Cements, Mortars and Concretes*. Elsevier, 2014.

[31] Shao-Dong Wang, Karen L Scrivener, and PL Pratt. Factors affecting the strength of alkali-activated slag. *Cement and Concrete Research*, 24(6):1033--1043, 1994.

[32] Peter Hewlett. *Lea's chemistry of cement and concrete*. Butterworth-Heinemann, 2003.

[33] RN Swamy and Ammar Bouikni. Some engineering properties of slag concrete as influenced by mix proportioning and curing. *ACI Materials Journal*, 87(3), 1990.

[34] S. C. Pal, A. Mukherjee, and S. R. Pathak. Investigation of hydraulic activity of ground granulated blast furnace slag in concrete. *Cement and Concrete Research*, 33(9):1481--1486, 2003.

[35] A.M. Neville. *Properties of Concrete*. ELBS Publication, Addison-Wesley Longman Limited, Essex, UK, 4th edition, 1996.

[36] M. Ben Haha, B. Lothenbach, G. Le Saout, and F. Winnefeld. Influence of slag chemistry on the hydration of alkali-activated blast-furnace slag — Part II: Effect of Al_2O_3. *Cement and Concrete Research*, 42(1):74--83, January 2012.

[37] M. Ben Haha, B. Lothenbach, G. Le Saout, and F. Winnefeld. Influence of slag chemistry on the hydration of alkali-activated blast-furnace slag — Part I: Effect of MgO. *Cement and Concrete Research*, 41(9):955--963, 2011.

[38] John PH Frearson and Denis D Higgins. Sulfate resistance of mortars containing ground granulated blast-furnace slag with variable alumina content. *ACI Special Publication*, 132, 1992.

[39] John L Provis and Jan Stephanus Jakob Van Deventer. *Geopolymers: structures, processing, properties and industrial applications*. Elsevier, 2009.

[40] Chao Li, Henghu Sun, and Longtu Li. A review: The comparison between alkali-activated slag (Si+Ca) and metakaolin (Si+Al) cements. *Cement and Concrete Research*, 40(9):1341--1349, September 2010.

[41] John L Provis and Jannie SJ van Deventer. *Alkali Activated Materials*. Springer, 2014.

[42] C Shi and RL Day. Selectivity of alkaline activators for the activation of slags. *Cement, Concrete and Aggregates*, 18(1), 1996.

[43] John L Provis and Susan A Bernal. Geopolymers and related alkali-activated materials. *Annual Review of Materials Research*, 44:299--327, 2014.

[44] AM Rashad, Y Bai, PAM Basheer, NB Milestone, and NC Collier. Hydration and properties of sodium sulfate activated slag. *Cement and Concrete Composites*, 37:20--29, 2013.

[45] Ye Guang. Numerical simulation of connectivity of individual phases in hardening cement-based systems made of blended cement with and without admixtures. Technical report, Microlab, TU Delft, December 2006.

[46] J Hill and J.H Sharp. The mineralogy and microstructure of three composite cements with high replacement levels. *Cement and Concrete Composites*, 24(2):191--199, April 2002.

[47] JJ Biernacki, JM Richardson, PE Stutzman, and DP Bentz. Kinetics of slag hydration in the presence of calcium hydroxide. *Journal of the American Ceramic Society*, 85(9):2261--2267, 2002.

[48] John M. Richardson, Joseph J. Biernacki, Paul E. Stutzman, and Dale P. Bentz. Stoichiometry of Slag Hydration with Calcium Hydroxide. *Journal of the American Ceramic Society*, 85(4):947--953, 2002.

[49] F. Bellmann and J. Stark. Activation of blast furnace slag by a new method. *Cement and Concrete Research*, 39(8):644--650, 2009.

[50] I. G. Richardson and G. W. Groves. Microstructure and microanalysis of hardened cement pastes involving ground granulated blast-furnace slag. *Journal of Materials Science*, 27(22):6204--6212, 1992.

[51] J. I. Escalante-Garcia and J. H. Sharp. The chemical composition and microstructure of hydration products in blended cements. *Cement and Concrete Composites*, 26(8):967--976, 2004.

[52] JI Escalante-Garcıa and JH Sharp. The microstructure and mechanical properties of blended cements hydrated at various temperatures. *Cement and Concrete Research*, 31(5):695--702, 2001.

[53] IG Richardson and GW Groves. The incorporation of minor and trace elements into calcium silicate hydrate (C-S-H) gel in hardened cement pastes. *Cement and Concrete Research*, 23(1):131--138, 1993.

[54] IG Richardson and GW Groves. The structure of the calcium silicate hydrate phases present in hardened pastes of white Portland cement/blast-furnace slag blends. *Journal of Materials Science*, 32(18):4793--4802, 1997.

[55] Guang Ye and Klaas van Breugel. Simulation of connectivity of capillary porosity in hardening cement-based systems made of blended materials. *Heron*, 54(2/3):163, 2009.

[56] J.I Escalante, L.Y Gómez, K.K Johal, G Mendoza, H Mancha, and J Méndez. Reactivity of blast-furnace slag in Portland cement blends hydrated under different conditions. *Cement and Concrete Research*, 31(10):1403--1409, October 2001.

[57] J.S. Lumley, R.S. Gollop, G.K. Moir, and H.F.W. Taylor. Degrees of reaction of the slag in some blends with Portland cements. *Cement and Concrete Research*, 26(1):139 -- 151, 1996.

[58] Karen Luke and Fredrik P Glasser. Selective dissolution of hydrated blast furnace slag cements. *Cement and Concrete Research*, 17(2):273--282, 1987.

[59] Vanessa Kocaba. *Development and Evaluation of Methods to Follow Microstructural Development of Cementitious Systems Including Slags*. PhD thesis, EPFL, 2009.

[60] W Hinrichs and I Odler. Investigation of the hydration of Portland blastfurnace slag cement: hydration kinetics. *Advances in Cement Research*, 2(5):9--13, 1989.

[61] Peter Hawkins, Paul D Tennis, and Rachel Jean Detwiler. *The use of limestone in Portland cement: a state-of-the-art review*. Portland Cement Association Skokie, IL, 2003.

[62] Anne-Mieke Poppe and Geert De Schutter. Cement hydration in the presence of high filler contents. *Cement and Concrete Research*, 35(12):2290--2299, 2005.

[63] G. Ye, X. Liu, G. De Schutter, A. M. Poppe, and L. Taerwe. Influence of limestone powder used as filler in SCC on hydration and microstructure of cement pastes. *Cement and Concrete Composites*, 29(2):94--102, 2007.

[64] Vangipuram Seshachar Ramachandran. Thermal analyses of cement components hydrated in the presence of calcium carbonate. *Thermochimica Acta*, 127:385--394, 1988.

[65] G Kakali, S Tsivilis, E Aggeli, and M Bati. Hydration products of C_3A, C_3S and Portland cement in the presence of $CaCO_3$. *Cement and Concrete Research*, 30(7):1073--1077, 2000.

[66] E Berodier and K Scrivener. Understanding the Filler Effect on the Nucleation and Growth of C-S-H. *Journal of the American Ceramic Society*, 97(12):3764--3773, 2014.

[67] Jean Péra, Sophie Husson, and Bernard Guilhot. Influence of finely ground limestone on cement hydration. *Cement and Concrete Composites*, 21(2):99--105, 1999.

[68] Kevin D Ingram and Kenneth E Daugherty. A review of limestone additions to Portland cement and concrete. *Cement and concrete composites*, 13(3):165--170, 1991.

[69] Barbara Lothenbach, Gwenn Le Saout, Emmanuel Gallucci, and Karen Scrivener. Influence of limestone on the hydration of Portland cements. *Cement and Concrete Research*, 38(6):848--860, June 2008.

[70] EJ Sellevold, DH Bager, E Klitgaard Jensen, T Knudsen, et al. Silica fume-cement pastes: hydration and pore structure. *Report BML*, 82:19--50, 1982.

[71] A Barker and Howard P Cory. The early hydration of limestone-filled cements. In *Blended cements in construction. Papers presented at the international conference*. University of Sheffield, UK, University of Sheffield, UK, September 1991.

[72] P. Pipilikaki and M. Beazi-Katsioti. The assessment of porosity and pore size distribution of limestone Portland cement pastes. *Construction and Building Materials*, 23(5):1966--1970, May 2009.

[73] Waldemar A Klemm and Lawrence D Adams. An investigation of the formation of carboaluminates. *Carbonate additions to cement, ASTM STP*, 1064:60--72, 1990.

[74] T. Matschei, B. Lothenbach, and F. P. Glasser. The role of calcium carbonate in cement hydration. *Cement and Concrete Research*, 37(4):551--558, 2007.

[75] Axel Schöler, Barbara Lothenbach, Frank Winnefeld, and Maciej Zajac. Hydration of quaternary Portland cement blends containing blast-furnace slag, siliceous fly ash and limestone powder. *Cement and Concrete Composites*, 55:374--382, 2015.

[76] Klaartje De Weerdt. *Blended cement with reduced CO_2 emission - utilizing the fly ash-limestone synergy*. PhD thesis, Norwegian University of Science and Technology, 2011.

[77] K. De Weerdt, M. Ben Haha, G. Le Saout, K. O. Kjellsen, H. Justnes, and B. Lothenbach. Hydration mechanisms of ternary Portland cements containing limestone powder and fly ash. *Cement and Concrete Research*, 41(3):279--291, 2011.

[78] Prinya Chindaprasirt and Sumrerng Rukzon. Strength, porosity and corrosion resistance of ternary blend Portland cement, rice husk ash and fly ash mortar. *Construction and Building Materials*, 22(8):1601--1606, 2008.

[79] M. Ghrici, S. Kenai, and M. Said-Mansour. Mechanical properties and durability of mortar and concrete containing natural pozzolana and limestone blended cements. *Cement and Concrete Composites*, 29(7):542--549, 2007.

[80] Hooton R Doug Bleszynski, Roland, Michael DA Thomas, and Chris A Rogers. Durability of ternary blend concrete with silica fume and blast-furnace slag: laboratory and outdoor exposure site studies. *ACI Materials Journal*, 99(5), 2002.

[81] M Sharfuddin Ahmed, Obada Kayali, and Wendy Anderson. Chloride penetration in binary and ternary blended cement concretes as measured by two different rapid methods. *Cement and Concrete Composites*, 30(7):576--582, 2008.

[82] MR Jones, RK Dhir, and BJ Magee. Concrete containing ternary blended binders: resistance to chloride ingress and carbonation. *Cement and Concrete Research*, 27(6):825--831, 1997.

[83] MI Khan, CJ Lynsdale, and P Waldron. Porosity and strength of PFA/SF/OPC ternary blended paste. *Cement and Concrete Research*, 30(8):1225--1229, 2000.

[84] M.D.a. Thomas, M.H. Shehata, S.G. Shashiprakash, D.S. Hopkins, and K. Cail. Use of ternary cementitious systems containing silica fume and fly ash in concrete. *Cement and Concrete Research*, 29(8):1207--1214, August 1999.

[85] Medhat H Shehata and Michael DA Thomas. Use of ternary blends containing silica fume and fly ash to suppress expansion due to alkali--silica reaction in concrete. *Cement and Concrete Research*, 32(3):341--349, 2002.

[86] Thanongsak Nochaiya, Watcharapong Wongkeo, and Arnon Chaipanich. Utilization of fly ash with silica fume and properties of Portland cement--fly ash--silica fume concrete. *Fuel*, 89(3):768--774, 2010.

[87] Mehmet Gesoğlu, Erhan Güneyisi, and Erdoğan Özbay. Properties of self-compacting concretes made with binary, ternary, and quaternary cementitious blends of fly ash, blast furnace slag, and silica fume. *Construction and Building Materials*, 23(5):1847--1854, 2009.

[88] Mateusz Radlinski and Jan Olek. Investigation into the synergistic effects in ternary cementitious systems containing portland cement, fly ash and silica fume. *Cement and Concrete Composites*, 34(4):451--459, April 2012.

[89] Kirk Vance, Matthew Aguayo, Tandre Oey, Gaurav Sant, and Narayanan Neithalath. Hydration and strength development in ternary portland cement blends containing limestone and fly ash or metakaolin. *Cement and Concrete Composites*, 39:93--103, 2013.

[90] Shashank Bishnoi and Karen L. Scrivener. μic: A new platform for modelling the hydration of cements. *Cement and Concrete Research*, 39(4):266 -- 274, 2009.

[91] S.J. Lokhorst and K. van Breugel. Simulation of the effect of geometrical changes of the microstructure on the deformational behaviour of hardening concrete . *Cement and Concrete Research*, 27(10):1465 -- 1479, 1997. Materials Research Society Symposium on Structure-Property Relationships in Hardened Cement Paste and Composites.

[92] Xian Liu, Guang Ye, Geert De Schutter, and Yong Yuan. Simulation of the microstructure formation in hardening self-compacting cement paste containing limestone powder as filler via computer-based model. *Materials and structures*, 46(11):1861--1879, 2013.

[93] Guang Ye and Klaas van Breugel. Microstructure simulation of portland cement blended with blast furnace slag. In *International RILEM symposium on Concrete Modelling (CONMOD'08)*, pages 791--800. RILEM Publications, 2008.

[94] C. Pignat, P. Navi, and K. Scrivener. Simulation of cement paste microstructure hydration, pore space characterization and permeability determination. *Materials and Structures*, 38(4):459--466, 2005.

[95] Shashank Bishnoi. *Vector modelling of hydrating cement microstructure and kinetics*. PhD thesis, Citeseer, 2008.

[96] Ashraf Ragab Mohamed, Mona Elsalamawy, and Marwa Ragab. Modeling the influence of limestone addition on cement hydration. *Alexandria Engineering Journal*, 54(1):1--5, 2015.

[97] Dale P. Bentz. Three-Dimensional Computer Simulation of Portland Cement Hydration and Microstructure Development. *Journal of the American Ceramic Society*, 80(1):3--21, 1997.

[98] D.P Bentz, V Waller, and F de Larrard. Prediction of Adiabatic Temperature Rise in Conventional and High-Performance Concretes Using a 3-D Microstructural Model . *Cement and Concrete Research*, 28(2):285 -- 297, 1998.

[99] D.P Bentz, O.M Jensen, A.M Coats, and F.P Glasser. Influence of silica fume on diffusivity in cement-based materials: I. Experimental and computer modeling studies on cement pastes. *Cement and Concrete Research*, 30(6):953 -- 962, 2000.

[100] Dale P. Bentz. Sebastien Remond. Incorporation of Fly Ash into a 3-D Cement Hydration Microstructure Model. Technical report, National Institute of Standards and Technology, 1997.

[101] Wei Chen, H. J. H. Brouwers, and Z. H. Shui. Three-dimensional computer modeling of slag cement hydration. *Journal of Materials Science*, 42(23):9595--9610, 2007.

[102] Toshiharu Kishi Koichi Maekawa, Tetsuya Ishida. *Multi-Scale Modeling of Structural Concrete*. Taylor & Francis, 2008.

[103] Xiao-Yong Wang and Han-Seung Lee. Modeling the hydration of concrete incorporating fly ash or slag . *Cement and Concrete Research*, 40(7):984 -- 996, 2010.

[104] G. De Schutter and L. Taerwe. General hydration model for portland cement and blast furnace slag cement . *Cement and Concrete Research*, 25(3):593 -- 604, 1995.

[105] Barbara Lothenbach, Karen Scrivener, and R. D. Hooton. Supplementary cementitious materials. *Cement and Concrete Research*, 41(12):1244--1256, 2011.

[106] Karen L Scrivener, Barbara Lothenbach, Nele De Belie, Elke Gruyaert, Jørgen Skibsted, Ruben Snellings, and Anya Vollpracht. TC 238-SCM: hydration and microstructure of concrete with SCMs. *Materials and Structures*, pages 1--28, 2015.

[107] Geert De Schutter. Hydration and temperature development of concrete made with blast-furnace slag cement. *Cement and Concrete Research*, 29(1):143--149, January 1999.

[108] Konish E. Sato, K. and K. Fukaya. Hydration of blast-furnace slag particle. volume 4 of *Proc. 8th ICCC*, pages 98--103, Rio de Janeiro, Brazil, 1986.

[109] Zhijun Tan, Geert De Schutter, Guang Ye, Yun Gao, and Lieven Machiels. Influence of particle size on the early hydration of slag particle activated by $Ca(OH)_2$ solution. *Construction and Building Materials*, 52:488--493, 2014.

[110] T. Kishi and K.. Maekawa. Thermal and Mechanical Modeling of Young Concrete Based on Hydration Process of Multi-Component Cement Minerals. pages 11--18. E&FN Spon, London, 1995.

[111] Zhijun Tan, Geert De Schutter, Guang Ye, and Yun Gao. A reaction kinetics model of blast-furnace slag in binary blended cement. In *International Congress on Durability of Concrete (ICDC-2012)*, pages 1--12, 2012.

[112] John L Provis, Peter Duxson, and Jannie SJ van Deventer. The role of particle technology in developing sustainable construction materials. *Advanced Powder Technology*, 21(1):2--7, 2010.

[113] Caijun Shi and Robert L. Day. A calorimetric study of early hydration of alkali-slag cements . *Cement and Concrete Research*, 25(6):1333 -- 1346, 1995.

[114] Z Rajaokarivony-Andriambololona, JH Thomassin, P Baillif, and JC Touray. Experimental hydration of two synthetic glassy blast furnace slags in water and alkaline solutions (NaOH and KOH 0.1 N) at 40 C: structure, composition and origin of the hydrated layer. *Journal of materials science*, 25(5):2399--2410, 1990.

[115] Dan Y. Goto S Otsuka Y., Ueki Y. Effects of the fineness of blast furnace slag on the hydration of high-sulfated slag cement. In *Proc. 13th ICCC*, Madrid, Spain, 2011.

[116] Huiwen Wan, Zhonghe Shui, and Zongshou Lin. Analysis of geometric characteristics of GGBS particles and their influences on cement properties. *Cement and Concrete Research*, 34(1):133--137, 2004.

[117] Karen L. Scrivener and André Nonat. Hydration of cementitious materials, present and future. *Cement and Concrete Research*, 41(7):651--665, July 2011.

[118] A. Gruskovnjak, B. Lothenbach, F. Winnefeld, R. Figi, S.-C. Ko, M. Adler, and U. Mader. Hydration mechanisms of super sulphated slag cement. *Cement and Concrete Research*, 38(7):983--992, 2008.

[119] Ruben Snellings, Gilles Mertens, and Jan Elsen. Supplementary cementitious materials. *Reviews in Mineralogy and Geochemistry*, 74(1):211--278, 2012.

[120] Ruben Snellings. Solution-Controlled Dissolution of Supplementary Cementitious Material Glasses at pH 13: The Effect of Solution Composition on Glass Dissolution Rates. *Journal of the American Ceramic Society*, 96(8):2467--2475, 2013.

[121] Q. Wang, P. Yan, and J. Feng. A discussion on improving hydration activity of steel slag by altering its mineral compositions. *J Hazard Mater*, 186(2-3):1070--5, 2011.

[122] Mason B. The constitution of some open-hearth slag. *J Iron Steel Inst*, 11:69–80, 1994.

[123] S.F. Han X. Shen M.S. Tang, M.Q. Yuan. The crystalline state of MgO, FeO and MnO in steel slag and the soundness of steel slag cemen (in Chinese). *J. Chin. Ceram. Soc.*, 7:35--46, 1979.

[124] F.P. Glasser. Chemistry of alkali-aggregate reaction. In R. Swamy, editor, *The alkali-Silica Reaction in Concrete*, pages 30--53, New York, 1992. Van Nostrand Reinhold.

[125] A Günlü M Öner, K Erdoğdu. Effect of components fineness on strength of blast furnace slag cement. *Cement and Concrete Research*, 33(4):463--469, 2003.

[126] Hiroshi Hirao Seiichi Hoshino, Kazuo Yamada. XRD/Rietveld Analysis of the Hydration and Strength Development of Slag and Limestone Blended Cement. *Journal of Advanced Concrete Technology*, 4:357--367, 2006.

[127] Pierre Mounanga, Muhammad Irfan Ahmad Khokhar, Rana El Hachem, and Ahmed Loukili. Improvement of the early-age reactivity of fly ash and blast furnace slag cementitious systems using limestone filler. *Materials and structures*, 44(2):437--453, 2011.

[128] Pierre Christian Germain Olivier Espion Bernard, Lebon Billy. Characterisation of new ternary cements with reduced clinker content. In *First International Conference on Concrete Sustainability*, 2013.

[129] K.L. Scrivener, T. Füllmann, E. Gallucci, G. Walenta, and E. Bermejo. Quantitative study of Portland cement hydration by X-ray diffraction/Rietveld analysis and independent methods. *Cement and Concrete Research*, 34(9):1541--1547, September 2004.

[130] Jo Dweck, Pedro Mauricio Buchler, Antonio Carlos Vieira Coelho, and Frank K Cartledge. Hydration of a Portland cement blended with calcium carbonate. *Thermochimica Acta*, 346(1-2):105--113, March 2000.

[131] B Kolani, L Buffo-Lacarrière, A Sellier, G Escadeillas, L Boutillon, and L Linger. Hydration of slag-blended cements. *Cement and Concrete Composites*, 34(9):1009--1018, 2012.

[132] Guang YE. *Experimental Study and Numerical Simulation of the Development of the Microstructure and Permeability of Cementitious Materials*. PhD thesis, Delft University of Technology, 2003.

[133] Lieven Machiels. *Zeolite occurrence and genesis in the Late-Cretaceous Cayo arc of Coastal Ecuador*. PhD thesis, University of Leuven, 2010.

[134] H.M. Rietveld. A method for including the line profiles of neutron powder diffraction peaks in the determination of crystal structures. *Acta Crystallogr*, 21:A228, 1966.

[135] H. M. Rietveld. A profile refinement method for nuclear and magnetic structures. *J. Appl. Crystallogr.*, 2:65--71, 1969.

[136] A. A. Coelho. *TOPAS-Academic: A Computer Programme for Rietveld Analysis, Address = http://www.topas-academic.net 2004.*

[137] R. W. Cheary and A. Coelho. A fundamental parameters approach to X-ray line-profile fitting. *Journal of Applied Crystallography*, 25(2):109--121, Apr 1992.

[138] R Vedalakshmi, A Sundara Raj, S Srinivasan, and K Ganesh Babu. Quantification of hydrated cement products of blended cements in low and medium strength concrete using TG and DTA technique. *Thermochimica Acta*, 407(1):49--60, 2003.

[139] Carlos Rodriguez-Navarro, Encarnacion Ruiz-Agudo, Ana Luque, Alejandro B Rodriguez-Navarro, and Miguel Ortega-Huertas. Thermal decomposition of calcite: Mechanisms of formation and textural evolution of CaO nanocrystals. *American Mineralogist*, 94(4):578--593, 2009.

[140] Elke Gruyaert, Nicolas Robeyst, and Nele De Belie. Study of the hydration of Portland cement blended with blast-furnace slag by calorimetry and thermogravimetry. *Journal of thermal analysis and calorimetry*, 102(3):941--951, 2010.

[141] Harald JUSTNES. How to Make Concrete More Sustainable. In *First International Conference on Concrete Sustainability*, 2012.

[142] Karen L. Scrivener Julien Bizzozero. Limestone reaction in calcium aluminate cement–calcium sulfate systems. *Cement and Concrete Research*, 76:159--169, 2015.

[143] Ana Fernández-Jiménez and F Puertas. Alkali-activated slag cements: kinetic studies. *Cement and Concrete Research*, 27(3):359--368, 1997.

[144] K. Luke and F.P. Glasser. Internal chemical evolution of the constitution of blended cements . *Cement and Concrete Research*, 18(4):495 -- 502, 1988.

[145] K. van Breugel J. Zhou, Ye Guang. Hydration of Portland cement blended with blast furnace slag at early stage. In R. Gagné M. Jolin J. Marchand, B. Bissonnette and F. Paradis, editors, *2nd International RILEM Symposium on Advances in Concrete through Science and Engineering*. RILEM Publications SARL, 2006.

[146] Sidney Diamond R.S. Barneyback Jr. Expression and analysis of pore fluids from hardened cement pastes and mortars. *Cement and Concrete Research*, 11(2):279 -- 285, 1981.

[147] Tatsuhiko Saeki and Paulo J. M. Monteiro. A model to predict the amount of calcium hydroxide in concrete containing mineral admixtures. *Cement and Concrete Research*, 35(10):1914--1921, 2005.

[148] Elke Gruyaert. *Effect of blast-furnace slag as cement replacement on hydration, microstructure, strength and durability of concrete*. PhD thesis, Ghent University, 2011.

[149] Thomas Matschei and Fredrik P. Glasser. Temperature dependence, 0 to 40 °C, of the mineralogy of Portland cement paste in the presence of calcium carbonate. *Cement and Concrete Research*, 40(5):763--777, 2010.

[150] S. Tsivilis, G. Kakali, E. Chaniotakis, and A. Souvaridou. A Study on the Hydration of Portland Limestone Cement by Means of TG. *Journal of Thermal Analysis and Calorimetry*, 52(3):863--870, 1998.

[151] Alessandra Mendes, Will P Gates, Jay G Sanjayan, and Frank Collins. NMR, XRD, IR and synchrotron NEXAFS spectroscopic studies of OPC and OPC/slag cement paste hydrates. *Materials and structures*, 44(10):1773--1791, 2011.

[152] Ivindra Pane and Will Hansen. Investigation of blended cement hydration by isothermal calorimetry and thermal analysis. *Cement and Concrete Research*, 35(6):1155--1164, June 2005.

[153] H. J. H. Brouwers. The work of Powers and Brownyard revisited: Part 1. *Cement and Concrete Research*, 34(9):1697--1716, 2004.

[154] Koichi Maekawa, Tetsuya Ishida, and Toshiharu Kishi. *Multi-scale modeling of structural concrete*. CRC Press, 2008.

[155] I.G Richardson. The nature of C-S-H in hardened cements . *Cement and Concrete Research*, 29(8):1131 -- 1147, 1999.

[156] Jan Bijen. Benefits of slag and fly ash. *Construction and Building Materials*, 10(5):309--314, July 1996.

[157] Thomas Schmidt, Barbara Lothenbach, Michael Romer, Karen Scrivener, Daniel Rentsch, and Renato Figi. A thermodynamic and experimental study of the conditions of thaumasite formation. *Cement and Concrete Research*, 38(3):337--349, 2008.

[158] Barbara Lothenbach and Frank Winnefeld. Thermodynamic modelling of the hydration of Portland cement. *Cement and Concrete Research*, 36(2):209--226, 2006.

[159] Sujin Song and Hamlin M Jennings. Pore solution chemistry of alkali-activated ground granulated blast-furnace slag. *Cement and Concrete Research*, 29(2):159--170, 1999.

[160] Yun Gao. *Multiscale Approach to Study the Heterogeneity and Ionic Diffusivity of Ternary Blended Cement Based Composites*. PhD thesis, Ghent University, 2013.

[161] European Committee for Standardization. Methods of testing cement - Part 1: Determination of strength, institution = European Committee for Standardization, organization = European Committee for Standardization, address = rue de Stassart, 36 B-1050 Brussels, February 2005.

[162] Jan Olek, MenashiI D Cohen, and Colin Lobo. Determination of surface area of portland cement and silica fume by mercury intrusion porosimetry. *ACI Materials Journal*, 87(5), 1990.

[163] Prinya Chindaprasirt, Chai Jaturapitakkul, and Theerawat Sinsiri. Effect of fly ash fineness on compressive strength and pore size of blended cement paste. *Cement and Concrete Composites*, 27(4):425--428, 2005.

[164] M. Heikal, H. El-Didamony, and M.S. Morsy. Limestone-filled pozzolanic cement. *Cement and Concrete Research*, 30(11):1827--1834, November 2000.

[165] Wieslaw Kurdowski. *Cement and concrete chemistry*. Springer, 2014.

[166] Dale P. Bentz. Influence of water-to-cement ratio on hydration kinetics: Simple models based on spatial considerations. *Cement and Concrete Research*, 36(2):238--244, February 2006.

[167] Z Guemmadi, M Resheidat, H Chabil, and B Toumi. Modeling the Influence of Limestone Filler on Concrete: A Novel Approach for Strength and Cost. *Jordan Journal of Civil Engineering*, 3(2):158--171, 2009.

[168] Zhijun Tan, Geert De Schutter, Guang Ye, and Yun Gao. The effect of limestone powder addition on strength of slag blended cement. In *Concrete under Severe Conditions: Environment and Loading (CONSEC-2013)*, volume 2, pages 1888--1898. RILEM Publications SA. RL, 2013.

[169] K. De Weerdt, K.O. Kjellsen, E. Sellevold, and H. Justnes. Synergy between fly ash and limestone powder in ternary cements. *Cement and Concrete Composites*, 33(1):30 -- 38, 2011.

[170] A Paul. Chemical durability of glasses; a thermodynamic approach. *Journal of materials science*, 12(11):2246--2268, 1977.

[171] Ei-ichi Tazawa, Shingo Miyazawa, and Tetsurou Kasai. Chemical shrinkage and autogenous shrinkage of hydrating cement paste. *Cement and concrete research*, 25(2):288--292, 1995.

[172] M. Bouasker, P. Mounanga, P. Turcry, a. Loukili, and a. Khelidj. Chemical shrinkage of cement pastes and mortars at very early age: Effect of limestone filler and granular inclusions. *Cement and Concrete Composites*, 30(1):13--22, January 2008.

[173] Antonio a. Melo Neto, Maria Alba Cincotto, and Wellington Repette. Drying and autogenous shrinkage of pastes and mortars with activated slag cement. *Cement and Concrete Research*, 38(4):565--574, April 2008.

[174] H. J. H. Brouwers. The work of Powers and Brownyard revisited: Part 2. *Cement and Concrete Research*, 35(10):1922--1936, 2005.

[175] S. J. Barnett, M. N. Soutsos, S. G. Millard, and J. H. Bungey. Strength development of mortars containing ground granulated blast-furnace slag: Effect of curing temperature and determination of apparent activation energies. *Cement and Concrete Research*, 36(3):434--440, 2006.